DOE/MC/24222-2790
(DE90000443)

Advanced On-Site Power Plant Development Technology Program

Final Report

Work Performed Under Contract No.: DE-AC21-82MC24222

For
U.S. Department of Energy
Office of Fossil Energy
Morgantown Energy Technology Center
P.O. Box 880
Morgantown, West Virginia 26507-0880

By
International Fuel Cells
P.O. Box 739
195 Governors Highway
South Windsor, Connecticut 06074

September 1989

TABLE OF CONTENTS

LIST OF FIGURES

LIST OF FIGURES (Cont'd)

LIST OF FIGURES (Cont'd)

LIST OF FIGURES (Cont'd)

LIST OF FIGURES (Cont'd)

LIST OF FIGURES (Cont'd)

LIST OF FIGURES (Cont'd)

LIST OF FIGURES (Cont'd)

LIST OF FIGURES (Cont'd)

LIST OF FIGURES (Cont'd)

LIST OF FIGURES (Cont'd)

LIST OF TABLES

LIST OF TABLES (Cont'd)

EXECUTIVE SUMMARY

The subject contract was initiated in August 1982 and the technical effort concluded in April 1989. The purpose of the technical effort was to establish a technology base for 200-kW on-site fuel cell power plants. It was conducted in two phases: 1) Component evaluation; and 2) Full-scale system verification. This contract was supplemented by a Gas Research Institute (GRI) contract which was conducted in the 1981 – 1986 time period. This GRI contract concentrated on 200–kW scale component design, thermal management/water treatment system analysis and redesign and advanced DC/AC inverter development.

The component evaluation phase of the contract was conducted in 1982 through 1985 and generally included subscale component tests, scale-up to full-size 200-kW hardware and full-size hardware tests of the cell stack (in Tasks 1 and 2), the power conditioner (in Task 3), the heat exchangers and ancillary components (in Task 4), and the fuel processor (in Task 5).

Booz, Allen and Hamilton Inc. (BAH) was contracted by DOE to perform an independent audit of IFC's projected cost to manufacture and assemble its 200 kW phosphoric acid fuel cell stack. The findings of this audit were presented to DOE/METC and NASA LeRC on June 2, 1987 at IFC – South Windsor, CT. The major conclusion of BAH's report was that – "no major uncertainties or concerns were identified with regards to IFC's overall cost estimates".

The full-size cell stack, fuel processor, heat exchangers, and ancillary components from the component development tasks were integrated into a dc system called the Verification Test Article (VTA). The VTA which was fabricated and tested under Task 7 allowed for system integration issues associated with the cell stack, fuel processor, thermal management, and water treatment subsystems to be explored under conditions similar to an actual fuel cell power plant.

Key accomplishments of this contract are as follows:

Component Evaluation

- The IFC Configuration B cell concept was incorporated into on-site stacks. Performance levels above the program goal of E + 20 mV were demonstrated. (This performance is equivalent to 650 mV at 200 ASF for full size cells).

- Low cost, fully-encapsulated serpentine coolers which offer improved tolerance to acid corrosion and flow blockage were incorporated into the on-site stacks.

- Advanced asymmetric silicon controlled rectifiers (ASCR's) were identified and incorporated into a 200-kW inverter bridge. An efficiency of 93.6 percent was achieved at full power.

- Alternative feedwater and cooling water pump configurations were identified and verified to improve reliability over previous 40-kW components
- An integrated heat exchanger assembly was developed for combining the fuel preheater, steam superheater and shift converter precooler functions of the fuel processor into a compact, low cost package. High reliability approaches for the burner air preheater and the water recovery condenser were also established.
- A low pressure drop (1/3 baseline) reformer catalyst was identified and successfully evaluated. This catalyst enabled the full-size reformer to be fabricated with fewer longer tubes.
- An up-fired reformer utilizing a modified commercial burner was developed and successfully tested.
- A new type of hydrodesulfurizer catalyst which does not require preconditioning and simplifies system control was verified for full-scale use.

Full-Scale System Verification

- The Verification Test Article (VTA) containing a full-height Configuration B cell stack, a full-scale fuel processor with six-tube reformer and new type of hydrodesulfurizer, an advanced thermal management and water treatment system, and necessary controls and monitors was successfully operated for nearly 2700 hours with an average power output of about 150 kWdc.
- The VTA start-ups were consistently under the five-hour design goal, and restarts from "hot hold" were accomplished in as little as thirty minutes. The success rate for VTA starts was nearly 90 percent which is very good for experimental hardware.
- The VTA operated stably over the full range of power up to 210 kWdc.
- Nearly two-thirds of the VTA operation was conducted at 180 kWdc (300 amp/ft^2 (ASF)) or above.
- The cell stack performance goal of E+20 mV was demonstrated.
- The advanced water treatment system in the VTA showed significant water quality improvement with no coolant blockage problems as existed in the 40 kW system. During the VTA operating life, the water treatment system was simplified by removing resin beds, redundant filters and an air regenerator heat exchanger without affecting performance.
- Emissions characteristics of the VTA were better than existing federal and state standards by at least an order of magnitude.

- Peak shaved fuel gas operation capability was added to the system and successfully evaluated.
- Full-power transient capability was successfully verified
- Full water recovery at rated power on a 95°F ambient day was demonstrated.
- The system was successfully used as a test vehicle for engineering changes to the on-site power plant design program.

A reconditioned 40 kW on site phosphoric acid fuel cell power plant was delivered and installed at METC in 1987. The power plant ran for 6960 hours. In October 1988 a decision was made to discontinue operation and the power plant was shipped back to IFC to be scrapped.

In conclusion, the component and system verifications performed in this program demonstrated the technical feasibility of advanced concepts in meeting performance requirements of on–site cogeneration applications and served as an important step toward future commercialization of on–site fuel cell power plants.

TASK 1 - CELL TECHNOLOGY

Subtask 1.1 - Electrode Catalyst Evaluation

OBJECTIVE

The objective of this task was to identify catalysts and electrodes suitable for scale-up to full-size cell hardware. To meet this objective, cell performance and endurance goals were established for subscale testing. The initial cell performance goal was referred to as E + 20 mv. This goal is equivalent to 682 mV per cell at 200 amps per square foot for subscale cells. The cell performance decay goal is referred to as E-line decay and represents a 43 mV per cell performance loss during 40,000 hours of operation.

SUMMARY

A series of subscale (2-inch by 2-inch) cell tests were run to evaluate cell configuration alternatives developed on the complementary GRI program and other IFC programs.

The first set of screening trials was conducted to identify the best cathode catalyst for scale-up. A catalyst layer formulation (using IFC GSB-18 catalyst) was identified which meets the initial cell performance and cell decay goals for cathodes.

Related subscale tests were also conducted to improve the wet-proofing of the IFC-developed HYCAN anodes, to evaluate low-iR matrix configurations and low-cost ribbed substrates made from an alternative carbon fiber (Fiber "D"), and to assess a new cell IFC configuration (called Configuration "B"). Subscale Configuration "B" cells have met or exceeded the performance goal for over 5000 hours.

ACCOMPLISHMENTS/CONCLUSIONS

The following items were accomplished with Configuration "B" cells and support the conclusion that Configuration "B" is superior to Configuration "A" and is, therefore, more desirable for future commercialization.

- The E + 20 mV cell performance and E-line cell decay goals have been met in subscale testing for over 5000 hours using the "B" configuration cell.
- A GSB-18 cathode catalyst layer and HYCAN anode catalyst layers were identified for scale-up to full-size cells.
- Use of a low iR matrix configuration and low-cost substrate material (made with Fiber "D") was verified in subscale tests.

DISCUSSION

The electrode performance improvement activity involved testing of laboratory scale (2-inch by 2-inch) single cells incorporating new catalyst layers and cell configurations developed in other programs. Figure 1.1-1 shows the test facility.

The first series of tests were directed toward evaluation of nine different subscale cells (referred to as Series I cells) with three different cathode catalysts on three different supports. One of the cathode catalysts, called GSB-18, was found to meet the initial on-site performance goal and was selected for further development.

Approaches to improve the cell performance decay of GSB-18 cathodes were investigated next. Four subscale cells (termed Series II cells) were fabricated with different wet-proofing approaches for the cathodes. All four cells were more hydrophobic than their predecessors (Series I cells), and two of the cells remained stable after special diagnostic testing. Those two cells were then subjected to stress tests to determine electrode performance stability. One of these cells (Cell No. 3638) was placed on endurance after completing stress tests and operated for a total of 17,000 hours. See Figure 1.1-2. Final cell performance was approximately E-10 mV.

The technology for the preparation of GSB-18 catalyst and electrodes transitioned from laboratory to shop in 1983. Prior to starting the first short stack in the program, pieces cut from full-size shop-made electrodes were built into 2-inch by 2-inch cells to obtain a preview of stack performance. One of these cells, Cell 3700, completed 7400 hours of operation. The performance versus time is shown in Figure 1.1-3. Although the performance level of cell 3700 was lower than that of 3638, it was stable and closely matched the average performance of the cells in the short stack.

In late 1983, kilogram-size batches of GSB-18 and GSB-26 catalysts were prepared and fabricated into 2.2-ft^2 electrodes. GSB-26 is a derivative of GSB-18 which showed improved performance in tests conducted in the complementary GRI program. Pieces cut from the full-scale cathodes were assembled into four subscale cells for the endurance testing. Apart from diagnostic tests following start-up, these cells (build No. 's 3739, 3751, 3771, and 3772) were run at 200 ASF without interference. All four cells performed better than the cells run in the 30-cell short stack. Although none of the cells attained the performance development goal of E + 20 mV, three cells were at or above E-line cell performance for 10,000 hours. See Figures 1.1-4 through 1.1-6.

(WCN-7028)

Figure 1.1–1. *Test Facility for Subscale Cells*

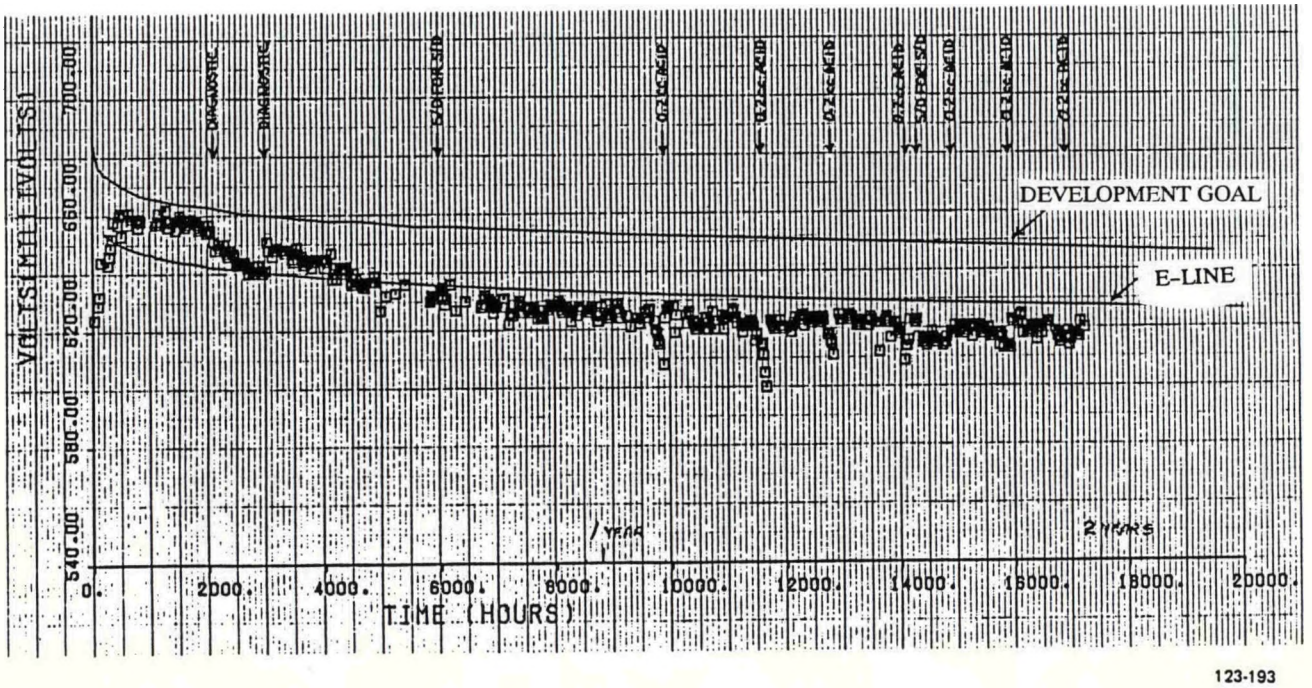

Figure 1.1–2. *Performance History of Cell 3638 with Lab–made Cathode*

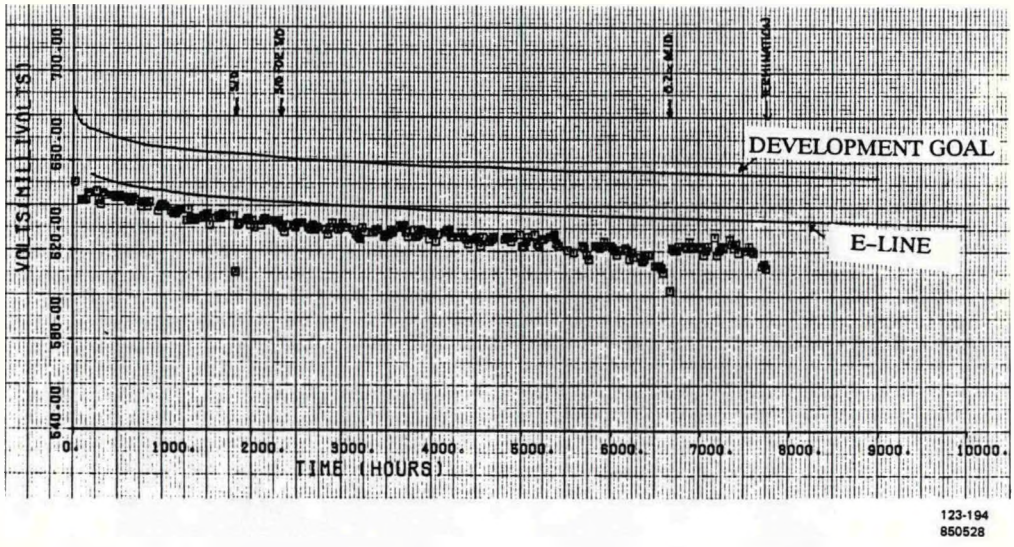

Figure 1.1–3. *Performance History of Cell 3700 with Shop–made Cathode*

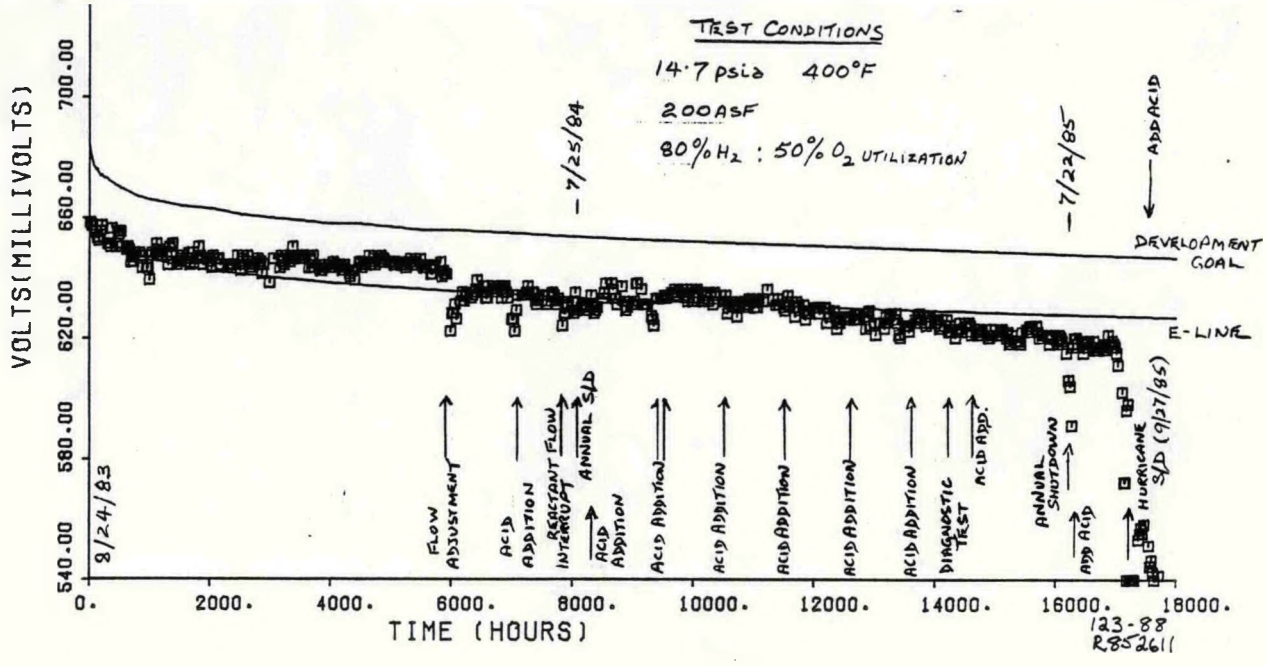

Figure 1.1–4. *Performance History of Cell 3739*

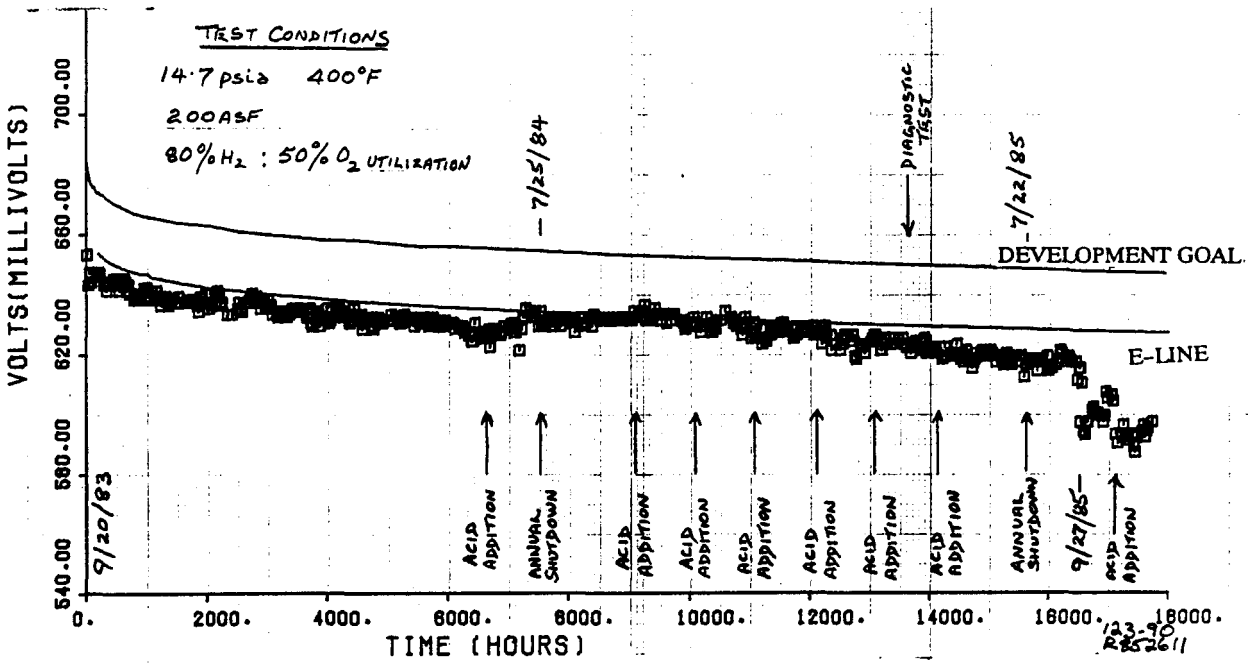

Figure 1.1–5. *Performance History of Cell 3751*

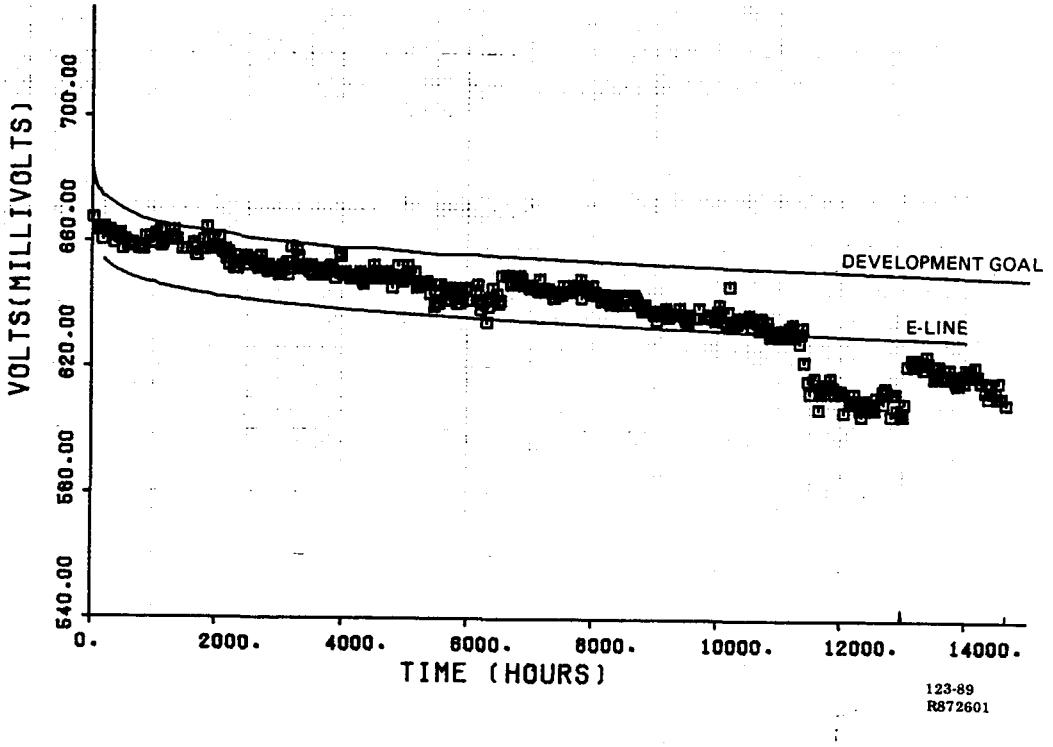

Figure 1.1–6. *Performance History of Cell 3771*

During 1984, work was directed toward improving life and reducing cost of the cell stack components. Areas covered were matrix configuration, anode stability, and substrate materials. Cell 3864 consisted of a HYCAN anode and GSB–18 cathode made in the shop using a low cost, ribbed substrate made from an alternative carbon fiber (Fiber "D"). A new matrix configuration was also utilized to reduce cell IR. As shown in Figure 1.1–7, cell 3864 operated near the E + 20 mV cell performance goal for over 4000 hours.

Also in 1984, evaluation of a new cell configuration (Configuration "B") was started. The first successful "B" configuration cell in this program was build No. 3890. This cell consisted of a lab–made HYCAN anode, GSB–18 cathode, and low–iR matrix. As shown in Figure 1.1–8, cell 3890 attained the on–site performance goal for almost 8000 hours. Another "B" configuration cell, build No. 3925, was also tested. As shown in Figure 1.1–9, cell 3925 performed above the program performance goal for 5000 hours.

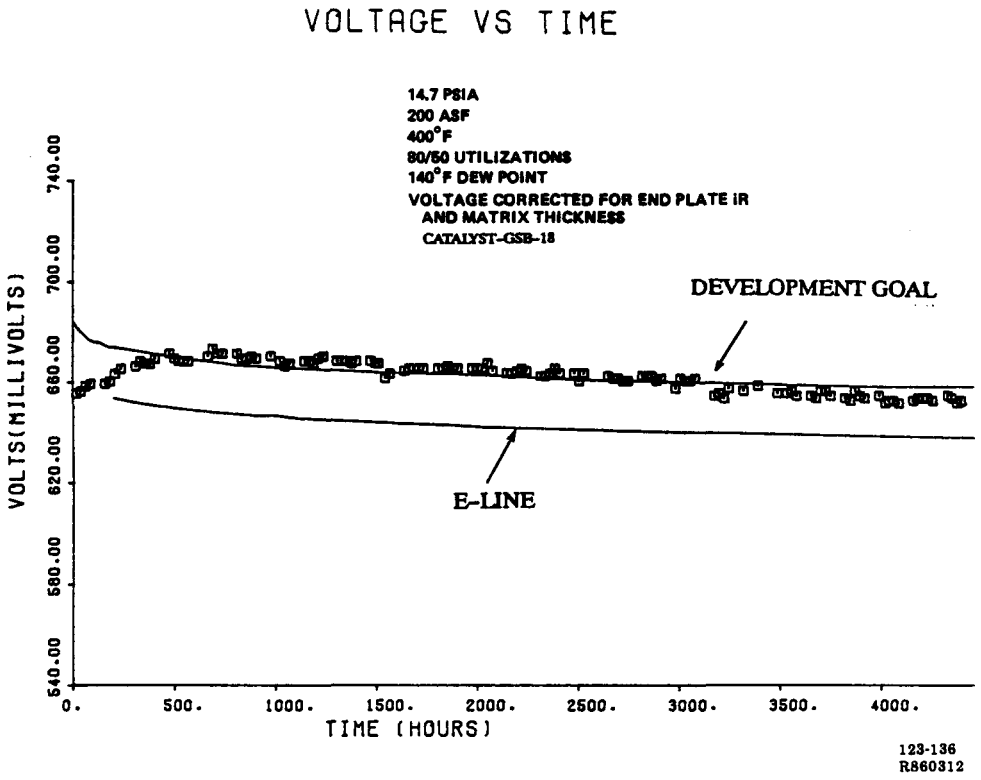

Figure 1.1–7. *Performance History of Cell 3864*

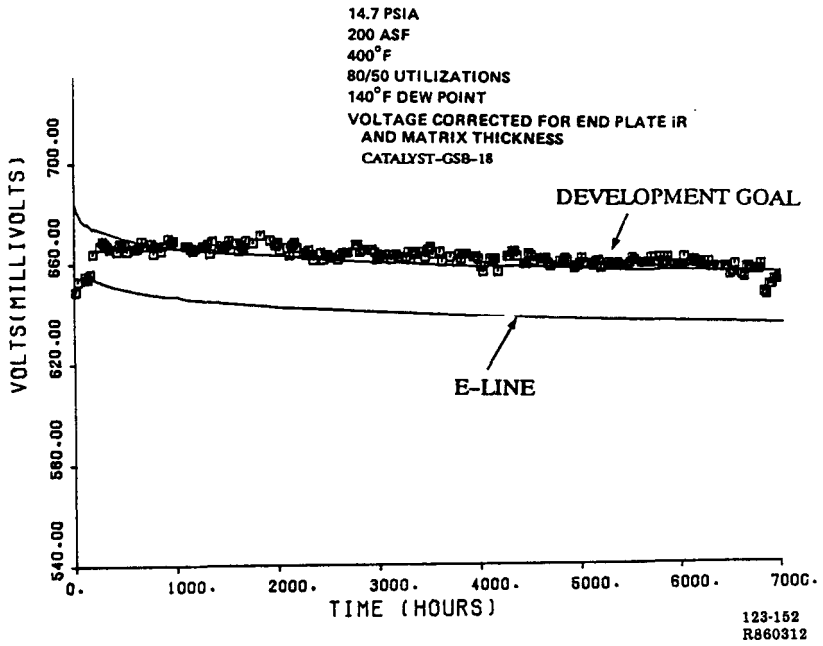

Figure 1.1–8. *Performance History of B–Configuration Cell 3890*

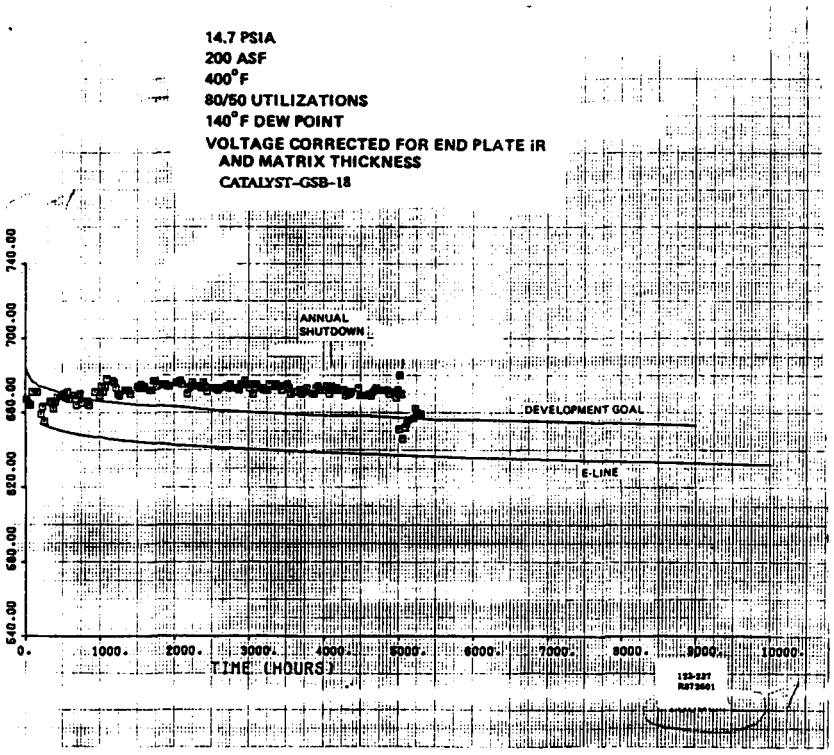

Figure 1.1–9. *Performance History of B–Configuration Cell 3925*

TASK 2 - CELL STACK DEVELOPMENT

Subtask 2.1 - Electrode Substrate Technology

OBJECTIVES

The objectives of this task are to investigate lower cost substrates and related repeat component materials and to increase the required electrolyte refill interval without compromising performance or cost.

SUMMARY

Studies showed that Configuration "B" cells could extend acid refill interval by 150 percent over original 40-kW Configuration "A" cells. This capability (along with the potential for lower cost components and improved cell performance) led to the decision to change from Configuration "A" to "B" cells.

The search for low-cost materials to fabricate substrates led to the identification of a new low cost fiber (called Fiber "D"). Engineering activities were directed toward manufacturing scale-up of substrates using Fiber "D". Heat treating requirements for Fiber "D" were initially investigated using a batch process. Later, continuous heat treating of Fiber "D" was evaluated using a furnace loaned from NASA. The heat-treated Fiber "D" was successfully formed into full-size Configuration "B" substrates for short stacks and the full-height stack in the Verification Test Article (VTA).

The Configuration "B" cells also use new particulate materials. Low-cost raw materials were identified in this program and formed into full-size parts for stack improvement activities.

ACCOMPLISHMENTS/CONCLUSIONS

- Configuration "B" cells displayed superior electrolyte storage compared to baseline 40-kW type Configuration "A" cells. The projected electrolyte refill interval was extended by 150 percent with Configuration "B" cells.
- A low-cost fiber (Fiber "D") was identified as a replacement for baseline carbon fibers in substrates.
- Continuous heat treating of Fiber "D" was demonstrated using a furnace on loan from NASA.
- Full-size substrates were formed using Fiber "D" for short stacks and the full-height stack.
- Low-cost particulate materials and processes were defined and scaled-up to fabricate over 1300 full-size Configuration "B" cell components for stacks.

DISCUSSION

Increased Electrolyte Storage

Two approaches to increase electrolyte storage and extend electrolyte refill interval were evaluated in this program. They were the dual porosity substrates for Configuration "A" cells and the Configuration "B" cell.

Earlier work had demonstrated the feasibility of constructing ribbed substrates for Configuration "A" cells with variable porosities adjusted to increase electrolyte storage in the ribs and increase gas diffusivity in the web or gas transport layer. A second generation dual porosity substrate with an advanced rib composition designed for additional electrolyte storage was evaluated in this phase of the program.

Substrate handsheets were formed with the advanced rib composition, as well as first generation dual porosity and standard substrates for comparison. Electrodes fabricated from these substrates were tested in 2-inch by 2-inch cells to determine performance as a function of electrolyte content. Since all web layers were nominally identical, performance stability at increasing electrolyte levels would serve to indicate the rib structure's ability to store the excess electrolyte.

The standard substrate cell with uniform porosity was tested satisfactorily at the baseline acid fill level of 30 percent, but would not operate after the first acid fill increment of 5 percent. The performance of the two second generation dual porosity cells are shown in comparison to the first generation cell in Figure 2.1-1. As expected, both types of dual porosity cells out performed the standard substrate with uniform porosity. The second generation dual porosity substrate also out performed the first generation substrate structure. The second generation dual porosity cells performed acceptably until the electrolyte fill was increased to 45 percent. The performance of both second generation dual porosity cells was about 12 mV above E-line at the 40 percent fill level. This fill level projects to a 50 percent increase in the time between acid refill intervals compared to the current 30 percent fill of conventional ribbed substrate cells.

Diffusion measurements as a function of electrolyte fill were also completed on the second generation dual porosity substrates. Figure 2.1-2 shows that dual porosity substrates have higher diffusion coefficients at equivalent fills than the single porosity substrates. The diffusion measurements are in agreement with subscale cell testing and show the performance of the dual porosity substrates to be less sensitive to electrolyte content than the conventional substrates, but the sensitivity to percent electrolyte fill is still greater than expected. The dual porosity substrate development effort was discontinued because improvements in acid storage were not as great as desired and an attractive alternative had been identified.

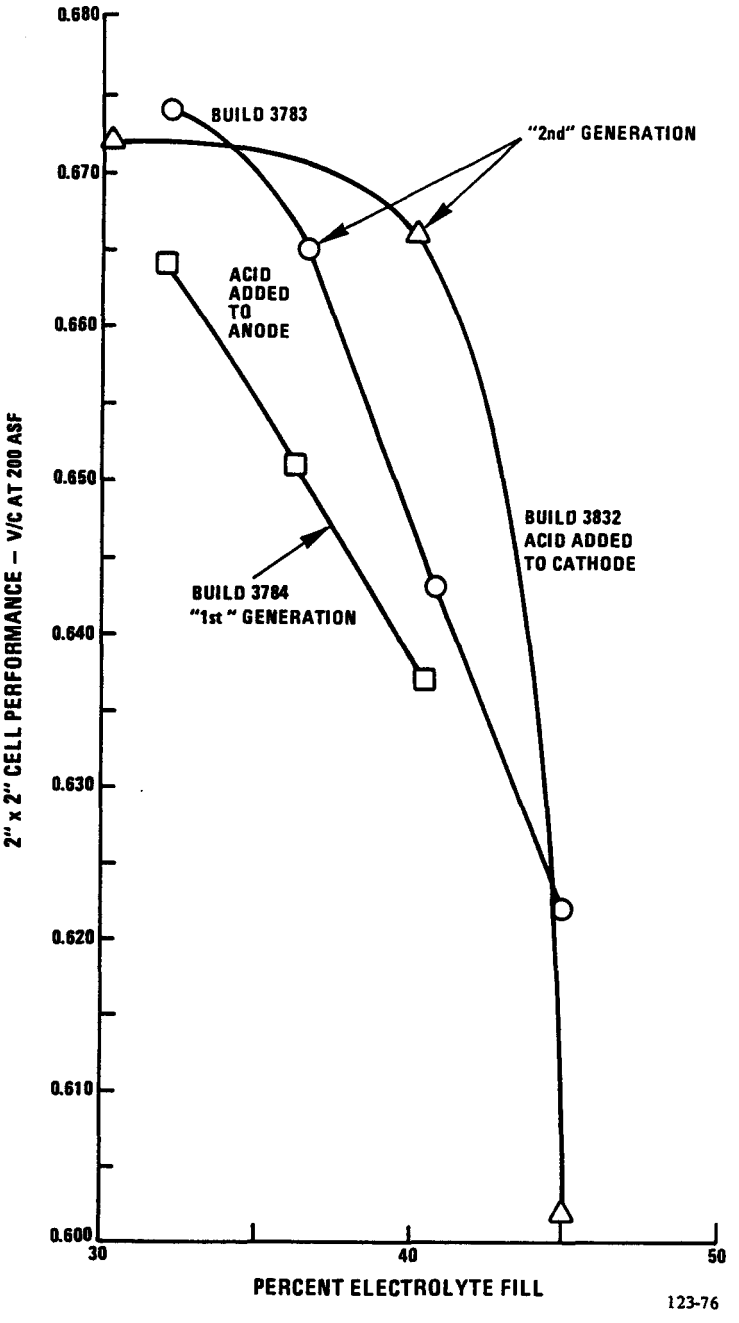

Figure 2.1–1. *Performance Comparison of Dual Porosity Cells*

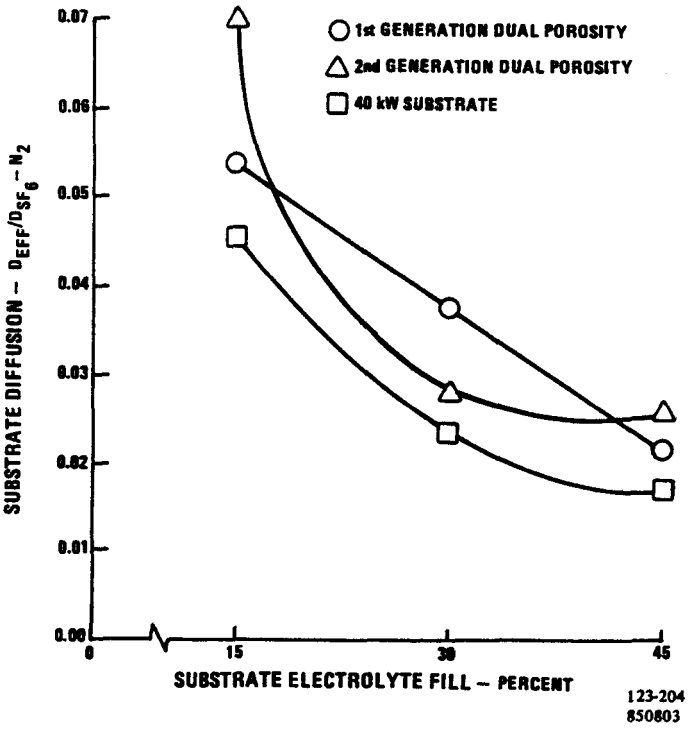

Figure 2.1–2. *Diffusivity Comparison of Configuration "A" Substrates*

IFC funded the conceptual development of an alternative cell configuration with high electrolyte storage capability. The alternative cell configuration was designated Configuration "B". Development tests had shown that the alternative cell configuration offered significant electrolyte storage increases using lower cost materials without penalty to cell thermal performance or electrical output. Two subscale cells were fabricated from the components of the second short stack for testing to determine performance as a function of electrolyte content. The test program was identical to that employed in evaluating dual porosity substrate structures, but the results were significantly better. See Table 2.1–1. Fill levels exceeded 50 percent without significant performance penalty, and the performance of both cells was above the E + 20 mV performance goal at the 50 percent fill level, which projects to a 150 percent increase in time between refill interval when compared to the baseline fill and 100 percent better than second generation dual porosity Configuration "A" cells.

Table 2.1–1. Electrolyte Fill Test for "B" Configuration Cells

Cell Fill, % Void Volume	30%	35%	40%	45%	50%
Cell Performance					
Cell 3891	E + 27	E + 26	E + 29	E + 30	E + 31
Cell 3892	E + 30	E + 28	E + 29	E + 26	E + 29

Low-Cost Substrate Materials

The program to form Configuration "B" substrates from commercially formed precursor materials was based on combining low-cost raw materials with conventional commercial forming processes to achieve low costs. The activity began in 1983 with laboratory scale handsheet samples being provided by several commercial material processors. After evaluation of these handsheet samples, a primary vendor was selected for scale-up activities.

The scale-up of commercially formed substrate structures was begun by attempting to reproduce a candidate composition on full-size production equipment. The material was produced on a 60-inch wide machine and the quantities produced were sufficient to estimate processing and material costs. Delamination and edge cracking occurred when this material was heat-treated.

A second generation material containing a different resin system was produced. No delamination or edge cracks were apparent, but many sheets developed cracks. The shape and extent of the cracks suggested thermal maldistribution during the heat-treat process. A carbonizing trial was undertaken to reduce the cracking by modifying the heat treat cycle. All of the second generation precursor sheets survived carbonization without cracks.

After completion of the experimental carbonizing trial, a full stack of second generation sheets was carbonized using the modified cycle. Again, all of the second generation precursor sheets survived carbonization in excellent condition. The full-sized sheets were then graphitized. Of the 38 parts graphitized, 29 were in satisfactory condition with the balance showing one or two cracks starting at center of an edge. These parts experienced a 25 percent linear shrinkage and 55 percent thickness shrinkage as a result of being heat-treated.

The commercially formed substrate precursors consistently yielded high mechanical strength but low thermal and electrical conductivity relative to the 40-kW substrates (Table 2.1-2). Experiments to improve these properties were not successful. The performance of full-size electrodes fabricated from the low-cost precursor substrates was also significantly below the standard substrate in 2-inch by 2-inch cell tests (Figure 2.1-3). Work on this material was, therefore, discontinued.

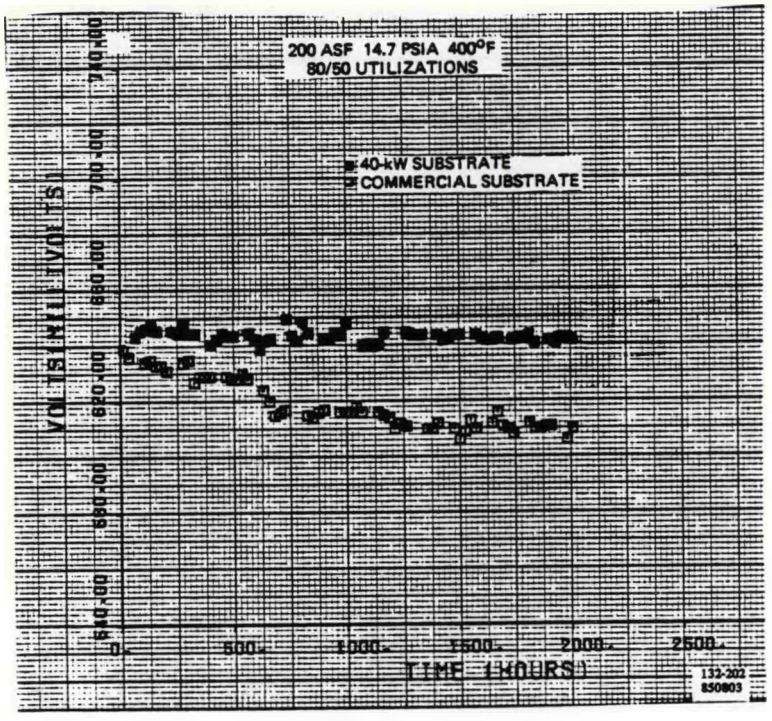

Figure 2.1–3. *Performance Comparison of Low–Cost Precursor Substrates to Standard Substrates*

IFC–funded efforts to develop a low–cost substrate material produced alternative to the commercially formed substrate precursors. The substrates were formed by process similar to that used for making 40–kW substrates, but with a new fiber (called Fiber "D"). Substrate handsheets were formed with the new material (Fiber "D"). As shown in Table 2.1–2, the material properties of the new, IFC substrate with Fiber "D" are similar to 40–kW experience and substantially better than substrates made by the commercial process.

Table 2.1–2. Substrate Property Comparison

Substrate	iR (mV/Mil/100 ASF X 10^{-2})	Thermal Conductivity (Btu/Hr/Ft/° F)	Flex Strength (psi)
IFC–Formed, with Fiber "D"	0.60	2.7	600
40–kW	0.50	4.0	400
Commercially–Formed	2.3	0.8	930

Based on the above data, Fiber "D" was selected for further improvement. The next sections report the manufacturing scale-up of Fiber "D" substrates which culminated in testing of full-size parts in short stacks and the full-height stack used in the Verification Test Article (VTA).

Fiber "D" Material Process Scale-up

The process technologies required to convert low-cost raw materials into Fiber "D" were evaluated at commercial scale. Raw materials were acquired in sufficient quantities to validate the initial processing steps on full-scale commercial equipment. Low-cost processes and materials were employed and processing was completed at nominal equipment throughput rates. Heat treating to complete the process and produce Fiber "D" was the central activity of this program.

Heat treating of Fiber "D" was initially conducted on a lab scale to provide material to form handsheets for physical property evaluation. The key heat treating variables were defined by comparing the handsheet properties to the various heat treat cycles and raw material processing variables. Preliminary continuous furnace equipment requirements and operating parameters were also defined in lab-scale heat treating experiments.

The first heat treat trials to produce Fiber "D" in full-size stack quantities were completed by batch process. The fiber produced in these trials was shown to be equivalent to the lab-scale product and was successfully used in full-size substrate forming trials. The batch process was the principal source of material used in developing Fiber "D" substrate properties, and the sole heat treat source for the third On-Site short stack in this program and the full-height power section electrode substrates.

Heat-treat trials were conducted at an equipment supplier to establish the feasibility of continuous processing of Fiber "D". Results from these trials compared well with laboratory scale tests and demonstrated that high commercial throughput rates were achievable. The Fiber "D" also fed smoothly through the equipment, and the initial results indicated that the finished fiber was acceptable for substrate forming.

A full-scale continuous furnace for heat treating Fiber "D" was acquired to evaluate and develop the process in production quantities. The furnace, on loan from NASA, was installed in November, 1985. The assembled furnace is shown in Figure 2.1-4. After feeder construction, checkout and run-in, 500 pounds of Fiber "D" were produced. The product fiber was identical to that produced in the batch process, except for the presence of a thin film of condensate that volatilizes at low temperature. Furnace changes to eliminate the unwanted condensate have been defined and will be evaluated in follow-on programs.

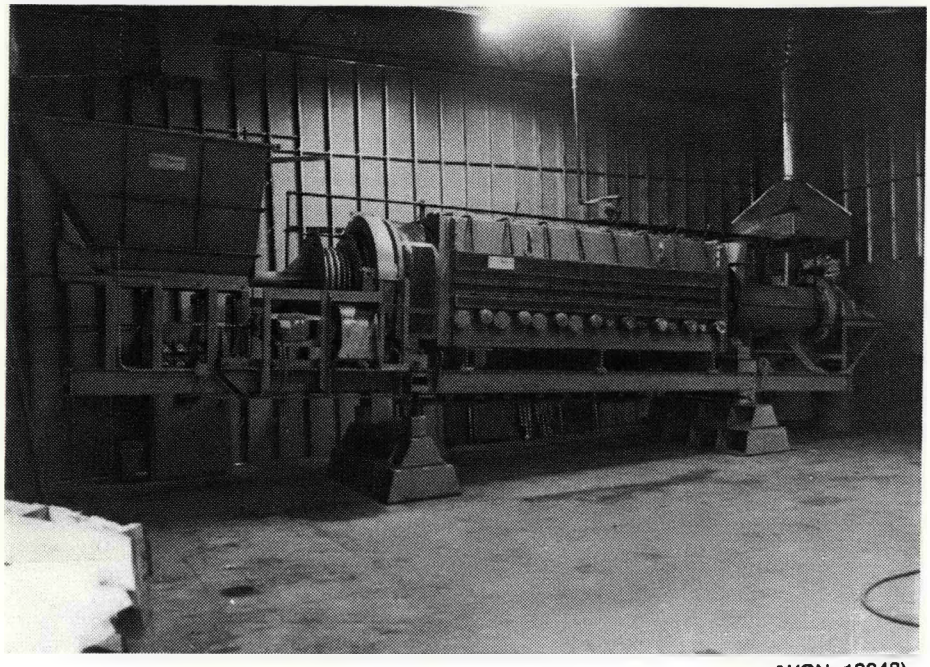

(WCN-13848)

Figure 2.1–4. *Furnace for Continuously Heat Treating Fiber "D"*

Substrate Forming Scale–Up

The initial full–scale Fiber "D" forming trials were completed using conventional double belt press, substrate forming equipment. Substrates were formed without difficulty and possessed adequate strength, flatness, and thickness uniformity. Heat treating was also completed by standard processes and equipment, and the physical properties were nominally equivalent to the baseline fiber. Flexural strength was marginally lower than baseline substrates and conductivity was better. The substrate forming trial is shown in progress in Figure 2.1–5.

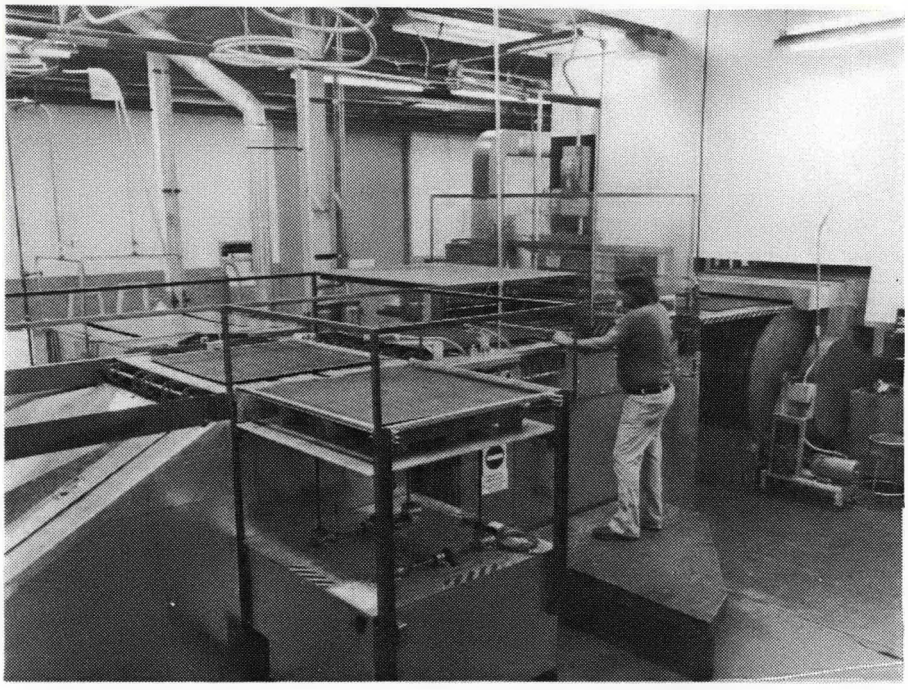

(WCN-13640)

Figure 2.1-5. *Forming Substrates with Fiber "D"*

Alternative in-house and commercial forming processes for the Configuration "B" electrode substrates were also evaluated. In-house forming trials were conducted under the parallel GRI technology development program. Results using the conventional forming equipment showed that considerable additional engineering was required. Lab-scale vendor trials demonstrated the feasibility of employing commercial processes. After a series of handsheet trials and pilot plant runs, the process was scaled-up by the vendor and 12,000 ft^2 of full-size, low-cost Configuration "B" electrode substrate material was manufactured for the third On-Site short stack in this program and the full-height power section. A comparison of key substrate physical properties for each of the processes evaluated is shown in Table 2.1-3.

Particulate Components

Three vendors were identified as suppliers of low-cost raw materials for forming components using particulate material rather than fiberous material. A comparison of component physical properties formed using each of the three vendors' raw materials is shown in Table 2.1-4.

Table 2.1-3. Substrate Property Comparison			
Parameter	**Units**	**Double Belt Formed**	**Commercially Formed**
Density	gms/cc	0.6	0.3
iR	MV/mil	2.5	1.2
Conductivity	Btu/Hr/Ft/° F	1.6	1.4

Table 2.1–4. Particulate Component Properties			
Precursor	**Electrical Resistance (mV/Mil/100 X 10^{-2})**	**Thermal Conductivity (Btu/Hr/Ft/° F)**	**Flex Strength (psi)**
Vendor A	0.30	8.0	1120
Vendor B	0.27	11.0	521
Vendor C	0.27	8.0	1920

Particulate components developed for the Configuration "B" cell were successfully scaled–up using conventional substrate forming and heat treating process equipment and technologies. The initial forming trial on the substrate former produced strong parts of uniform thickness and density. All samples showed excellent conductivity and strength.

Cell Stack Cost Audit

Another element of activity on this contract was related to the cell stack cost assessment task. The major objective of the cost assessment task was to establish the effect of technology developed in the program on cell stack component cost and provide an assessment of the progress toward achieving established cost goals. A cost assessment system, previously developed by IFC, was used to establish a valid and reliable assessment of cell stack cost. The cost data used in the assessment were collected as part of "cost tracking" activities associated with the actual fabrication of cell components during the program. The validity of the manufactured cost assessment was reviewed by an independent, third–party auditor. An audit of IFC's cell stack cost estimate was completed in June, 1987 by representatives from Booz, Allen & Hamilton, Inc. following the completion of the full–height VTA stack fabricated under this contract. The independent audit verified IFC's assessment and established a baseline projected cost for producing 200-kW cell stacks using the Configuration B cell design.

Subtask 2.2 - Cooler Technology

OBJECTIVES

The objectives of this subtask were to reduce cooler cost and improve cooler reliability.

SUMMARY

An improved cooler configuration, the encapsulated serpentine cooler, was introduced at the beginning of the program based on its development in the GRI program. The coolers used in the 40-kW field test used relatively complex tube arrays with many parallel flow paths for the cooling water. The serpentine tube array consists of a single tube. The basic simplicity of the serpentine array results in a cost one-third of conventional arrays. The arrays are encapsulated in holders to protect the tube arrays from acid attack and to conduct stack waste heat to the tubes. Heat transfer evaluations indicated that the encapsulated serpentine cooler has better heat transfer characteristics than conventional coolers, and the cooler spacing could be increased from 5 cells/cooler to up to 10 cells/cooler. The overall benefit of using serpentine coolers is a reduction of 80 percent in stack cooler cost.

An additional benefit of the serpentine cooler is that orifices (often called snivvies) are not required to distribute the cooling water flow between coolers in the stack. During the 40-kW field test, coolers typically had to be chemically cleaned every 2000-hours to prevent blockage of snivvies and subsequent loss of cooling water flow to cell stack coolers. By eliminating flow orifices (snivvies), the serpentine coolers can save the cost and inconvenience of periodic chemical cleaning and improve the reliability of cell stack cooling.

Activities in this task were directed toward the engineering and fabrication of full-size encapsulated serpentine coolers for short stacks and the full-height stack in the Verification Test Article (VTA). Fluid flow studies, heat transfer tests, cooler holder material evaluations, and erosion/corrosion tests were conducted to select and improve configurations for stack testing. Coolers accumulated as much as 7000-hours of operation in short stacks without evidence of acid corrosion on the outside of tube arrays or erosion/corrosion on the inside.

The improvement of cooler hose integrity was also addressed. Teflon hoses with and without reinforcing were tested for durability at 200-kW on-site operating conditions. A woven stainless steel-reinforced Teflon hose with modified swaged connections was defined with burst pressures in the 5000-7000 psig range. This is 20 times greater than the 250 psig design pressure of the cooling water system.

ACCOMPLISHMENTS/CONCLUSIONS

- A low-cost encapsulated serpentine cooler offering improved tolerance to acid corrosion and flow blockage was developed. The new cooler reduces cooler cost by more than 80 percent.

- Encapsulated serpentine coolers were fabricated and successfully tested for up to 7000-hours in cell stacks. No coolant-side corrosion was noted in stack tests.

- Woven steel-reinforced Teflon hoses with modified swaged connections were made to meet 200-kW design requirements for dielectric coolant hoses over the projected power plant life.

DISCUSSION

Cost and reliability improvements for cell stack cooling were achieved by defining the encapsulated serpentine cooler and the stainless steel reinforced cooler hoses. The following sections describe various aspects of design and development activities.

Cooler Design

The heat transfer characteristics of the 3/8-inch bare metal serpentine cooler were analyzed. Heat removal requirements can be satisfied by a cooler spacing of 10 cells/cooler for cells operating at 200 ASF with E + 20 mV cell performance.

The fluid dynamic analysis of the 3/8-inch tube diameter cooler was completed. The flow characteristics of this cooler configuration are such that flow control orifices are not required to prevent cooler-to-cooler flow maldistribution. A test program was initiated to define the influence of oxygen content and velocity on erosion-corrosion inside 3/8-inch horizontal tubes.

The simplicity of the serpentine cooler results in a cost which is one-third of that of the conventional cooler. The 3/8-inch bare metal serpentine cooler allows the cells per cooler to be increased from five to ten. The combination of these results in a cost reduction of more than 80 percent on a $/KW basis when compared to the cooler configuration used in the 40-kW plant.

Cooler Heat Transfer Rigs

A subscale heat transfer rig was designed and constructed to provide convenient means of screening candidate cooler materials and configurations before committing to testing in the full-size heat transfer rig. This rig is also used to measure the thermal conductivity of cell components. The subscale rig has a 6-inch by 6-inch planform area and utilizes a 3/8-inch diameter serpentine array with pitch of 1.5 inches. All candidate coolers are fabricated to fit this array, allowing results to be measured against a standard. The basic operating principal of the subscale heat transfer rig is identical to the full-size rig. The data collection and reduction process for the subscale heat transfer rig was computerized to provide rapid readout of cooler performance. The subscale heat transfer rig is shown in Figure 2.2–1.

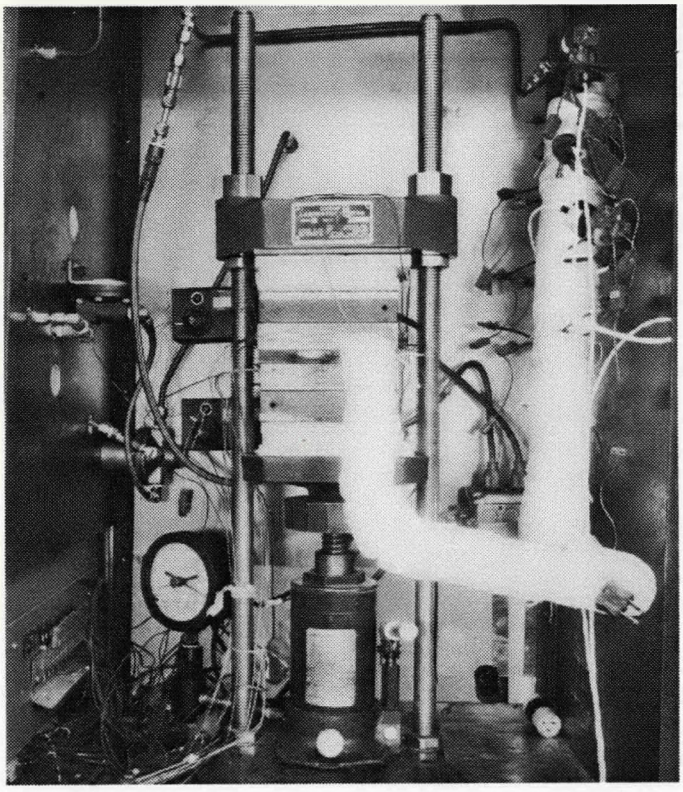

(WCN-11013)

Figure 2.2–1. *Subscale Cooler Installed in Heat Transfer Rig*

Initially, a cooler assembly of the type used in the first 30-cell stack was tested in the subscale heat transfer rig to establish a baseline for comparison. This assembly consisted of a copper array with a fibrous cooler holder. The same type cooler was tested with a stainless steel array to provide an additional baseline. The thermal resistance data of these coolers are shown in Table 2.2–1. Results are in agreement with the full-size heat transfer rig. Additional testing was conducted to support the cooler and design activity.

Table 2.2–1. Initial Subscale Heat Transfer Rig Test Results

Cooler Holder	Cooler Tube	Thermal Resistance Hr-Ft^2 °F/Btu
Fiber A	Copper	0.0082
Fiber A	Stainless Steel	0.0091

A full-size heat transfer rig was constructed to test coolers of 27-inch by 27-inch planform size that are being engineered for the 200-kW cell stack. The rig consists of a test cart containing an electrical heater control system that will simulate the heat flux in a cell stack, and a cooler assembly representative of the cooler arrangement found in a cell stack. A schematic of the rig is shown in Figure 2.2–2.

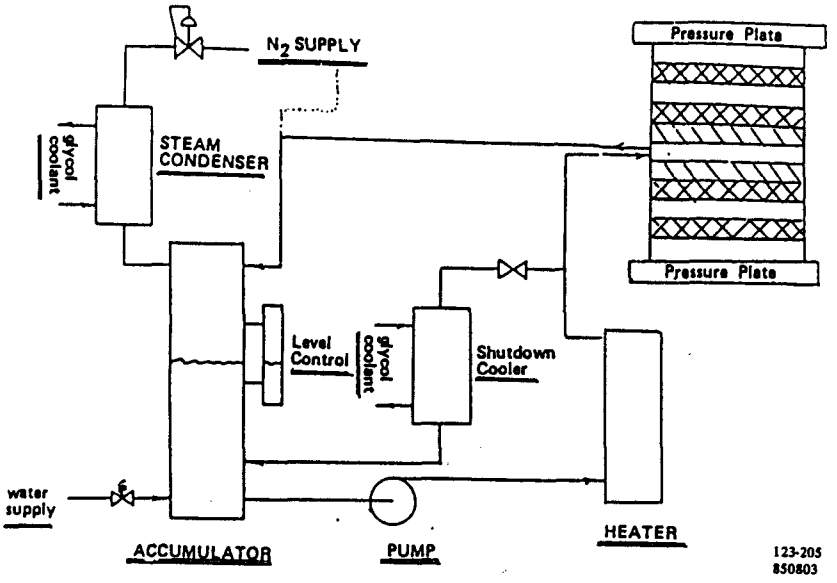

Figure 2.2–2. *Schematic for Full–Size Heat Transfer Rig*

The first test of a 27-inch by 27-inch cooler was conducted using a test cooler which was the same design as the encapsulated cooler used in the 30-cell short stack. Figures 2.2–3 and 2.2–4 show the new heat transfer rig with the test cooler installed. The measured thermal resistance of the cooler was 0.0095 hr ft²°F/Btu. This agreed with the results obtained for a similar cooler tested earlier in the 20–inch 20-inch heat transfer rig. Additional testing was conducted to support the cooler development and design activity.

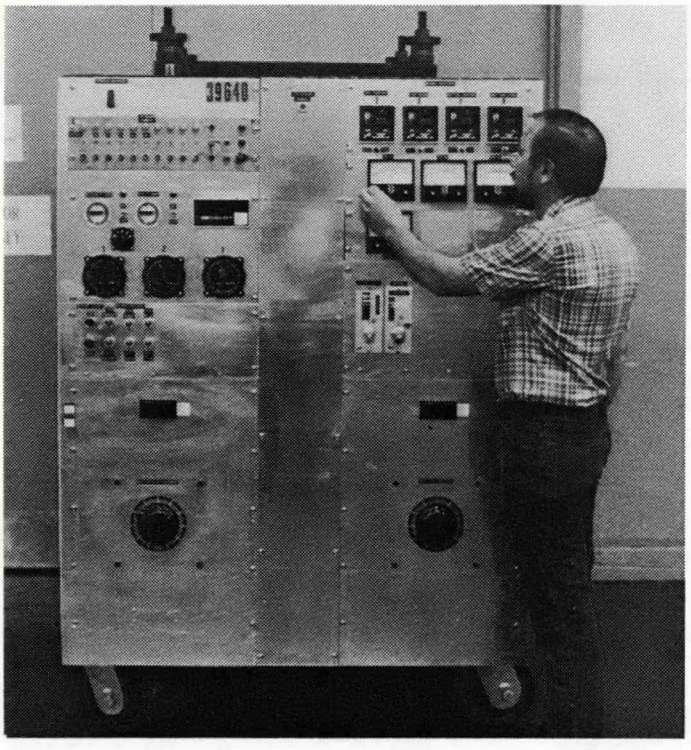

(WCN-12034-6)

Figure 2.2–3. *Heat Transfer Test Rig for Full–Size Coolers*

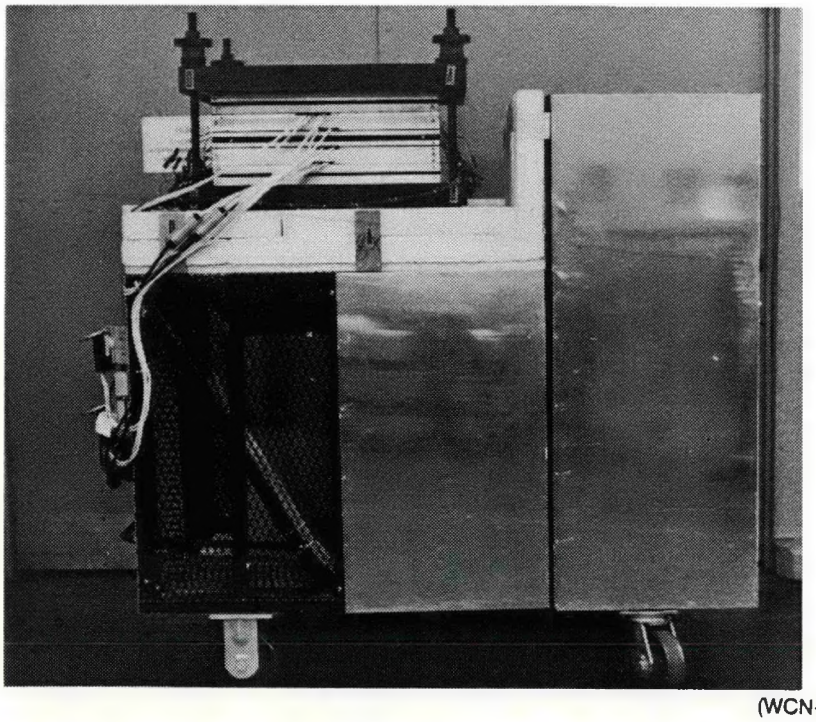

(WCN-12034-7)

Figure 2.2–4. *Full–Size Cooler Installed in Heat Transfer Rig*

Cooler Holders

Alternative cooler holders were investigated to improve thermal performance and reduce cost. Evaluation of cooler holders includes fabrication trials, testing in subscale and full-scale heat transfer rigs, and determination of projected cost. Three types of cooler holders were evaluated.

The first type of cooler holder to be evaluated utilized solid graphite. Subscale heat transfer tests were conducted to evaluate the solid graphite cooler holder as a means of obtaining higher cooler thermal conductivity (Table 2.2–2). For the case of zero nominal clearance between the tube and holder, the thermal resistance is slightly lower than the baseline. When the tube-to-holder clearance is 2.5 mils nominal, the thermal resistance is considerably higher. The results indicated that thermal caulks would be required to accommodate the tube to holder clearances.

Two commercially available thermal caulks were evaluated. Solid cooler holders with a tube to holder clearance of 2–3 mils were used in conjunction with the thermal caulks. These results are included in Table 2.2–2.

Table 2.2–2. Subscale Heat Transfer Rig Test Results

Cooler Holder	Cooler Tube	Tube to Holder Fit	Caulk Thermal	Thermal Resistance Hr-Ft^2 °F/Btu
Graphite Fiber	Stainless Steel	Interference	None	0.0091 (Baseline)
Solid	Stainless Steel	Zero nominal clearance	None	0.0081
Solid	Stainless Steel	2-3 mil clearance	None	0.0365
Solid	Stainless Steel	2-3 mil clearance	Commercial Type A	0.0093
Solid	Stainless Steel	2-3 mil clearance	Commercial Type B	0.0112
Solid	Stainless Steel	2-3 mil clearance	Type A with 9% Graphite	0.0083
Solid	Stainless Steel	2-3 mil clearance	Type A with 20% Graphite	0.0089

The second type of cooler to be evaluated was metallic cooler holders. Two materials, zinc and aluminum, were evaluated to obtain higher holder thermal conductivity. Subscale heat transfer testing of the zinc holders showed that high thermal resistance occurred because of poor tube to holder contact at the operating temperature. This was found to be due to the difference in thermal expansion between the holder and cooler tube materials that caused the tube to separate from the holder. Subscale heat transfer test shows that coolers with aluminum holders had a thermal resistance about 15 percent lower than the conventional fiber holder. However, testing in simulated cell environments showed that aluminum holders developed high electrical resistance even with protective nickel plating. No further activity with metal holders was conducted.

Development of a more conductive and lower cost cooler holder fabricated from a particulate material was initiated during 1984 under the parallel Electric Utility Technology and Development Program, DOE Contract DE-AC01-82FE60338. This approach appeared suitable for On-Site applications and was the third cooler holder type to be evaluated.

Subscale heat transfer tests indicated that a thermal caulk is required to accommodate the dimensional tolerances associated with the particulate holder. A total of four thermal caulk materials were tested with particulate holders in the subscale heat transfer rig. These materials include a commercial caulk, a commercial caulk with 5 percent graphite powder added, and two IFC proprietary formulations (Types A and B). The test results indicated that the IFC Type A thermal caulk was the most effective.

A 3.7-ft^2 cooler fabricated with a particulate cooler holder and the IFC Type A thermal caulk was tested in the full-scale heat transfer rig. Testing was initially conducted at 40 psi axial load to simulate initial stack conditions. Three thermal cycles from 350 to 150°F were conducted during this segment of the test. Axial load was reduced to 10 psi, to evaluate the influence of lower axial loads, and seven thermal cycles were conducted.

Cooler thermal resistance was calculated to be about 40 percent lower than a cooler with a baseline fiber holder. No change in thermal resistance due to the thermal cycles or the reduction in axial load was observed during the test period. These results are shown in Figure 2.2–5.

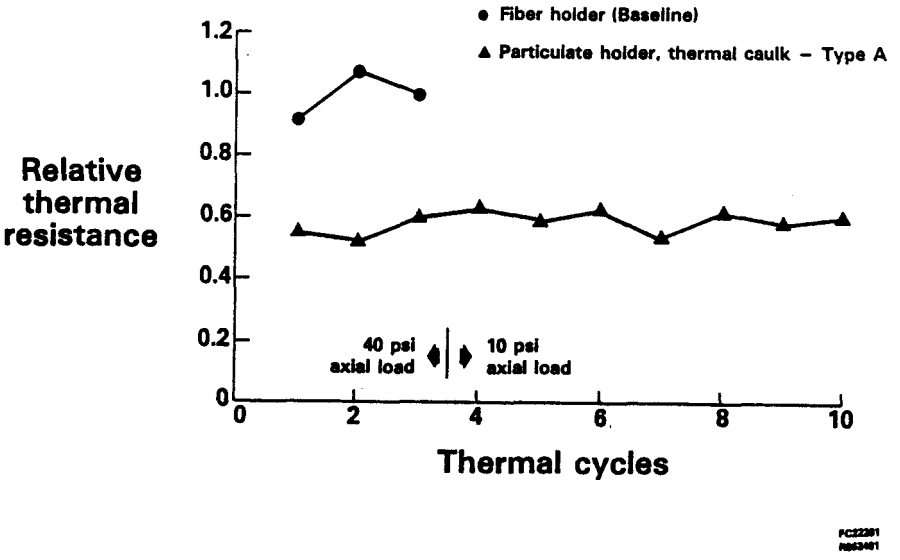

Figure 2.2–5. *Thermal Resistance Comparison of Full–Size Coolers*

Erosion-Corrosion Tests

The heat transfer rig was redesigned to evaluate cooler erosion and corrosion issues associated with changes in coolant system operating conditions. The two key changes were (1) the increase in water/steam velocity in serpentine coolers and (2) the increase in dissolved oxygen in the water loop.

Major changes to the rig consisted of increasing the power density of the heaters to increase the heat flux to the coolers, increasing the coolant flow, addition of a feedwater system that will allow the dissolved O_2 level to be controlled, and the addition of ion–exchange beds that will allow pH to be controlled. A schematic of the test stand is shown in Figure 2.2–6.

In the first build of the erosion-corrosion rig, a stainless steel serpentine cooler and a stainless steel inlet manifold were tested for 3144 hours to evaluate erosion-corrosion under a high coolant oxygen level. The coolant oxygen content was in the range of 400-600 PPB during the first 1900 hours and then decreased to 30-40 PPB over the last 1200 hours. The test conditions and coolant properties are shown in Table 2.2–3. No significant changes in pressure drop or thermal profile occurred during the 3144 hours of testing (Figures 2.2–7 through 2.2–9).

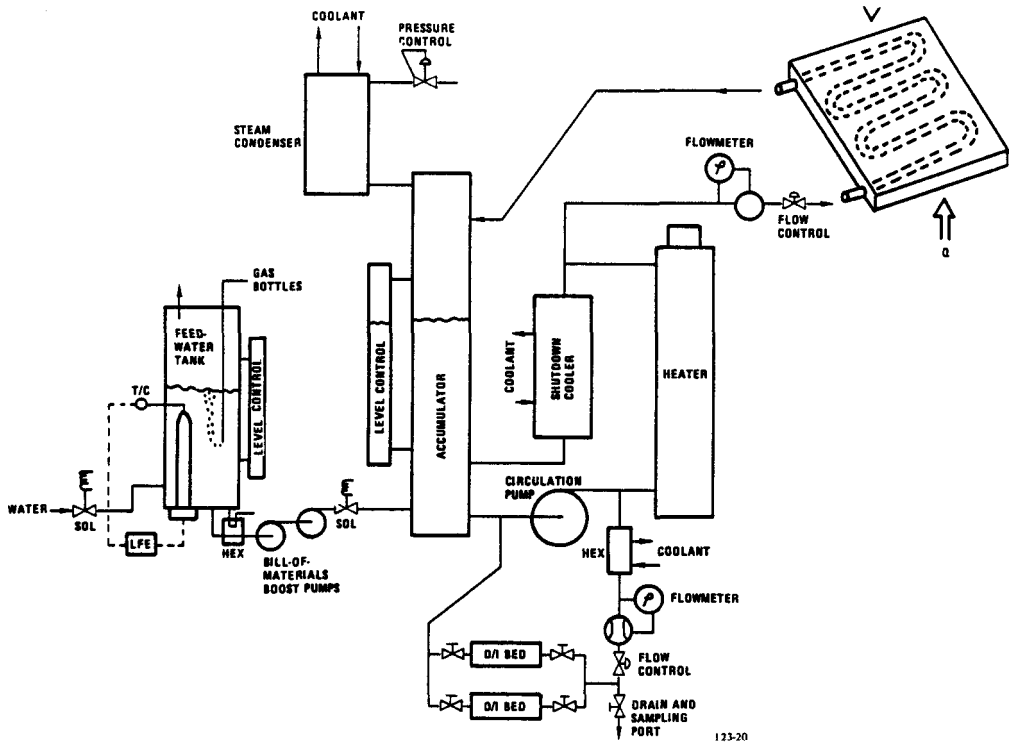

Figure 2.2–6. *Schematic For Erosion–Corrosion Tests*

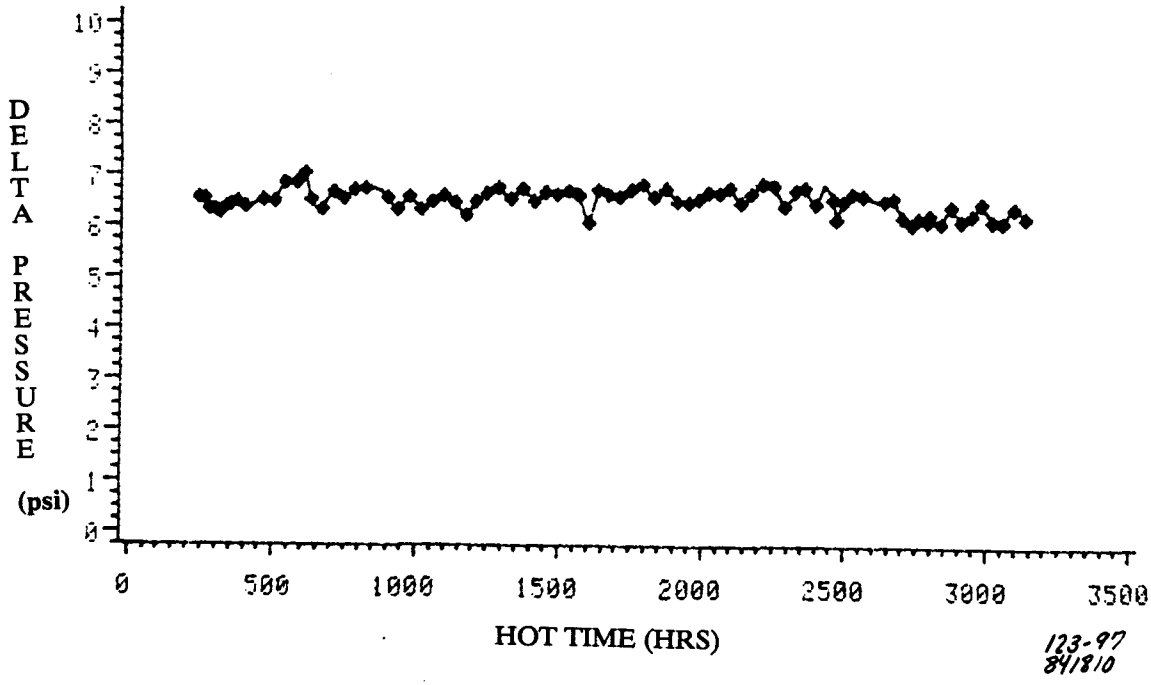

Figure 2.2–7. *Erosion–Corrosion Rig Pressure Drop History for Build 1*

Table 2.2-3. Erosion-Corrosion Rig - Build 1

Test Conditions	Time Averaged Values: Beginning of Test 25 - 50 Hours	Time Averaged Values: 3038 - 3061 Hours
Coolant Flow Rate, pph	165	165
Coolant - Inlet Temperature, °F	338	343
- Inlet Pressure, psig	128.6	126.5
- Delta P Across Cooler, PSID	6.7	6.2
Heat Input to Cooler, Watts	5940	5730

	270 Hours	1321 Hours	1935 - 2111 Hours	2498 Hours	2978 - 2999 Hours
Coolant Properties					
Oxygen Content (PPB)	600	400	40	30	30
pH	8.15	-	7.8	7.99	7.6
Conductivity (umho)	1.3	0.85	0.38	0.7	0.45
Turbidity (NTU)	0.5	-	0.25	3.1	3.3

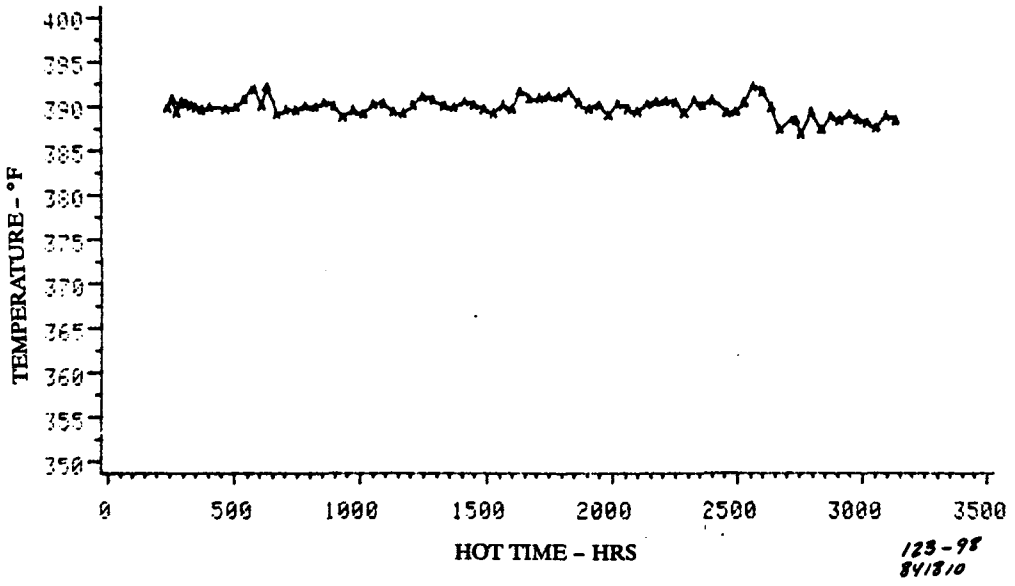

Figure 2.2–8. *Erosion–Corrosion Rig Temperature History For Bottom Cooler In Build 1*

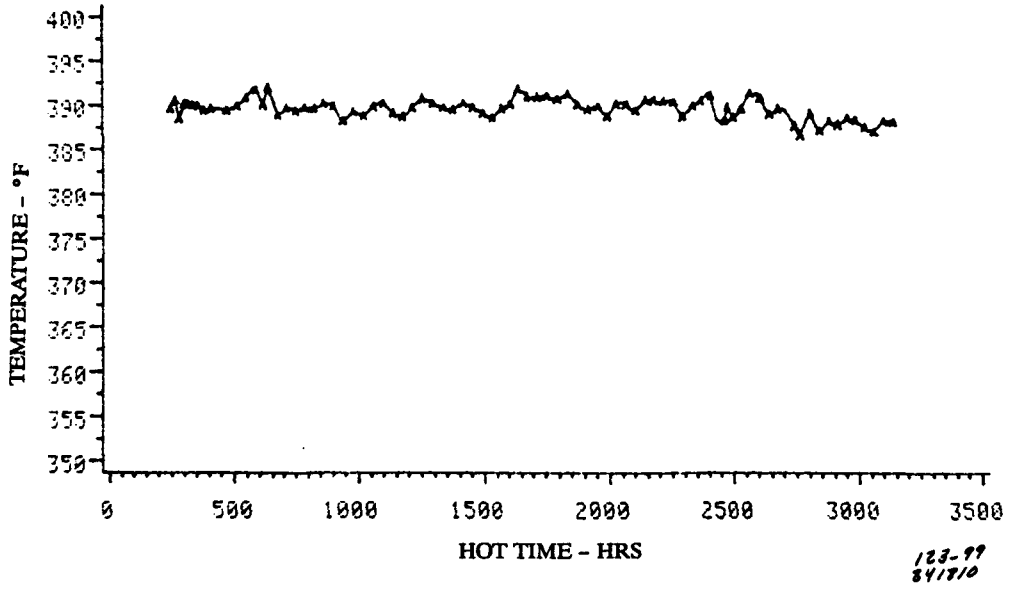

Figure 2.2–9. *Erosion–Corrosion Rig Temperature History for Top Cooler In Build 1*

The stainless steel serpentine cooler array was removed from the cooler assembly for the post-test evaluation. Radiographs showed no significant change in wall thickness of the array. Metallographic cross sections showed the wall thickness to be unchanged from the inlet to exit of the array. These results indicate no measurable erosion-corrosion occurred during this test.

A metallographic cross section of the inlet tube on the manifold showed there was no significant change in the diameter and no measurable corrosion at the tip of the tube. A deposit (average thickness of about 0.001 inch) was present on the wall of the tube. Elemental analysis showed the material to be primarily copper and iron. The source of the copper is components in the feedwater treatment module and the coolant cart.

In the second build of the erosion-corrosion rig a stainless steel serpentine cooler and a stainless steel inlet manifold were tested for 6070 hours to evaluate the erosion-corrosion under a low coolant oxygen level. The test conditions and coolant properties are shown in Table 2.2–4. There was no significant change in pressure drop or thermal profile of the cooler since the 1600-hour point when the heat input was adjusted to increase the steam exit velocity to the desired level, as shown by the data in Figures 2.2–10 through 2.2–12.

The cooler array and coolant inlet manifold were subjected to post-test evaluation. A radiograph of the cooler array showed no significant differences in tube wall thickness throughout the array. Metallographic cross sections showed the wall thickness to be unchanged from the inlet to exit of the array. These results indicate no measurable erosion-corrosion occurred during this test.

A metallographic cross section of the stainless steel inlet tube on the manifold showed no measurable corrosion at the electrically positive tip of the tube. A deposit with a maximum thickness of approximately 25 mils was present on the inside wall of the inlet tube near the tip. The deposit was analyzed by x-ray diffraction and identified to be iron oxide in the form Fe_2O_3.

In the third build of the erosion-corrosion rig, a cooler array fabricated from lower cost stainless steel tubing was tested. This tubing reduces the cost of the serpentine array by 40-50 percent. About 3,500 hours of testing were accumulated. Test conditions and coolant properties are shown in Table 2.2–5.

Table 2.2–4. Erosion – Corrosion Rig – Build 2

Test Conditions	91–115 Hours	1121–1145 Hours	1754–1777 Hours	3070–3094 Hours	4342–4366 Hours	6039–6063 Hours
Coolant Flow Rate, PPH	165	165	165	165	165	165
Coolant – Inlet Temperature, ° F	342	340	348	348	349	348
– Inlet Pressure, PSIG	122.6	125.2	128.9	129.8	129.4	130.0
– P Across Cooler, PSID	5.4	4.5	5.8	5.7	5.9	5.8
Heat Input to Cooler, Watts	5288	5084	5552	5543	5566	5470
Coolant Properties	**605 Hours**	**1064 Hours**	**1414 Hours**	**2770 Hours**	**4255 Hours**	**6050 Hours**
Oxygen Content (PPB)	60	30	30	40	40	40
pH	7.6	7.6	7.0	7.2	7.7	7.5
Conductivity (umho)	0.25	0.61	0.44	0.33	0.32	0.45
Turbidity (NTU)	6.3	6.3	3.1	3.1	0.8	–

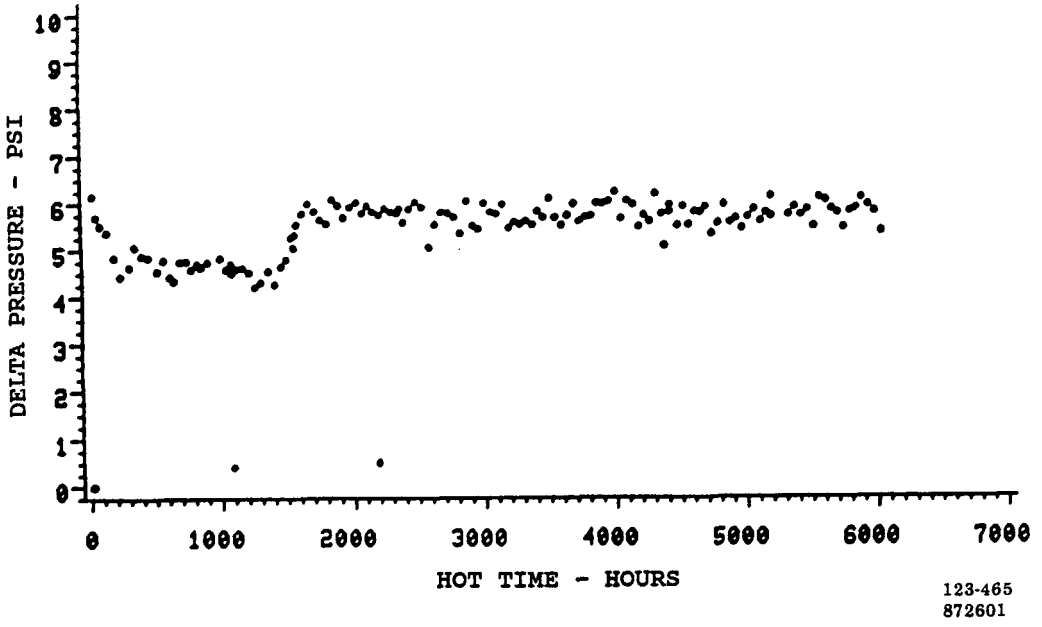

Figure 2.2–10. *Erosion–Corrosion Rig Pressure Drop History for Build 2*

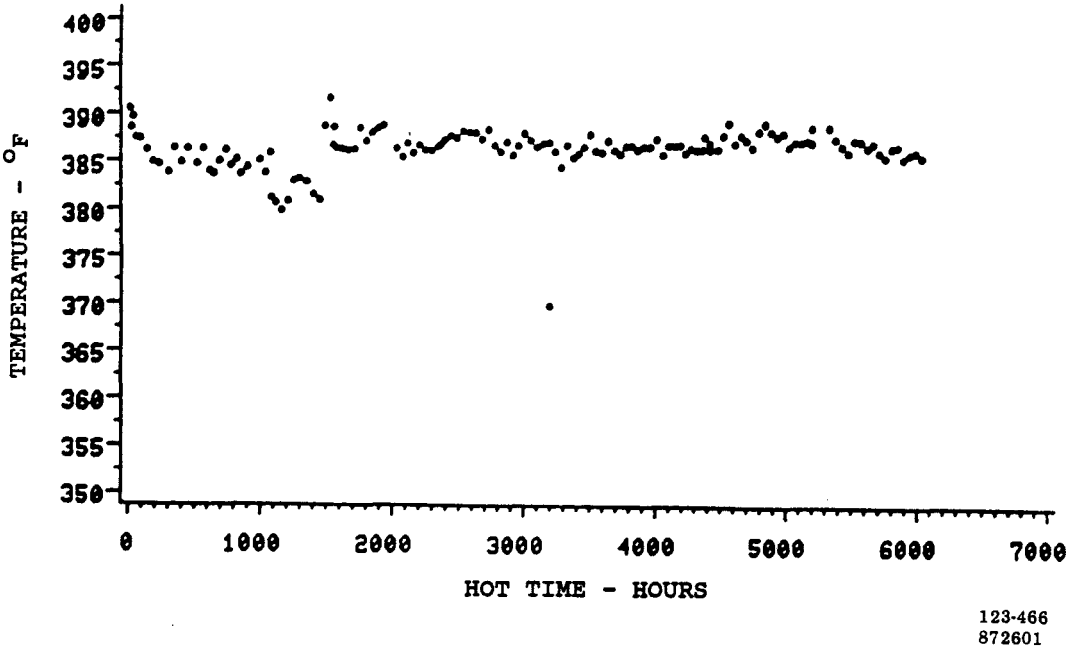

Figure 2.2–11. *Erosion–Corrosion Rig Temperature History for Bottom Cooler In Build 2*

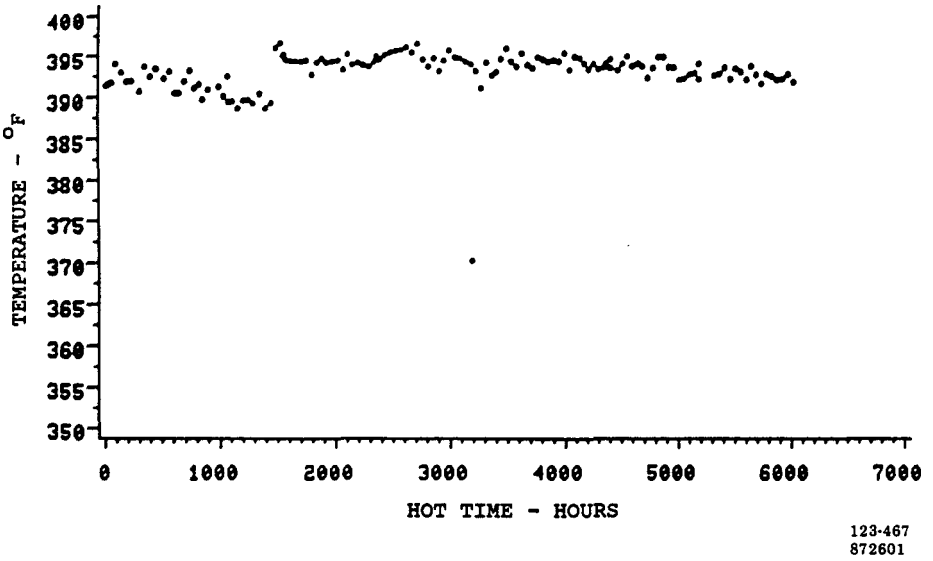

Figure 2.2–12. *Erosion–Corrosion Rig Temperature History for Top Cooler In Build 2*

Table 2.2–5. Erosion-Corrosion Rig – Build 3

Test Conditions	453-477 Hours	813-837 Hours	1351-1375 Hours	2461-2485 Hours	2461-2485 Hours
Coolant Flow Rate, PPH	165	165	165	165	165
Coolant					
– Inlet Temperature, °F	348	347	346	347	350
– Inlet Pressure, PSIG	132	132	131	131	136
– ΔP Across Cooler, PSID	7.0	7.0	7.0	7.2	6.9
Heat Input to Cooler, Watts	6606	6661	6517	6572	6493
Coolant Properties	**310 Hours**	**928 Hours**	**1696 Hours**	**2415 Hours**	**3193 Hours**
Oxygen Content (PPB)	30	35	20	25	20
pH	6.6	6.4	7.5	6.4	8.2
Conductivity (μmho)	0.43	0.35	0.38	0.43	0.40
Turbidity (NTU)	2.6	1.0	1.0	1.2	0.9

Fabrication of Encapsulated Cooler Assemblies

Cooler assemblies were fabricated for the 30-cell stack testing in Subtask 2.4. The assemblies contained a 3/8-inch single-element bare copper serpentine cooler array and a totally encapsulated cooler holder configuration. The design was developed under the GRI On-Site Technology Development Program.

The completely encapsulated cooler assemblies for the 30-cell stack were characterized. The measured iR across the cooler assemblies averaged 13 mV at 100 ASF, or to 1.3 mV/cell at 10 cells per cooler. A gas leak check was made on each cooler assembly to check for leaks at the cooler tube penetrations between the bonded halves of the cooler holder. No leaks were observed. Application of an aggravated 100 psi axial load did not initiate cracks in the sections of the plate associated with the tube bend gaps.

Post-Test Evaluation of Encapsulated Coolers

Encapsulated coolers from the first and second On-Site short stacks were evaluated. One cooler in the first short stack was tested for 5200 hours and the other two for 7125 hours. The

coolers were disassembled to determine the condition of the copper cooler arrays. There was no acid corrosion of the copper arrays and no acid present in the holders.

Five coolers with stainless steel arrays were tested for 5051 hours in the second short stack. Examination of the disassembled coolers showed no acid corrosion of the arrays and no acid in the holders. These results verify the encapsulation concept was effective in preventing acid penetration.

Cooler arrays from the first and second short stacks were examined metallographically for erosion-corrosion. Cross sections showed that tube wall thickness was unchanged from the inlet to exit of the array. This indicates no significant erosion-corrosion occurred in either the copper or the stainless steel arrays.

Dielectric Coolant Hoses

The coolers are connected to a coolant manifold with a dielectric hose to prevent electrical shorting. The serpentine cooler requires a thick wall Teflon® hose with about a 3/8-inch O.D. and a 0.150-inch wall thickness. Tests were run to establish short-term and long-term burst characteristics of this hose. Initial trials to clamp this hose to the cooler nipples were successful and showed no leakage at 600 psi and room temperature. No leakage was measured after 15 thermal cycles from 70°F to 425°F. Room temperature burst pressure is 1100-1200 psi, which translates to a 400-450 psi burst pressure at 400°F.

Short-term burst pressure data was generated as a function of temperature. See Table 2.2–6. Burst pressures above 250 psig are adequate for 200-kW operation.

Table 2.2–6. Short–Term Burst Pressure of Thick Wall Teflon Hoses

No. of Samples	Temperature, °F	Burst pressure, psi
1	375	500
1	375	490
2	400	460
1	425	420

A test program was conducted to characterize the long-term burst strength of thick wall Teflon® hoses. Testing was conducted at temperatures of 350, 375, and 400°F. The hoses were 3/8-inch diameter Teflon® with a 0.150 inch wall thickness. The tests were conducted using the procedure in ASTM-D-2837 for evaluating thermoplastic hose material. Testing was conducted under subcontract by a testing laboratory familiar with this procedure.

The hoses that were tested at 350°F and 375°F reached the planned 10,000 hours. None of the 400°F hoses reached 10,000 hours because of an accidental overtemperature. This affected eight hoses that had reached 6300 to 7300 hours at the time of the overtemperature.

The failed hoses from the 10,000 hour test program were categorized with respect to type of failure. The types of failure include leakage between the clamped hose and tube, short axial splits and 1/8-inch long, and burst failures that resulted in axial splitting. Table 2.2–7 shows the breakdown of these failures for each test temperature.

Table 2.2–7. Failure Summary for Teflon ® Dielectric Hoses

Type of Failure	350°F	375°F	400°F
Leakage at Clamp	6	2	0
Short Axial Split	3	7	7
Burst – Axial Split	10	13	15
(Non-Failures)	6	11	8*

***Testing discontinued because of overtemperature**

Failures caused by leakage between the hose and tube were due to surface oxidation of the copper tubes. Cooler tube material was changed from copper to stainless steel during this program; therefore, the oxidation problem is limited to this test program.

Hoses that failed because of short axial splits were analyzed by the supplier. The results indicate these failures are caused by foreign material inclusions or processing defects. Approximately 80 percent of burst and short axial split failures initiated or occurred near the end of the hose. This is attributed to reduced wall thickness at the ends. The hoses were drilled out at the ends to increase the inside diameter slightly to match the size of the tube.

The balance of the hoses failed by bursting, which is the expected failure mechanism. A statistical analysis was conducted to determine the maximum acceptable operating temperature of the hoses for a 40,000-hour power plant life. These results, shown in Table 2.2–8, were determined from log-log regression analyses. It is concluded that the hose configuration tested is acceptable for use up to 350°F. Since normal 200-kW operating temperatures range up to 375°F, an activity was initiated to evaluate hose configurations with higher pressure capability.

Table 2.2-8. Statistical Analysis of Thick Wall Teflon® Dielectric Hoses

Temperature	100,000 Hour Pressure (1)	100,000 Hour Lower Confidence Level (LCL) (2)	LCL Ratio (3)	Probability of Failure in 40 k Hours
350°F	327.3 psig	275.9 psig	0.843	0.035% (at 120 psig)
375°F	256.8 psig	178.8 psig	0.696	0.91% (at 169 psig)
400°F	210.7 psig	150.8 psig	0.716	44.1% (at 232 psig)

Note: (1) Pressure at which 50% of samples fail in 100,000 hour.
(2) Pressure at which 2.5% of samples fail in 100,000 hours.
(3) LCL/100,000 hour pressure (0.85 is required).

Thin-walled Teflon® hoses with fiberglass braid reinforcement were tested because these hoses were expected to have higher pressure capability and to cost less than the thick wall Teflon® hose.

Initial testing showed that the connector clamp design used on the thick walled Teflon® hose was not adequate for the reinforced of thin wall Teflon® hose. Four 7/16-inch diameter reinforced hoses were tested at 300 psi and 375°F. After 75 hours of testing, one of the samples experienced failure at the connector clamp. This indicated that a new clamp design was required, and the supplier of the reinforced hose developed a replacement swaged clamp connector.

Burst testing showed that the initial pressure capability of the fiberglass reinforced thin-walled Teflon hose with swaged connector clamps was about 2000 psi at 400°F. This is at least four times higher than the thick-walled Teflon hose. A group of eight hoses was then tested at 500-700 psi and 400°F to determine endurance capability at this pressure, which represents two to three times coolant system design pressure. All eight of the hoses failed within 800 hours. The failures were attributed to pressure cycling that causes abrasion of the fiberglass braid and not the swaged connector clamp.

Activity was initiated to evaluate a woven stainless steel reinforcement as an alternative to fiberglass reinforcement. Stainless steel reinforced hose has a high burst strength (8,000-9,000 psi), has the ability to withstand pressure cycling, and is comparable in cost to

fiberglass reinforced hose. The stainless steel reinforced hose assembly requires a design modification to provide the dielectric protection intrinsic to the fiberglass reinforcement. The coolant hose supplier provided twelve cooler hose assemblies with two versions of swaged connector for short-term endurance testing. The hoses were aged at 420°F and pressure levels of 500 and 1000 psig. Burst strength was measured after approximately 200, 400, 800, and 1600 hours of aging. Two hoses with the basic swaged connector failed during the aging process. Test results are shown in Table 2.2–9. The results show that hoses with a basic swaged connector have burst pressures in the 1000-2000 psi range while hoses with a modified swaged connector have burst pressure in the 3000-6000 psi range. This is over 10 times the coolant loop design pressure. Based on this testing, stainless steel hoses with the modified swaged connector was selected for use on the GRI short stack, the third short stack in this program, and the full-height stack used in the Verification Test Article (VTA). The hoses performed successfully in the short stacks and the VTA stack.

Table 2.2–9. Testing of Stainless Steel Reinforced Teflon ® Hose

		Burst Pressure at 420 °F (psi)			
		Basic Swaged Connector		Modified Swaged Connector	
Aging Time (Hours)	Aging Temperature (°F)	500 psi Aging	1000 psi Aging	500 psi Aging	1000 psi Aging
184	420	1500 1700	1900 1900	4800 3300	3200 4700
416	420	1800 1800	1400 1800	3400 3200	6000 4600
848	420	1100 1200	1600 *	4500 2800	4300 3000
1649	420	1900 *	1800 1750	4800 5000	3200 5100

*Failed during aging

Subtask 2.3 – Non-Repeat Component Technology

OBJECTIVES

The objective of this task was to reduce fabrication cost and improve durability by improving non-repeat component technologies.

SUMMARY

Special emphasis was directed toward improving reactant manifold integrity. An improved manifold retention approach using standard, commercially–available hardware was defined. A flow test simulator was constructed and procedures developed to ensure uniform flow distribution to the cell stack, and to evaluate alternative plumbing arrangements. Extensive testing was conducted to determine manifold coating delamination causes and to establish test procedures to evaluate improved coatings. A new, lower cost PFA coating system with excellent adhesion characteristics was identified through these efforts.

Alternative techniques were evaluated for fabricating the reactant and coolant manifolds. Trials to form a full-scale reactant manifold made entirely from glass-reinforced plastic were continued and a mold formed. Laser welding of coolant flow nozzles to the main coolant manifold pipe assemblies was evaluated.

Efforts in the areas of materials development resulted in producing a family of corrosion resistant fluoroelastomers for sealing, adhesion, and component protection applications. A low-cost substitute for nickel plating electrical take-off hardware was also developed.

Three acid refill concepts identified in a complementary GRI program were evaluated using quarter-scale mockups: drip wicking, acid injection, and spray. The spray approach was selected for scale-up after it was judged to be fastest and most reliable. Refill of a 40-kW stack containing 270-cells was successfully completed in one hour. A portable acid spray cart was fabricated and used to refill a second 40-kW stack. The acid spray approach was also used to refill a short stack from subtask 2.4 after 6100–hours of operation, and performance was essentially unchanged as a result of the refill.

ACCOMPLISHMENTS/CONCLUSIONS

- Defined and tested an improved manifold retention system.
- Uniform flow distribution in manifolds was verified using a test simulator.
- Established new test procedure to evaluate manifold coating adhesion at stress conditions.
- Identified a new and lower cost PFA coating system with unique stability at stress conditions.

- Fabricated tooling to mold full-size reactant manifolds from glass-reinforced PPS.
- Developed commercially available nickel power based ceramic coating to replace higher cost nickel plating.
- Hardware was defined and constructed for a portable acid refill system.
- Two 40-kW stacks and a short stack from Subtask 2.4 were successfully refilled with acid.

DISCUSSION

Manifold Retention to Cell Stack

A cell stack structural mockup was constructed to establish installation procedures and to check the fit of the reactant manifolds and retention hardware.

Figure 2.3-1 shows the structural mockup with the manifolds installed and loaded. The procedures required to install the manifolds and apply the sealing load were straightforward, and the fit was good. Several washers were employed for seal load follow-up, and the strap and tee-bolt dimensions were increased for better stability and ease of assembly.

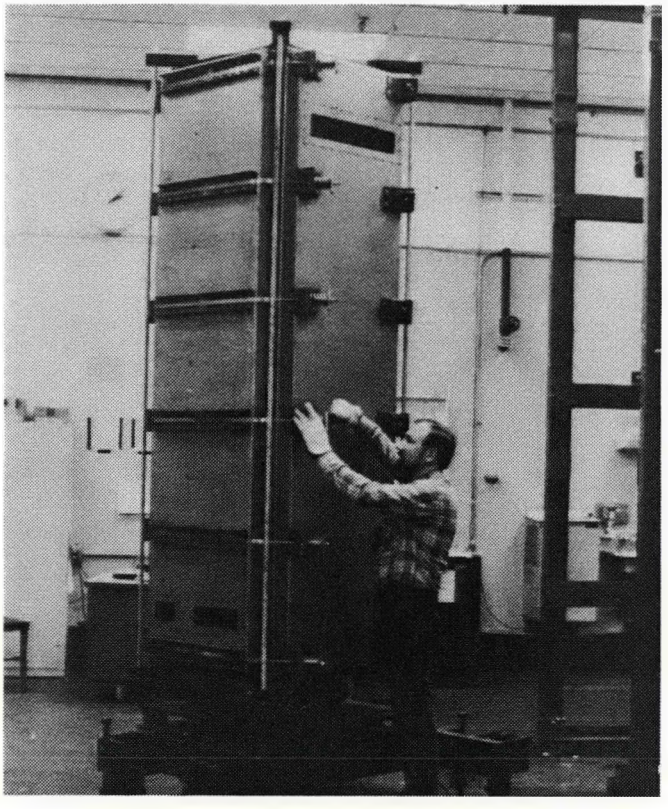

(WCN-13281)

Figure 2.3-1. *Full-Size Reactant Manifolds and Retention Hardware Installed on Mockup*

An alternative approach to manifold retention was also defined, and prototype hardware was fabricated for evaluation. This approach used commercially available springs and standard packaging bands. The mechanical feasibility of this approach was demonstrated on a short stack mockup. Structural analysis indicated that the approach would be acceptable with additional straps to carry the shipping loads, and additional follow-up springs located to eliminate friction as a factor in determining seal loading.

Reactant Flow Distribution

A test rig was constructed to evaluate reactant manifold design concepts and to ensure uniform flow distribution to all cells. Tests were conducted to validate general manifold sizing and to evaluate alternative nozzle configurations and baffling arrangements.

The test rig consists of a blower, flow metering equipment, flow straighteners, a stack simulator, and the test manifold. The setup is shown schematically in Figure 2.3–2. The key item is the stack simulator, formed by dividing the flow field into adjoining compartments. Stack pressure drops were simulated by covering the compartments with permeable cloth. A pitot tube inserted into the compartment exhaust opening was used to measure local flows for comparative analysis. The compartments can be seen in Figure 2.3–3.

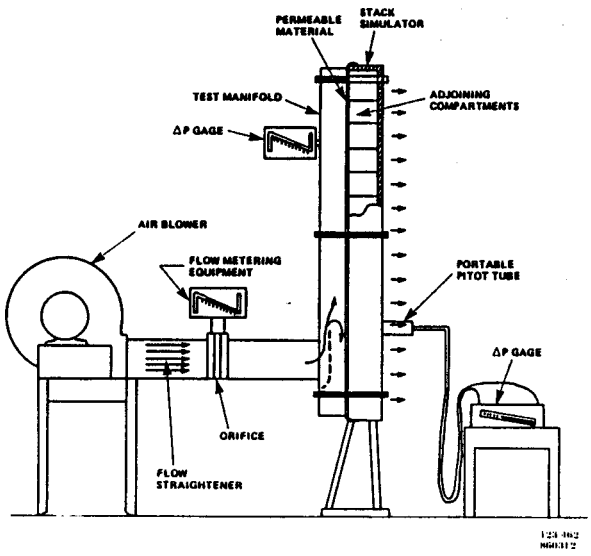

Figure 2.3–2. *Setup for Reactant Flow Distribution Tests*

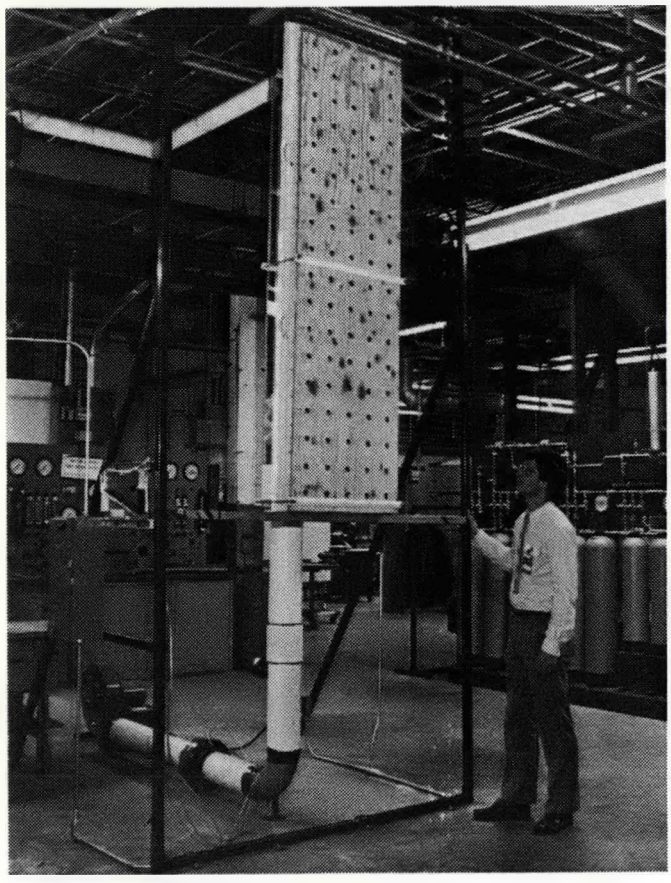

(WCN-15572-33)

Figure 2.3–3. *Reactant Flow Distribution Testing*

The compartmentalized stack simulator was calibrated by measuring the flow through each chamber at a constant pressure drop. The results indicated a considerable flow variation from edge to center due to variations in covering cloth permeability. The stack simulator was recalibrated by adding cloth layers until the flow through each compartment was nominally the same at the selected supply pressure. The results were a considerable improvement, and the calibration was judged satisfactory for preliminary testing. The calibration results are shown in Figure 2.3–4.

The initial test series evaluated alternative air inlet arrangements. Circular air inlet piping was tested first. There was some scatter in the data, as shown in Figure 2.3–5, but there did not appear to be any systematic flow maldistribution. The simulated stack pressure drop was reduced from 1.8 to 1.3 times the design value by removing 2 of the 6 layers of cloth from each compartment. Overall flow distribution was not affected. Flow at the bottom of the manifold was slightly lower than the norm in both tests. To correct this, the internal baffle was relocated closer to the manifold wall in a series of steps. Figure 2.3–6 compares results obtained at the original and optimum baffle locations.

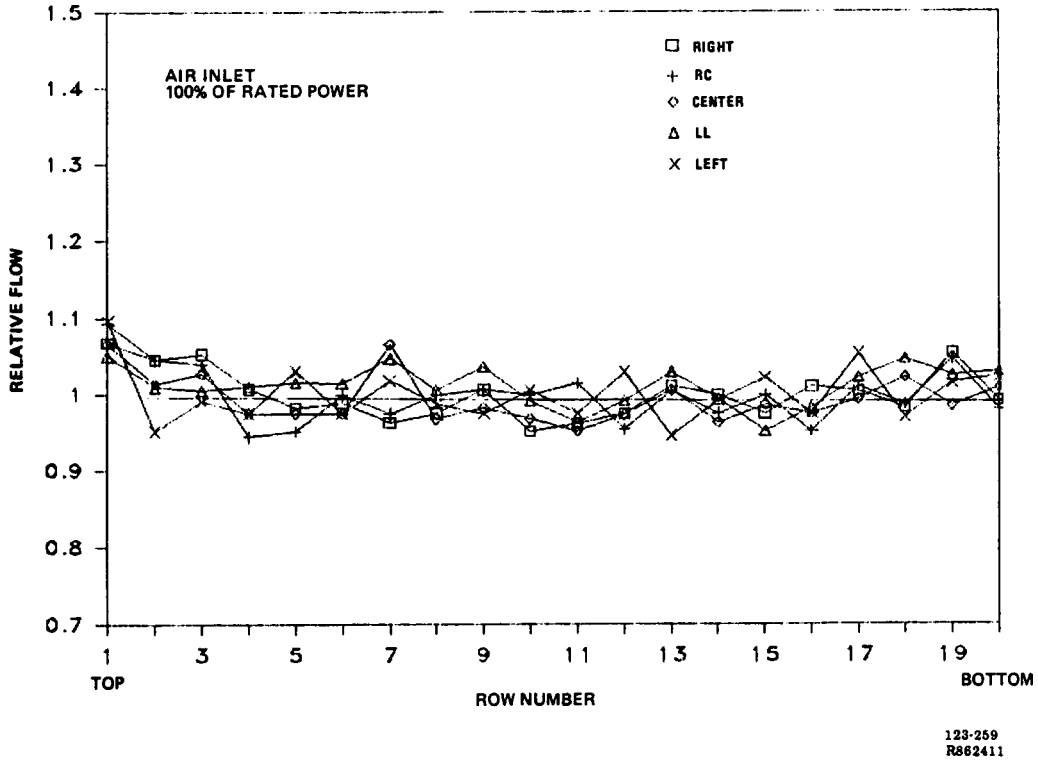

Figure 2.3–4. *Reactant Flow Distribution Calibration Results*

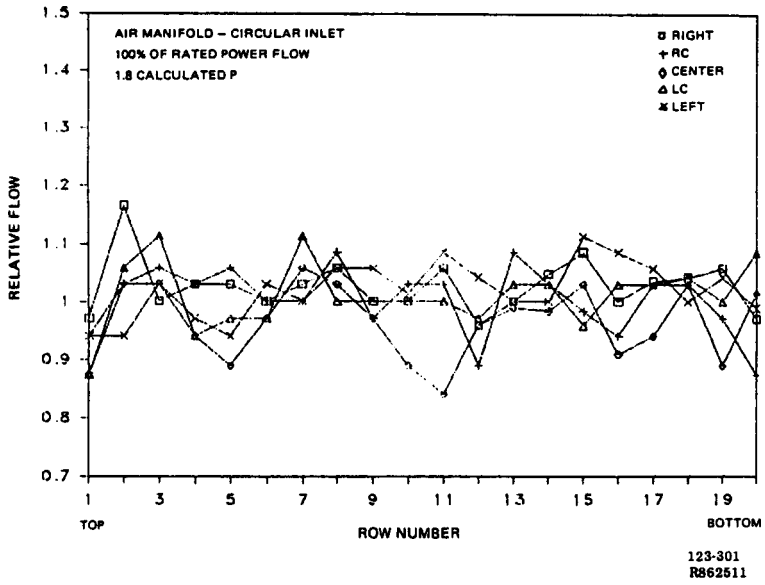

Figure 2.3–5. *Initial Air Flow Distribution Results*

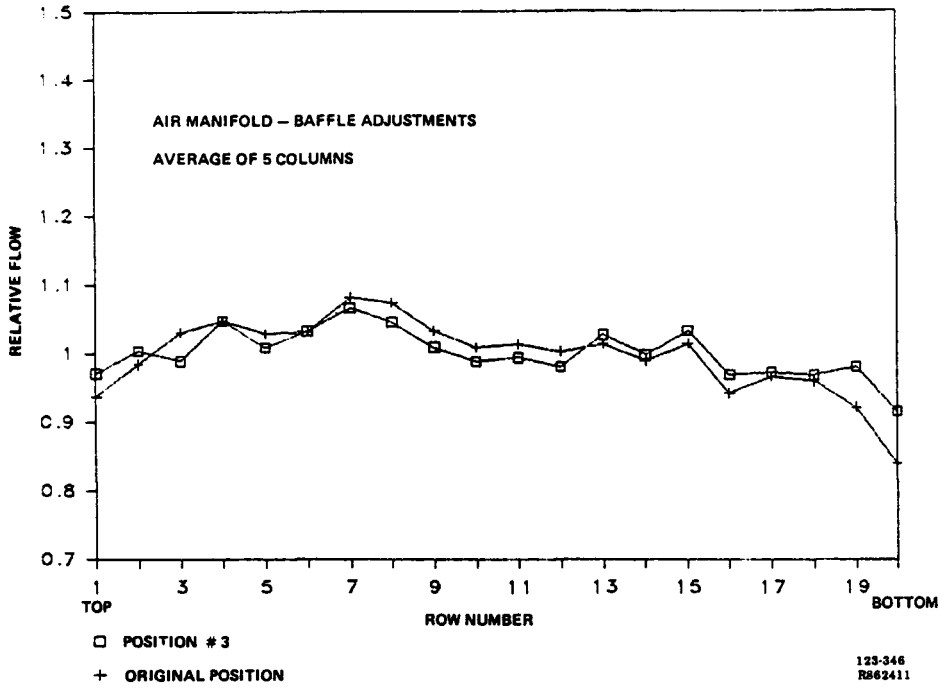

Figure 2.3–6. *Comparison of Air Flow Distribution Results Before and After Baffle Adjustment*

A new type of stack simulator cloth covering was evaluated prior to initiating fuel manifold flow tests. The cloth is offered in a series of weights with flow and pressure drop characteristics similar to power plant fuel and air flows. The cloth is manufactured for commercial applications requiring uniform flow characteristics over broad areas, the basic requirement of the stack simulator. The stack simulator was recovered with a single layer of the new cloth selected to match power plant rated fuel flow conditions and calibrated. The results were a significant improvement, and greatly simplify installation and calibration.

Testing of the fuel inlet manifold were performed on the flow distribution rig. Figure 2.3–7 shows the flow distribution data for rated flow. Except for the middle of the bottom row, the data is within the desired $\pm$ 10 percent. Modifications to the baffle were made to remedy this local maldistribution.

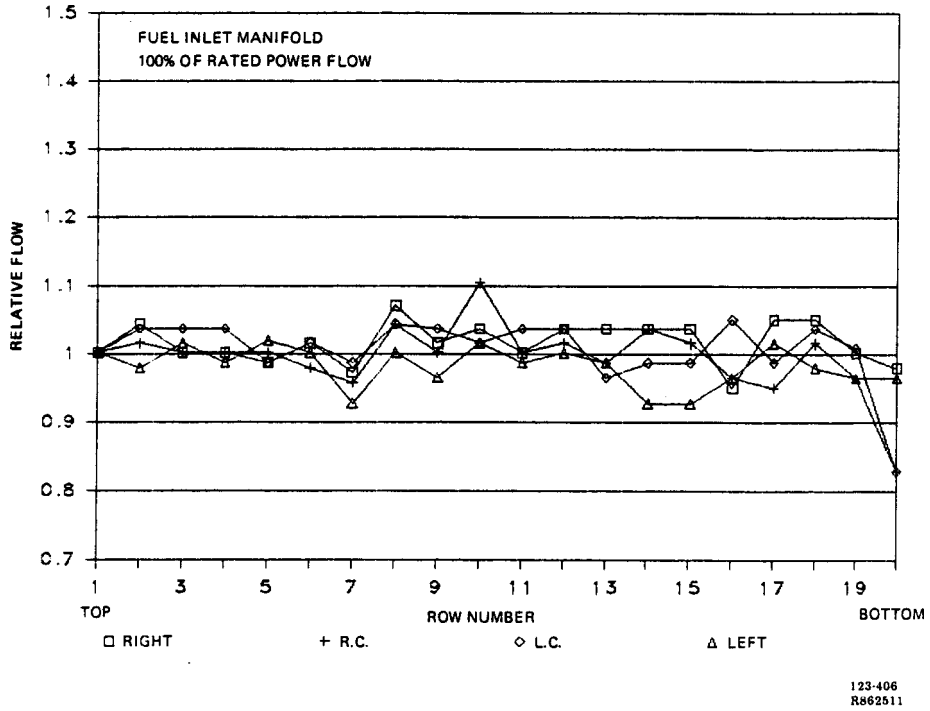

Figure 2.3–7. *Fuel Flow Distribution Results*

Reactant Manifold Coatings

The manifold coating effort progressed in three stages. In the first stage, vendor-coated corner and strip samples were screened to evaluate materials and processes. In the second stage, short stack manifolds were coated to evaluate vendor application technique and to test promising candidates at power plant operating conditions. In the third stage, coating systems warranting additional scale-up were applied to full-size manifolds to evaluate vendor production techniques.

Strip samples and short stack manifold coatings were tested by subjecting the coating to steam at low temperature. The coating system that could resist loss in peel strength and delamination under this screening procedure was unique. The first samples received were in the form of corner and strip samples. All samples showed well adhering, uniformly thick coatings without flaws. Peel strength was not exceptional but did not substantially change after being subjected to saturated steam. Short stack and full-height stack manifolds were coated with similar results in good workmanship: the coatings were flawless and uniformly thick. The stack manifolds all successfully passed 500 volt wet-spark and steam screening tests. The coating system was employed in all sensitive locations in the full-height power section and was recommended for other components requiring acid protective coatings.

Reinforced Plastic Reactant Manifold

A reinforced plastic manifold improvement effort was conducted. The manufacturer of the high temperature PPS resin developed the capacity to produce prepreg (resin-impregnated fiberglass cloth) of sufficient width for fabrication of a full-size manifold. The manifold design was modified to include provisions for an acid drain and instrumentation and was reviewed with a manufacturer. Orders were placed for molding materials and the required mold. The initial resin manufactured was unsatisfactory and was replaced.

Post-test examination of the reinforced plastic manifold that ran for 1897 hours on the first 30-cell NASA short stack did not reveal any corrosive attack to the PPS or glass reinforcement. Reduced flexural strength was measured in the areas of greatest acid concentration and was attributed to mechanical damage of the composite in these areas during installation of reactant exit and drain fitting. A program was started to determine the flexural strength of the reinforced plastic material as a function of time and temperature. Initial results indicated there is a 20-25 percent difference in the flexural strength, as measured parallel and perpendicular to the direction of the fiberglass reinforcement.

Tests to evaluate the flexural strength and creep of the molded PPS/fiberglass material, as a function of time and temperature, were conducted. Figures 2.3–8 and 2.3–9 show the flexural data to 5000 hours. Flexural creep data has also been obtained at 400°F on two samples stressed at 1200 psi in a three-point flexural configuration. See Table 2.3–1. Permanent set is the deflection from the horizontal, measured at room temperature with no load.

Table 2.3-1. Flexural Creep Data (Two Samples at 400°F at 1200 psi)

Time (hours)	Permanent Set (inches)	
	#1	#2
600	0.040	0.030
1100	0.045	0.035
2130	0.075	0.060

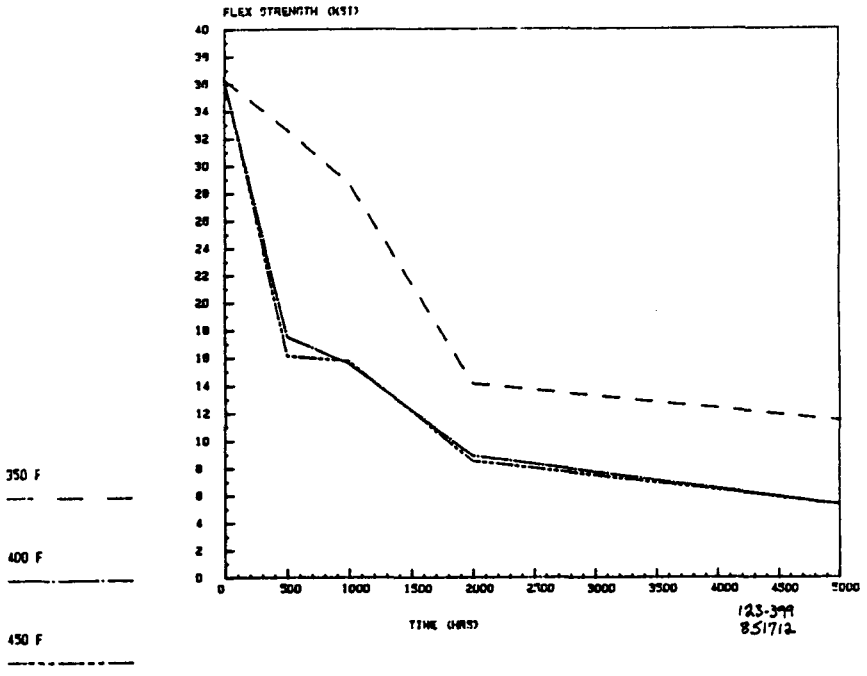

Figure 2.3–8. *Room Temperature Flexural Strength of PPS/Fiberglass After Aging At Temperature*

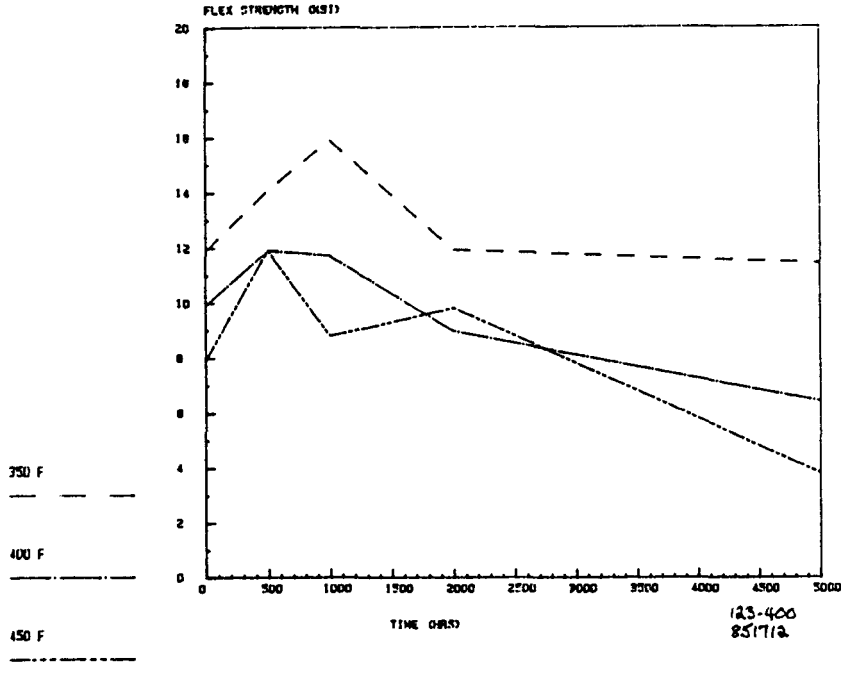

Figure 2.3–9. *Flexural Strength of PPS/Fiberglass Measured at Temperature*

The dividers for two manifolds in the GRI Short Stack were fabricated from bulk injection molded PPS. The flexural requirements and corrosion resistance requirements for this application are much less severe than the formed shell. No detectable corrosion or other defects were noted during post-test analysis. Figure 2.3–10 shows a divider installed on the fuel inlet manifold.

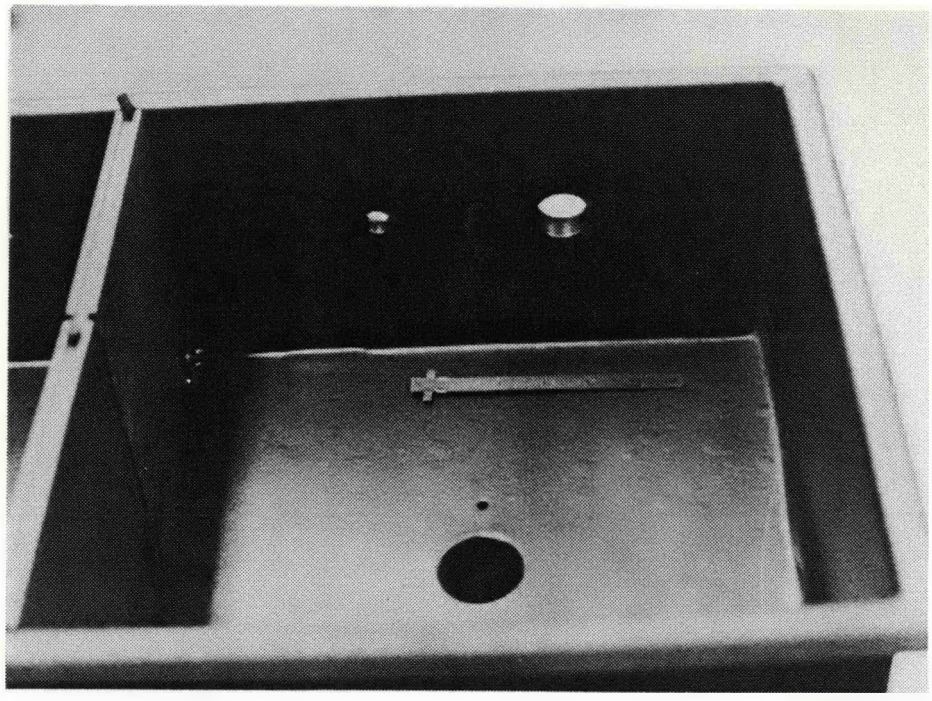

(WCN-13799)

Figure 2.3–10. *Manifold Divider For Short Stack*

Coolant Manifold Nozzle Attachments

Alternative methods of attaching nozzles to the coolant manifold were evaluated. Conventional welding techniques are effective but are also expensive and tend to distort the manifold.

Several laser welding vendors were supplied materials for trials to determine power requirements and other weld parameters. Several approaches were attempted based on equipment flexibility and fixturing capacity. The approach, shown in Figure 2.3–11, was successful on a trial basis.

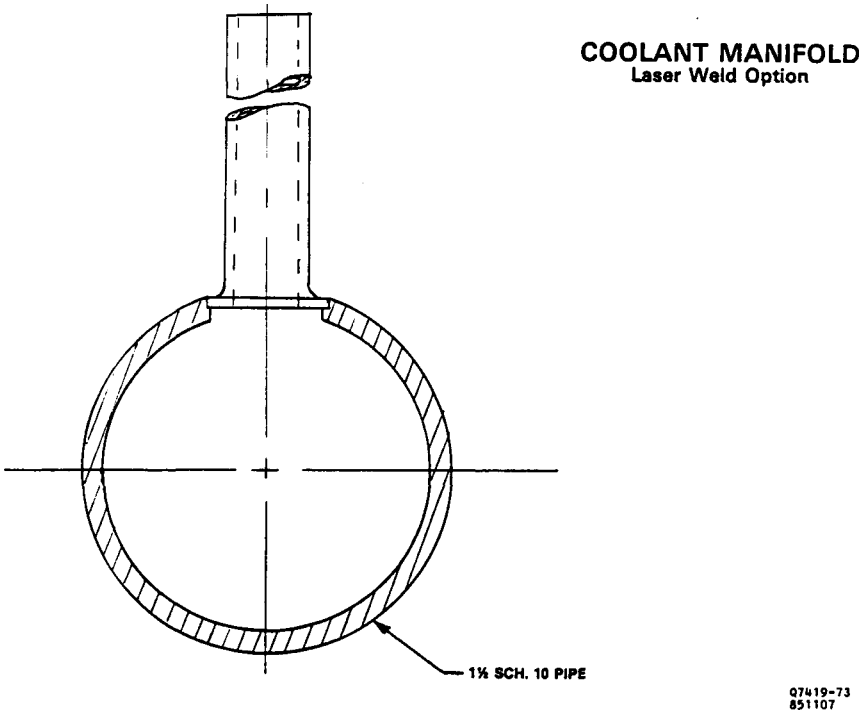

Figure 2.3–11. *Laser Welding Option For Coolant Manifold*

Nickel Plating Replacement

To eliminate the expense involved in nickel plating the pressure plates, alternative methods of maintaining adequate electrical contact were considered. The most attractive method replaces the nickel plate with a commercially–available, nickel powder based ceramic coating. Tests were started to evaluate the long-term stability of the material that is temperature rated far above the 400°F requirement. Carbon steel plates were coated on both sides and sandwiched between fuel cell substrates for conductivity measurements. Four coated samples were evaluated for over 2600–hours. Figure 2.3–12 shows the voltage drop measurements. The values are stabilizing at an acceptable rate. The measured electrical drop shown is the total for coated surfaces at 100 ASF. The impact of one coated surface at the nominal power plant rated load of 200 ASF is essentially the same as two coated surfaces at 100 ASF.

The nickel powder based coating was also evaluated in the third on-site short stack. The coating was used as a substitute for the standard pressure plate nickel plating between the pressure plates and load take-offs, and performed satisfactorily in over 1000 hours of stack testing.

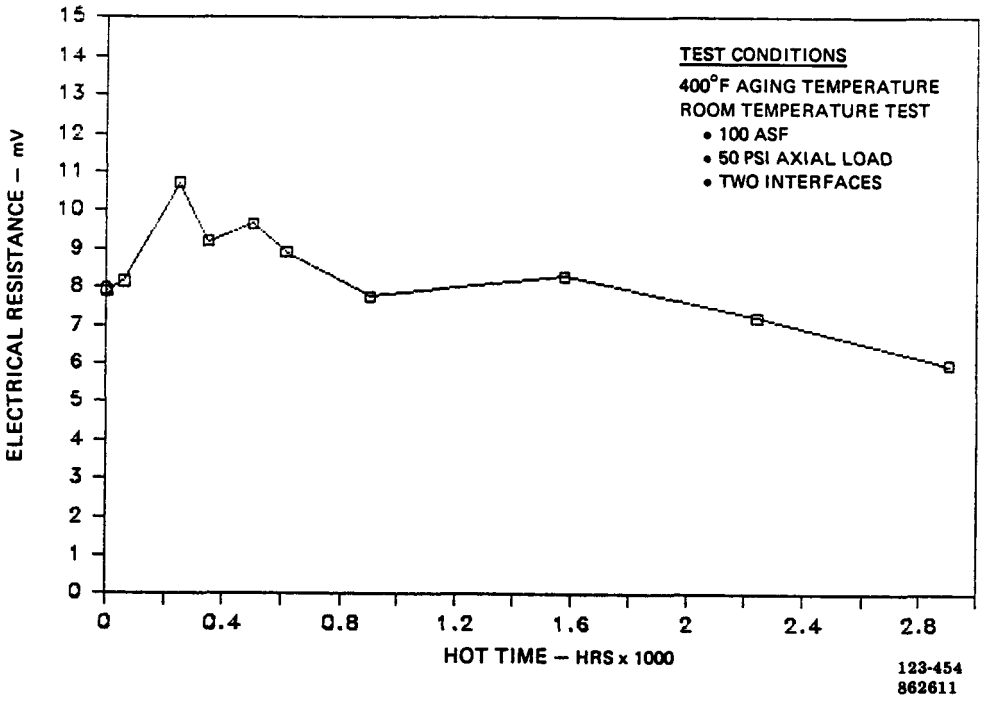

Figure 2.3–12. *Electrical Resistance History of Pressure Plate Coating*

Acid Refill

Three approaches were evaluated for refilling acid into cell stacks: drip-wick, acid injection, and acid spray. The three fill concepts have several common features: acid is added to a non-operating stack, one electrode of each cell is saturated with dilute acid, and acid slowly redistributes within the cell as the acid is concentrated to operating concentration during a modified stack start-up cycle.

The drip-wick approach to acid addition is a subject of a patent disclosure and, therefore, not discussed.

The acid injection approach adds acid to each cell by a small diameter Teflon® tube. This tube is inserted into a reactant flow channel at each cell. The individual tubes are gathered into a bundle, and the bundle is sealed to form an acid distribution reservoir. A quarter-scale, 12-cell mockup of this approach was evaluated. During acid addition, the flow channel containing the Teflon tube is the first to fill with acid. The acid flows out of this channel and is laterally transported across the face of the stack by the tabs on the separator plates. The acid is wicked into the cell by the reactant flow channels. The excess acid cascades down the face of the stack and is collected from the bottom of the reactant manifold. The mockup was disassembled and gravimetrically verified that the substrates were saturated with acid.

The spray approach adds acid to the cell by spraying the face of the stack with acid. A plexiglas manifold was built to fit the quarter-scale, 10-cell mockup. Candidate spray nozzles were

mounted into this manifold. Acid was applied to the face of the stack and wicked down the flow channels. Within 15 minutes the flow channels were visually saturated. Teardown analysis confirmed that the substrates were filled. No obvious acid distribution or acid containment problems were observed.

Since the spray approach was the fastest and most reliable method for acid refill in subscale tests, this approach was selected for scale-up.

The first acid refill trial was conducted on a used 40-kW stack containing 270 cells. This stack was assembled with 90 new cells, located in 6-cell substacks throughout the entire stack. The new cells were filled with varying amounts of acid: dry, 10, 20, and 30 percent full reservoirs. A photograph of the cell stack and acid refill cart are shown in Figure 2.3-13. The refill test involved spraying the entire face of one side of the stack until all cells including the gas channels were full of acid and acid was cascading uniformly down the opposite side of the stack. The acid in the stack was then conditioned, the stack was disassembled, and acid inventory data (Figure 2.3-14) was obtained on each of the 90 new cells.

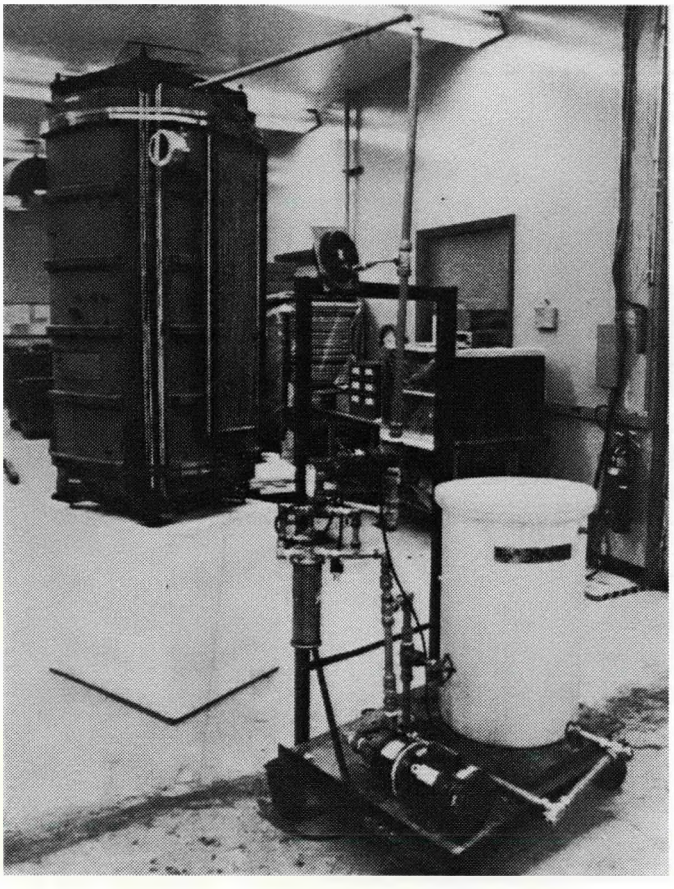

(WCN-10844)

Figure 2.3-13. *Cell Stack With Acid Refill Cart*

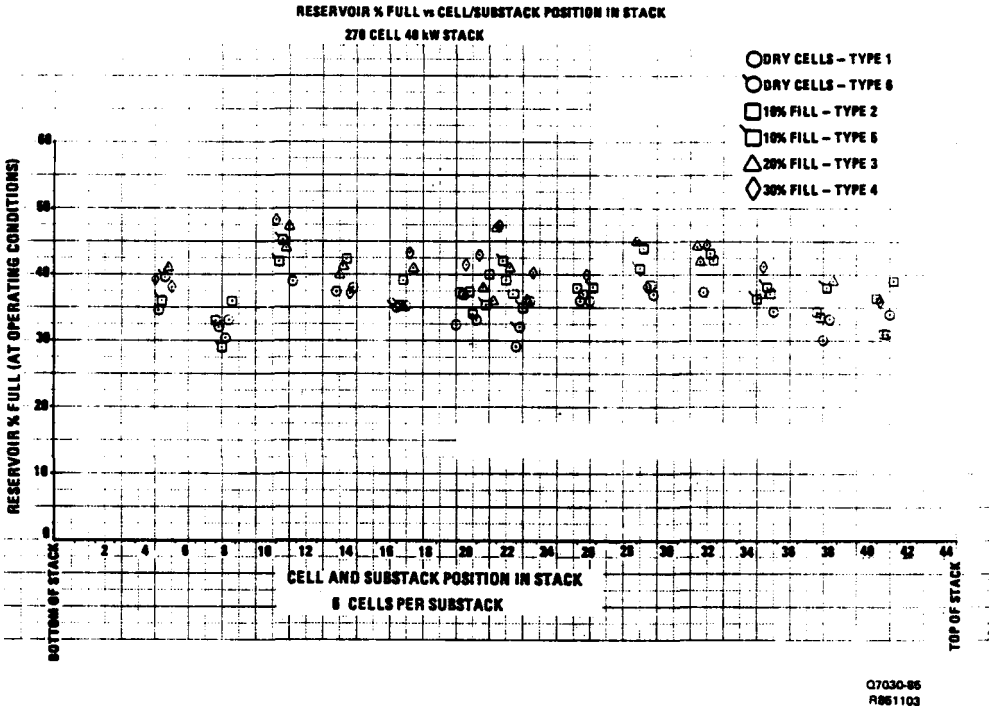

Figure 2.3–14. *Acid Inventory After Refill*

A survey of nozzle and spray system manufacturers was conducted. The objective was to select a commercially available spray nozzle that would be compatible with the fuel cell environment and would provide an acid spray pattern for refilling each cell in an assembled stack. The nozzles that were selected for evaluation were made of Teflon®, operated at low pressures and low flows, were compatible with 1/4 and 3/8-inch plumbing, and were, in some cases, of non-clogging design. The results of these evaluations led to the selection of a solid cone spray nozzle. Solid cone spray nozzles were used to refill a 30-cell stack being tested in Subtask 2.4 and a second 40-kW stack. Figure 2.3-15 shows the portable acid spray cart that was used along with the spray nozzles for the refill trial on this stack.

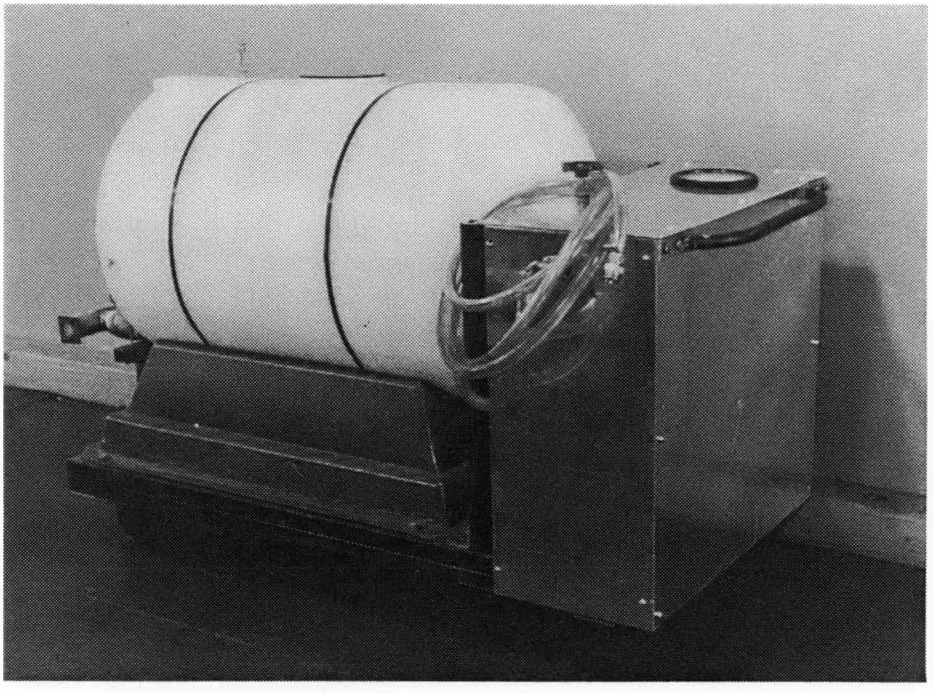

(WCN-13013-10)

Figure 2.3-15. *Portable Acid Spray Cart*

Subtask 2.4 – Cell Stack Testing

OBJECTIVE

The objective of this task is to evaluate the operational capabilities of stack components developed in other tasks. Included in this are evaluation of new design configurations, compatibility of new materials, and performance and decay characteristics of advanced catalysts.

SUMMARY

The cell stack components that were demonstrated successfully in subscale cells and rig tests were scaled up for test in short stacks of full area cells. The stacks built and tested in this program incorporated a number of improvements developed in this program and complementary GRI and private programs.

The first short stack in this program used Configuration "A" cells. The second and third short stacks and the full-height stack for the Verification Test Article (VTA) were fabricated with the new Configuration "B" cells. As detailed in Subtasks 1.1 and 2.1, the new Configuration "B" cells have superior performance and electrolyte management capabilities and use lower cost materials than Configuration "A" cells.

About 15,000 hours of short stack test time were accumulated in this task. In addition to cell test experience, this testing provided the opportunity to evaluate acid refill and water treatment approaches.

ACCOMPLISHMENTS/CONCLUSIONS

The first short stack was successfully refilled with acid after 6000-hours of operation and then run for an additional 1200-hours to prove performance after the refill, and the second short stack was operated with a subscale water treatment system to show that cooler plugging was no longer a problem.

- Short Stack No. 1 accumulated over 7200 hours of operation.
- An acid approach was successfully used to refill the Short Stack No. 1 after 6000 hours of operation.
- Short Stack No. 2, the first stack to be built with "B" configuration cells, accumulated 5051 hours of operation including 25 thermal cycles.
- A subscale water treatment system was tested with Short Stack No. 2 for the final 2166 hours of testing. The subscale system included a simulated section of the 40-kW cooler manifold to monitor restriction of coolant flow. No restriction was noted.
- Short Stack No. 3 accumulated over 2500 hours of operation including 16 thermal cycles. All components were in good visual condition after testing.
- A 305-cell full-height stack was fabricated using "B" configuration cells for test in the Verification Test Article (VTA) under Subtask 7.2.

DISCUSSION

Three short stacks (utilizing full-size 200-kW cells) were built and tested. The full-height stack for the Verification Test Article (VTA) was also fabricated as part of this stack. Fabrication and testing of each of these stacks is discussed below.

Short Stack No. 1

The first short stack in this program was assembled with the following features:

- Thirty-two (32) Configuration "A" cells with 3.7-ft^2 active area.
- GSB-18 cathode catalyst and HYCAN anode catalyst with both dry mix and wet mix anode catalyst formulations.
- Totally encapsulated, single-element serpentine coolers with ten cells per cooler.
- Integral end plate and current collector configuration.

A photograph of the completed stack prior to applying thermal insulation and installing in the test facility is shown in Figure 2.4-1.

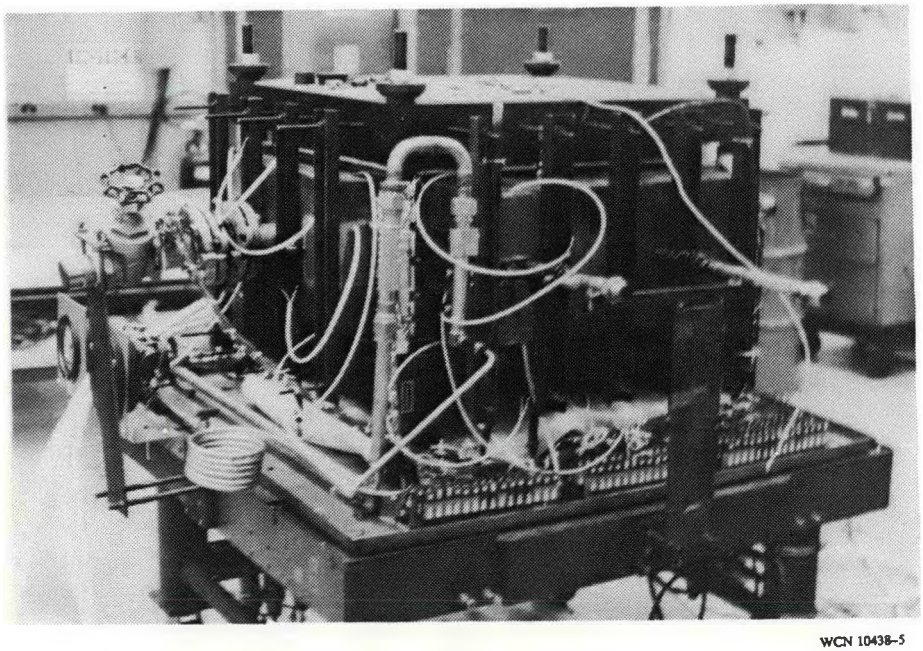

Figure 2.4-1. *Short Stack No. 1*

The endurance test conditions for this stack were 14.7 psia reactant pressures and 400°F average cell temperature. Typical operating conditions were 200 ASF, 80 percent fuel utilization, 60 percent air utilization and 148°F fuel dew point. A total of 7125 hours of operation, including 22 thermal cycles were completed. The test was interrupted at 5000 hours, and the stack was disassembled for inspection and reassembled for additional testing. The stack was tested for an additional 2175 hours prior to the final post-test inspection.

Cell performance curves versus current density and time are shown in Figures 2.4–2 and 2.4–3. This data shows that the average performance of all cells remained within 10 mV of E-line until the mid-test inspection and rebuild. The performance then decreased approximately 20 mV but improved during the next 200 hours of operation. The average cell performance was not changed by the acid refill, but cells with dry mix anode catalyst formulation were more sensitive to the inspection/rebuild and the acid refill test. The cells with wet mix anode catalyst formulation improved with test time after the rebuild and were within a few millivolts of E-line at the end of the test.

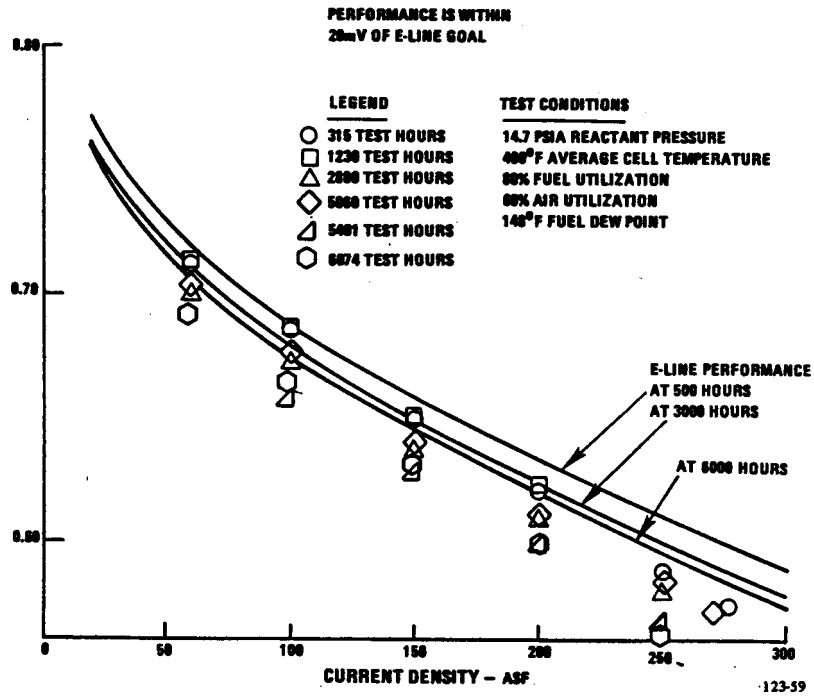

Figure 2.4–2. *Short Stack No. 1 Performance Calibration at Various Operating Time*

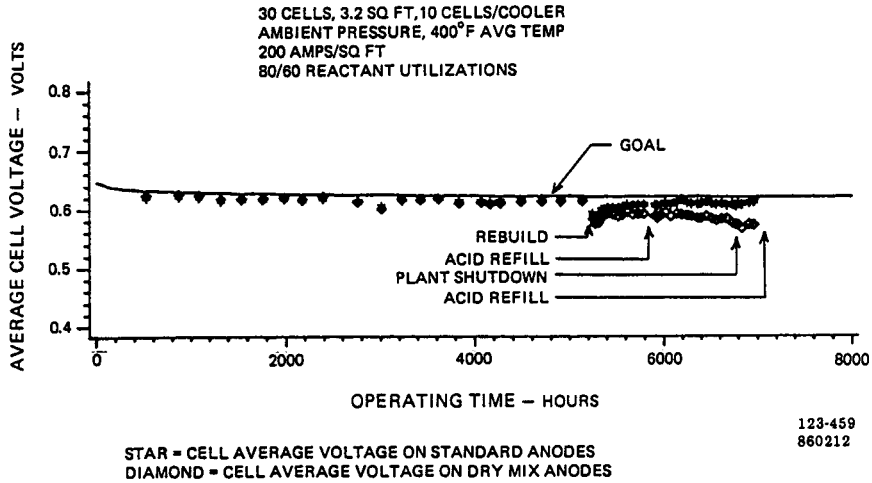

Figure 2.4–3. *Short Stack No. 1 Performance History at 200 ASF*

As stated above, mid–test and post–test inspections were conducted. The following observations apply to both inspections:

- The general condition of all components was excellent.
- There was no evidence of cell package defects or deterioration.
- The carbonized separator plates were in acceptable condition.
- Acid inventory data showed that the cells were uniformly filled.
- Cooler assemblies were in excellent condition with no evidence of corrosion or restriction in flow.
- The reactant gas manifold seal leakage and cell package crossover remained low and acceptable throughout the life of the stack.
- Protective coatings on the reactant gas manifolds were defect–free.

Short Stack #2

The second short stack was the first stack to be fabricated with the new "B" Configuration cells. Special features are listed below:

- Thirty-two (32) "B" Configuration cells with 3.7-ft2 active area.
- GSB-18 cathode catalyst and HYCAN anode catalyst; both dry mix and wet mix anode and cathode catalyst formulation.
- Improved edge seals on cell package.
- Reduced matrix thickness.
- Encapsulated cooler assemblies with eight cells per cooler.
- Reactant manifolds with PFS and PPS protective coatings and strap/spring retention system.
- Integrated end plate, pressure plate, and power takeoff.

The endurance test was conducted at 14.7 psia reactant pressures and 400°F average cell temperature. The cell operating conditions were 80 percent fuel utilization, 60 percent air utilization, and 148°F fuel dew point.

The average cell performance calibration data are presented in Figure 2.4-4. This is a plot of the average cell voltage versus current density. Data at 500-hours exceeded the goal. The cell stack operated for over 5000 hours. The cell performance history is presented in Figures 2.4-5 and 2.4-6. Figure 2.4-5 presents the average cell voltage at the 300 ASF design conditions versus operating time. The final 300 ASF performance level is 30 mV below the E + 20 mV goal. Figure 2.4-6 compares the 200 ASF performance history of this stack to that of the first short stack.

An acid collector rig was tested on the cathode exhaust of this stack. The collector operated for 590 hours, and the expected amount of acid was collected.

A post-test inspection of this stack was conducted. This inspection included a visual inspection of all components and the measurement of acid inventory in each cell component. The following significant observations were made:

- Defects noted in Cell 28 were caused by impurities entrapped during stack assembly.
- The axial load decrease with operating time was acceptable. These data are presented in Figure 2.4-7.
- The acid inventory is uniformly distributed among the cells.

- The encapsulated coolers were in excellent condition. There was no evidence of acid within the assembly and no corrosion deterioration of the materials.
- There were no restrictions in the coolant system. These coolers operated for the final 2166 hours with the subscale water treatment system.
- The reactant gas manifold protective coatings showed no deterioration.
- The reactant gas manifold leakage was at a very low level throughout the test. The gas manifold seals showed excellent conformity of the seal to the irregularities on the edge of the cell stack.

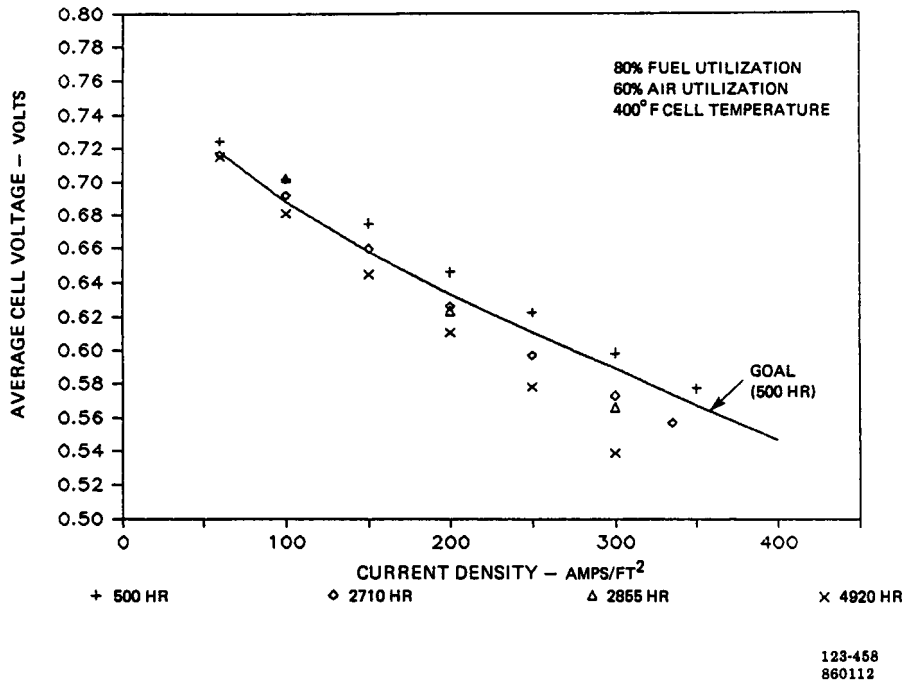

Figure 2.4–4. *Short Stack No. 2 Performance Calibrations at Various Operating Times*

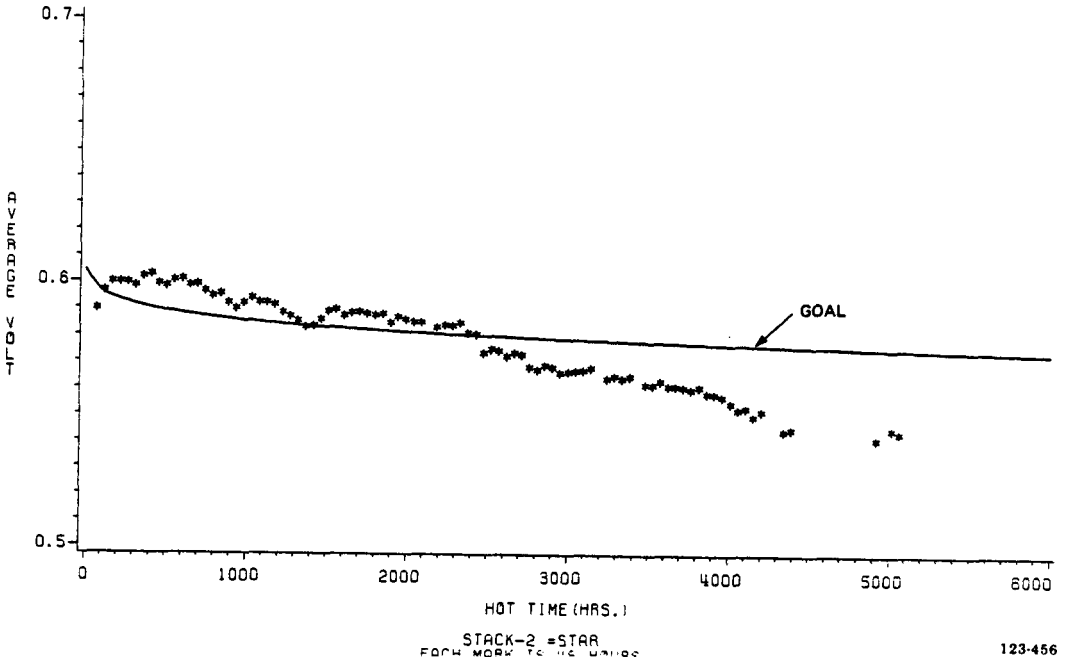

Figure 2.4–5. *Short Stack No. 2 Performance History* at 300 ASF

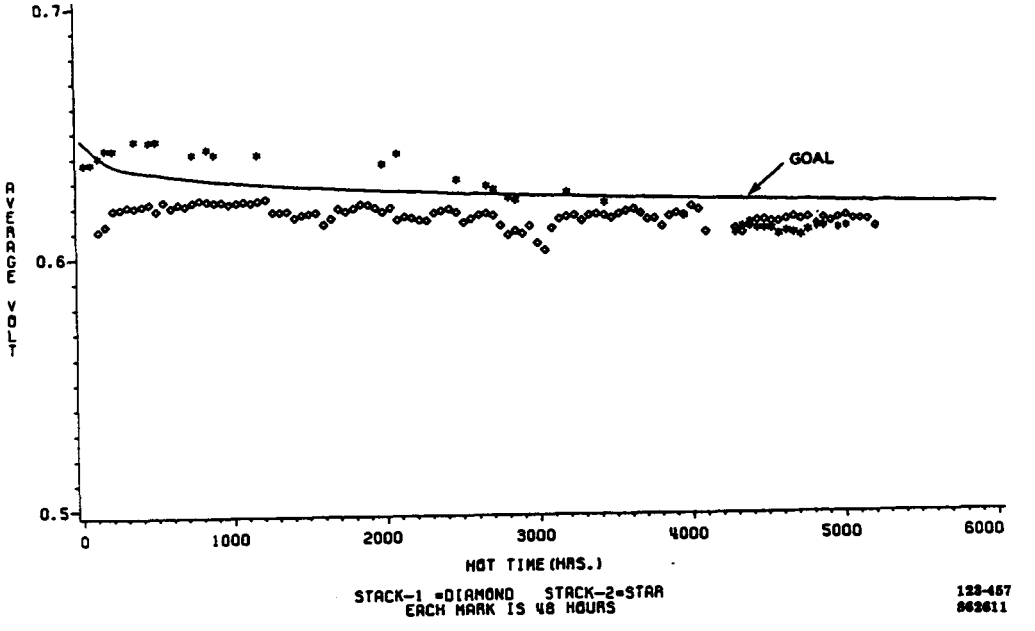

Figure 2.4–6. *Performance History Comparison of Short Stacks No. 1 and No. 2 at 200 ASF*

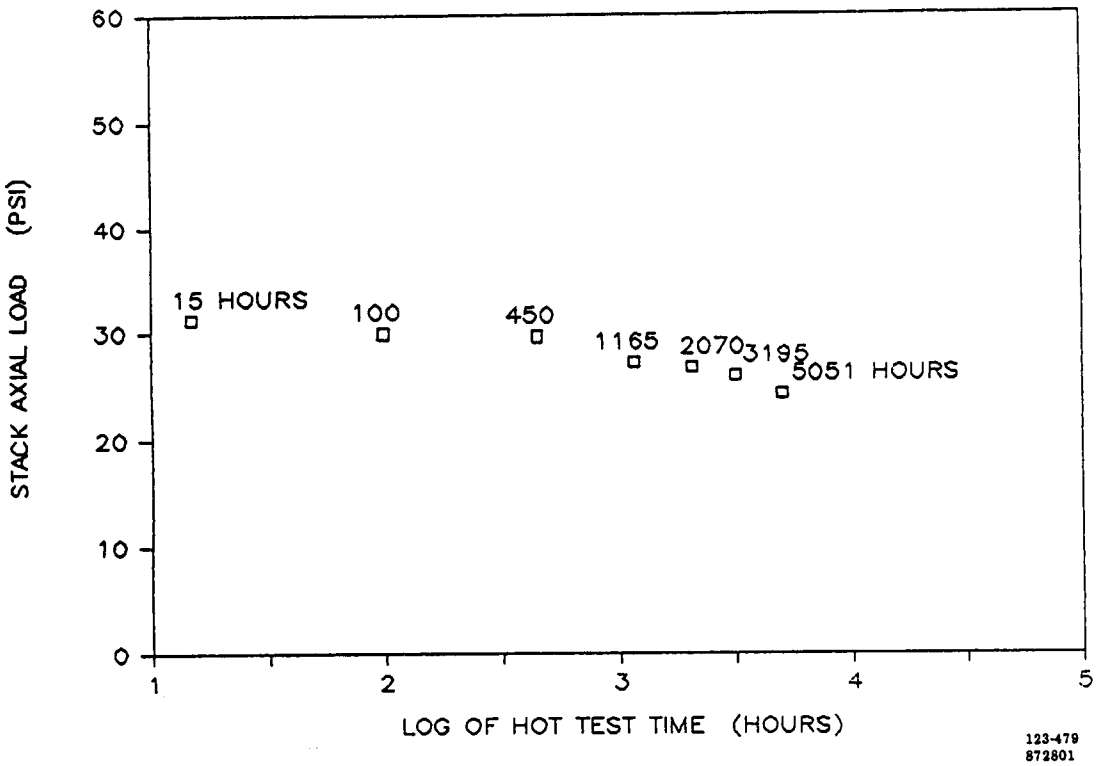

Figure 2.4–7. *Stack No. 2 Axial Load History*

Subscale Water Treatment Testing

A subscale water treatment system was tested with Short Stack No. 2 for the last 2166 hours of the testing. A schematic of this water treatment system is presented in Figure 2.4–8. The system included a cathode exhaust condenser that returns water condensed from the cathode exhaust to the cooling water system. Carbon dioxide was added to this condensate to simulate burner exhaust condensate. The subscale system also included a simulated section of a 40–kW cooler manifold to monitor restriction of coolant flow. No restriction in coolant flow was noted during this test period.

The stack water inlet manifold was operated for 3737 hours at 200 volts above the stack potential. This higher voltage simulates the potential of the water inlet manifold on a full–size stack. There was no restriction in flow during this test, and the post–test inspection showed this manifold to be free of deposits.

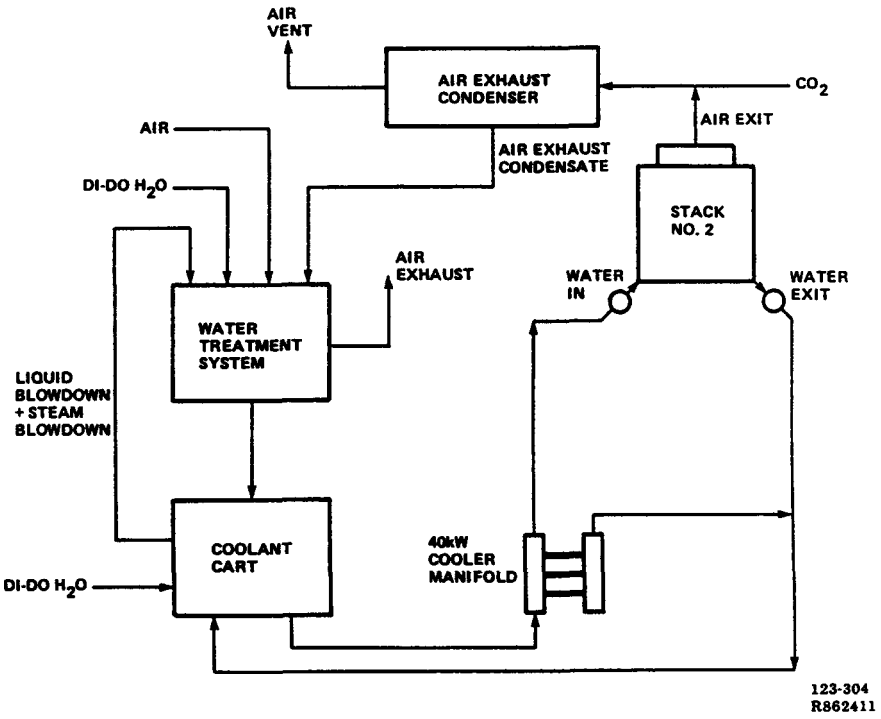

Figure 2.4–8. *Schematic for Short Stack Water Treatment Tests*

Short Stack No. 3

In 1986, the third and final short stack of the program was assembled. This stack contained the following features:

- Twenty–eight (28) "B" Configuration cells with 3.3 ft2 active area.
- GSB–18 cathode catalyst and HYCAN anode catalyst.
- Encapsulated cooler assemblies; seven cells per cooler.
- Reduced matrix thickness.
- Advanced acid management features.
- Integral end–plate configuration.
- Reactant gas manifolds with advanced protective coatings.

Testing was conducted at loads up to 365 ASF. The average cell temperature was 405°F at 300 ASF and 410°F at 365 ASF. Typical fuel and air utilization were 80 percent and 60 percent, respectively.

A total of 2522 load hours, 2635 hot hours and 16 thermal cycles were completed during testing. The cell performance history at 300 ASF is shown in Figure 2.4–9. Cell performance was

at or above the goal for over 1000-hours and was stable throughout the test although a 5 to 20 mV per cell increase in hydrogen gain was noted in "B" Configuration cells without conventional separator plates. At the end of performance testing; the cell stack was stored for approximately six months at 130°F.

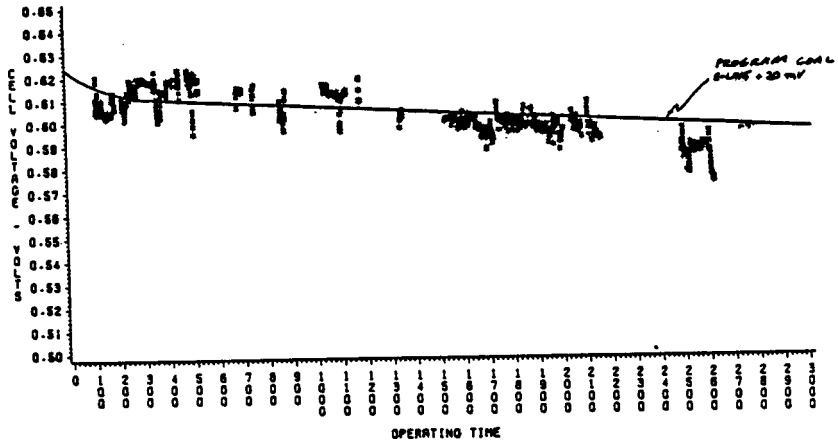

Figure 2.4-9. *Short Stack No. 3 Performance History at 300 ASF*

The cell stack was restarted for a short (2-day) performance calibration prior to post-test inspection. Results of this performance calibration (at about 2630 hours) are compared to previous calibrations in Figures 2.4-10 through 2.4-12. A 20 mV loss in average cell was experienced between 1650 hours and 2625 hours. See Figure 2.4-10. About two-thirds of this loss is associated with the six months of storage at 130°F. No significant change in hydrogen and oxygen gains occurred between 1617 and 2630 hot hours.

The cell stack electrolyte was conditioned, and the stack was removed from the test stand for post-test inspection. Visually, all components were in good condition. Electrical isolation and reactant gas leakage are acceptable. The axial load loss history is presented in Figure 2.4-13 and is as expected.

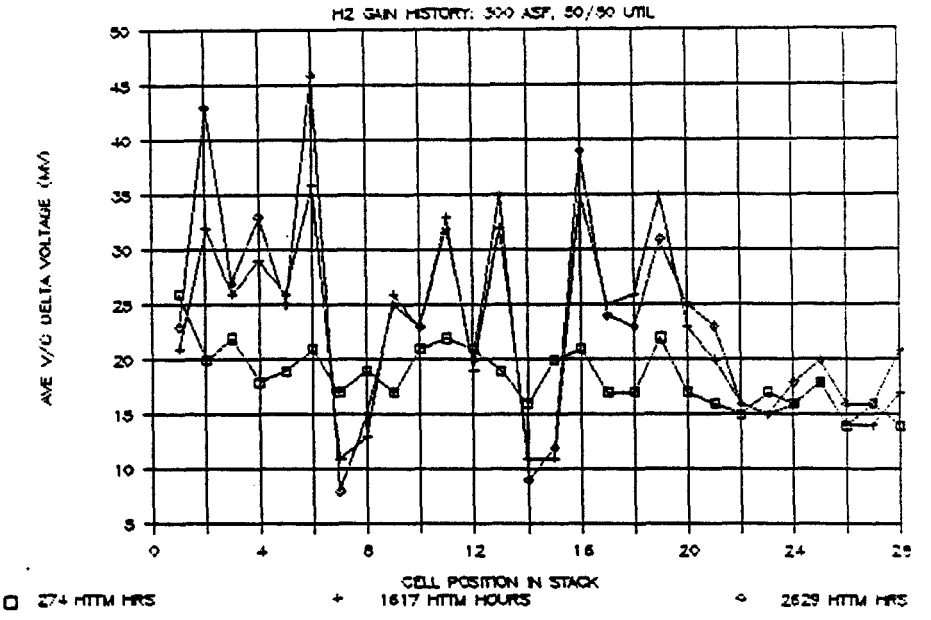

Figure 2.4–10. *Short Stack No. 3 Performance Calibrations*

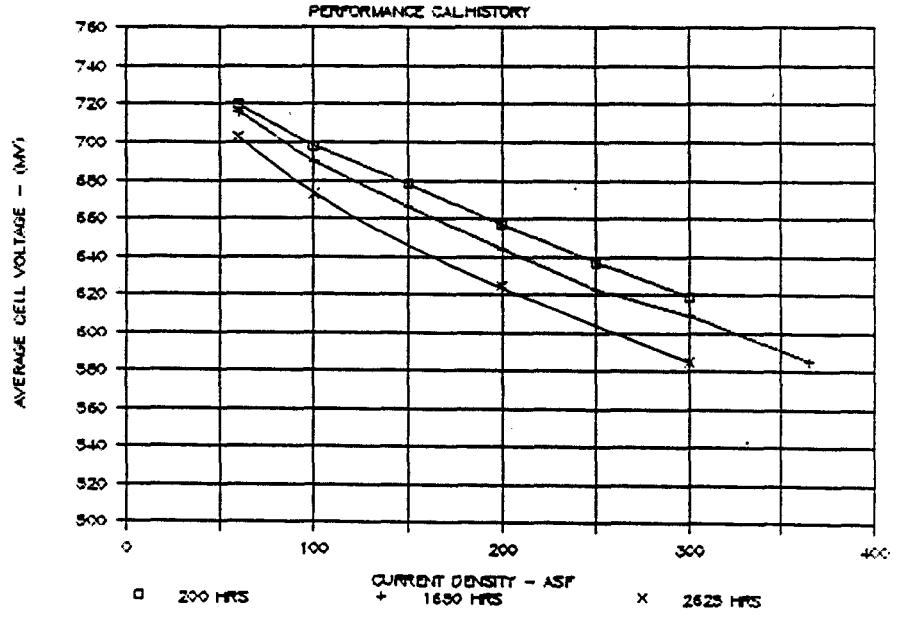

Figure 2.4–11. *Short Stack No. 3 Hydrogen Gains*

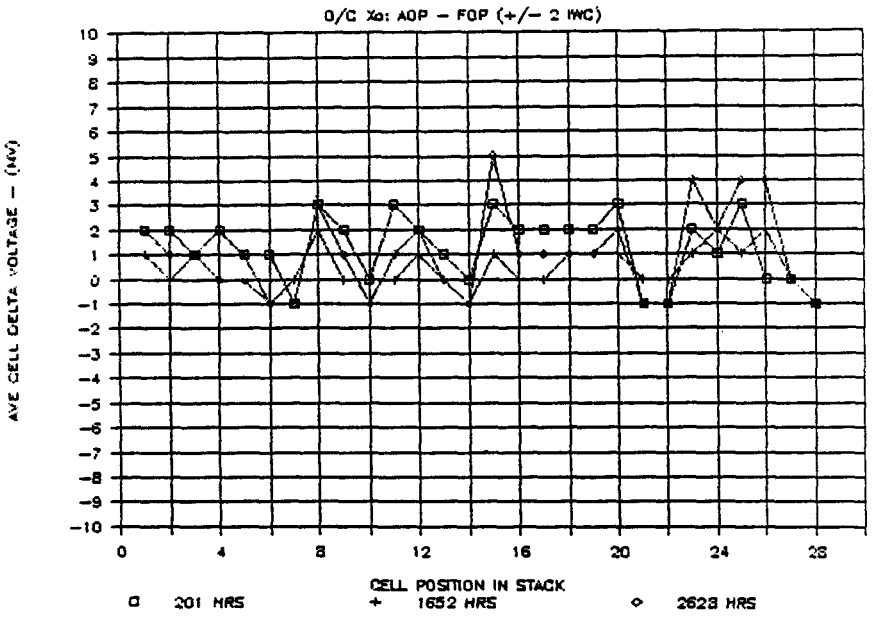

Figure 2.4–12. *Short Stack No. 3 Cross–Pressure Sensitivity at Open–Circuit*

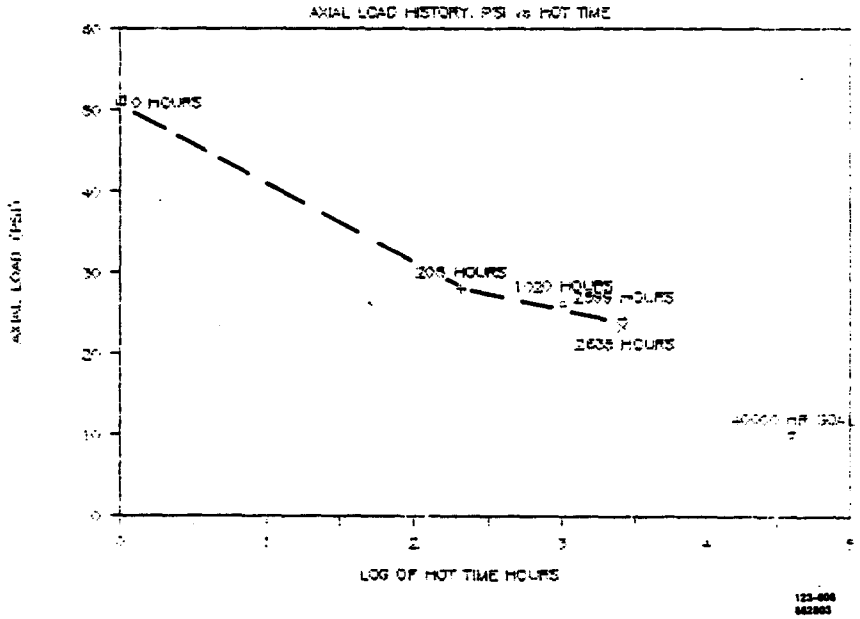

Figure 2.4–13. *Short Stack No. 3 Axial Load History*

Electrolyte inventory measurements of individual cells were completed. This data was reviewed to assess cell package electrolyte management. No significant cell–to–cell acid transfer was evident in either the baseline Configuration "B" cells or in those "B" cells containing conventional separator plates.

Full Height Stack

Fabrication and assembly of a full-size 308-cell stack was conducted in 1986. This stack contains the same design features as the third short stack. The full-height stack was mounted on a test cart and delivered for installation and testing in the Verification Test Article under Subtask 7.2. A photograph of the full-height stack is shown in Figure 2.4-14.

(WCN-14308-11)

Figure 2.4–14. *Full–Height Stack During Fabrication*

TASK 3 - POWER PROCESSOR DEVELOPMENT

Subtask 3.1 Define Inverter Technology

OBJECTIVE

The inverter is an electrical system which converts dc power from the fuel cell stack into utility-grade AC power for the customer. The objective of this subtask was to establish the design approach, control circuit options, and semiconductor technology for a high efficiency, low cost inverter.

SUMMARY

The approach taken in this subtask was first to evaluate the impact of advanced semiconductor and power circuit technologies, control concepts, and improved magnetic components on inverter cost and efficiency. The basic inverter system design, as established in the 1982 GRI program, was modified and updated as a result of these optimization studies, system tradeoff studies, and identified beneficial technologies. A detailed electrical design was then established, along with a GRI-sponsored conceptual mechanical packaging design, for use in performance estimates and definition of the brassboard inverter which was built and tested in Subtask 3.2.

The initial inverter design was a 200-kW, two-bridge unit with 93.6 percent efficiency at rated power. Use of a low loss output transformer, auxiliary commutation for surge (ACS) circuitry, and advanced asymmetrical silicon controlled rectifiers (ASCR's) were identified for increasing efficiency to 95.4 percent and, therefore, selected for evaluation on the brassboard inverter. A brassboard is a rigidly structured unit to allow evaluation of critical electrical, thermal and mechanical packaging parameters and performance. Other trade-off studies were used to select forced air-cooling for bridges and multi-megawatt control hardware (developed under a separate DOE contract) for the main control unit of the brassboard.

ACCOMPLISHMENTS/CONCLUSIONS

- Established an inverter bridge electrical design with calculated efficiency up to 95.4 percent.
- Identified ASCR's for testing in the brassboard inverter and transistors for advanced technology evaluations in complementary GRI programs.
- Selected forced air cooling for inverter bridges.

DISCUSSION

Initial Inverter Definition

Previous studies performed under a GRI-sponsored effort evaluated power circuit technology and identified designs that would improve cost and/or efficiency. The study determined

that the individual commutation circuit provided both cost and efficiency advantages over the Split-C commutation circuit used in the 40-kW on-site inverter.

The individual commutation circuit was tested in a one-quarter scale powerpole to confirm its feasibility for the on-site inverter. The 1983 NASA On-Site effort in this subtask then became one of providing a detailed on-site inverter system electrical design using identified technologies from tradeoff and optimization studies which, with mechanical design support from a parallel GRI program, would provide Subtask 3.2 with the necessary information for fabricating brassboard inverter hardware.

Other on-site program activity established a rating of 200 kW for the development inverter, defined the system for initial development as grid-connected only, provided an estimate of the fuel cell dc operating characteristics, and defined the ac utility line interface voltage. From this governing set of criteria the inverter system depicted in Figure 3.1-1 was established. The primary elements are:

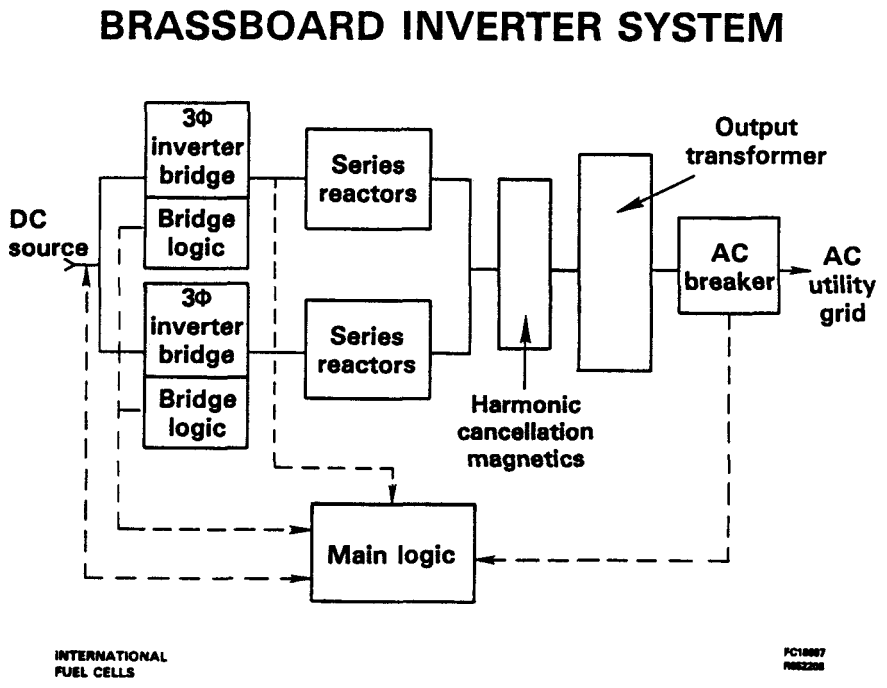

Figure 3.1-1. *200-kW Brassboard Inverter System*

- Two three-phase inverter bridges utilizing pulse width modulation for control of fundamental and harmonic voltages (the two bridges operate 30° displaced into a delta-wye transformer to magnetically eliminate the 5th/7th harmonics and their conjugate pairs).
- Series reactors which provide the bulk of the system's 22 percent impedance for the controls to work against and which provide a buffer between the bridges and the utility line.

- A full isolation two-winding power transformer that provides a voltage match between the bridge outputs and the utility line, as well as grounding isolation.
- The control and protection logic, which provides all necessary operating, regulating, and protective functions for automatic, unattended operation. The logic is comprised of two parts, bridge logic and main logic. The bridge logic was defined in Subtask 3.2.

After establishing the basic inverter system, an electrical circuit schematic for the bridges, series reactors, and output transformer was detailed by defining the specific component values necessary to meet the on-site performance requirements. That configuration was then reviewed to insure functionality, with proper safety margins and optimization of components to achieve maximum performance. The end result was an on-site inverter capable of delivering 200 kW into an electric utility line with a calculated efficiency of 93.6 percent at rated power.

A series of optimization and trade-off studies were then conducted on the inverter design to improve the inverter performance and/or reduce cost. As discussed in the following sections, results from these studies can raise the inverter efficiency by a total of 1.8 percent up to 95.4 percent at rated power.

Output Transformer Selection

The output transformer was the first area to be studied as part of optimization studies. Typical commercial magnetics in this power range have full load losses between 5 percent and 2 percent of rating. Initial estimates of efficiency had assumed 2 percent. Several manufacturers were queried as to the cost and weight penalties in designing a transformer for 1 percent loss at full load. Initial feedback was not promising, with little detail provided. One manufacturer did show an interest in analyzing this question, however, and estimated that an output transformer with a 1 percent full load loss would weigh 27 percent more and cost 20 percent more than a 2 percent loss design. Since the 20 percent cost increase was much less costly than achieving equivalent dc module efficiency, the 1 percent transformer was included in the brassboard system, and the full load inverter efficiency estimate was improved by 1 percent.

Circuit Optimization

Another possibility for efficiency improvement was in the use of auxiliary commutation for surge circuitry (ACS). The baseline design incorporated one main commutation circuit sized to handle the energy required to commutate off the peak current necessary to handle surges at the minimum dc operating voltage. The ACS concept is to:

1. Use a smaller main commutation circuit for normal full load current plus an approximate 30 percent margin to handle minor perturbations,
2. Use ACS whenever the current exceeds the 30 percent margin, to handle surges and faults.

This concept was investigated previously for MW-scale inverters. Evaluation of ACS designed for the 200-kW brassboard inverter showed the results in Table 3.1-1.

Table 3.1-1. Auxiliary Commutation For Surge Effect On Efficiency

Load	Commutation Circuit Losses (Watts) Without ACS	With ACS	Delta	System Efficiency Increase (%)
Full Load	828	462	366	0.2
Half Load	1,116	702	414	0.4
Quarter Load	1,884	1,452	432	1.0

The 0.2 percent improvements at full load, when viewed as a function of the cost of the ACS on a system basis, resulted in a break-even situation. The ACS provides more substantial benefits in grid-independent inverter designs which require higher overload and benefit more from part power efficiency improvements. Since grid-independent designs will be required for broad applicability, the ACS was incorporated into the brassboard design for technology evaluation.

Semiconductor Selection

The third area for optimization utilized the results of semiconductor device investigations. Semiconductor evaluations and forecasts were performed as an on-going effort in this task. Initial forecasts (performed in 1983) considered near-term projections for SCR's (silicon carbide rectifiers), ASCR's (asymmetrical SCR's), and GTO's (gate turn-off thyristors) for use as the main thyristor in the inverter. The ASCR was selected for initial testing in the brassboard since reductions in forward drop from 1.7 v to 1.3 v were projected for the near-term. The reduction in forward drop can increase the calculated inverter efficiency by 0.6 percent.

Later semiconductor evaluations and forecasts expanded the candidate list for inverter switching devices to include RCT's (reverse conducting thyristors) and transistors as new devices became available. This program focused on the development testing of the ASCR inverter in the 1983-1985 while a complementary GRI program considered use of advanced semiconductor switching devices. (The GRI effort led to the successful testing of a transistor inverter in 1987).

Inverter Cooling Definition

Different methods for cooling the brassboard inverter bridges were considered as part of optimization studies. Once the electrical circuit was defined and the semiconductors identified, estimated losses were calculated. The parallel GRI effort provided a mechanical packaging concept from which the cooling study could evolve, using the estimated losses for the semiconductors and other components. The study included three types of cooling:

- Forced air
- Liquid
- Heat pipe

Table 3.1-2 shows results for the analysis of forced air cooling with extruded aluminum heat sinks. The maximum calculated semiconductor junction temperature is 109°C, with 120°F ambient inlet cooling air. The acceptable junction temperature limit is 125°C, with 115°C preferred for margin. A similar analysis for liquid cooling showed equivalent performance can be obtained, but at a much higher cost. Cost estimates based on parts requirements alone showed liquid cooling to be twice as costly. Also, previous studies and experience proved heat pipes to be cost effective at cooling loads significantly higher than those of the 200-kW inverter. The forced air/heat sink method was the logical choice to meet requirements at the minimum cost.

Table 3.1-2. Bridge Cooling Summary

Item	Watts Loss Each	Qty. Per Bridge	CFM Air Req'd Each	Calculated Junction Temp. °C
Main Thyristor	345	6	80	109°
Commutation Thyristor	170	6	80	108.7°
Main Diode	100	6	30	92°
Commutation Diode	75	6	30	91.5°
Clamp Diode	75	6	40	107°
Heat Load Due to Other Components			1410 Watts	
Total Air Flow Per Bridge			1560 CFM	
Max Inlet Air Temp.			43.3 °C	
Max Exit Air Temp			50.7 °C	

Inverter Control Definition

Inverter bridge controls for the brassboard inverter were sufficient to operate the inverter power poles but did not contain the logic necessary to operate the inverters connected to the utility grid. A main logic was required to provide real and reactive power control, utility line related protection, and synchronization with the utility line.

Two approaches for obtaining a main control unit brassboard testing were evaluated:

1. A laboratory constructed breadboard version with the basic control functions but limited protection and no diagnostic features.

2. Procurement of a second set of the hardware designed for multimegawatt converters (under DOE Contract DE-AC01-79ET29079) that provide more sophisticated control and protection functions than required and also contain a sophisticated level of diagnostics.

The evaluation showed that the actual costs were not significantly different, but that two significant advantages were offered in the multimegawatt design: it provided excellent hardware and software flexibility (necessary to evaluate the control concepts required for the on-site power processor), and its diagnostics would greatly simplify the checkout and evaluation process. The multimegawatt design was selected for testing on the brassboard in Subtask 3.2. The version of the main inverter control unit that was selected is shown in the block diagram in Figure 3.1-2.

Conceptual studies showed that bridge and main controls could be combined into one package on future production versions. (The separate configuration was selected for test flexibility on the brassboard). Table 3.1-3 shows a comparison of the brassboard configuration to the possible future version.

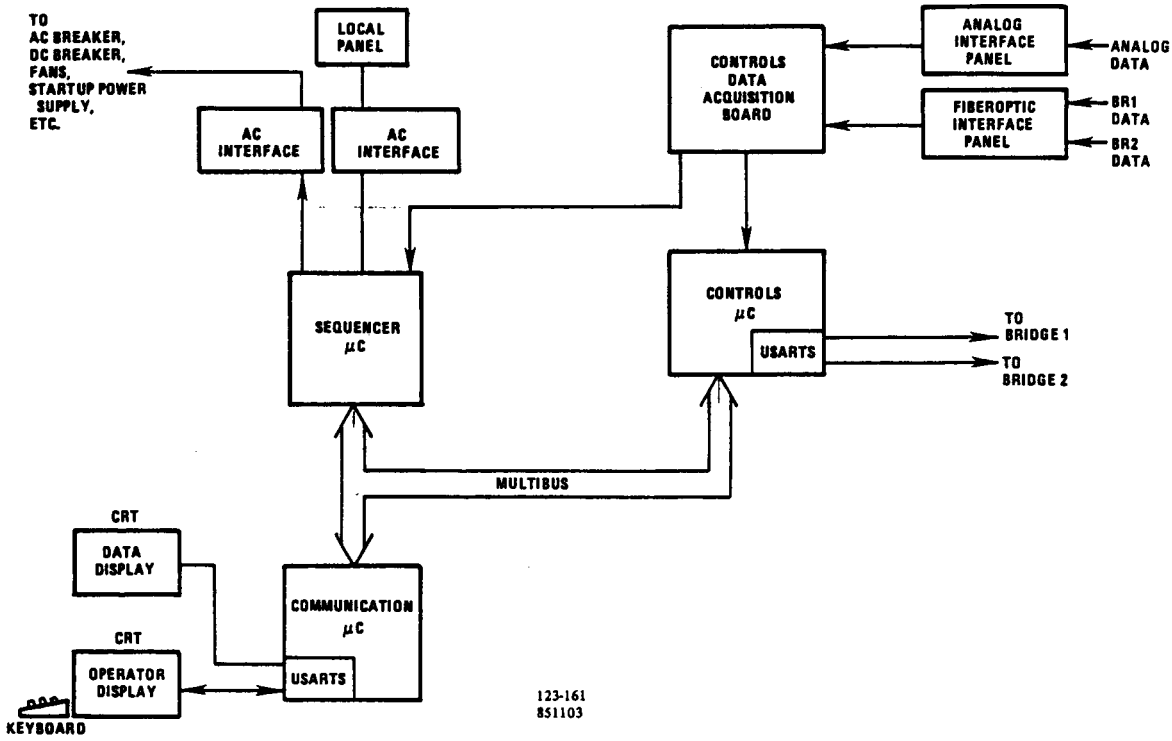

Figure 3.1–2. *Block Diagram of Main Inverter Controller*

Table 3.1–3. Simplified Baseline Inverter Control Unit Comparison to Brassboard

	Brassboard	Baseline
Circuit Boards		
Total	10	8
Custom	5	5
Off–the–Shelf	5	3
Interface Panels	11	5
Chasis	3	1
Power Supply Assembly	3	1
Cabinet	3	1

Subtask 3.2 Verify Inverter Technology

OBJECTIVE

The objective of this task is to construct a 200-kW brassboard inverter and verify its basic technologies and resolve any design or system deficiencies.

SUMMARY

The 200-kW brassboard two–bridge ASCR inverter was fabricated in 1984 and completed testing in 1985. Functionally, the two–bridge inverter performed as designed; however, data obtained showed part power efficiency to be lower than expected. The cause of this lower efficiency was determined, and the means to achieve the design goal was identified.

ACCOMPLISHMENTS/CONCLUSIONS

- The 200-kW two–bridge ASCR inverter functioned as designed during testing.
- Final measured brassboard efficiency after optimization of selective commutation was 93.6 percent at full power. The quarter power efficiency was 84.6 percent and could be increased to 87.6 percent by identified design optimizations.

DISCUSSION

A subcontract was placed with a commercial electrical/electronics equipment manufacturer to provide a mechanical design (funded by GRI) and construct two bridges and the series reactors for the 200-kW brassboard inverter. The brassboard inverter bridge logic, which was conceptually identified and based on distributed microprocessor technology under an earlier GRI study, was carried from the conceptual design to a detailed hardware and software design. A bridge logic vendor was selected to deliver two sets of brassboard bridge logic, one for each of two brassboard bridges. A vendor procurement for a low loss output transformer was also established. All this equipment was received by early 1984. The following sections describe tests performed on this equipment and analyses in support of these activities leading to successful test of the ASCR brassboard inverter system.

Brassboard Bridge Static Checks

The brassboard inverter bridges and controls underwent the static evaluation portion of the test plan. The wiring and circuitry verifications and circuit element measurements resulted in minor corrections.

Static voltage tests to 350 volts dc resulted in a per bridge total of 470 milliamps static current drain, as compared to a calculated value of 475 milliemes and a measurement by the fabrication vendor of 440 milliamps.

Bridge Dynamic Pole Testing

The individual 200-kW brassboard powerpole tests were completed. Figures 3.2–1 through 3.2–3 provide a summary comparison of the test data versus the results of powerpole modeling on UTC's hybrid digital/analog simulator. Results were in close agreement with predictions.

In addition, the dynamic characteristics of the auxiliary commutation circuitry were determined, with operation within 10 percent of predicted. Figure 3.2–4 depicts typical dynamic data taken with a digital storage scope. The auxiliary commutation circuitry is designed for limited duty cycle operation, which requires use of storage instruments.

System Integration

The bridge control unit was procured from vendors, bench tested, delivered to the bridges, and installed.

The 200-kW inverter bridge and main control units were integrated with the brassboard bridges and isolated operation was verified. In addition, power wiring was installed from the 200-kW test dc power supply to the bridge inputs and from the bridge outputs to the system output transformers. Current transformers, switchgear, and the ac utility line ties were completed and pre–line–parallel checkout was completed.

The bridge and main control units were verified as being correctly wired, then the thyristor gate signal circuitry design was verified by operating the control and observing the gate signals. Figure 3.2–5 shows typical oscilloscope pictures of the thyristor gate signals used to derive critical parameters such as peak gate current (I peak), rate of change of current (di/dt), reverse current, and pulse width. All of the data were in agreement with calculated design values.

Dynamic Isolated Testing

Once operation of the thyristor gating signals was confirmed, each powerpole was operated individually (at no load but at high dc input voltage) with the new controls. Multiple powerpoles were operated simultaneously, then each entire bridge, and finally both bridges simultaneously. The objective of this testing was to observe powerpole operating parameters and confirm that operation of multiple poles did not cause dynamic anomalies through interaction between the poles. Interaction anomalies that can occur are circuit resonance on the dc input bus or oscillating currents between bridges. No anomalies were observed due to interaction between poles or bridges, but some other minor control anomalies were discovered and corrected.

Hybrid Computer Simulation

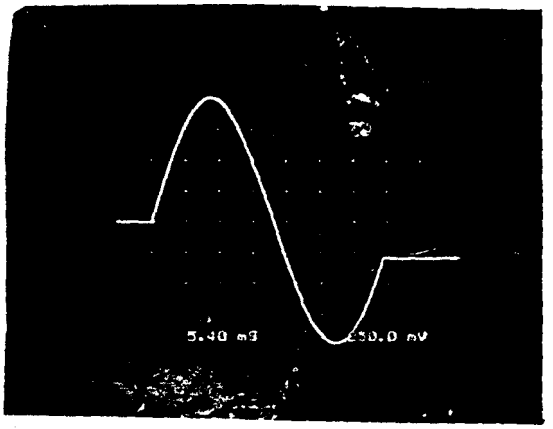

I=500 A/Div, T=10.8 μs/Div

$I_{P(1st\ pulse)}$=2000A

$T_{P(1st\ pulse)}$38.6 μs

$I_{P(2nd\ pulse)}$=1948A

$T_{P(1st\ pulse)}$=38.6 μs

Range for
12 Switch
Assemblies

$I_{P(1st)}$=1960-2100A

$T_{P(1st)}$=39.0=40.5 μs

$I_{P(2nd)}$=1800-1900A

$T_{P(2nd)}$=38.0-40.0 μs

Mean

$I_{P(2nd)}$=1825A

$T_{P(2nd)}$=39.25μs

Pole 1A Comm Current and Voltage

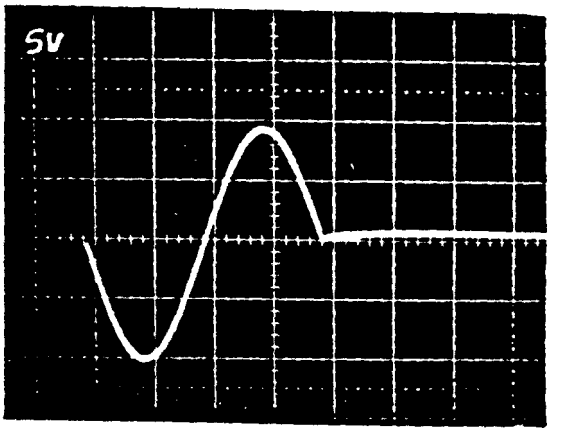

I=1000 A/Div, T=40 μs/Div

$I_{P(1st)}$=2000A

$T_{P(1st)}$=40.0μs

$I_{P(2nd)}$=1900A

$T_{P(2nd)}$=40.0 μs

123-164
850528

Figure 3.2–1. *Commutation Circuit Current at 250 Vdc*

Hybrid Computer Simulation

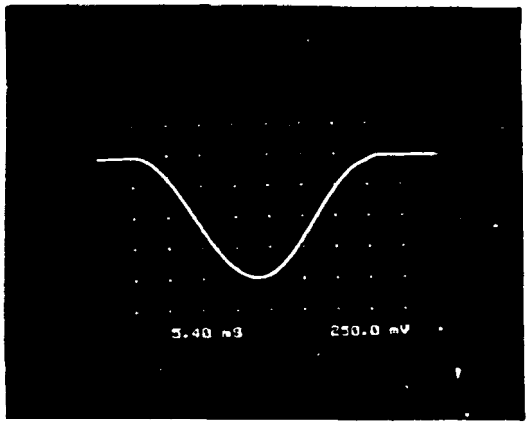

V=125 V/Div, T=10.8 μs/Div

$V_{peak\text{-}to\text{-}peak}$=500 volts

Pole 1A Comm Cap Voltage

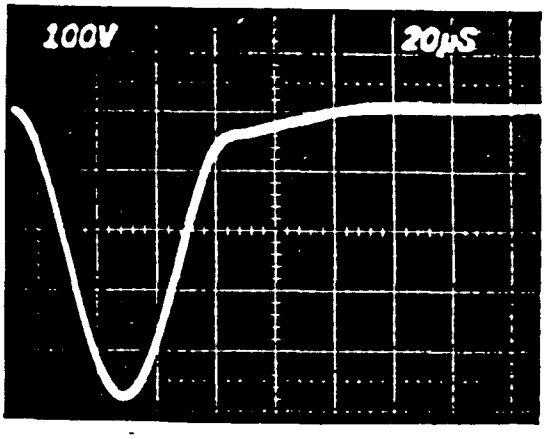

123-166
850528

V=100 V/Div, T=20 μs/Div

$V_{peak\text{-}to\text{-}peak}$=485 volts

Range for
12 Switch
Assemblies

$V_{p\text{-}p}$=485-510 volts

Mean

$V_{p\text{-}p}$=497 volts

Figure 3.2–2. *Commutation Capacitor Voltage at 250 Vdc*

Hybrid Computer Simulation

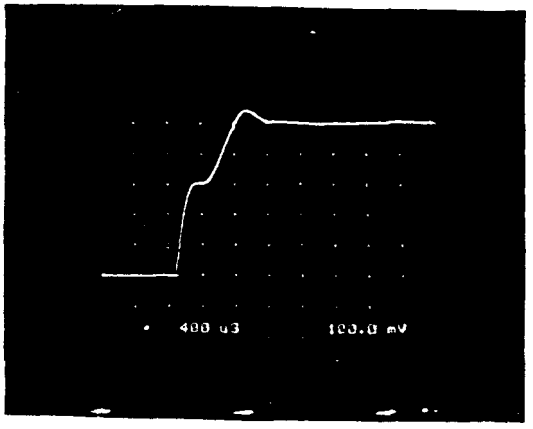

V=50 V/Div, T=800 ns/Div
10-90% dv/dt=180V/μs

Pole 1A Lower Main ASCR

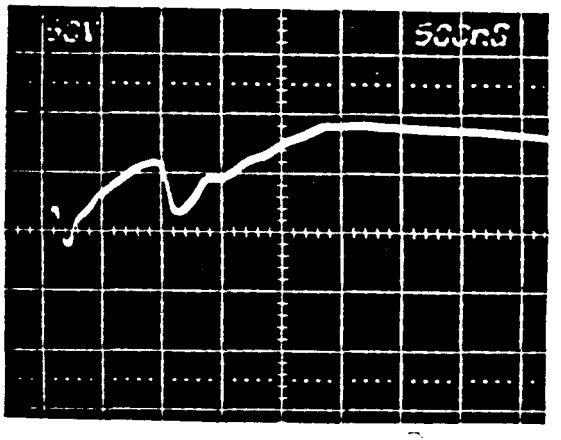

V=50 V/Div, T=500 ns/Div
10-90% dv/dt=210 V/μs

123-168
850528

Range for
12 Switch
Assemblies

10-90% dv/dt=70-315v/μ

Mean

10-90% dv/dt=199v/μs

Figure 3.2–3. *Main Switch ASCR Turn–Off Voltage at 250 Vdc*

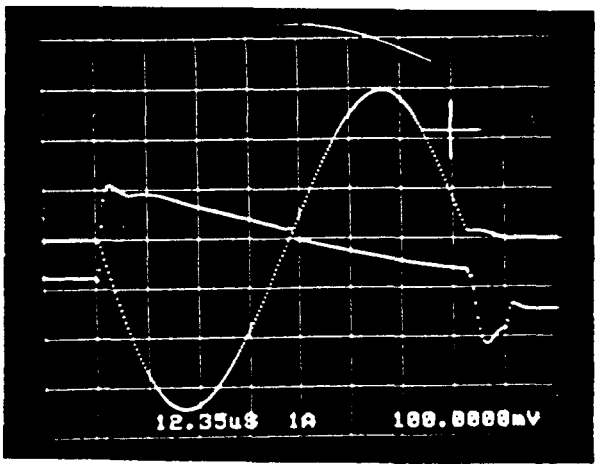

Aux. Comm. Current (Lower) 100 A/Div.

IP_1 = 340A TP_1 = 12,35 x 3.8 = 47.7 µs

IP_2 = 300A TP_2 = 12.35 x 3.6 = 45 µs

Voltage Across Q6 10 V/Div

Vdc = 190 Volts Vc5 = 225 Volts

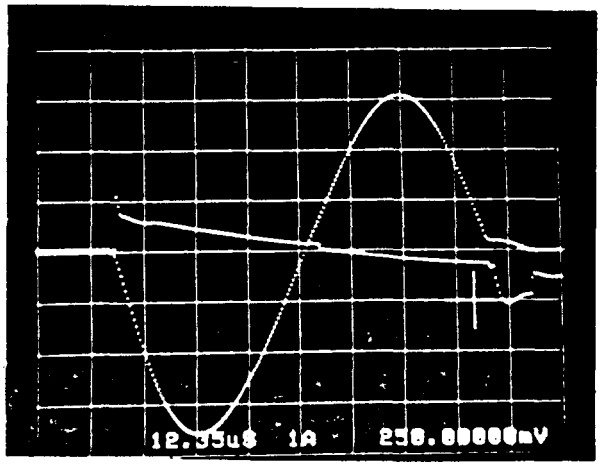

Aux. Comm. Current (Lower) 200 A/Div.

IP_1 = 800A TP_1 = 12.35 x 3.75 = 47 µs

IP_2 = 610A TP_2 = 12.35 x 3.6 = 45 µs

Aux. Comm. Voltage Q6 25 V/Div.

123-173
850528

Figure 3.2–4. *Typical Auxiliary Commutation Circuit Data*

Upper Main

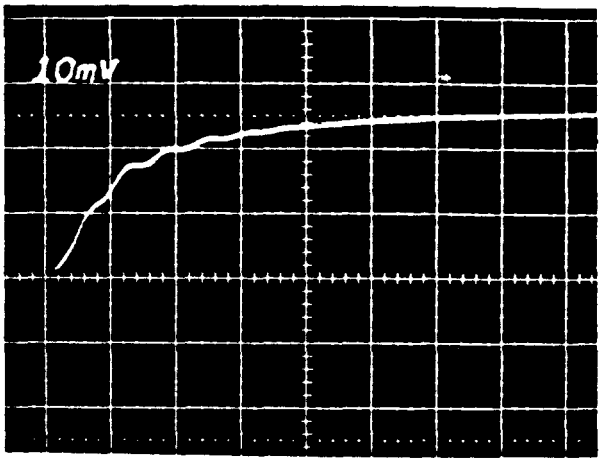

Vert. - 5Δ di/dt = 0.95Δ/μsec, 10%-90%

Upper Main

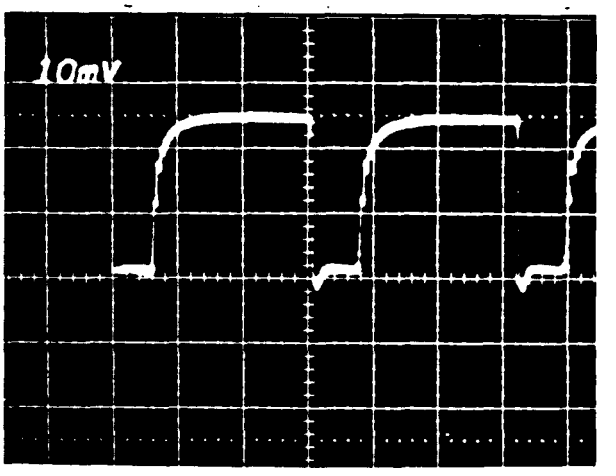

Horz. - 5 μsec/div. Turn On/Turn Off Sequence

Upper Comm.

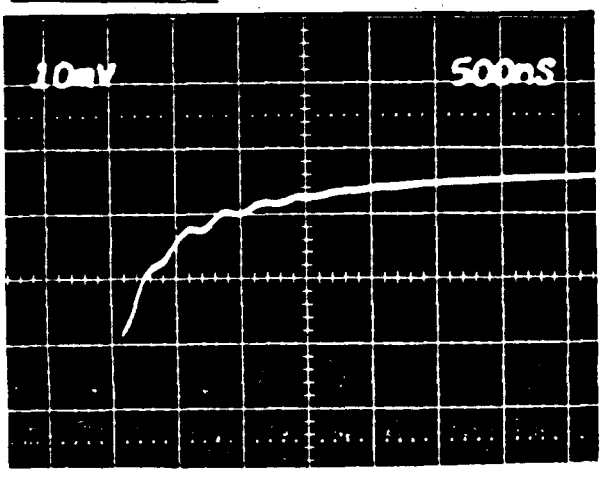

Vert. - 5Δ div. di/dt = 1.00 Δ/μs 10%-90%

Upper Comm.

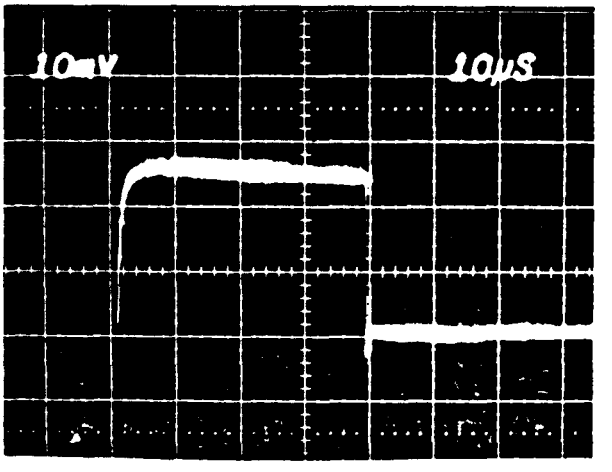

Turn On/Turn Off Sequence

123-171
850528

Figure 3.2–5. *Typical Gate Drive Oscilloscope Data*

Line Parallel Preparation

Final preparations for line paralleling the 200-kW brassboard inverter were completed. The correct operation of the output transformer was verified. Its input (primary) and output (secondary) voltages were measured with the secondary side of the transformer connected to the utility line (Figure 3.2–6). Secondary currents were also measured, which represent transformer magnetizing current. Magnetizing kilovoltamperes (kVA) was then calculated; it is also shown in Figure 3.2–6. Next, transformer phasing was checked, as shown in Figure 3.2–7. This chart recorder data shows the phase relationship of transformer primary to secondary connections and confirms the proper phase relationship of inverter input to the transformer and utility line output.

In addition to the output transformer, a line variac was installed in the test setup, along with a transfer switch to allow the utility line interface voltage levels to be varied for test purposes. The input to the variac comes from the inverter and the output is connected to the utility line.

Output transformer secondary energized from 480 Vac line with primaries disconnected.

Secondary Voltage (RMS)

VAN = 269.3 v	VAB = 466.5 v
VBN = 268.0 v	VBC = 462.6 v
VCN = 267.3 v	VCA = 464.5 v

Primary Voltage RMS

WYE Connections

VAN = 67 v	VAB = 130 v
VBN = 71 v	VBC = 130 v
VCN = 83 v	VCA = 130 v

Delta Connections

VAN = 52 v	VAB = 130 v
VBN = 87 v	VBC = 130 v
VCN = 89 v	VCA = 130 v

Secondary Current RMS

I_A = 188 ma x 60 = 11.3 amps I_B = 194.1 x 60 = 11.6 amps I_C = 176.4 ma x 6 = 10.6 amps

Voltages on 8 Channel Recorder

Secondary	VAN, VBN, VCN
Primary	VAB1, VAB2

- o Steady State
- o Transient

Magnetizing KVA = 3 Vcc i_c = 9.0 KVA

Figure 3.2–6. *200-kW Brassboard Output Transformer Test Results*

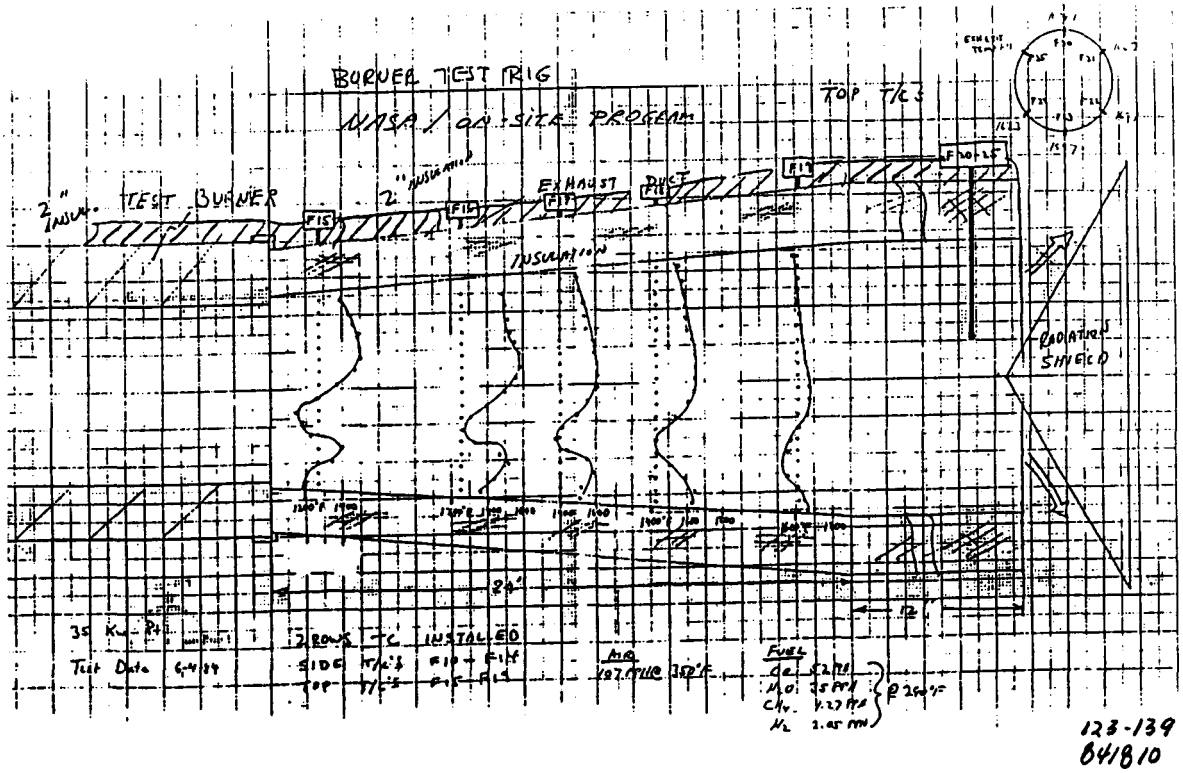

Figure 3.2–7. *Phasing for 200-kW Output Transformer*

The following other line parallel preparations were also completed:

- All of the different pulse width modulated switching patterns that the inverter produces at various operating conditions were evaluated.
- The control for limiting dc circulating current in the ac output was confirmed to be operational.
- Real and reactive power controls were verified.
- Protection set levels were verified to be as desired.
- Test instrumentation was installed to observe line parallel operation.
- Controls analog data acquisition calibrations were verified.

Initial Line Parallel Testing

The brassboard inverter automatic sequence to line parallel operation was successfully verified. Once the inverter was operating in parallel with the utility line, dynamic running currents and voltages were observed at power outputs up to 100 kW. During this brassboard functional checkout effort, several problems and anomalies were identified and resolved. Of particular significance were the resolution of unstable operation and a blown pole fuse. The unstable operation was due to instability of the synchronizing circuits (which synchronize the

inverter output with the utility line). The synchronizing circuit was unstable because of harmonic distortion in the utility line signal used for synchronization. The problem was resolved by adding an active filter network to the utility line synchronizing signal, which removed the harmonic distortion. The blown fuse was caused by an incorrect thyristor gate drive signal, attributed to a hardware problem. Fixing the hardware problem corrected the gate drive signal.

Further testing revealed problems with the facility dc power supply (used to simulate dc power from the fuel cell stack) and the current sense circuitry in the inverter. The dc power supply was originally limited to 150 kW output at the 190 vdc minimum voltage requirement of the inverter. A variac was installed in the ac feed to the power supply to correct the problem. Voltage spikes on the pole overcurrent protections signal were found to be inadvertently activated. A resistor – capacitor filter was added to the input of the current sensor circuit and shunt leads were relocated to eliminate the noise in the current sense circuitry.

Line Parallel Operation

After correcting the problems noted in the initial line parallel tests, the 200-kW brassboard two–bridge ASCR (Asymmetrical Silicon Controlled Rectifier) inverter was operated over the full power range. Unfortunately, while running at full power (200 kW) in parallel with the utility line, a diode failure occurred within an inverter power switch.

Examination of the failed diode showed the failure to be caused by overcurrent. Investigation of powerpole design, and dynamic tests revealed no problems in the powerpole. Higher–than–expected peak dc voltage switching transients were observed and corrected by changing the dc input filter capacitor wiring arrangement to reduce lead inductance. This change reduced the switching transients by 50 percent. Inverter controls were also investigated, and several anomalies were found and corrected. Once the anomalies were corrected, inverter testing was resumed with no further diode problems.

Operating data over the full power range indicated that operation was stable but part power efficiency was lower than expected. Analysis of the problem showed that incorrect operation of the selective commutation feature was the primary cause. The "selective commutation" feature eliminates unnecessary activation of the power switching pole commutation circuits. Commutation circuits are stored energy circuits required to turn off the main power semiconductors (ASCR's) by applying a pulse of current.

Operation of selective commutation was characterized to determine why selective commutation was not as effective as desired. Circuit operation was observed for 50 kilowatt operation at 229 Vdc input and 239 volts dc input, and for 100 kilowatts operation at 217 volts dc and 228 volts dc input. At the lower voltage levels, selective commutation occurred only 5.5 percent of the time in one 360 degree cycle, versus an anticipated 44 percent of the commutations expected to be selectively commutated. At the higher voltage levels, selective commutation

occurred only 11 percent of the time. Observation of current waveforms determined the reason selective commutation was not as effective as expected was harmonic currents in the output current waveform. Analysis of the output current waveform showed that if the harmonics were removed, selective commutation would operate effectively.

Additional analysis of inverter design was performed to determine how the current harmonics might be eliminated. It was found that adding a small harmonic canceling transformer would have the desired effect. The harmonic reduction transformer was designed, built, and installed on the brassboard inverter to improve the effectiveness of the selective commutation feature. Inverter tests showed that the harmonic reduction transformer reduced harmonic currents and improved operation of selective commutation as predicted. Figures 3.2–8 and 3.2–9 show the difference in pole output current with and without the harmonic reduction transformer, at 50 kilowatt load. The figures show that harmonic current is reduced considerably by the harmonic reduction transformer.

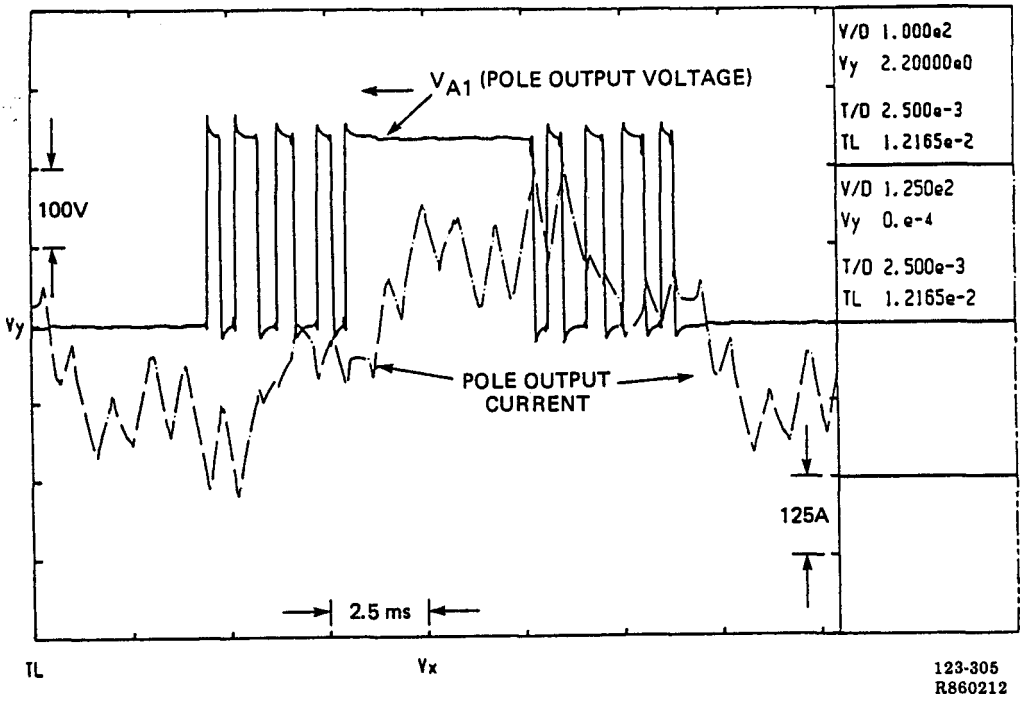

Figure 3.2–8. *Operation With Harmonic Reduction Transformer*

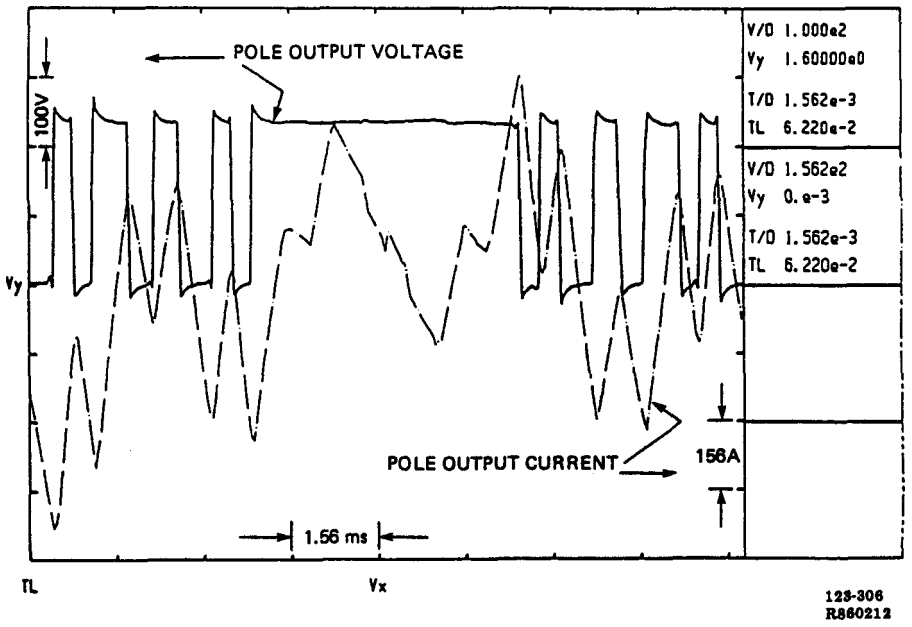

Figure 3.2–9. *Operation Without Harmonic Reduction Transformer*

Performance testing of the brassboard inverter was completed with the harmonic reduction transformer installed. Figure 3.2–10 shows inverter efficiency curve at the end of testing (in May 1985) with optimum selective commutation operation. The optimum operation of selective commutation was achieved by operating at +0.95 power factor at part power. Final measured brassboard inverter efficiency after optimization of selective commutation is 84.6 percent at quarter power and 93.6 percent at full power. Predicted efficiency with an optimized inverter design is 87.6 percent at quarter power and 93.8 percent at full power. The optimized design efficiency can be obtained if lower loss controls, cooling fans, commutation circuits, and an optimized harmonic canceling transformer are installed.

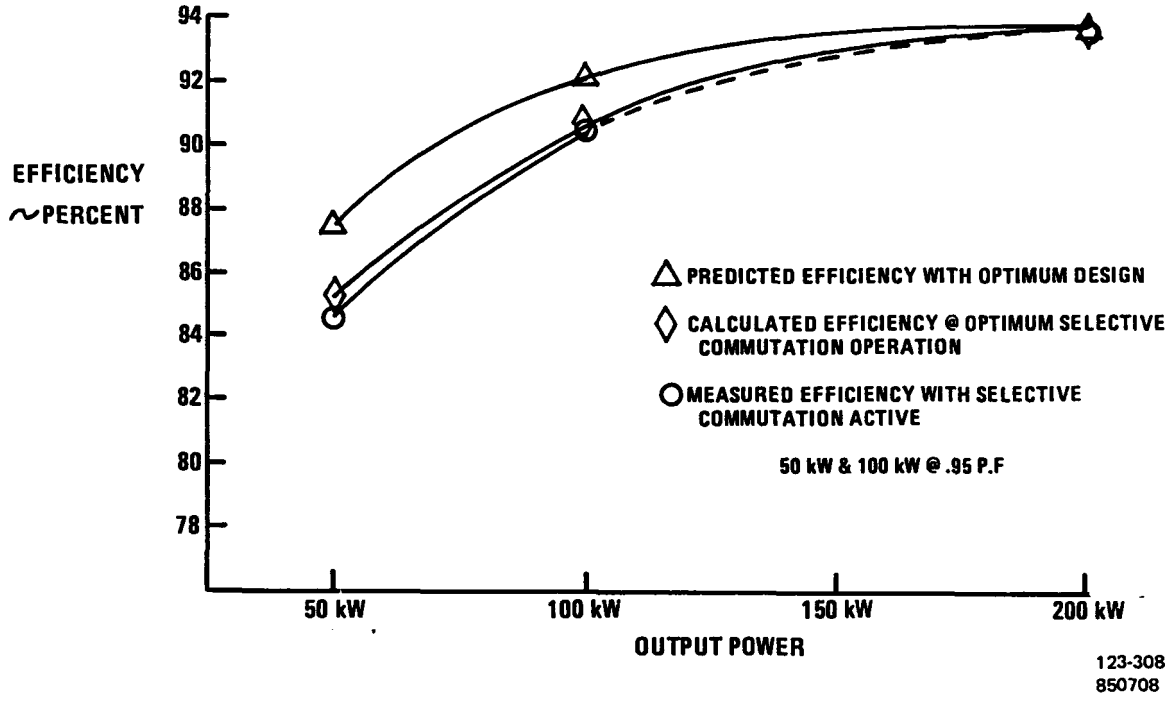

Figure 3.2–10. *Inverter Efficiency*

TASK 4 - HEAT EXCHANGER DEVELOPMENT

OBJECTIVE

The objectives of this task were to define and verify low-cost, high reliability heat exchangers and pressure vessels to be included in the verification test rigs. The approach taken was to survey vendors to identify hardware for the specific power plant applications and to conduct selective component evaluation tests to ensure that low-cost selections reliably meet performance and environmental requirements for the On-Site power plants.

SUMMARY

Eight (8) heat exchangers in the on-site fuel cell power plant were addressed as part of this task. Emphasis was placed on defining simple, low-cost configurations which could provide years of dependable service in a fuel cell power plant. In all cases, suitable units meeting system performance requirements were identified and fabricated for use in the Verification Test Article (VTA).

This task also addressed defining a low-cost configuration for separating steam for the fuel processor from the 2-phase cell stack cooling water stream. An assembly using a pressure vessel as a hot well and a commercial centrifugal separator for final steam separation was defined and fabricated for verification testing.

ACCOMPLISHMENTS/CONCLUSIONS

- A compact heat exchanger assembly which houses all three (3) process fuel heat exchangers (the fuel preheater, steam superheater, and shift converter precooler) was defined and fabricated for the Verification Test Article (VTA)
- An all-welded rippled plate heat exchanger was selected for the burner air preheater in the VTA after performance verification tests.
- A standard, commercial hot well/separator assembly design was selected and built to meet the steam separator function on the VTA.
- A small shell-and-tube heat exchanger was selected and fabricated to reject cell stack waste heat in the VTA.
- A Teflon® - coated tubular heat exchanger was selected and packaged with a demister to remove acid vapor from the cathode exhaust.
- A water recovery condenser core consisting of a stainless steel desuperheating section and a phenloic - coated carbon steel condensing section was fabricated for the VTA after successful subscale testing.

DISCUSSION

Process Fuel Heat Exchangers

The concept of packaging the three process fuel heat exchangers (the fuel preheater, steam superheater, and shift converter precooler) in a single enclosure was developed in the complementary GRI program to reduce the cost, size, and complexity on future on-site power plants. The assembly is called the Integrated Heat Exchanger.

A vendor for Integrated Heat Exchanger was identified, and a purchase order for the unit to be used in verification testing was placed. IFC provided assistance in the enclosure design since the vendor was not familiar with the design of high temperature (1000°F) fuel enclosure. After construction, the tube-sides of the assembly were pressure tested to 500 psig to ensure structural integrity.

FIgure 4-1 shows the Integrated Heat Exchanger received for verification testing. It was assembled and successfully tested with the fuel processor subsystem (subtask 5.4). Unfortunately, the unit was damaged by contaminants in facility water before insertion in the Verification Test Article (VTA). A second integrated heat exchanger was fabricated and successfully used in the VTA without further problems.

(WCN-13725)

Figure 4–1. *Integrated Heat Exchanger Assembly*

Burner Air Preheater

The burner air preheater is designed to recover energy in the reformer exhaust, raising the efficiency of the fuel processor.

Vendor surveys conducted in this program to identify low-cost air preheater designs indicated that standard shell and tube heat exchangers were too expensive for this application. Units designed to regenerate the exhaust gas from boilers and heat treating furnaces were more appropriate.

Four of the candidate heat exchangers for the air preheater application identified in the GRI program were selected for experimental evaluation under this task. In selecting these units an attempt was made to provide a variety of reduced cost heat exchanger types and geometries. This selection provided various options for packaging this unit. The units selected represent tube array, ripple plate, and compact formed plate configurations.

The experimental evaluation program included start-up, design and off-design performance, 100-hour endurance and 100-cycle tests. The 100-hour steady state and 100-cycle tests were performed to provide assessment of structural integrity. Post-test inspections of the heat exchangers were also conducted.

One of the heat exchanger candidates, a rippled metal plate unit, was particularly attractive because it met performance and cost requirements. One drawback to this specific unit was the durability of the ceramic potting that provides the sealing between the hot and cold side streams. An alternate vendor offered an all-welded ripple plate heat exchanger. A full-scale unit was procured and tested to verify performance. Results of the testing are shown in Table 4-1. Heat transfer test performance was slightly short of the goal for the verification rig, the deviation from the performance goal was within the accuracy of the measurement capability of the test set-up and would not affect operability. Figure 4-2 shows the all-welded unit that was selected for the verification test rig.

Table 4-1. Air Preheater Test Results		
	Performance Objective	**Test Results***
Pressure Drop (IWC)		
– Cold Side	1.3	0.20
– Hot Side	0.8	0.32
Heat Duty (BTU/Hr)	49,300	48,752
Effectiveness	68%	67%

* Corrected for change in thermodynamic properties between test fluid and power plant fluid.

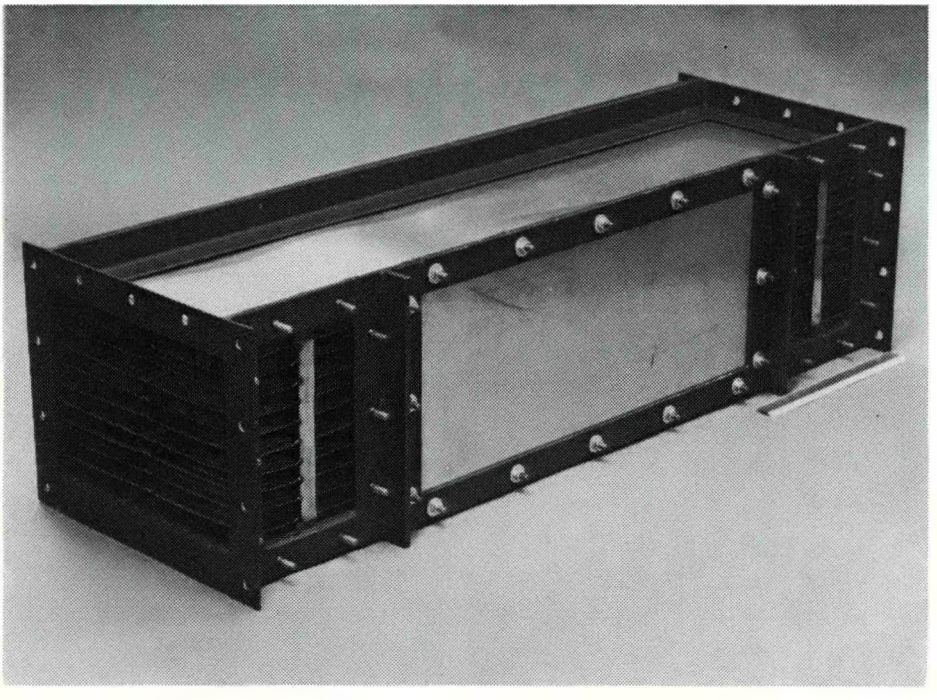

(WCN-13727)

Figure 4-2. *Reformer Burner Air Preheater*

Hot Well/Separator

The function of the hot well and separator are to take the 2-phase stream from the cell stack cooling water exit, provide steam to the fuel processor, and return liquid water to the cooling pump. Previous studies indicated that the lowest cost configuration for the hot well/separator was individual units for the two components rather than an integrated unit. Individual units were sized and procured for use on the verification test rig. Figure 4-3 shows the hot well vessel inverted on a shipping pallet. Additional ports were included on the top of the hot well vessel for instrumentation and inspection during verification rig testing. Figure 4-4 shows the in-line steam separator selected for verification rig testing.

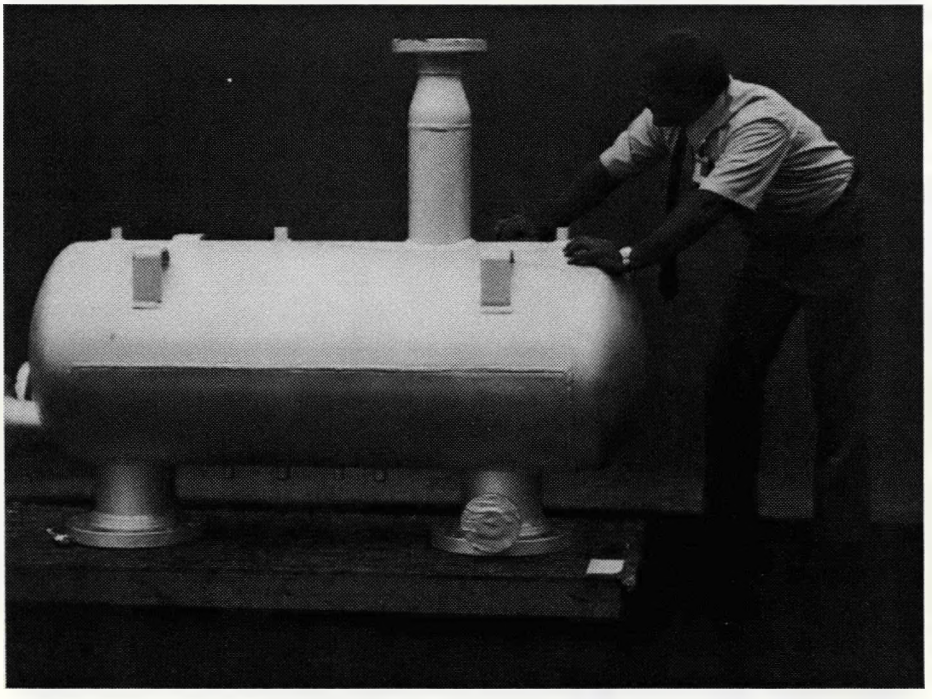

(WCN-13726)

Figure 4-3. *VTA Hot Well Vessel*

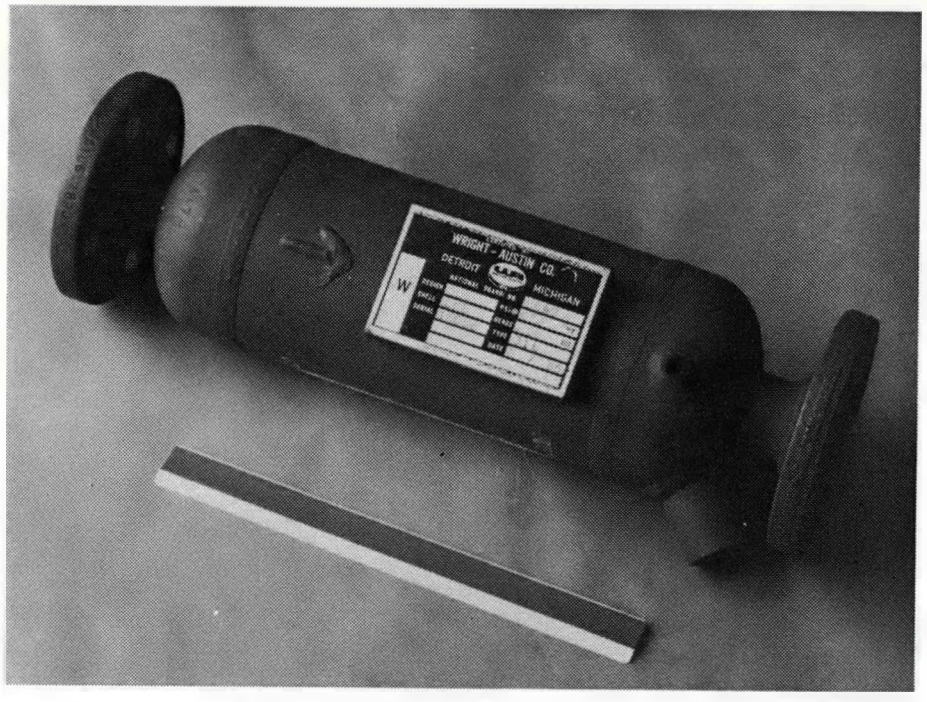

(WCN-13713)

Figure 4–4. *VTA Steam Separator*

Water Recovery Condenser

The water recovery condenser condenses and collects the water from the gaseous exhaust of the Verification Test Article (VTA). The water is used to generate steam for reforming of natural gas. Condensing water from the process exhaust stream enables the VTA (and on–site fuel cell power plants built by IFC in general) to be water self–sufficient.

Previous efforts to identify a low–cost water recovery condenser for the 200-kW power plant indicated that a fined tube core would meet the requirements. To prevent phosphoric acid corrosion, the candidate material selected for the inlet section was stainless steel. Carbon steel with phenolic coating for carbonic acid resistance was selected for the rear section based on subscale material testing.

A subscale condenser was designed and fabricated for testing in conjunction with a short developmental fuel cell stack. Cathode exhaust gas from the stack was passed through the subscale condenser, and the condensate water from the gas stream was used for subscale water treatment system testing. Testing conducted on the water recovery condenser was done without a cathode exhaust regenerator between the cell stack and the condenser.

Figure 4–5 shows the subscale unit on test. Performance of the unit over 2166 hours of test was within predictions.

Tear-down inspection of the condenser cores revealed minor corrosion on the stainless steel inlet section and no corrosion on the following phenolic-coated sections. The rate of buildup of corrosion deposits on the fins of the inlet section was judged to be acceptable for at least a full year of operation under expected power plant operating conditions. Periodic maintenance would entail in-situ washing of corrosion deposits from the fined surfaces of the inlet section.

After the design approach for the water recovery condenser was confirmed by successful subscale testing, a unit was fabricated for the Verification Test Article (VTA).

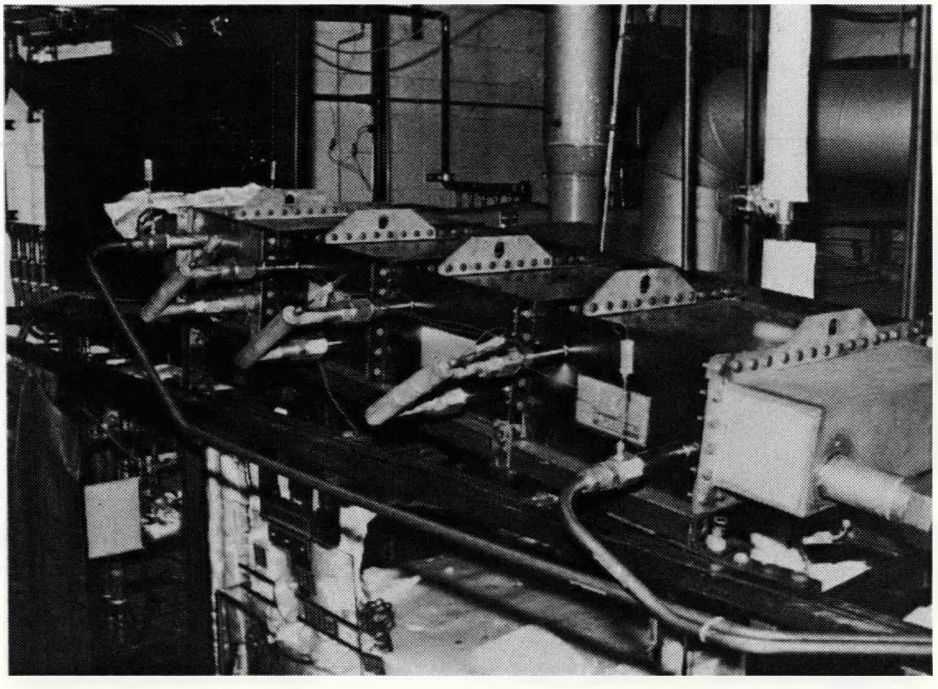

(WCN-13572-21)

Figure 4-5. *Subscale Water Recovery Condenser*

Thermal Control Heat Exchanger

The thermal control heat exchanger is used to reject cell stack waste heat from the cooling water system. Investigation of candidate heat transfer core configurations for the thermal control heat exchanger indicated that the lowest cost, most reliable unit would be a standard shell and tube unit. Selected configuration was a 5–inch diameter by 48–inch long U–Tube unit with the tubes seal welded to the tube sheet to ensure leak tight service. Stainless steel material was selected for both the tube and shell sides of the unit. Figure 4–6 shows a sketch of the unit for the Verification Test Article (VTA).

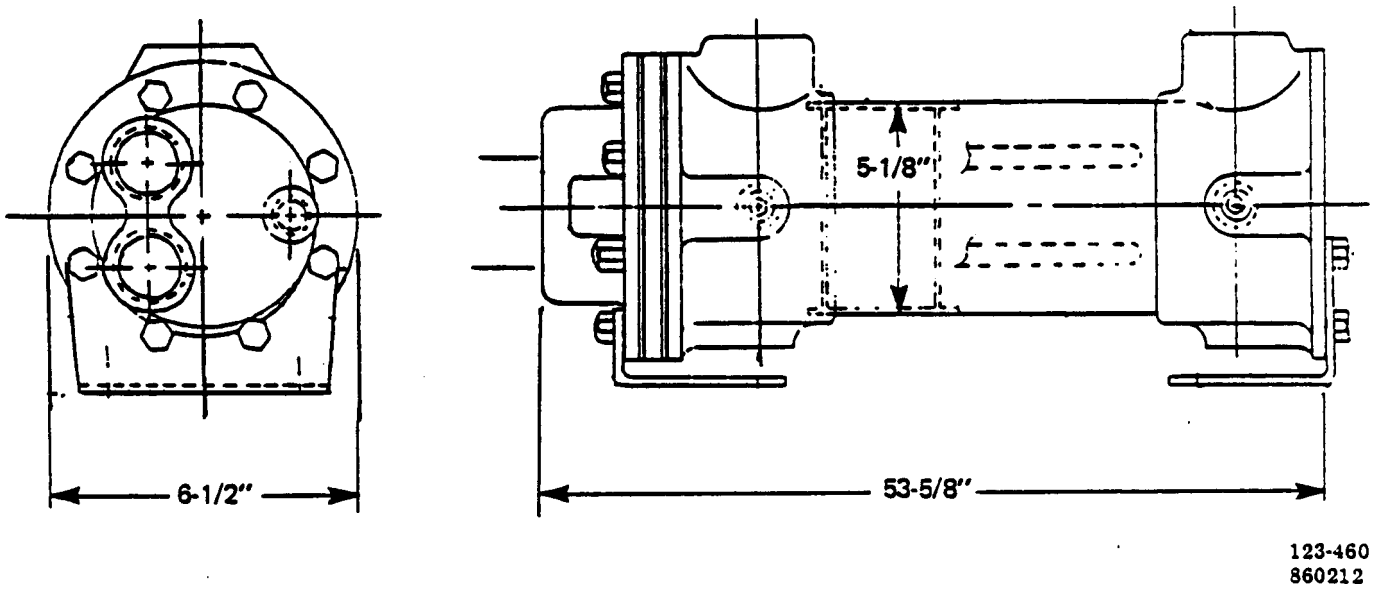

Figure 4–6. *Thermal Control Heat Exchanger*

Acid Condenser

The purpose of the acid condenser is to remove the small amount of phosphoric acid vapor in the cathode exhaust before the exhaust gas enters the water recovery condenser. Various types of component configurations and materials ranging from a Teflon® tube heat exchanger to water spray cooler were considered. Water spray coolers were rejected due to system complexity associated with these configurations, and attention was focused on defining a low–cost, reliable configuration. This effort led to selection of a Teflon® – covered tubular heat exchanger cooled by cathode inlet air flow. A photograph of a prototype core is shown in Figure 4–7. The heat exchanger is called the cathode air regenerator on the Verification Test Article (VTA).

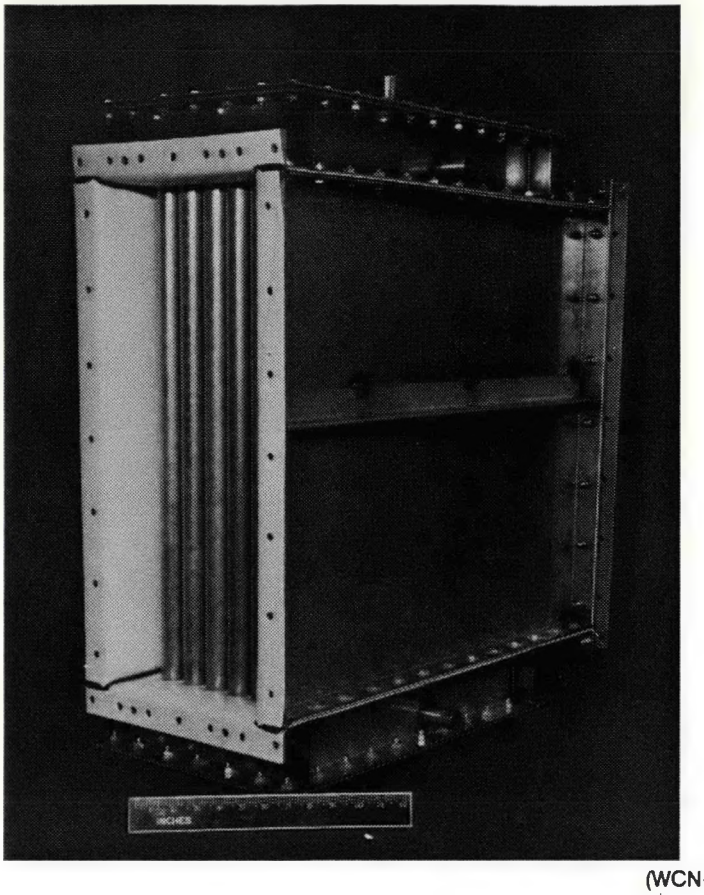

(WCN-10710)

Figure 4–7. *Prototype Cathode Air Regenerator Core*

A sketch of the cathode air regenerator used on the VTA is shown in Figure 4–8. The tubes are aluminum; the tube sheets and side–wall enclosure are made of carbon steel. All surfaces exposed to the cathode exhaust stream that contain phosphoric acid are covered with Teflon®. The size of the enclosure was selected to accommodate an internal acid separator.

The cathode air regenerator was tested successfully on the VTA for approximately 1500 hours of operation. No problems with functionality or material compatibility were encountered. The regenerator was eliminated from the VTA when water treatment analyses indicated the acid condenser function was no longer needed.

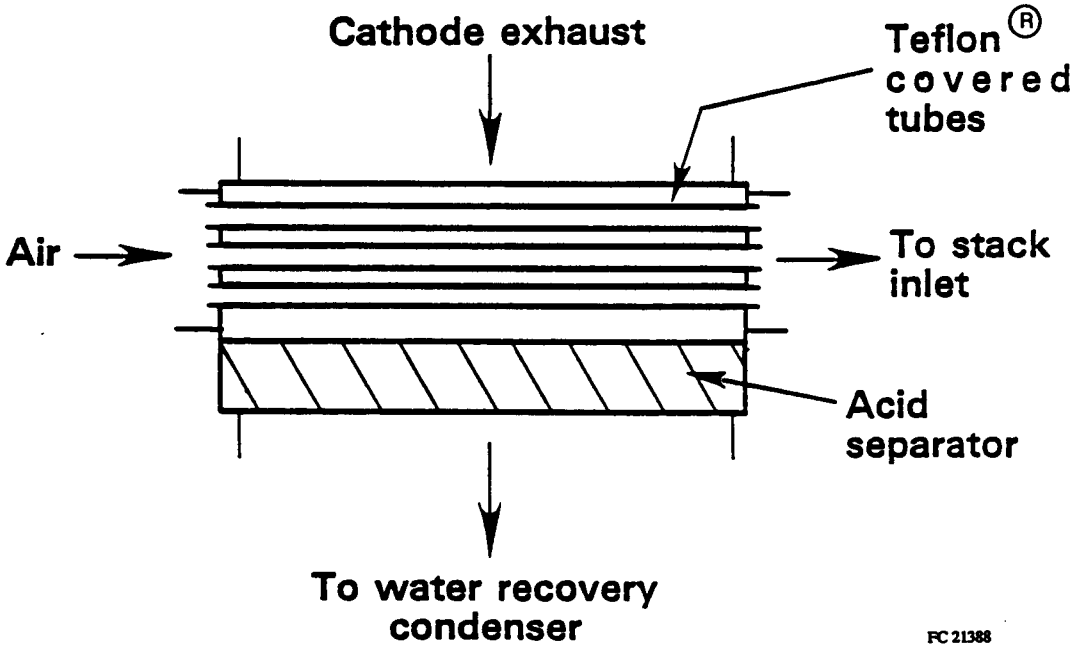

Figure 4–8. *Cathode Air Regenerator Configuration*

TASK 5 - FUEL PROCESSOR DEVELOPMENT

Subtask 5.1 - Develop Fuel Processor Catalyst Technology

OBJECTIVE

The objective of this subtask is to identify hydrodesulfurization and low temperature shift catalysts which minimize the bed sizes and reforming catalysts and optimize the reformer packaging by increasing the allowable tube length without increasing pressure drop.

SUMMARY

Several reforming catalysts were identified which have significantly lower pressure drop than the 40-kW catalyst. Low pressure drop reforming catalyst is important to the design of the 200-kW development reformer because it reduces cost and volume by allowing the required catalyst volume to be packaged into fewer, longer tubes while maintaining low fuel system pressure drop. The catalysts were identified via visits and telephone conversations with catalyst vendors. Of eight candidate catalysts tested, four were found to have performance equivalent to that of the 40-kW catalyst. One of these (HGC-4014) has been selected for evaluation in the endurance test in Subtask 5.2.

An alternative to 40-kW shift converter catalyst was identified. Since the long-term life characteristics of the 40-kW catalyst are already known, this new catalyst was selected for endurance testing in Subtask 5.2.

Conventional hydrodesulfurization catalysts require presulfiding prior to becoming active and are normally operated at several hundred pounds of pressure in order to obtain adequate activity and endurance to completely desulfurize fuel for several years. The desulfurizer previously designed for the On-Site power plant was capable of completely desulfurizing natural gas near atmospheric pressure; however, it was quite large, had a limited life and required expensive presulfiding. Tests run in this task identified a hydrodesulfurization catalyst that does not require presulfiding and is potentially smaller and less expensive than the baseline catalyst. This catalyst (called PSD-12) is a noble metal catalyst manufactured by IFC. It was selected for further endurance testing in Task 5.2.

ACCOMPLISHMENTS/CONCLUSIONS

- A reform catalyst (HGC-4014) was identified having 35 percent of the pressure drop of the baseline 40-kW power plant and same performance. Use of this catalyst will enable reformers to be built with fewer tubes.
- An alternative to the 40-kW shift converter catalyst was identified.
- An alternative to the 40-kW hydrodesulfurizer catalyst was identified. The catalyst can operate at subambient pressures without expensive catalyst presulfiding.

DISCUSSION

Reform, shift converter, and hydrodesulfurizer catalysts were evaluated at 200-kW operating conditions in subscale rigs. The following sections describe these tests and present results.

Reform Catalyst Evaluations

Reformer catalyst testing was conducted in an electrically heated subscale reactor capable of testing catalysts under controlled temperature conditions. The pressure drop and heat transfer effects in this reactor are analogous to those found in full-scale reformers. A diagram of the reactor is shown in Figure 5.1–1. The reactor was 46.5 inches in length and had an I.D. of 1.38 inches. Gas sample taps were located at intermediate positions along the length of the reactor so that the degree of fuel conversion could be determined along the length of the reactor as well as at the reactor exit. The temperature in each of the reactor sections were controlled by separate heaters that could be adjusted to maintain constant wall temperatures for a variety of conditions. A photograph of the reactor installed in the furnace is shown in Figure 5.1–2.

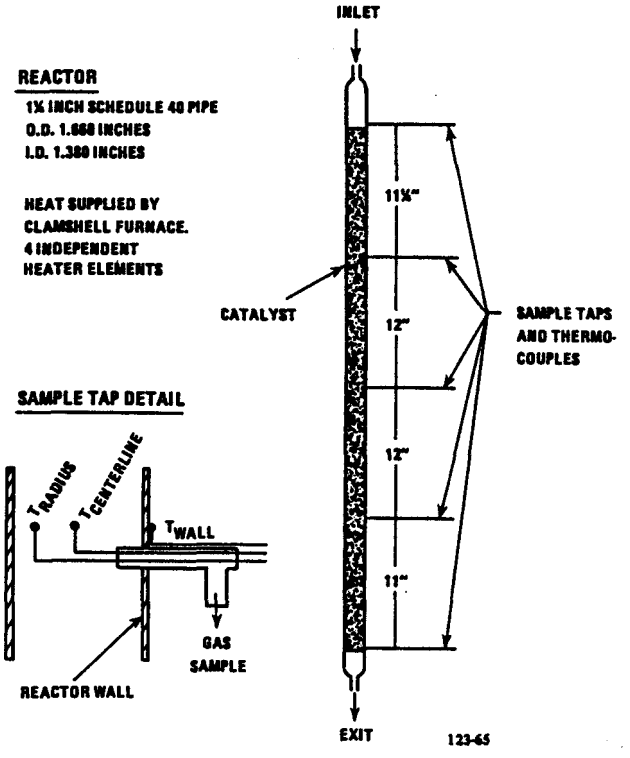

Figure 5.1–1. *Diagram of Subscale Reactor for Testing Reform Catalysts*

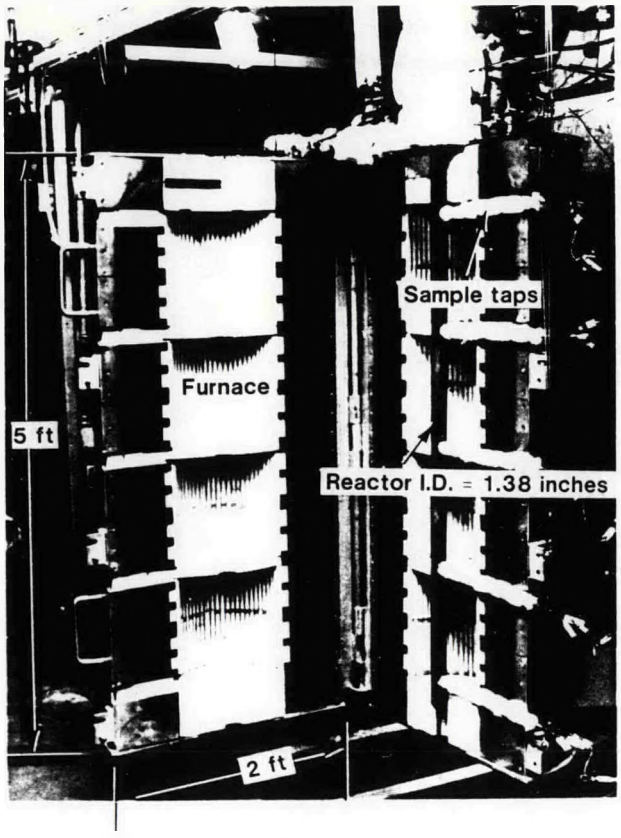

Figure 5.1-2. *Subscale Reactor in Furnace*

A total of eight candidate catalysts plus the 40-kW reformer catalyst were tested. Data is summarized in Table 5.1-1. Figure 5.1-3 shows a comparison of the data for the 40-kW catalyst to three of the most promising candidates. As shown by the data in the figure, varying degrees of pressure drop reduction can be attained while maintaining good reform conversion at the reactor exit. Reforming conversion for these catalysts was also measured at the intermediate gas sample taps along the length of the reactor. The results indicate that there is very little difference in reform conversion between the 40-kW catalysts and the low pressure drop catalysts (Figure 5.1-4). The data presented in the two figures above were taken at a mass flux (lbs. of fuel/hr. per unit reactor cross section) equal to the mass flux used in the 200-kW reformer design. Reactants were fed to the reformer at 650°F and the same reactor wall temperature profile was maintained for all the catalysts with a 1400°F wall temperature at the exit. Tests were also run at more severe conditions where the mass flux was twice that of the present 200-kW design mass flux with the wall temperature raised to 1500°F at the reactor exit. Results of these more severe conditions are also listed in Table 5.1-1. The reform conversions in this table show only a small difference between most low pressure drop catalyst and the 40-kW catalyst.

HGC-4014 has been selected as the reforming catalyst for the endurance test, since its small size permits design of a reformer with a thinner bed than would be possible with some of the other catalysts. The thinner bed minimizes the catalyst volume required.

Table 5.1-1. Performance of Low ΔP Catalysts

Catalyst	Shape	Size	Normalized delta-P (1)	Fuel Conversion (θ) (2) Design Flux	Fuel Conversion (θ) (2) 2X Design Flux	Commercial Experience
40 kW	Pellets	3/16x1/8	1.0	.96	.97	Yes
HGC-2000	Pellets	5/32x3/16	.92	.94	.94	Yes
HGC-1009	Pellets	1/4x1/4	.45	.91	.84	Yes
HGC-4014	Rings	5/16x5/16	.35	.96	.94	Yes
HGC-8001	LPDS	1/4"	.25	.91	—	No-Lab
HGC-2003	Rings	7/16x7/32	.14	.95	.94	Yes
HGC-3011	LPDS Cross-Partioned	3/8"	.07	.94	.92	No-Pilot
HGC-4012	Rings	5/8x5/16	.07	—	—	Yes
HGC-2004	Rings	7/16x7/16	.04	.90	.88	Yes

Notes: (1) Average of hot reform test data at 1 and 2X design flux.

(2) Fuel conversion, $= \frac{CO + CO_2}{CO + CO_2 + CH_4}$

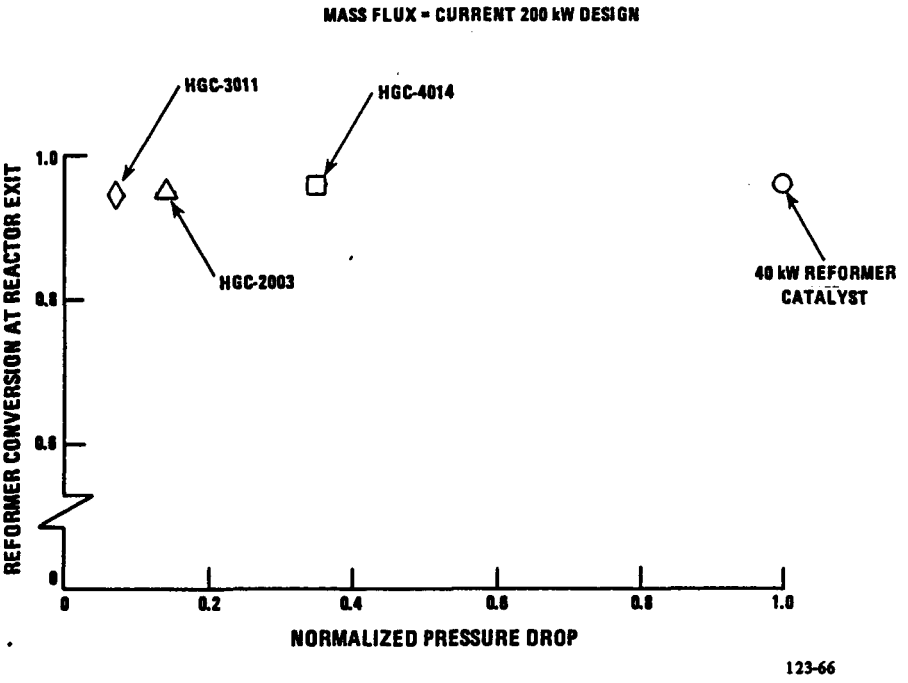

Figure 5.1–3. *Reform Catalyst Performance Comparison*

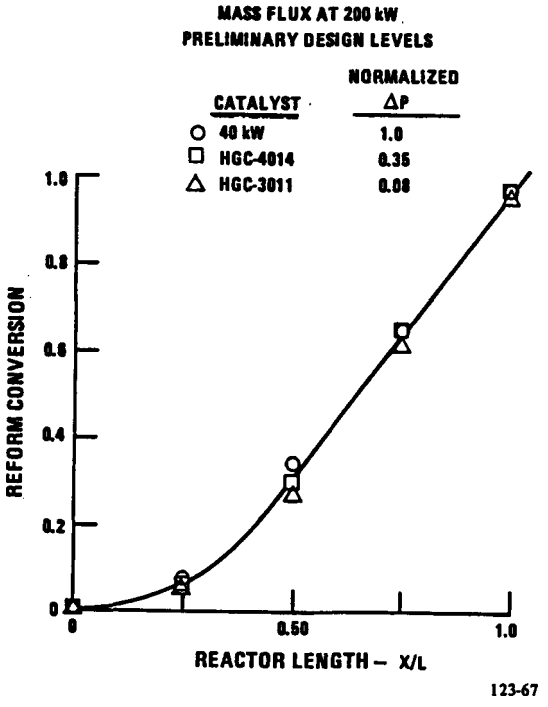

Figure 5.1–4. *Reform Catalyst Performance versus Length*

Alternative Shift Converter Catalyst Identification

At the beginning of this program, there was only one known source for shift converter catalyst having activity comparable to that of the 40-kW catalyst. An effort was made to identify an alternative source for such a catalyst. A vendor whose performance data showed that its activity was higher than that of the 40-kW shift catalyst. For this reason, it was selected for endurance testing in Subtask 5.2. If the claimed performance improvement could be verified at the low pressure conditions used in the 200-kW power plant, then the volume of the power plant shift converter could be reduced.

Hydrodesulfurizer Catalyst Testing

Different hydrodesulfurizer catalysts were evaluated in electrically heated subscale reactors capable of testing catalysts under controlled temperature and pressure conditions. In order to simulate power plant conditions, the hydrodesulfurizer must be operated under vacuum conditions of -1 to -4 psig. A controlled vacuum was obtained by exhausting the hydrodesulfurizer into the suction side of a nitrogen-driven ejector. Catalyst performance was determined by injecting a known quantity of thiophane, a stable sulfur compound used as an odorant, and measuring the conversion of thiophane to hydrogen sulfide at various sample taps along the length of the reactor.

Thiophane was added to the reactor by bubbling a small quantity of reactant gas through a container of thiophane (sulfurizer). A diagram of the test apparatus is shown in Figure 5.1-5. It can be seen from this diagram that the sulfur level in the gas stream was maintained constant by controlling the sulfurizer temperature and pressure. The sulfur level was determined by withdrawing and analyzing a gas sample from the sample tap (shown directly after the sulfurizer back-pressure regulator) but before the simulated shift converter recycle was mixed with the methane. The many heaters and thermocouples installed on the rig allowed control of the catalyst temperature in each of the three catalyst test beds.

The first catalyst tested was a noble metal on alumina catalyst manufactured at IFC and designated PSD-12. Much of the initial testing was used to verify the analytical procedure and ensure reproducibility of sulfur analysis at very low sulfur concentrations. Subsequent tests were run to verify performance for use in the endurance test. Results from this test, shown in Table 5.1-2, verified that PSD-12 was capable of operating in the endurance train. No catalyst decay was observed during over 500 hours of operation, and less than 0.05 parts power million of sulfur was detected exiting the reactor over the range of conditions expected in the power plant.

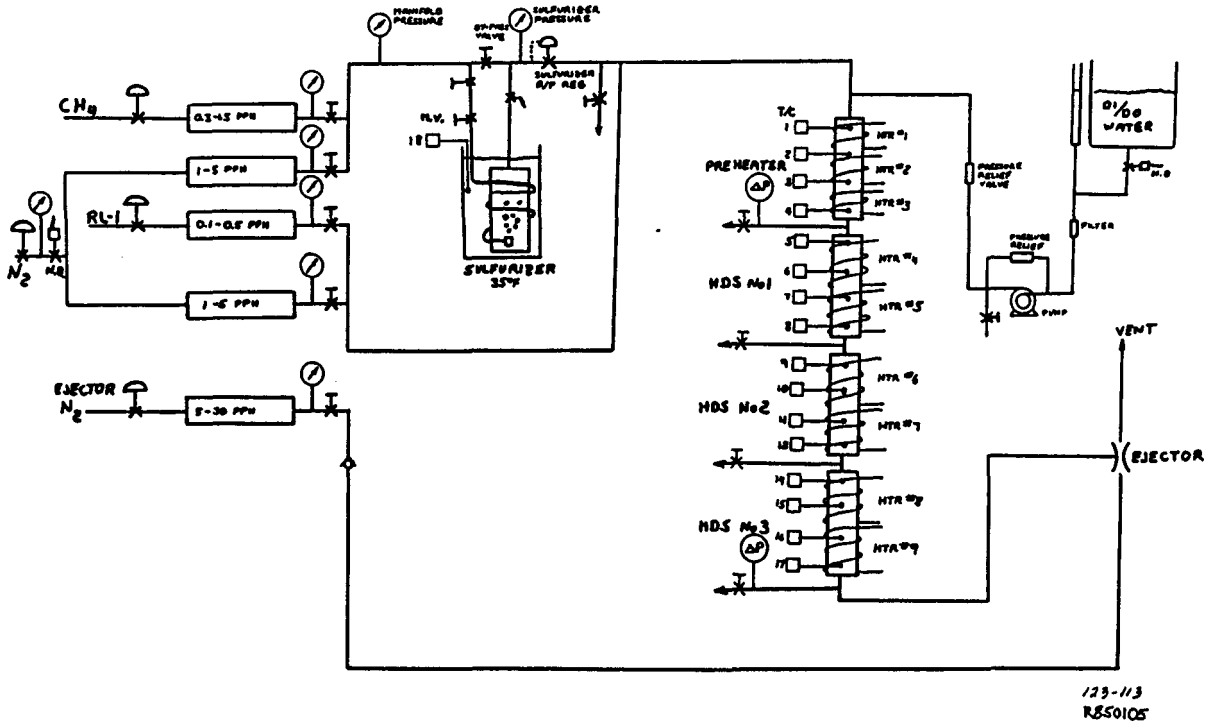

Figure 5.1–5. *Schematic For Subambient Hydrosulfurizer Catalyst Testing*

Table 5.1–2. Hydrodesulfurizer Test Results of PSD-12 Catalyst

Catalyst Weight	0.542 lbs
Fuel Flow	0.81 lbs/hr
Recycle Flow	12%
HDS Pressure	-1 psig

Sulfur Analysis

Temperature	Into HDS	Exit HDS No. 1	Exit HDS No. 2	Exit HDS No. 3
450°F	28.5 PPM	8.8 PPM	1.2 PPM	0.3 PPM
500°F	28.4 PPM	2.5 PPM	< 0.05 PPM	-
550°F	31.8 PPM	1.3 PPM	< 0.05 PPM	-

The second hydrodesulfurizer catalyst tested, PCB-9269, has the potential to further minimize desulfurizer cost and volume. Tests at 500°F and 575°F were conducted with simulated recycle gas varying from 2.5 percent to 12 percent during the over 3000 hours of testing. After 800 hours of testing, the catalyst slowly decayed. No changes in pressure or in recycle rate eliminated the decay, and testing was, therefore, discontinued.

Another commercial hydrodesulfurizer catalyst (PCB-9506), with a potential cost advantage over the PSD-12 catalyst, was evaluated for 1700-hours at 600°F, the minimum temperature recommended by the vendor. Results indicated that a temperature higher than the present minimum recommended by the manufacture was required to obtain the desired performance and life. Since raising the temperature of the hydrodesulfurizer in the present power plant configuration would not provide a cost or system benefit, testing of PCB-9506 catalyst was discontinued.

Based on the catalyst evaluations conducted in this task, PSD-12 hydrodesulfurizer catalyst was selected for endurance testing in Subtask 5.2.

Subtask 5.2 – Fuel Processor Catalyst Endurance Testing

OBJECTIVE

The objective of this task was to verify the durability of fuel processor catalysts identified in Subtask 5.1 and thereby qualify catalysts for use in full-scale fuel processor and Verification Test Article (VTA).

SUMMARY

A subscale fuel processing rig was constructed and tested for over 2000-hours. During this test period, throughput and operating conditions were varied over the entire range expected in power plant operation. Based on successful completion of this test, new reform, shift converter, and hydrodesulfurizer (HDS) catalysts were qualified.

After completion of fuel processing train testing, the subscale rig was modified to conduct extended testing of the new noble metal HDS catalyst, PSD-12. This testing (conducted for over 9000-hours) served to establish benefits in terms of extended overhaul periods and system simplicity associated with the use of PSD-12.

ACCOMPLISHMENTS/CONCLUSIONS

- A new low pressure drop reform catalyst (HGC-4014) demonstrated stable performance over 2000-hours of testing. Use of this catalyst will require fewer tubes in the full-scale reformer (Subtask 5.3) and, therefore, reduce cost.
- An alternative shift converter catalyst operated stably during the 2000-hour endurance test with activity 40 percent greater than the baseline. Use of this catalyst reduces the required catalyst volume by 40 percent.
- A noble metal HDS catalyst (PSD-12) was qualified for use in full-scale rigs based on successful testing for over 9000-hours. As summarized in Table 5.2–1, the new catalyst reduces the projected cost and weight for HDS catalyst, extended the overhaul interval, and simplifies the system by eliminating 50 percent of the HDS controls.

Table 5.2–1. Comparison of HDS Catalysts

	Baseline Catalyst	PSD-12
Relative cost per kW (including activation)	1.0	0.57
Relative weight	1.0	0.4
Overhaul interval	16,000 hours	40,000 hours
Activation	Yes	No
Relative recycle	1.0	0.2
Relative fuel controls required	1.0	0.5

DISCUSSION

Subscale Fuel Processor Catalyst Train

A fuel processor catalyst train using reform, shift converter, and hydrodesulfurizer catalyst identified in Subtask 5.1 was constructed. It was constructed from standard tubing and pipe sections, instrumented for temperature and gas sampling, filled with catalyst, and connected in series. Electrical heaters maintained temperatures similar to those expected in a power plant, and a steam ejector was used to reduce the hydrodesulfurizer pressure to the level expected in a power plant. A schematic of the endurance train is shown in figure 5.2–1 and a photograph showing the actual hardware in Figure 5.2–2.

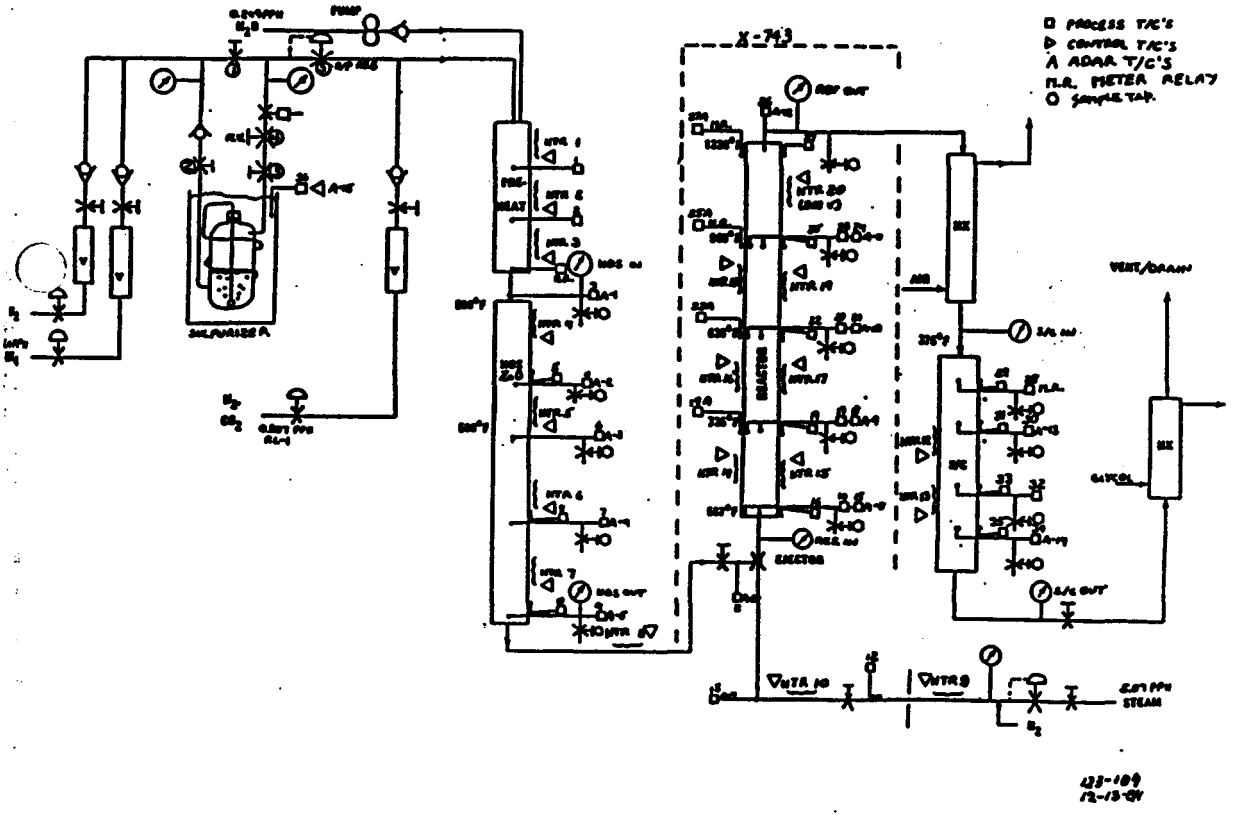

Figure 5.2–1. *Schematic For Subscale Fuel Processor Catalyst Train Test*

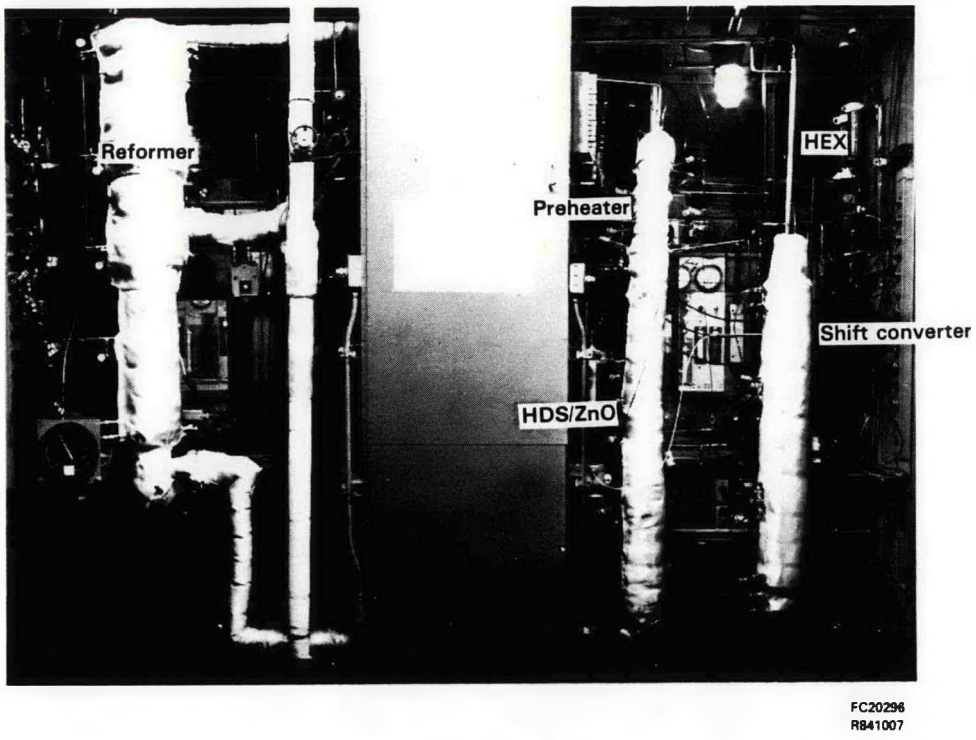

Figure 5.2–2. *Subscale Fuel Processor*

During over 2000 hours of endurance testing, hydrodesulfurizer and low pressure drop reformer catalysts tested in the Subtask 5.1 as well as an alternative shift catalyst, for use in an on-site power plant were qualified. All of the catalysts tested were stable throughout the test and demonstrated the expected activity. Figure 5.2–3 shows shift conversion, reformer conversion, and hydrodesulfurizer exit sulfur concentration versus run time. Performance of all three reactors was steady with time, with undetectable sulfur exiting the desulfurizer for the entire period.

Reformer performance at 125 hours was very similar to the reformer results from catalyst screening tests completed in Subtask 5.1. At 1958 hours, the endurance train reformer bed temperatures were adjusted to exactly match those used in a previous catalyst screening test at 120 hours. Figure 5.2–4 shows that the endurance test catalyst provided slightly higher fuel conversion than the previous catalyst test after 120 hours, indicating very stable reformer performance.

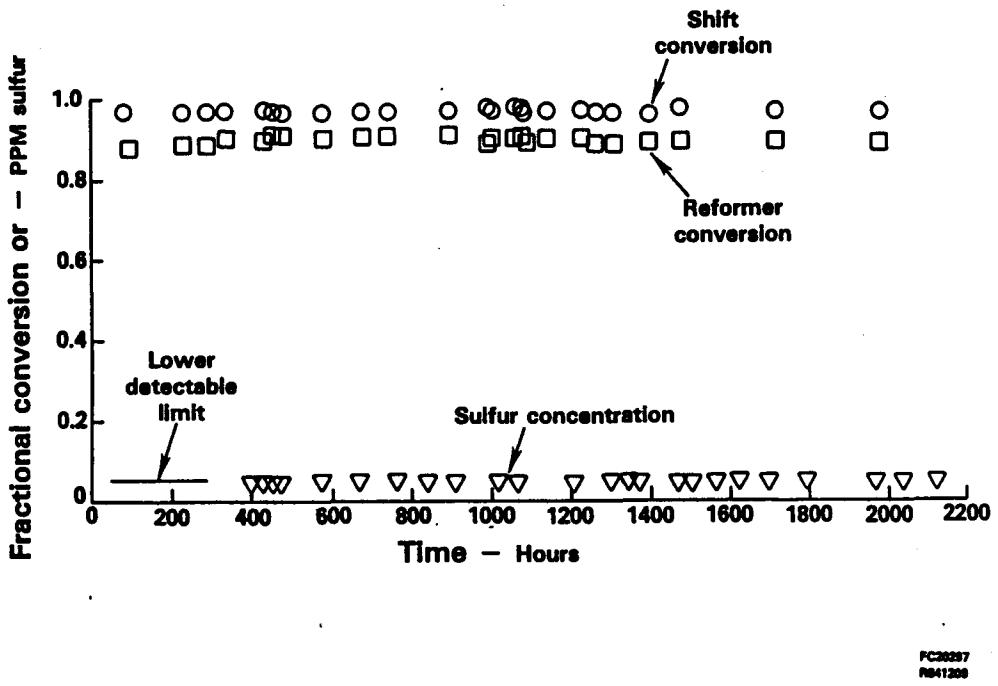

Figure 5.2–3. *Subscale Fuel Processor Performance*

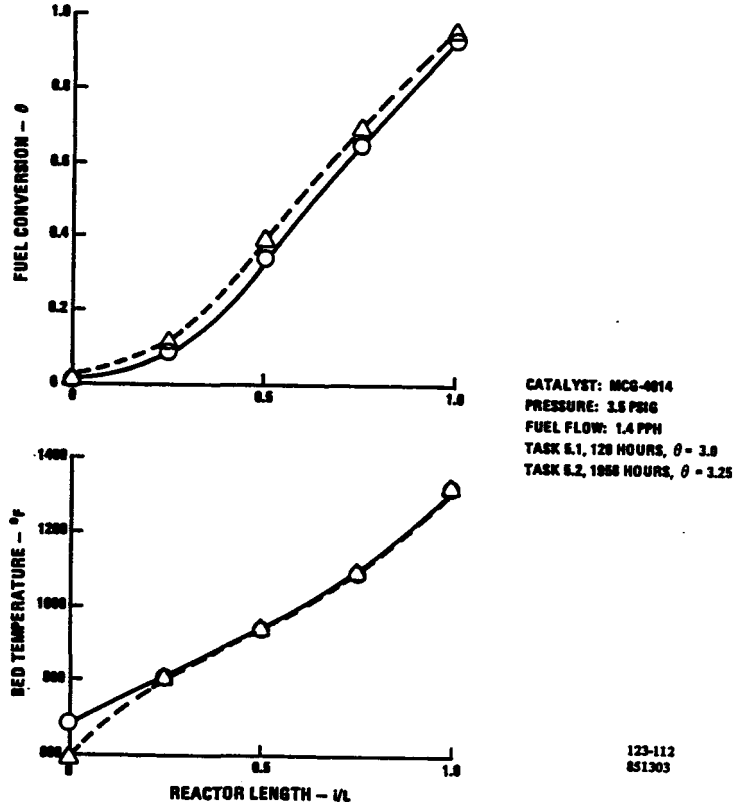

Figure 5.2–4. *Subscale Reform Catalyst Performance Comparison After 120 Hours and 1958 Hours of Operation*

Results of low temperature shift converter catalyst tests indicate that the HGC-4015 shift catalyst is more active than the baseline catalyst. Figure 5.2–5 compares the measured performance obtained at the different shift converter inlet temperatures with the calculated performance computed for an adiabatic bed containing catalyst 1.4 times as active as fresh baseline shift converter catalyst. The measured data follow the predicted performance very closely, indicating that the HGC-4015 catalyst is about 40 percent more active than the baseline catalyst and is more than adequate as an alternative catalyst for the power plant.

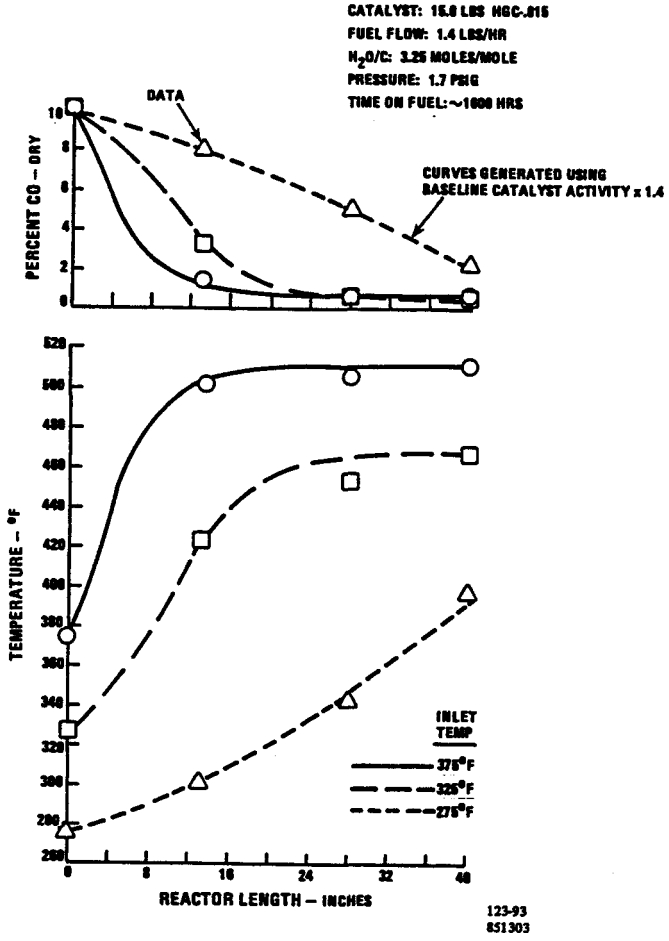

Figure 5.2–5. *Subscale Low Temperature Shift Converter Catalyst Performance*

The PSD-12 hydrodesulfurizer catalyst showed no decay throughout the initial 2077 hours of the endurance test; however, a major upset in performance occurred at 2077 hours when the rig shut down automatically because of loss of steam and a valve failure caused liquid thiophane to leak onto the catalyst. This resulted in poisoning of the reformer and shift converter as well as the hydrodesulfurizer catalyst. Both reformer and shift converter catalysts were poisoned to the extent that they could no longer perform their function; however, the hydrodesulfurizer was still capable of desulfurizing the fuel to less than detectable sulfur levels (less than 0.05 parts per million).

Subscale Hydrodesulfurizer Testing

The rig used for fuel processor catalyst train testing was modified to allow further endurance testing of PSD-12 hydrodesulfurizer (HDS) catalyst. The only changes from endurance train testing were 1) to change the ejector to one with a greater range of secondary fluid pressures, 2) to change the ejector driving fluid from steam to nitrogen, 3) to remove the downstream reform and shift converter reactors. A schematic of the test apparatus in Figure 5.2–6 shows the location of all thermocouples, heaters, and sample tags. The hydrodesulfurizer contained 591 grams of PSD-12 HDS catalyst and 5453 grams of zinc oxide sulfur absorbent, and was fabricated from 3.5 inch stainless steel tubing. The ejector was used to control the subatmospheric pressure of the HDS, and the sulfur level was maintained constant through the use of a sulfurizer that took a small bypass stream and saturated it with thiophane, a stable (difficult to remove) sulfur compound used by some gas utilities as an odorant. Sulfur concentrations were determined by drawing samples from individual sample taps into a Dohrmann Sulfur Analyzer.

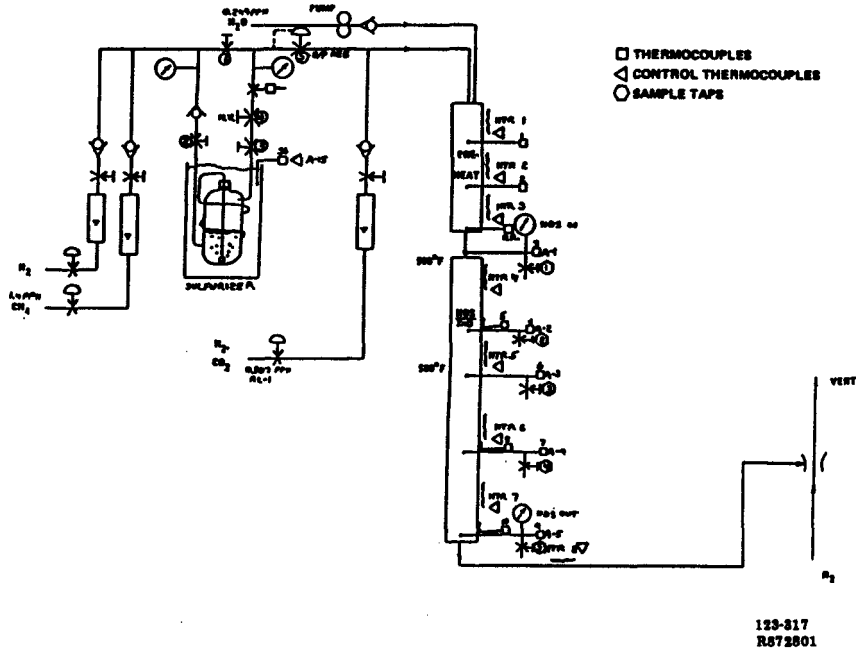

Figure 5.2–6. *Schematic For Subscale Hydrodesulfurizer Catalyts Test*

As shown in Figure 5.2–7, PSD-12 HDS catalyst was evaluated for a total 9267-hours (including the first 2077-hours in subscale fuel processor catalyst train prior to the sulfur upset).

Settings for hydrogen recycle, HDS pressure and temperature were varied over the entire operating range expected during actual power plant operation. Based on successful completion of this endurance test, the catalyst was qualified for use in the full-scale fuel processor test (Subtask 5.4) and the Verification Test Article (Subtask 7.2).

The benefits of using PSD-12 noble metal catalyst over the previous baseline 40-kW HDS catalyst were clear after completing the endurance test:

1. The catalyst activity is stable enough to extend the overhaul interval from 16,000-hours to 40,000 hours with 60 percent less catalyst.

2. The relative cost of PSD-12 is 43 percent less than the 40-kW catalyst (including the cost of activation).

3. The ability of the PSD-12 to operate over wider ranges of temperature, pressure, and recycle enable a simpler control system with 50 percent fewer valves.

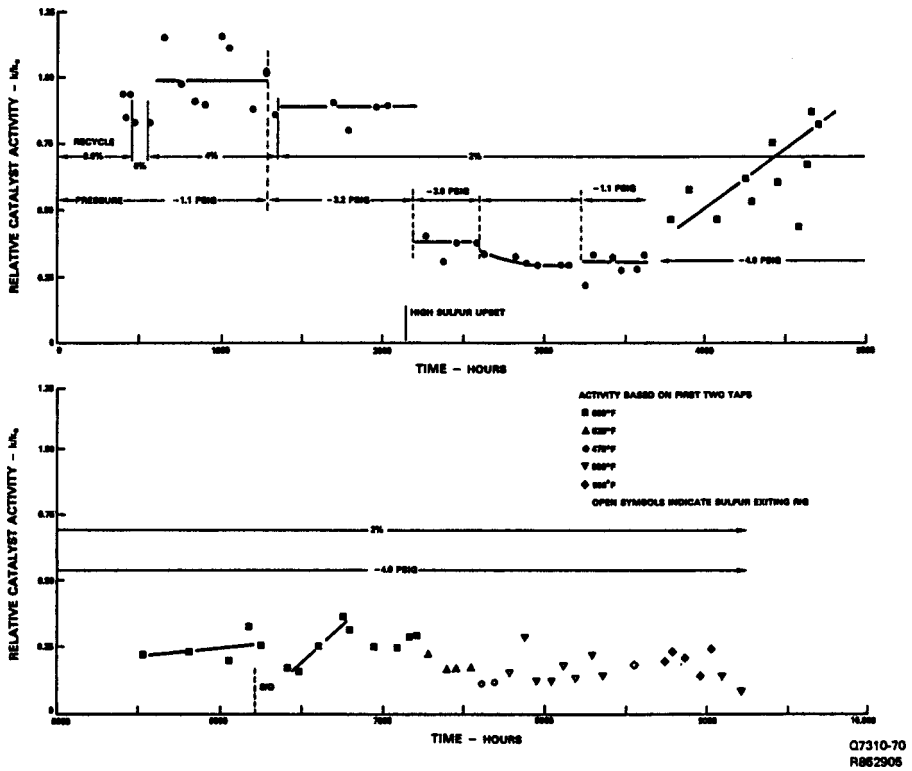

Figure 5.2–7. *PSD–12 HDS Catalyts Performance History*

Subtask 5.3 - Verify Reformer Technology

OBJECTIVE

The objective of this subtask was to fabricate a 200-kW on-site development reformer and to demonstrate the operational capabilities of the assembly before insertion in the full-scale fuel processor assembly in Subtask 5.4.

SUMMARY

A full-size development reformer was fabricated and tested for 708 hours. During the test period, there were 28 thermal cycles to 1000°F or greater. Tests included performance mapping over the full operating range up to 200 kW; full power up-transients from minimum flow to 200-kW; and parameter testing at 200 kW to determine the effects of process steam/fuel carbon ratio, burner air/fuel ratio (ER), process pre-heat temperature, and burner pre-heat temperatures on performance.

After successfully completing the performance tests and a post-test inspection, the reformer assembly was delivered to the full-size fuel processor for further testing.

ACCOMPLISHMENTS/CONCLUSIONS

- Modified a commercial burner and verified it met start and operating requirements associated with the reformer burner.
- Defined an up-fired burner configuration which could distribute flow evenly over reformer tubes.
- Fabricated a full-size 6-tube reformer assembly, corrected burner and insulation deficiencies noted in early testing and added high temperature shift catalyst extra/reform catalyst to improve performance.
- Verified the basic reformer design in over 700-hours of operation.

DISCUSSION

Burner Testing

Initial testing of an industrial burner was undertaken to identify any problem areas that might require modification prior to conducting more comprehensive performance tests. The burner was operated on both natural gas and a low-Btu fuel gas composition to simulate depleted anode exhaust gas. A preliminary assessment of burner ignition, heat release, turndown ratio, flame length, and temperature pattern did not reveal any major problem areas on either natural gas or low-Btu fuel. Burner pressure drop was, however, unacceptably high when burning low-Btu fuel gas due to the larger volumetric flow when operating with this fuel. Based on these test results, it was determined that this burner could not be modified

sufficiently to reduce the pressure drop to acceptable levels. After consultation with the burner manufacturer, a larger burner model was selected that projects to meeting the pressure drop goals.

The larger commercial burner was then procured and installed in the test stand. Modifications were made to the stand to accommodate the larger burner dimensions. In addition, a traverse system was installed to allow rapid measurement of radial and axial temperature profiles. A schematic of the test rig showing the traverse system is shown in Figure 5.3–1 and photographs of the larger burner installed in the stand are shown in Figure 5.3–2. The new traverse system consists of two traversing actuators, each driving five thermocouples.

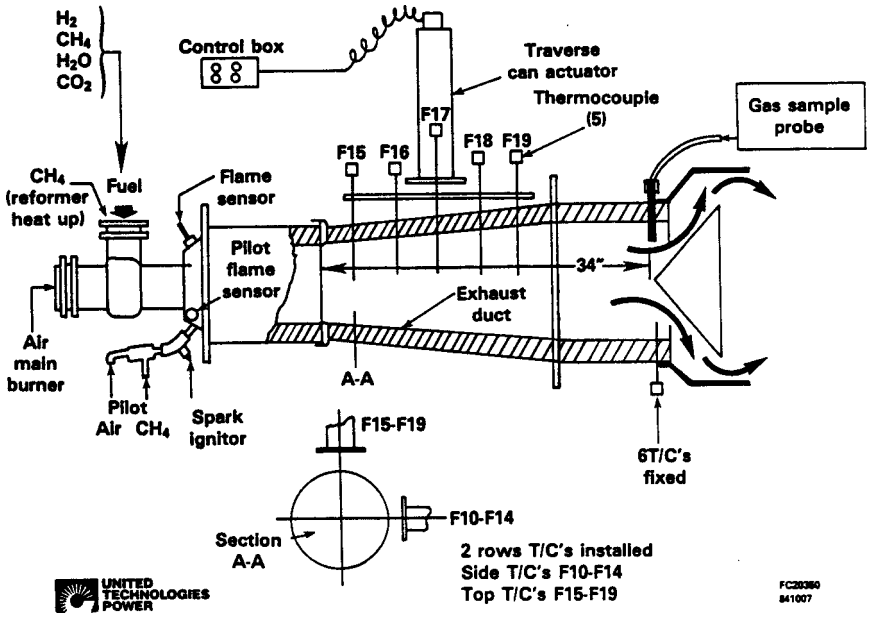

Figure 5.3–1. *Schematic of Burner Test Rig*

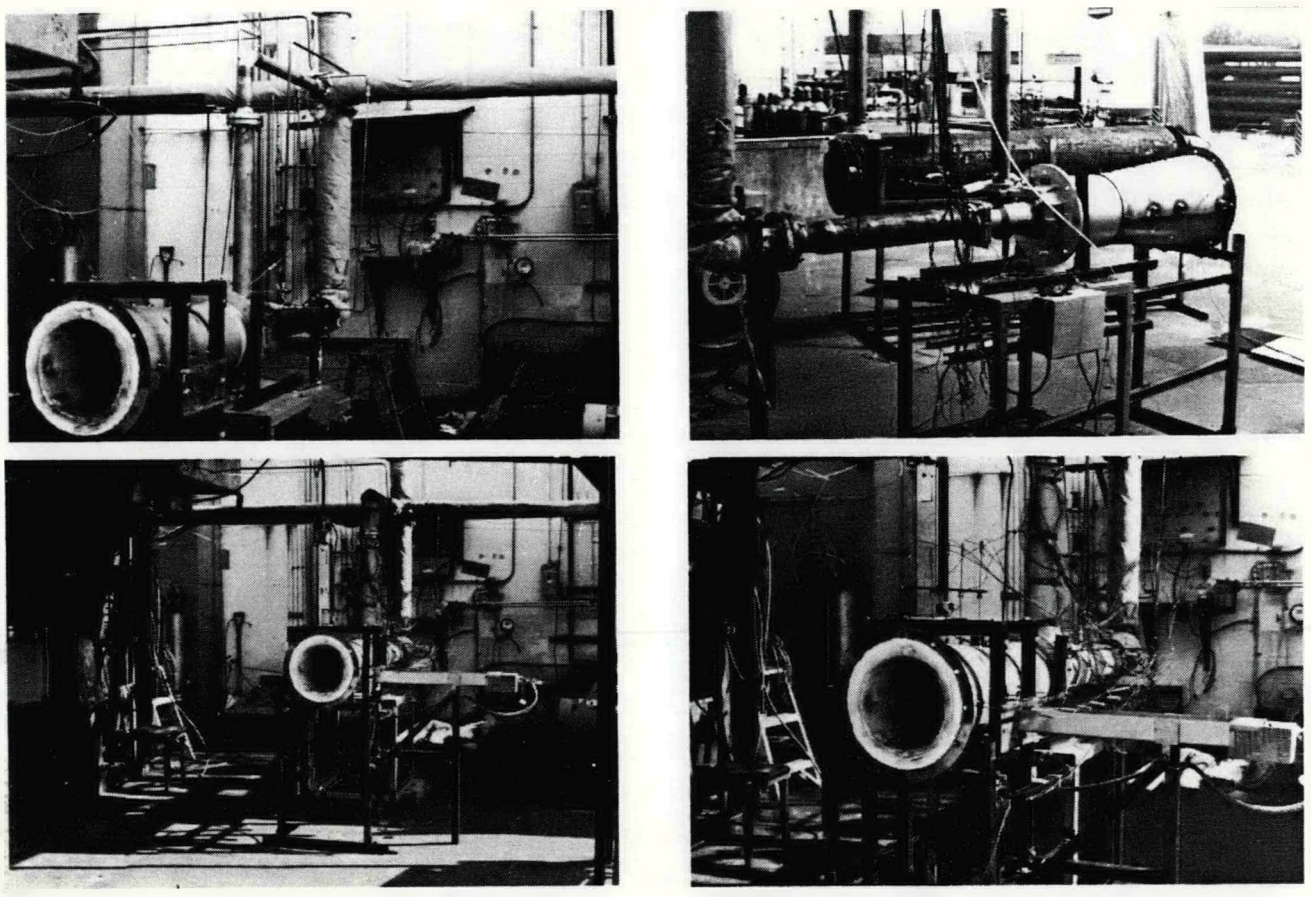

Figure 5.3–2. *Burner Installed in Test Rig*

Burner air and fuel side pressure drop versus power level are shown compared to earlier, smaller burners in Figures 5.3–3 and 5.3–4. At the 100 percent design point, the air side ΔP was 0.45" H_2O and the fuel side ΔP was 0.45" H_2O. Pressure drop data was obtained at both hot and cold flow conditions to assure the validity of the measurements because of the very low pressure drop involved. The data scatter for the burner air side, shown in Figure 5.3–3, is minimal and follows a 2-to-1 slope as expected, except for the lowest flows. The fuel side exhibited more scatter, as shown in Figure 5.3–4. The curve shown on the plot in Figure 5.3–4 is based on both the hot test data and nitrogen data point, which was corrected for the molecular weight difference.

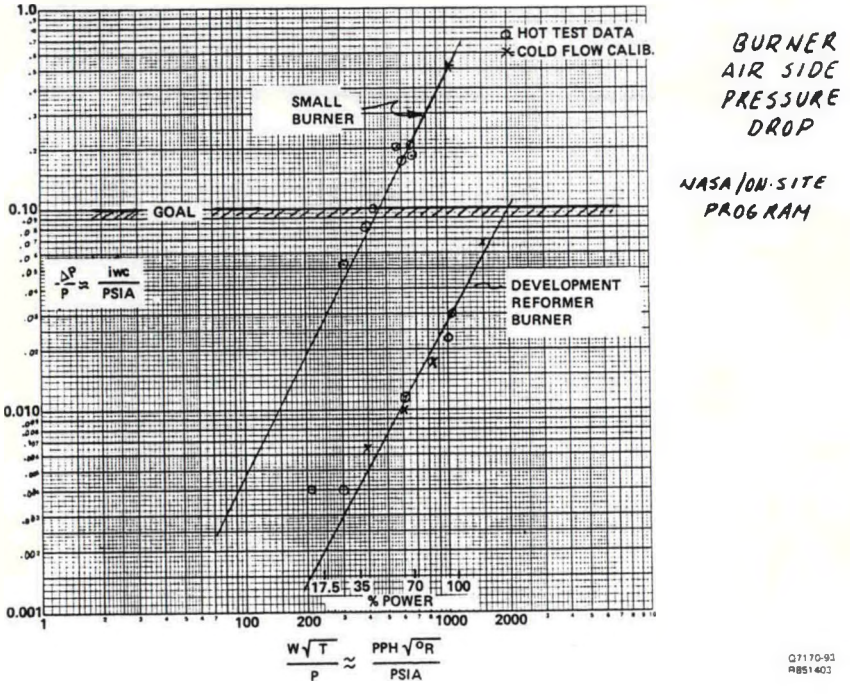

Figure 5.3–3. *Burner Air–Side Pressure Drop Characteristic Comparison*

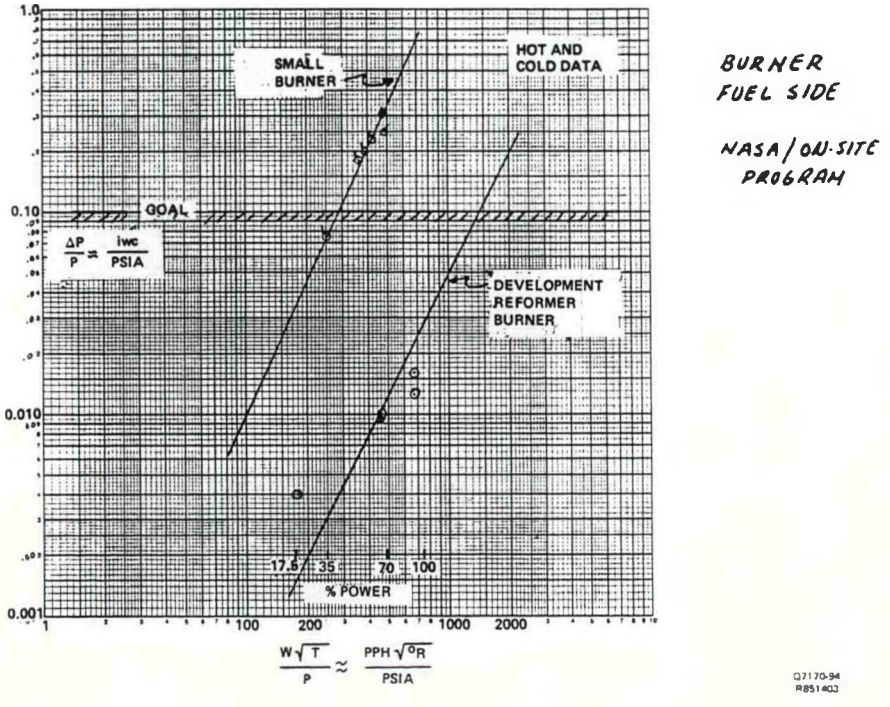

Figure 5.3–4. *Burner Fuel–Side Drop Characteristic Comparison*

Radial and axial temperatures provided at the 200-kW power flows are shown in Figure 5.3–5 for the side thermocouple traverse and in Figure 5.3–6 for the vertical thermocouple transverse. (Refer to figure 5.3–1 for burner rig test set-up). The profiles are similar to those obtained from the smaller commercial burner. Audible and visual characteristics observed at the maximum flow point were excellent. No discernible flame structure was visible, the exhaust being clear and clean. The burner exhibited no combustion noise, such as rumble or oscillations, and the flow appeared to be smooth and steady.

A gas sampling probe was located 34 inches from the burner discharge (shown in Figure 5.3-1) to obtain gas analysis samples to measure burner combustion efficiency. Gas analysis equipment was installed to measure CO using a non-dispersive infrared (NDIR) analyzer and total hydrocarbon as CH_4 using a flame ionization detector. Measurements indicated that burner emissions were unacceptably high.

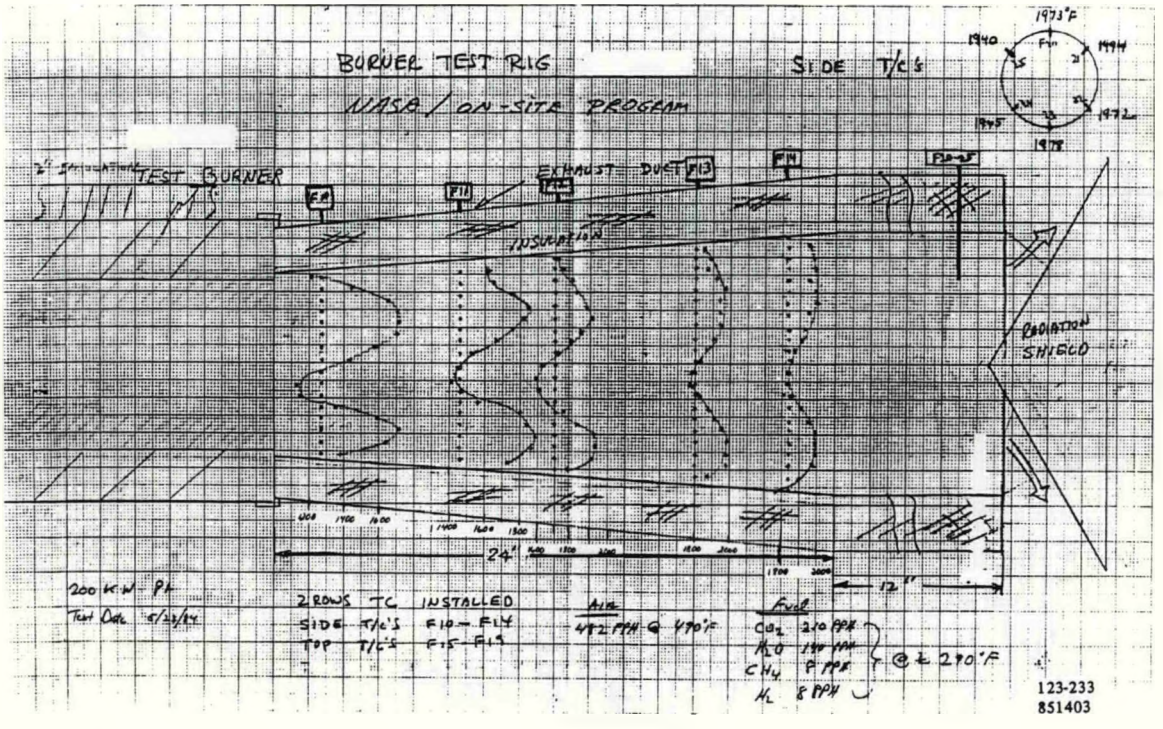

Figure 5.3–5. *Development Burner Temperature Profiles for Side Traverse*

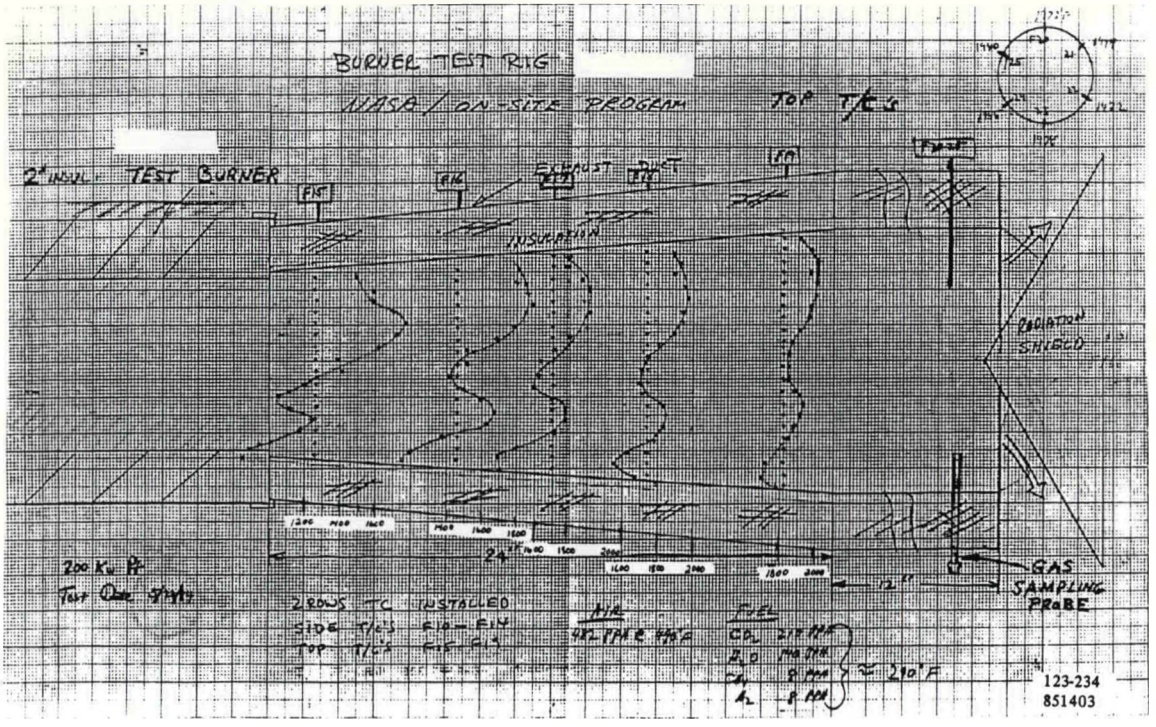

Figure 5.3–6. *Development Burner Temperature Profiles for Vertical Traverse*

The high concentrations of CO and CH_4 indicated that further testing would be required. The first step was to modify the test rig to more closely match the development reformer dimensions and heat loss. A schematic of the revised test rig is shown in Figure 5.3–7. The exhaust duct is internally insulated, has a 9" diameter, and is 72" long, duplicating the geometry of the burner gas path in the burner sleeve of the 200-kW development reformer. A radiation shield and deflector assembly was installed at the back end of the duct to reduce thermocouple radiation losses. The presence of high levels of unburned CO and CH_4 in the exhaust of the burner "as is" (called mod 1) were then reconfirmed in the modified test stand.

Two modifications of the burner were then evaluated to lower the emissions. As shown in Figure 5.3–8, each of the modifications (called mods 2 and 3) progressively lowered emissions with the mod 3 burner design producing acceptable results. Measurements taken at three radial points in the exhaust duct of mod 3 showed no more than 70 ppm CO and no measurable CH_4.

Operation of the natural gas start torch and burner were also found to be acceptable with burner mod 3, and the duplicate burner for the development reformer was procured and modified.

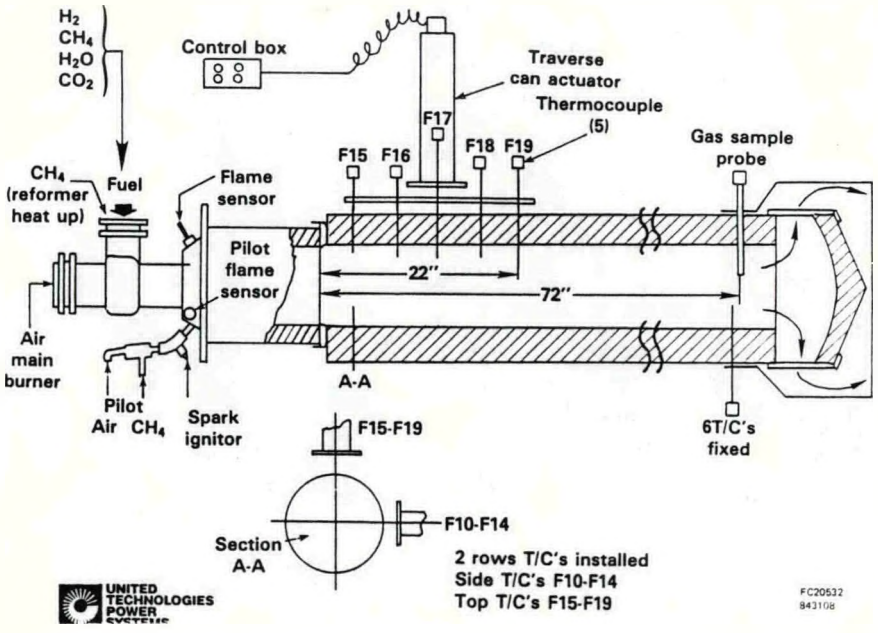

Figure 5.3–7. *Modified Burner Test Rig*

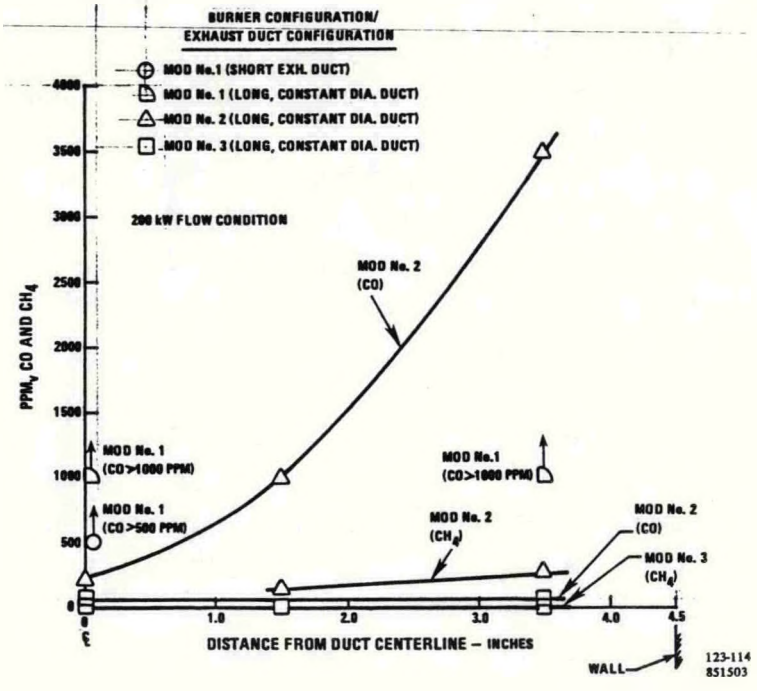

Figure 5.3–8. *Burner Emissions Reduction*

Water Table Testing

Visual flow testing was initiated on a water table using a two-dimensional model representation of the 200-kW development reformer burner configuration. The objective of these tests was to define an acceptable burner gas flow path geometry within the burner cavity to provide uniform burner gas flow and, therefore, maintain uniform reformer tube temperatures.

Water table testing of a two-dimensional model of an early version of the up-fired development reformer burner cavity indicated that more flow was going to the outer diameter than the inner diameter. The flow pattern obtained during this testing is shown in Figure 5.3–9.

Modifications to the up-fired burner gas path were tested to improve the balance between the inner and outer flow paths. The results of this showed that shortening the burner riser was beneficial. See Figure 5.3–10. The development reformer design was modified to permit easy adjustment of the burner riser height to facilitate fine-tuning required to obtain acceptable tube temperature uniformity.

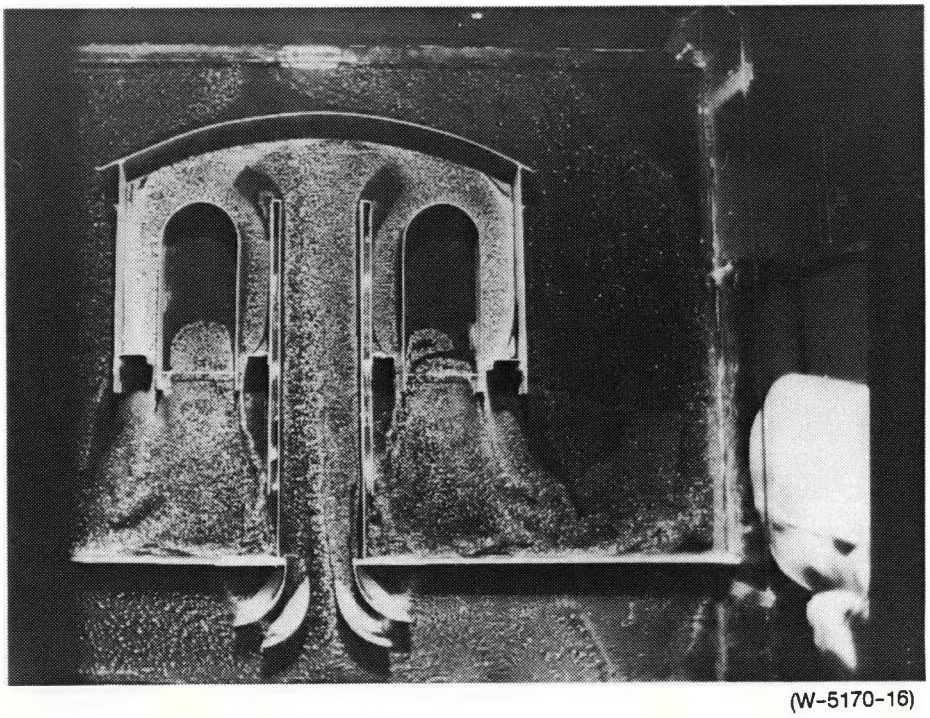

(W-5170-16)

Figure 5.3–9. *Flow Pattern in Reformer Burner Cavity with Original Riser*

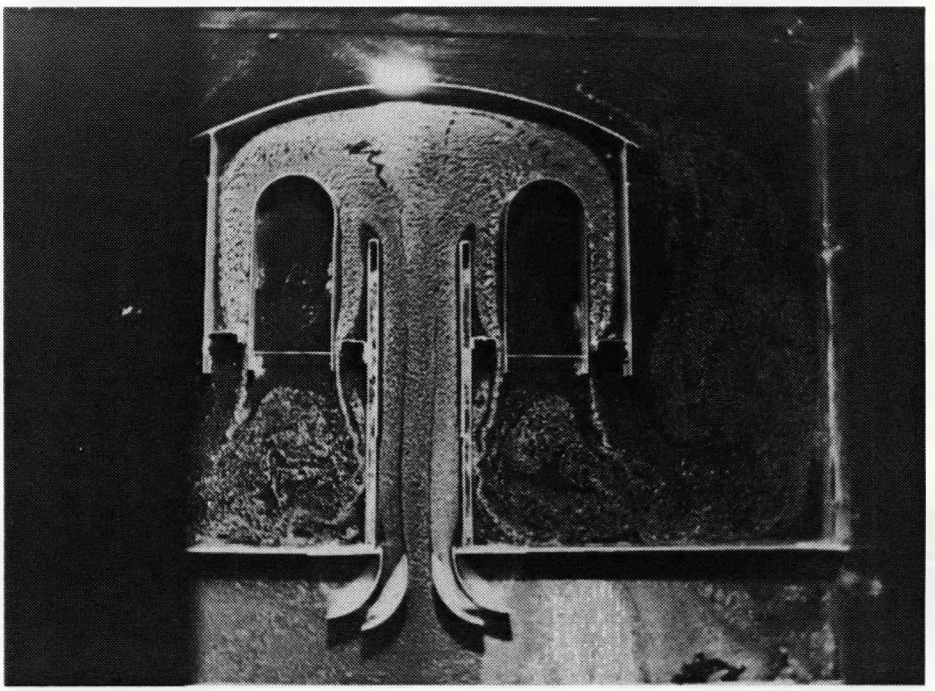

(WO-1298)

Figure 5.3-10. *Flow Pattern in Reformer Burner Cavity With Riser Shortened*

A water table model of a down-fired configuration was also evaluated. The flow patterns showed very little expansion from the inlet. Jet flow persisted all the way to the top of the middle tube, which then acted as a flow deflector. The flow pattern also showed two large recirculation zones on either side of the center tube. Modifications to improve the flow distribution would require either a much shallower dome angle (probably 10°) resulting in an undesirable reformer height or physical flow deflectors, which would present durability problems in the hot exhaust stream. No further effort was conducted on this configuration, and only the up-fired burner was used in the development reformer.

Development Reformer Fabrication

The 200-kW development reformer fabrication was completed in 1984. The design of this reformer was provided under a parallel GRI-sponsored contract. The selected design consists of six tubes. The tubes are heated by a single industrial burner. A summary of the 200-kW development reformer design is compared to the 40-kW power plant reformer in Table 5.3–1.

Table 5.3–1. Summary of Development Reformer Design

	40-kW Reformer	200-kW Development Reformer
Number of Tubes	4	6
PPH Fuel Processed/Tube	4.5	15
PPH Natural Gas Processed Per Square Foot Tube Surface	1.0	1.2
Tube Material	Wrought 310 S. Stl	310 S. Stl Pipe
Catalyst Size	0.7" Dia. x .14" Long	.31" D x .31" L .13" Hole
Burner Type	6 Fuel/Air Nozzles Per Reformer Tube, Separate Natural Gas Start Nozzles	Single Burner For Start And Steady State
Heat Transfer Enhancement	Lower Metal Sleeves With 1" Ceramic Balls in the 1.75" Gap	Ceramic Sleeves
Package Dimensions	36" Diameter x 49" High	56" Diameter x 10' High

The major sheet metal parts of the reformer (tubes, dome, cylinder, and skirt) are shown during fabrication in Figure 5.3–11. The reformer tube subassemblies, process inlet and exhaust manifolds, and pigtails were welded and heat treated to relieve stresses. The low pressure drop catalyst was loaded into the reformer tubes, and the tubes were individually flow checked using nitrogen to assure uniform process gas flow distribution. The caps were welded to the reformer tubes, and the entire process side of the reformer was successfully pressure checked for leaks. The completed tube-manifold assembly was mounted on the reformer

support structure and transporter cart, and the lower tube thermocouples and skirt were installed. The burner gas cylindrical shell and dome were then lowered on the assembly, and the burner was installed. The completed reformer assembly is shown in Figure 5.3-12.

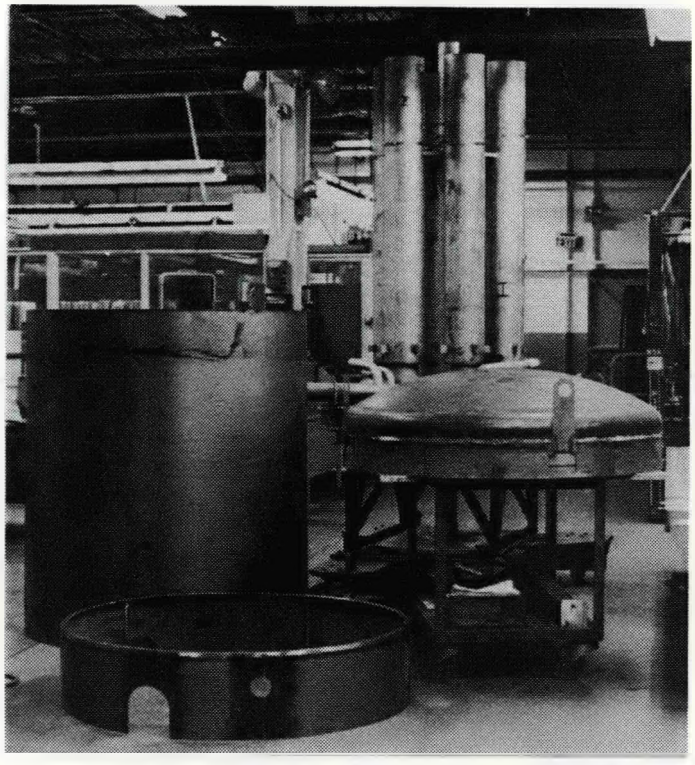

(WCN-13063)

Figure 5.3-11. *Development Reformer During Fabrication*

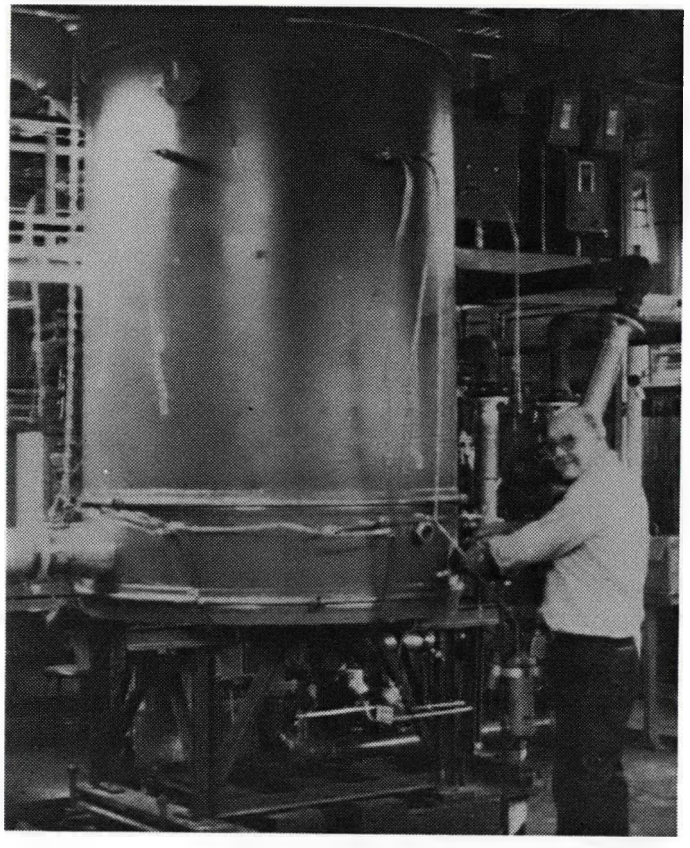

(WCN-13252)

Figure 5.3–12. *Completed Development Reformer Assembly*

Facility Modification

During 1984, the 200-kW development reformer test facility was designed, and construction was completed. All gas delivery systems, piping, heaters, controls, and thermocouples were installed. Final stand checkouts of these items and the hookup automatic data acquisition and retrieval (ADAR) system were completed prior to test startup in 1985. A schematic showing the development reformer test facility requirements is shown in Figure 5.3–13. An elevation drawing of the test facility is shown in Figure 5.3–14.

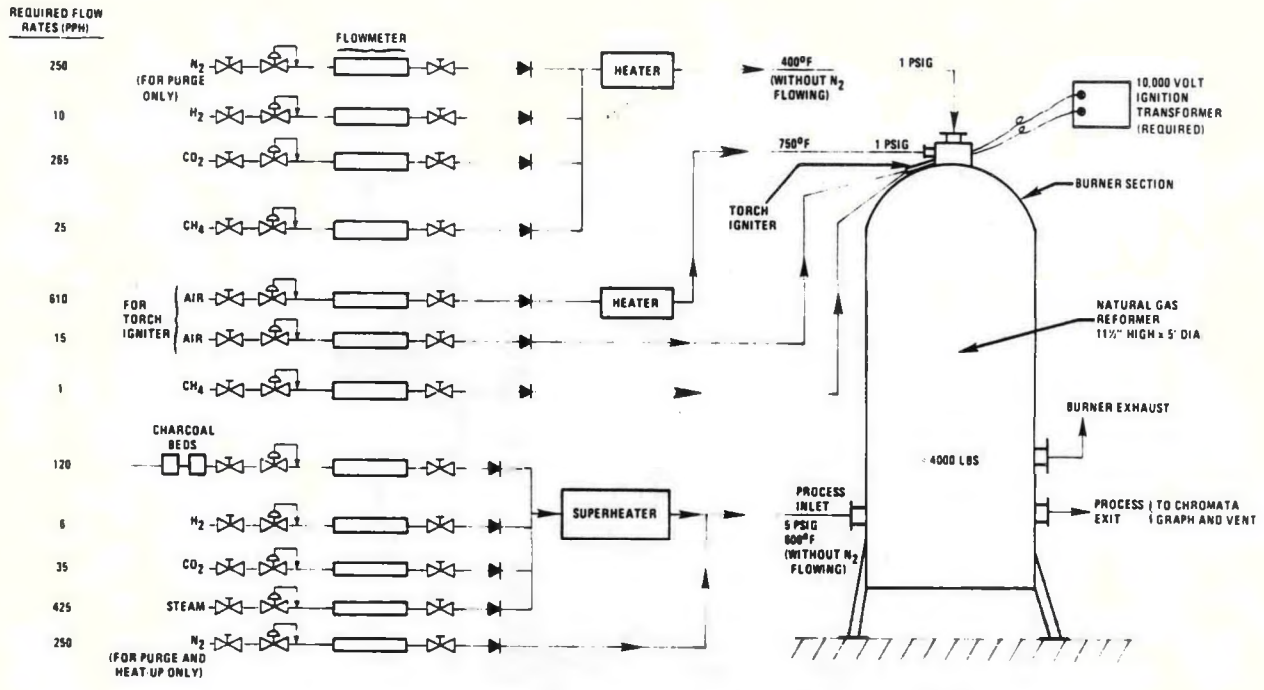

Figure 5.3–13. *Schematic For Development Reformer Testing*

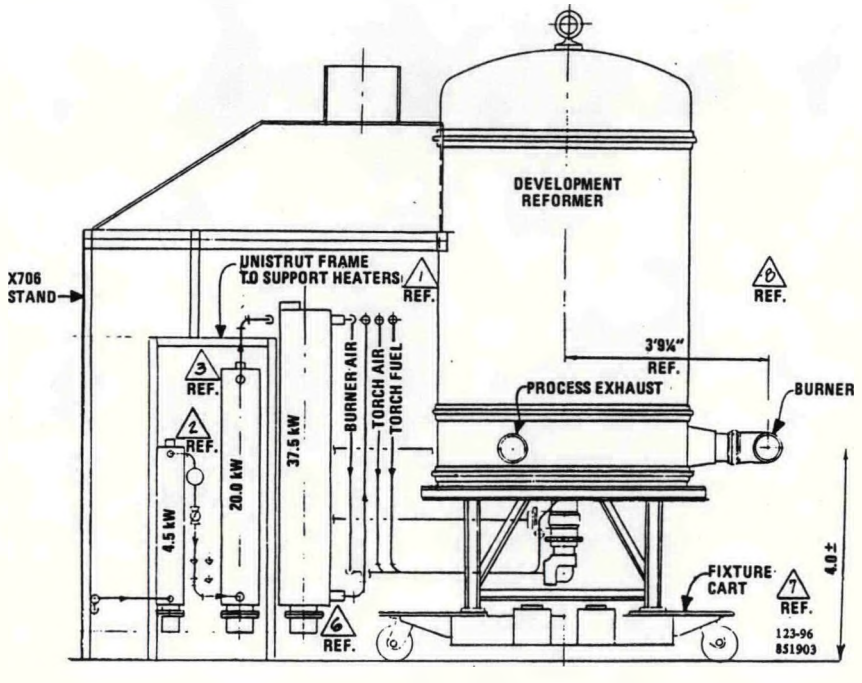

Figure 5.3–14. *Elevation Drawing of Development Reformer Test Facility*

Initial Reformer Testing

Initial testing of the 200-kW development reformer indicated several problems with the reformer burner. Each of these were addressed and corrected as follows:

1. Burner temperatures during startup and steady-state operation exceeded the manufacturer's long-term temperature rating limit of 750°F. A replacement burner rated for long-term operation up to 1000°F was purchased and installed. Both burners are shown in Figure 5.3–15. The burner casting was also changed from 304 to 310 stainless steel to provide long-term corrosion resistance.

(WCN-13573-18)

Figure 5.3–15. *Original and Upgraded Reformer Burners*

2. Occasional flameouts were experienced during startups as air preheat temperature increased. A burner modification that improved stability was fabricated and checked out on the burner test facility. The burner ignition and stability envelopes are shown in Figure 5.3–16 for 60°F air and air preheated to 500-600°F after burner modifications were completed.

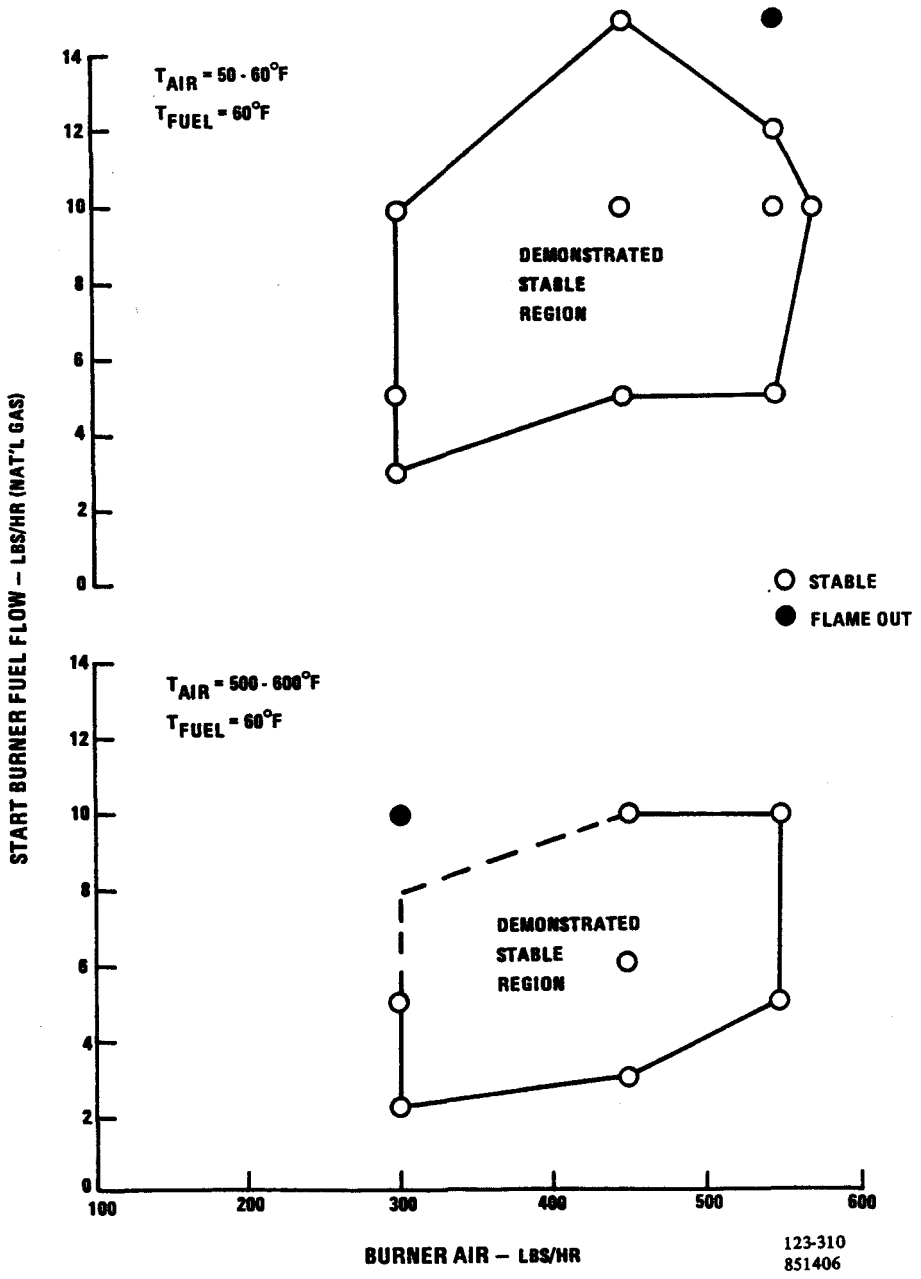

Figure 5.3–16. *Burner Operating Envelopes After Modifications*

3. The burner flame sensor (flame rod) signal on simulated anode gas fuel became too weak for reliable operation with the flame controller unit. The flame sensing deficiency was corrected by incorporating a more sensitive (ultraviolet) detector in a location where it would "view" a larger volume of flame.

After completing the development activities described above, reformer burner operation and stability improved significantly, and activities focused on testing the reformer. As shown in Figure 5.3–17, the reformer heatup was typically accomplished in 2-1/2 hours, and operation over the full power range was demonstrated.

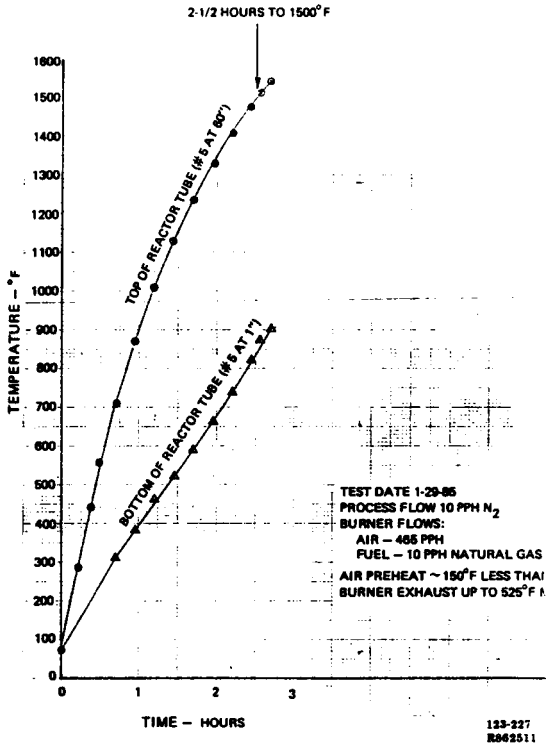

Figure 5.3–17. *Development Reformer Heatup*

Reformer Modifications

After 168-hours of operation, the reformer was shutdown for inspection. The following items were found and corrected:

1. The hot face insulation in the reformer dome had begun to erode and tear in the area surrounding the splash plate. The insulation was upgraded by the addition of a 1-inch-thick layer of insulation board to the hot face. A close-up view of the upgraded insulation is shown in Figure 5.3–18.

2. A small weld crack was repaired at the base of a thermocouple penetrator. Additional smaller leaks in the lower and middle vessel closure clamp seals were corrected.

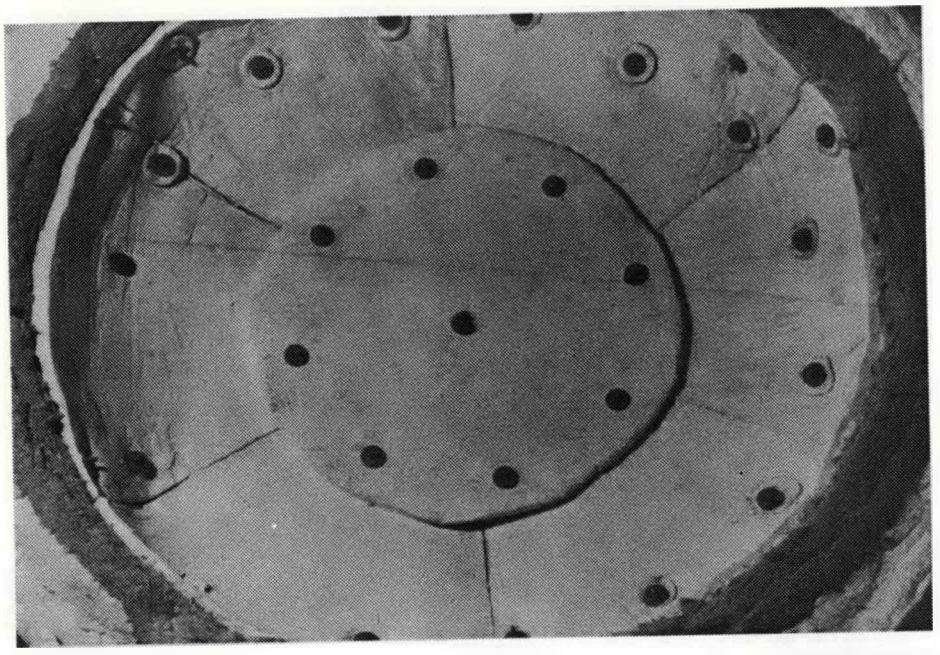

(WCN-13655)

Figure 5.3–18. *Upgraded Insulation in Reformer Dome*

Catalyst Addition

High temperature shift catalyst was added to the regenerator tube inside the reformer while the reformer was shutdown. Test results of the modified reformer are compared to the original build in Table 5.3–2. As expected, the addition of high shift catalyst lowered the exit carbon monoxide (CO) content and increased pressure drop. Upgrading the insulation also reduced the reformer heat loss but the reformer fuel conversion did not increase as much as expected.

After a total of 306-hours of operation the reformer was again shutdown for inspection. During the period, extra reform catalyst was added to the reform tubes.

Table 5.3-2. Effect of Development Reformer Modifications on Performance at 200-kW Flows

Parameter	Original Build	Modified Reformer	Change
Process ΔP ("H_2O)	30.6	50.4	+19.8"
Process Exit CO (% Dry)	10.9	7.2	-3.7%
Fuel Conversion (%)	92.2	92.5	+0.3%
Heat Loss Btu/Hr	29,600	20,600	-9000 Btu/Hr

Performance Tests

The reformer was operated for an additional 402-hours (708-hours total) after completing the reformer modifications described previously. During this period, performance mapping at 80-kW, 140-kW, and 200-kW flows was conducted. This flow range represents operation over the full ac power range from zero net power to 200-kW rated power. Figure 5.3-19 compares the performance of the original build to the modified reformer at 200-kW flows. Efficiency of the modified reformer is consistently above the original build. Table 5.3-3 compares the test results for the modified reformer to predictions. All values other than efficiency are "as expected". The efficiency is about 3 percent below predicted because of insufficient heat transfer within the reformer. This deficiency will not effect operability in the full-scale fuel processor or Verification Test Article (VTA) and can be corrected in future designs.

By 1985, the full-scale fuel processing system configuration was defined, and operating conditions for the reformer in the system were re-estimated. The major changes from previous test conditions were a reduction in the burner air to fuel ratio from 120 percent to approximately 105 percent of stoichiometric, and a reduction in process and burner inlet temperatures to reflect more realistic heat losses. Performance maps were completed at conditions simulating 140-kW and 200-kW flows. The average top tube, burner exhaust and process exhaust temperatures plus reformer efficiency are plotted as a function of fuel conversion in Figure 5.3-20 for 200-kW flow settings. The reformer efficiencies shown in these curves are slightly lower than the earlier results as a consequence of the lower pre-heat temperatures. The average top-tube temperature at a fuel conversion of 87.7 percent was 1493°F. The temperature was uniform, varying from 1482°F to 1509°F for a tube average. Maximum variation around a tube was 105°F on tube No. 5.

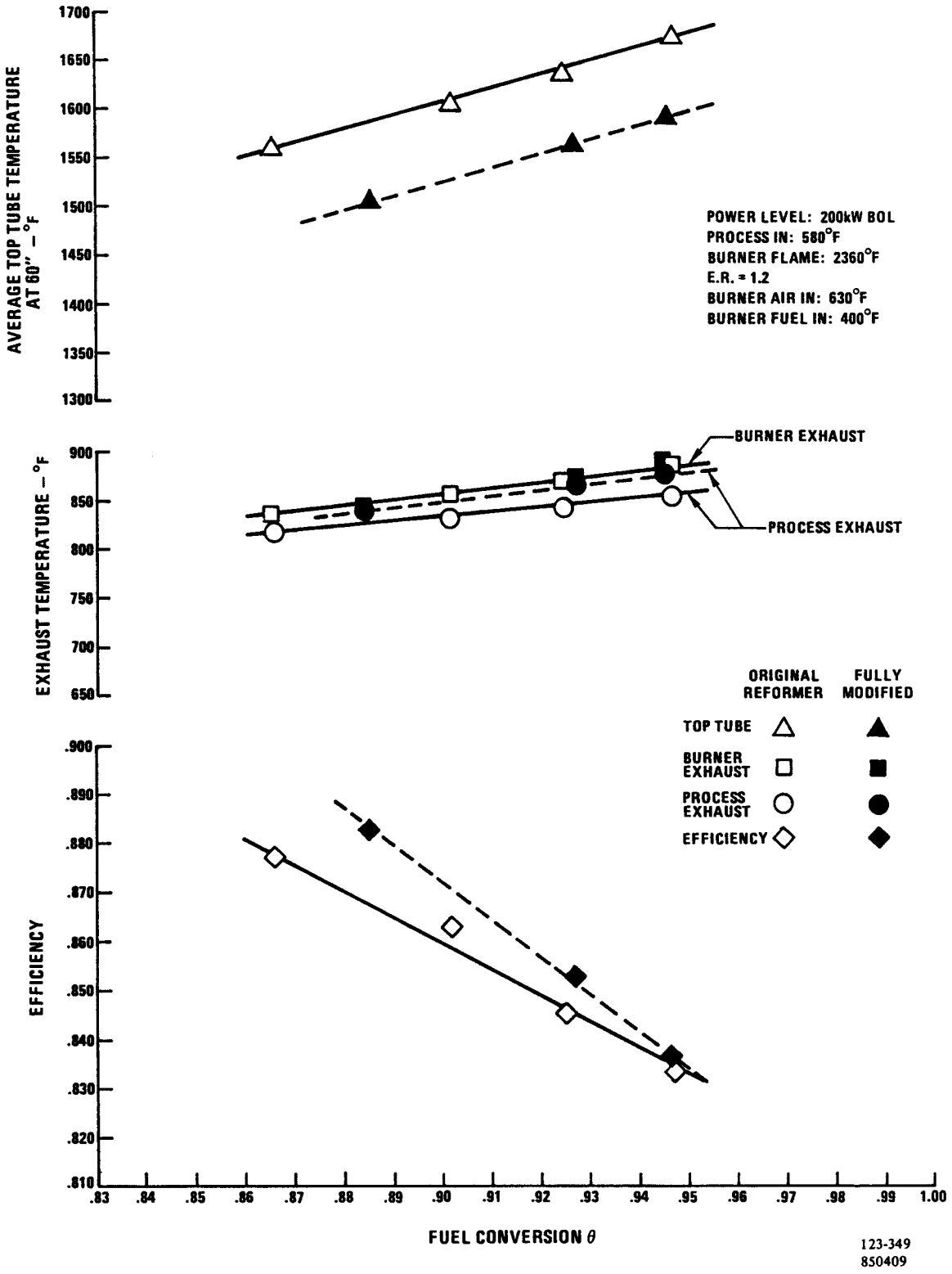

Figure 5.3–19. *Reformer Performance Comparison*

Table 5.3-3. Reformer Performance Summary at 200-kW

Item	Predicted	Fully Modified Reformer Performance
Pressure Drop		
Process	60 In H_2O	56 In H_2O
Burner Fuel	3.5 In H_2O	3.2 In H_2O
Burner Air	3.5 In H_2O	2.2 In H_2O
Heat Loss	20,000 Btu/Hr	15-30,000 Btu/Hr
*Efficiency @ 92.5% fuel conversion	88%	85 $\pm$1%

$$\text{*Efficiency} = \frac{\text{Heating Value of Hydrogen Converted}}{\text{Heating Value of Fuel to Reformer Burner}}$$

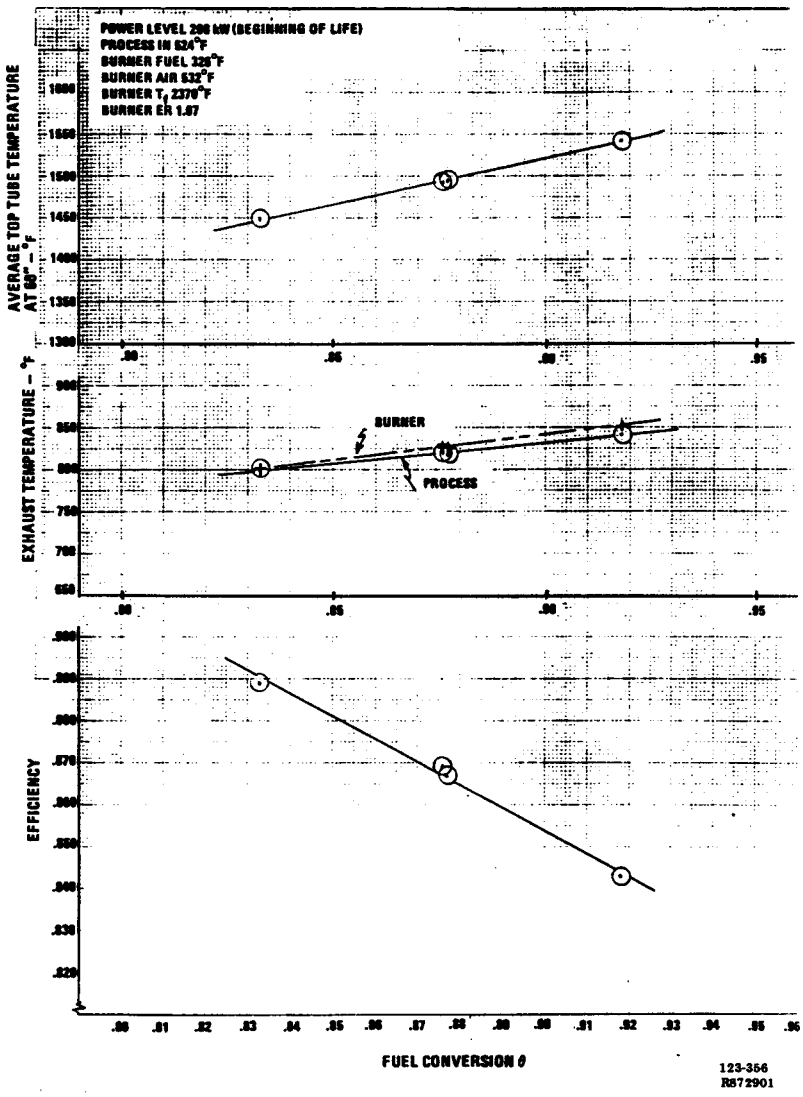

Figure 5.3–20. *Reformer Performance at 200–kW*

The transient response of the modified development reformer during full power transient from 80-kW (approximately zero net ac power) to 200-kW (rated power) was evaluated. Continuous recordings of process exhaust CH_4, CO_2, and CO (dry gas basis) together with tabulated values for power level, fuel conversion, average reformer top-tube temperature, are shown in Figure 5.3–21 as a function of time. After the flow change, fuel conversion decreased from 87.7 percent at 80-kW flows to a minimum of 70.4 percent at the 200-kW flows. After five minutes, the fuel conversion began to increase in response to the rapidly rising top-tube wall temperature. Performance stabilized after about 30 minutes. This information wasu utilized to define control requirements needed to provide a continuous supply of hydrogen to the cell stack during transients.

The effect of process steam/fuel carbon ratio on performance is shown on Table 5.3–4 at a fixed 200-kW fuel flow level. Increasing steam/fuel carbon ratio from the baseline value of 3.17 to 3.68 improves fuel conversion and shift conversion. Conversely, decreasing the steam flow to achieve a steam/fuel carbon ratio of 2.68 reduces fuel conversion and increases exit carbon monoxide content.

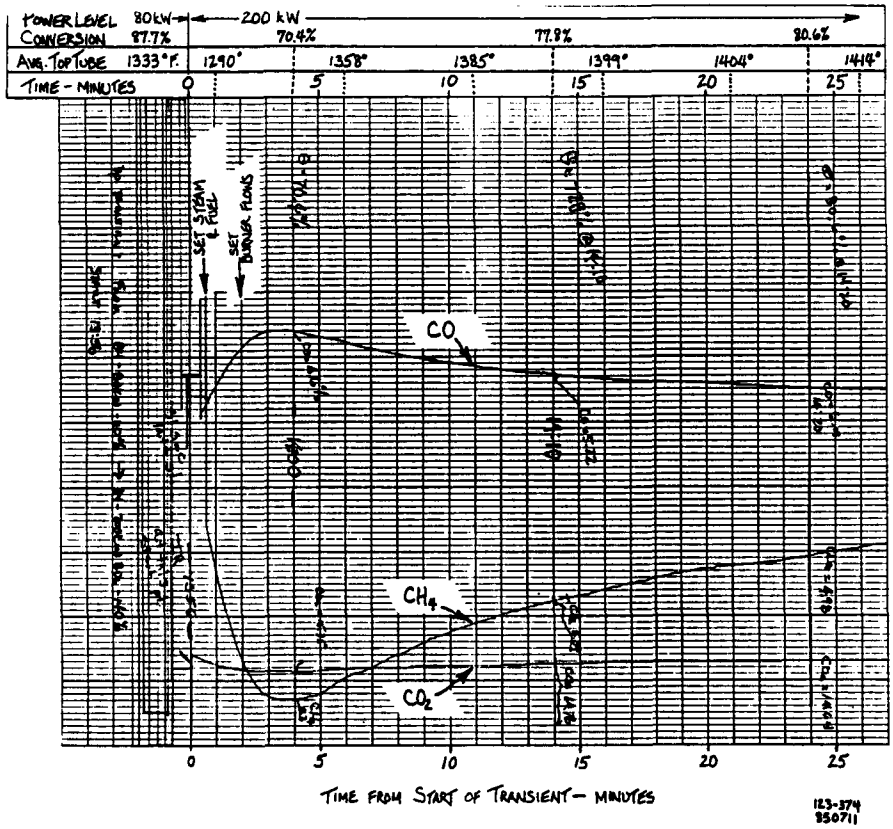

Figure 5.3–21. *Reformer Performance During Full–Power Up–Transient*

Table 5.3–4. Effect of Steam/Fuel Carbon Ratio on Modified Development Reformer Performance

Test Point	Steam/Fuel Carbon	Fuel Conversion (%)	Exit CO (%)
Low Steam	2.68	84.5	8.0
Baseline	3.17	85.5	7.1
High Steam	3.68	85.9	6.2

The effect of burner air/fuel equivalence ratio (ER) on performance at 200-kW flows is shown in Figure 5.3–22. Burner air was adjusted to vary the burner ER from 1.025 to 1.23 (1.00 = stoichiometric), while measuring the reformer fuel conversion. Optimum fuel conversion was obtained at ER's of 1.05 to 1.13. This represents a gain of about 1 percent in conversion over the fuel conversion obtained at a 1.20 ER typical of the 40-kW power plants.

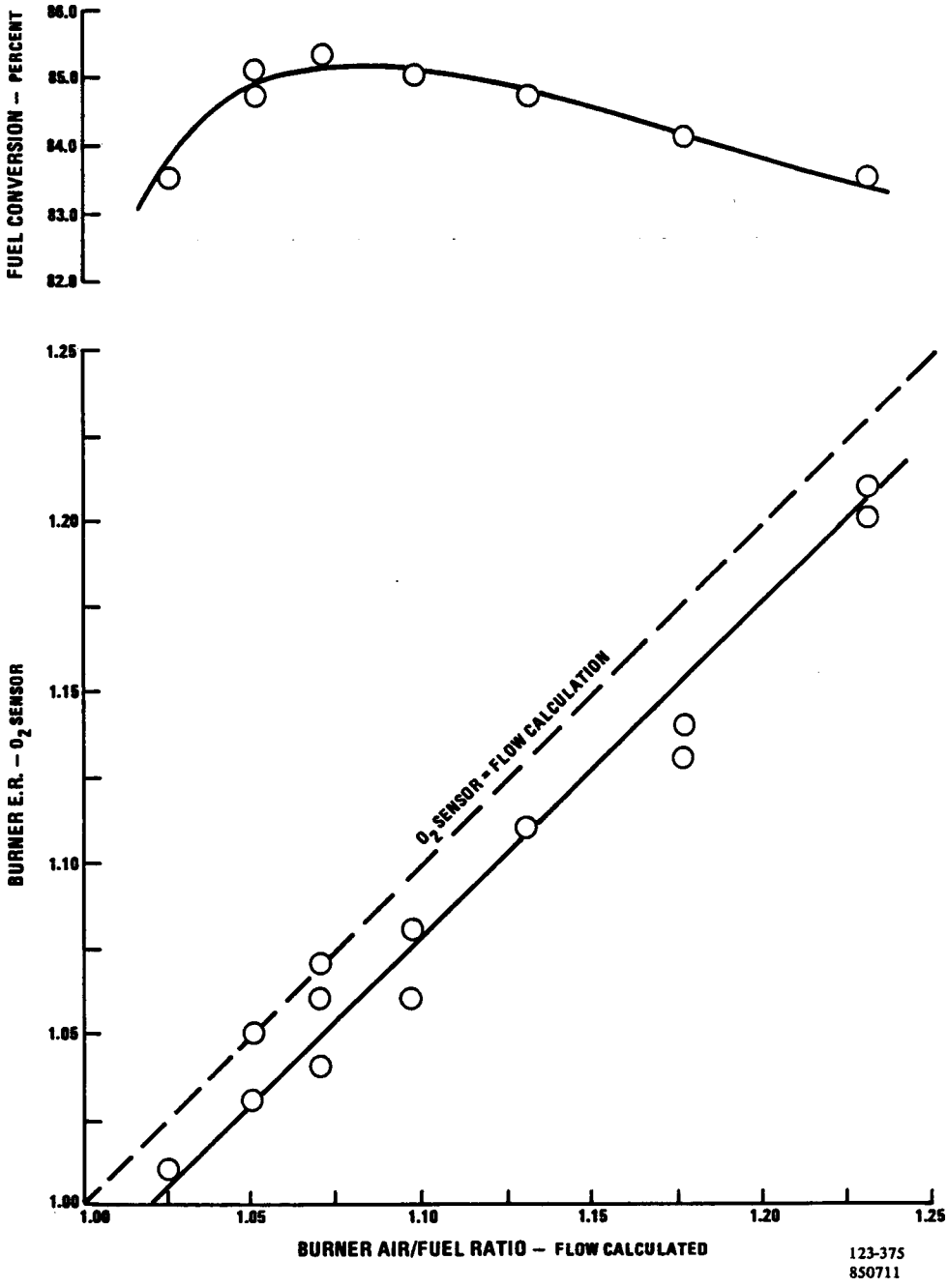

Figure 5.3–22. *Reformer Performance Response to Burner ER Changes*

The effect of process and burner gas pre-heat temperatures on performance is shown in Tables 5.3–5 and 5.3–6. For these tests, the reformer fuel conversion was measured at 200-kW flows as the pre-heat temperatures were varied from the baseline value (±100°F for process pre-heat and burner air pre-heat and ±75°F for burner fuel pre-heat). The results show that fuel conversion increases by about 1.4 percent per 100°F of added pre-heat in either the process feed or burner air. The fuel conversion increases by about 1.8 percent per 100°F of added pre-heat to the burner fuel. The greater sensitivity of the reformer to the burner fuel pre-heat is due to the higher heat capacity of burner fuel stream compared to burner air stream. The 75°F change in the burner fuel has the same impact on the adiabatic flame temperature as a 100°F change in the burner air.

Table 5.3.5. Effect of Process Pre-Heat Temperature On Modified Development Reformer Performance at 200-kW Flows

Test Point	Process Inlet Temperature (°F)	Fuel Conversion (%)
-100° F	418	85.4
Baseline	520	87.0
+100° F	618	88.1

Table 5.3.6. Effect of Burner Pre-Heat Temperatures on Modified Development Reformer Performance at 200-kW Flows

Test Point	Burner Fuel Inlet (°F)	Burner Air Inlet (°F)	Adiabatic Flame Temperature (°F)	Fuel Conversion (%)
-100° F Air	322	430	2336	85.8
-75° F Fuel	250	532	2338	86.1
Baseline	323	531	2374	87.0
+100° F Air	320	628	2405	88.6
+75°F Fuel	400	533	2407	88.8

Endurance Testing

Endurance testing was conducted over a 176-hour period including 96 hours at 200-kW flows, 52 hours at 140-kW flows, and 28 hours at 80-kW flows. Performance data including average top-tube temperature, fuel conversion, reformer process pressure drop, and dry gas exit carbon monoxide content are plotted for this period in Figure 5.3–23.

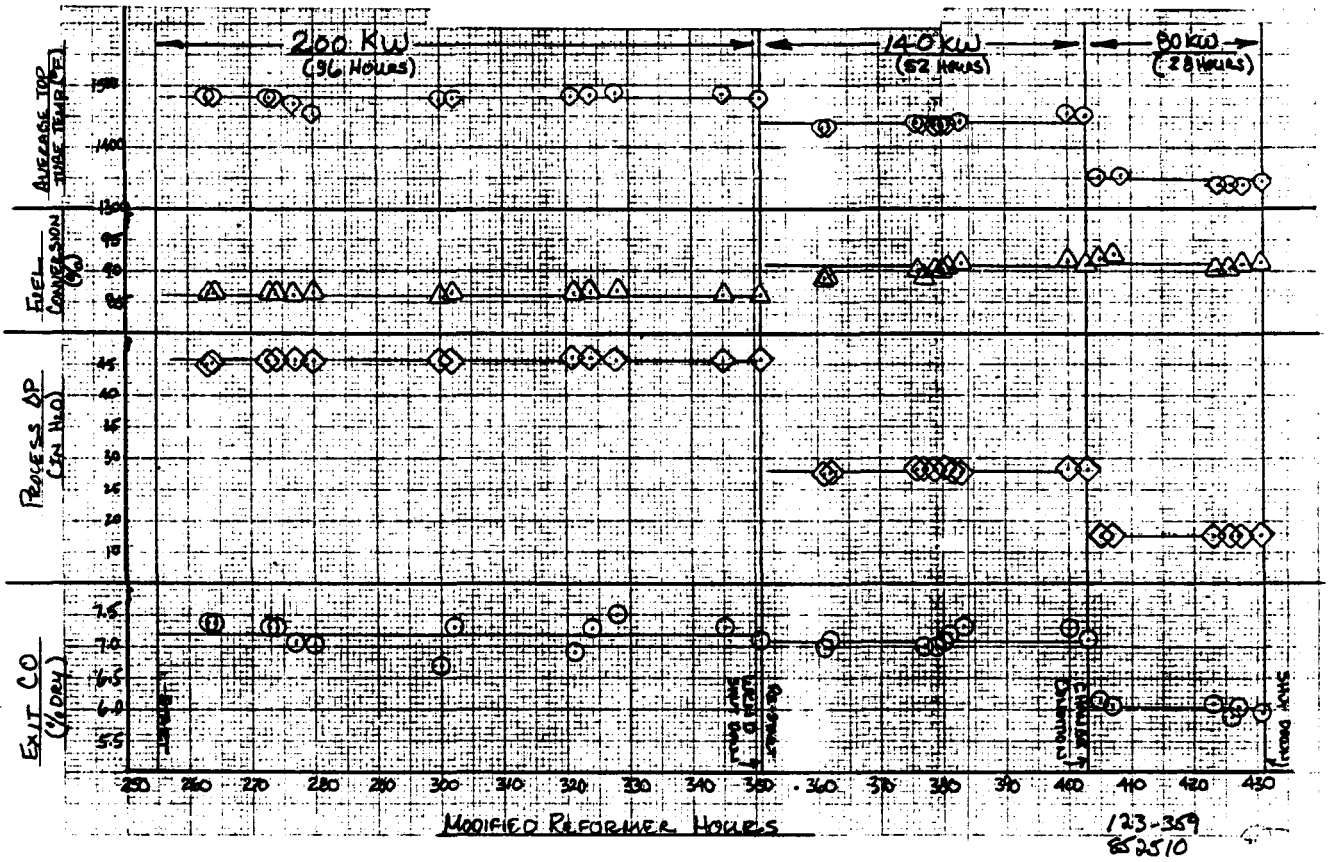

Figure 5.3–23. *Reformer Performance History*

Post-Test Inspection

Post-test inspection revealed that all reformer external parts and reformer tubes were in good condition. Some shrinkage was evident in the loose insulation packed around the outside of the burner heat transfer sleeves. The fiberboard insulation material added to the inside surface of the reformer dome exhibited a hard, firm surface after 540 hours of test operation. Two small shrinkage cracks developed in the splash plate.

Subtask 5.4 – Fabricate Full-Scale Fuel Processor

OBJECTIVE

The objective of this task is to fabricate a full-scale fuel processor, verify the functionality of the fuel processor, and deliver it to the Verification Test Article.

SUMMARY

The full-scale fuel processor consists of a reformer, a Low Temperature Assembly (LTA) which contains hydrodesulfurizer and low temperature shift catalyst beds, an integrated heat exchanger assembly, a burner air preheater, a process air blower, steam ejector, and related auxiliary components required to control the subsystem. All equipment was fabricated and assembled as part of this activity except the development reformer from Subtask 5.3 and heat exchangers from Task 4.0.

After completing modifications to the test facility, the fuel processor system was successfully started and operated for over 350-hours to verify proper operation over the full power range. The fuel processor was then moved to the Verification Test Article (VTA) test stand, integrated with the Water Treatment System, and completely checked out prior to operation in the VTA with the full-height cell stack.

ACCOMPLISHMENTS/CONCLUSIONS

- Fabricated a full-scale Low Temperature Assembly (LTA) containing hydrodesulfurizer and low shift catalysts.
- Identified a steam ejector which meets system pumping requirements and verified its operation with an electric actuator.
- Verified acceptable operation of the fuel processor system over the full power range.

DISCUSSION

The heat exchangers and reformer assembly for the full-scale fuel processor were provided by Tasks 4.0 and 5.3, respectively. The following sections describe fabrication and checkout of the remaining major components (the Low Temperature Assembly and steam ejector), assembly of the entire fuel processing rig, and verification test results.

Low Temperature Assembly (LTA) Fabrication

The design of the LTA was completed under the parallel GRI contract. A sketch of the vessel design is shown in Figure 5.4–1. The design consists of a central hydrodesulfurizer (HDS) vessel with a wrap-around, low-temperature shift converter (LTSC) vessel. Both catalysts beds are sized for a five-year life. Vessel heat-up during startup and standby operation is accomplished by replaceable cartridge heaters that are mounted through the top of the vessel.

The HDS catalyst requires no preactivation before use, and the LTSC activation requirements are simplified compared to those for the 40-kW power plant.

The LTA vessels were completed and mounted to a transportation cart. The HDS/absorber and LTSC catalysts were then added to the vessels. Pressure testing and thermal insulation completed preparation prior to installation into the fuel processing facility. Figure 5.4–2 shows the assembly prior to insulating.

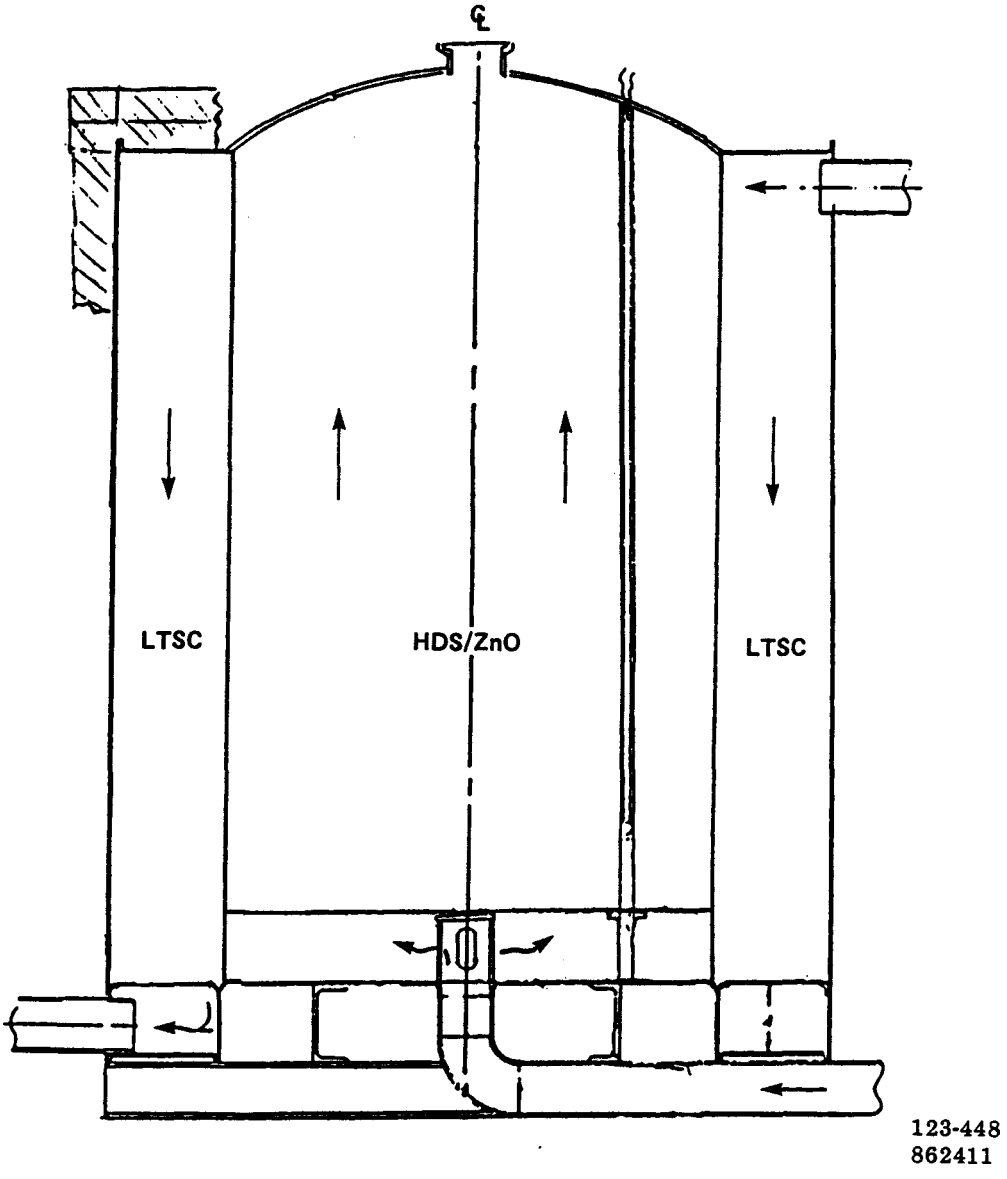

Figure 5.4–1. LTA Configuration

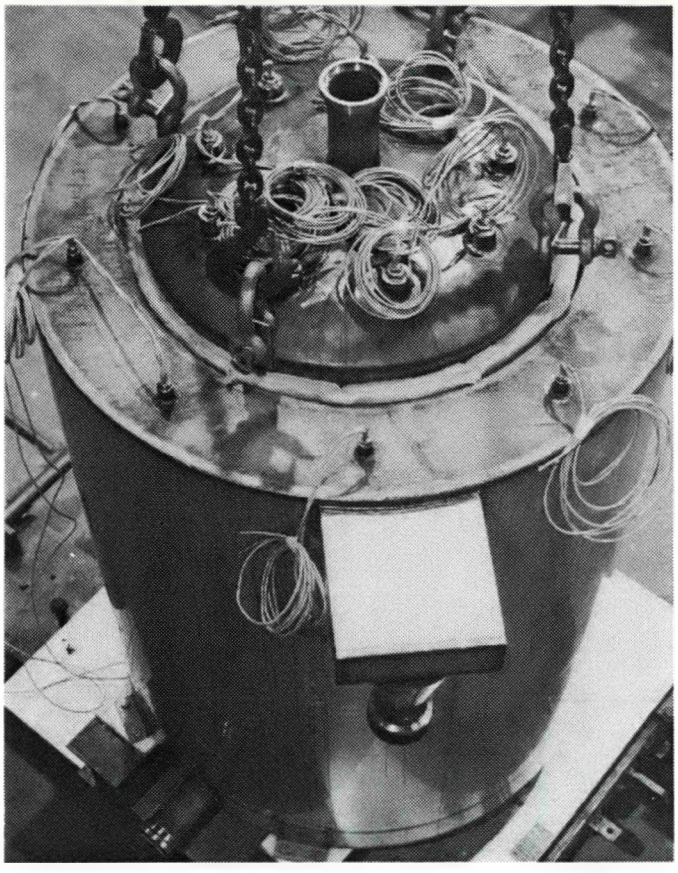

(WCN-13839)

Figure 5.4–2. *Assembly Prior to Insulating*

Steam Ejector Selection

One objective of this subtask was to make a variable area ejector to meet pumping requirements of the system at desired fuel and steam consumption rates. The approach taken was to adapt commercially-available devices for each of the functions.

A survey identified several possible vendors for variable area ejectors. Although pneumatically actuated units were available, none offered an electrically operated unit. Electric actuation was desirable since ancillaries are not required and interfacing to the microprocessor controller was simplified. Two candidate ejectors were procured without actuators and tested. An electric actuator was procured separately. Figure 5.4–3 shows the actuator mounted to Candidate A ejector. A photograph of Candidate B (without actuator) is shown in Figure 5.4–4.

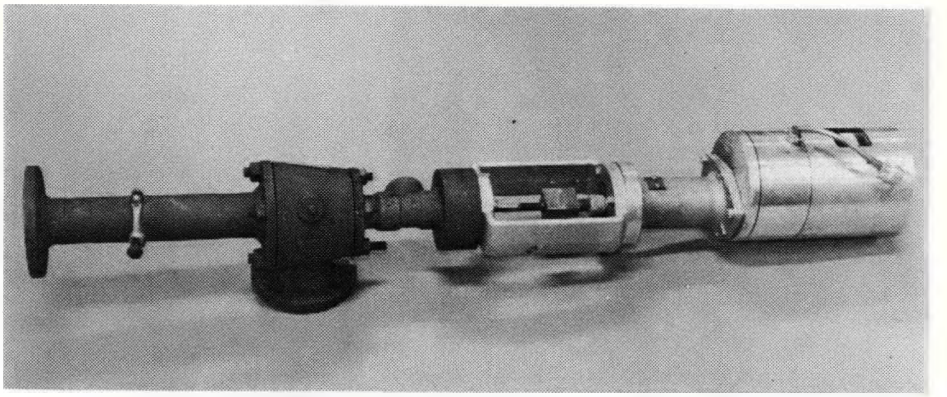

(WCN-13837)

Figure 5.4–3. *Candidate A Ejector With Actuator*

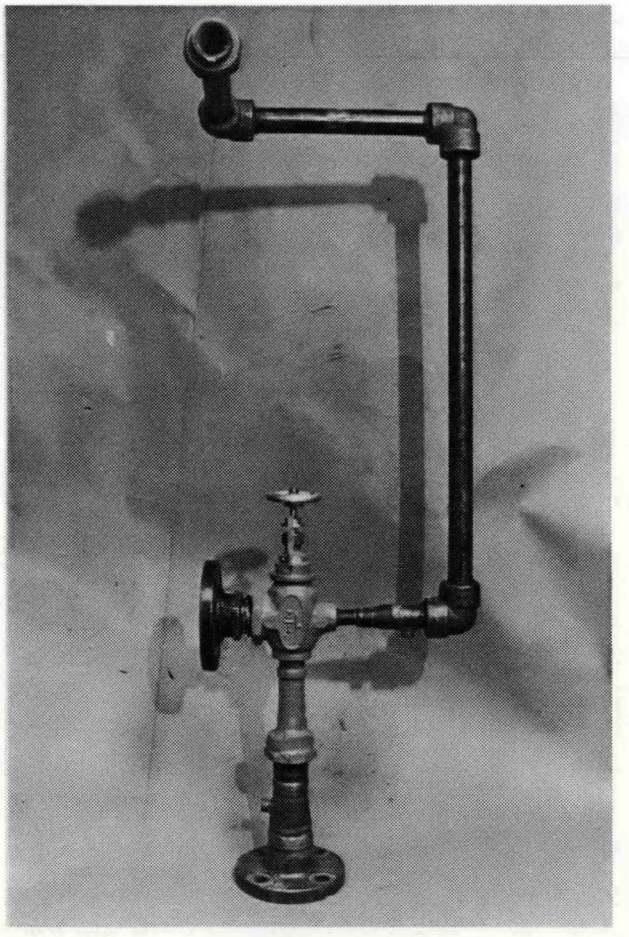

(WCN-13574-15)

Figure 5.4–4. *Candidate B Ejector Without Actuator*

The Candidate B ejector most closely matched power plant requirements in initial bench testing. The performance map obtained for this candidate is given in Figure 5.4–5. Candidate A approached the desired performance at low power levels but failed to provide sufficient ΔP at high power levels, as shown in Figure 5.4–6. The electric actuator was installed on Candidate B, and further testing was conducted. The candidate met all desired characteristics over the full operating range except overflow capacity was limited to 10 percent rather than the desired 25 percent. Candidate B was selected for use in the full-scale fuel processor because 10 percent overflow (above steady-state 200-kW flow) was an adequate margin for initial operation in the Verification Test Article (VTA). Figure 5.4–7 shows the ejector mounted on the fuel processor.

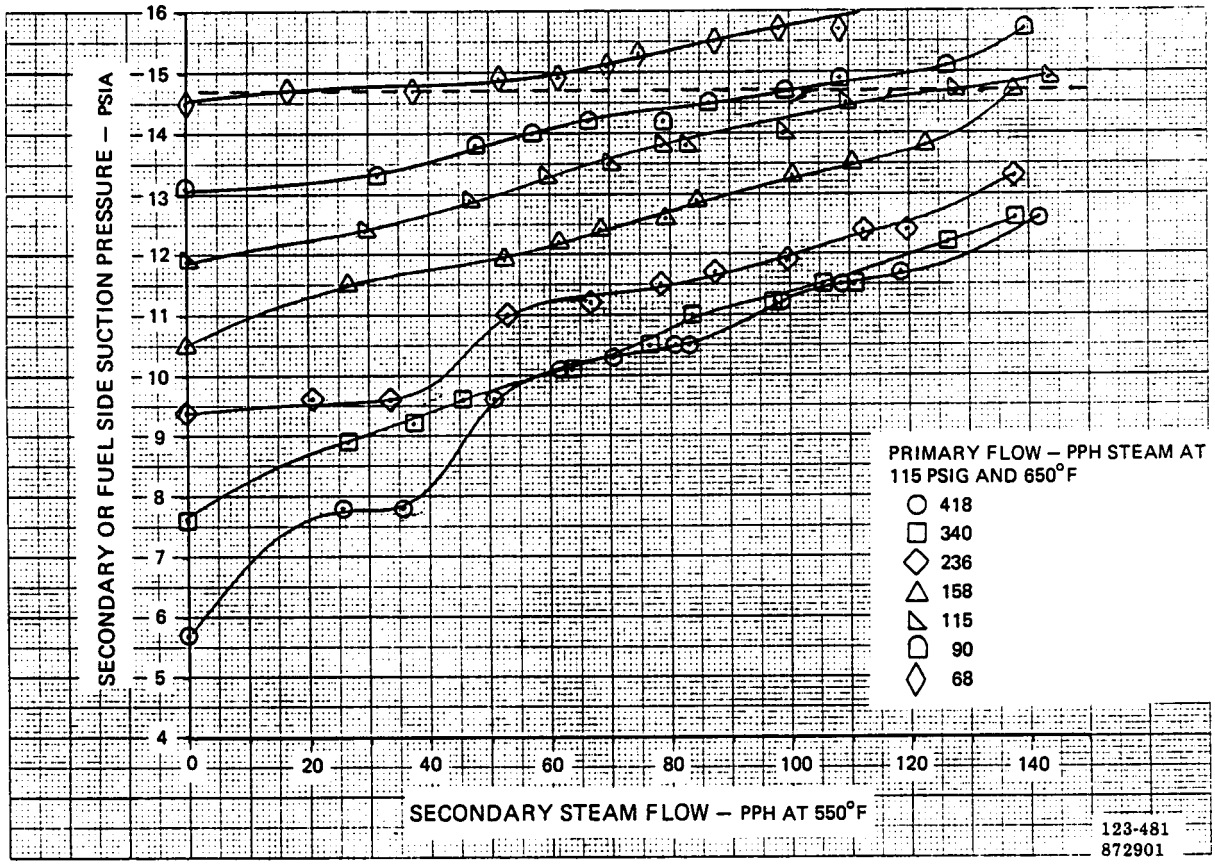

Figure 5.4–5. *Performance Map for Candidate B Ejector*

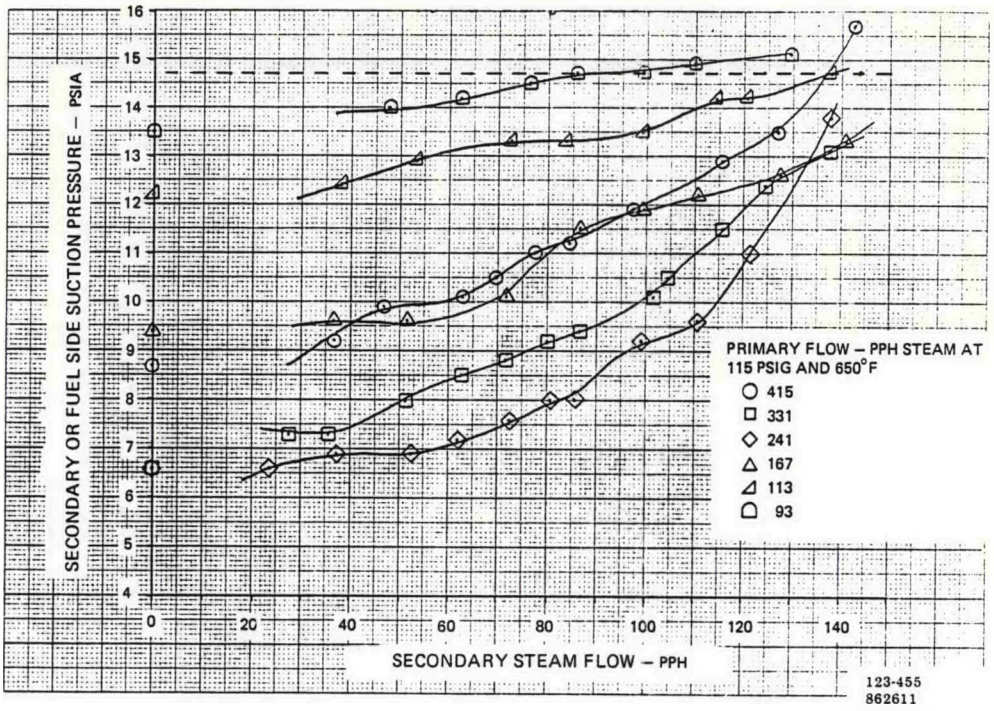

Figure 5.4–6. *Performance Map for Candidate A Ejector*

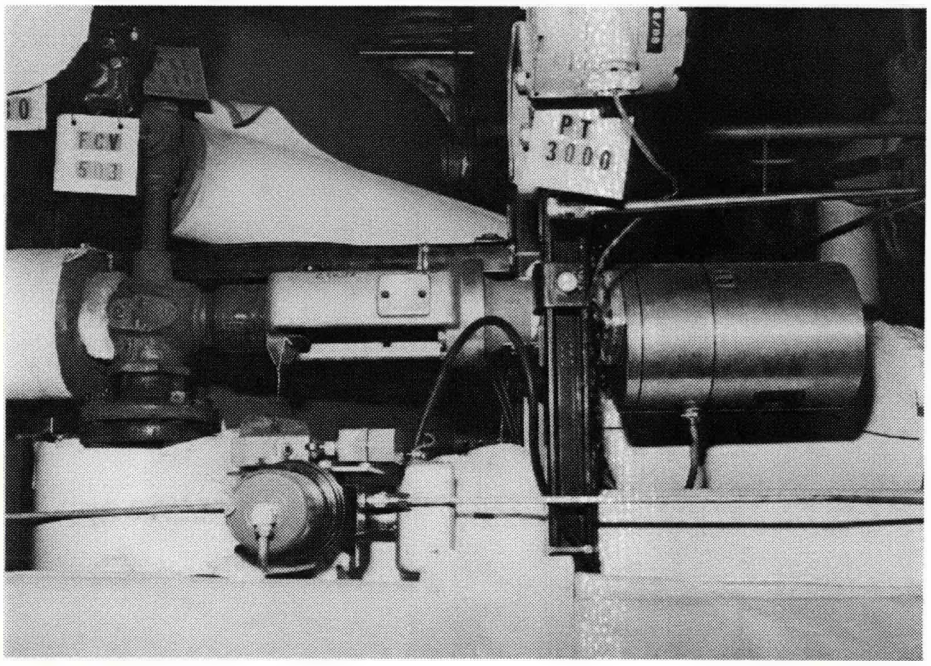

(WCN-14045)

Figure 5.4–7. *Candidate B Ejector Installed in VTA*

Fuel Processor Description

The Low Temperature Assembly (LTA), the integrated heat exchanger assembly (from Task 4.0), the burner air preheater (from Task 4.0), and the steam ejector were installed in the test stand with the development reformer (from Subtask 5.3). A schematic of the subsystem and an illustration of the hardware orientation are shown in Figures 5.4–8 and 5.4–9, respectively.

The fuel processor valves and sensors were integrated with a programmable controller to permit either manual and automatic control of the fuel processor. The control hardware was assembled into a control panel. The software for the programmable controller was provided by a parallel GRI program.

Figure 5.4–10 is a photograph of the completed fuel processor.

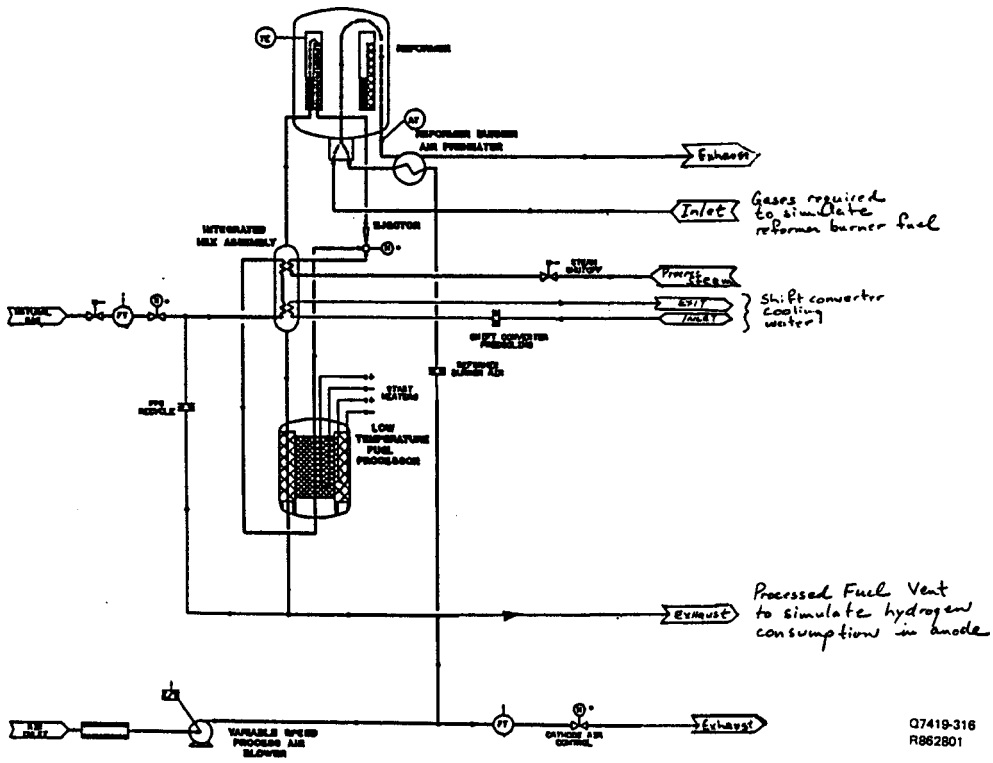

Figure 5.4–8. *Fuel Processor Flow Schematic*

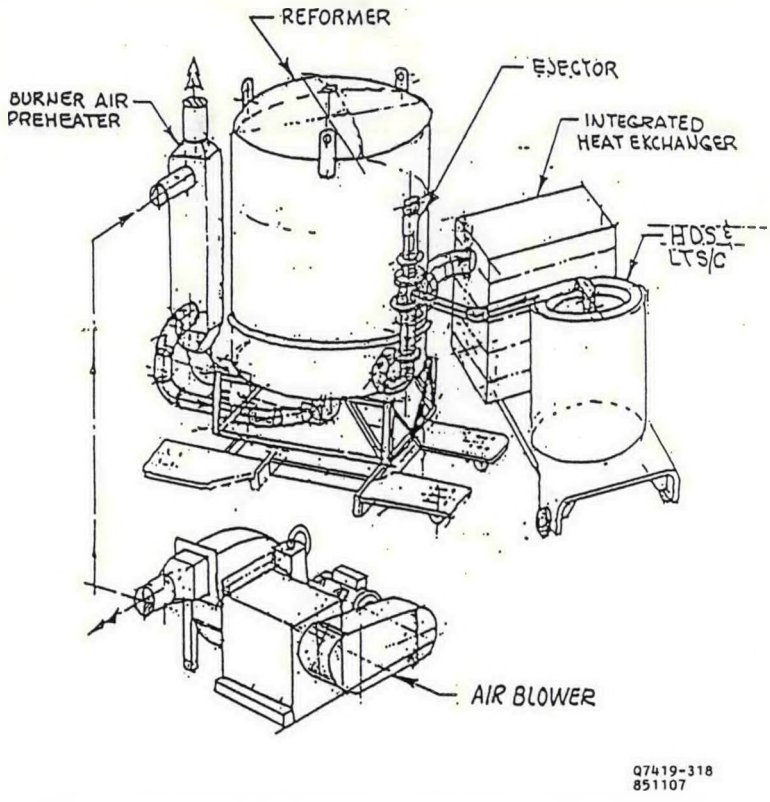

Figure 5.4–9. *Fuel Processor Configuration*

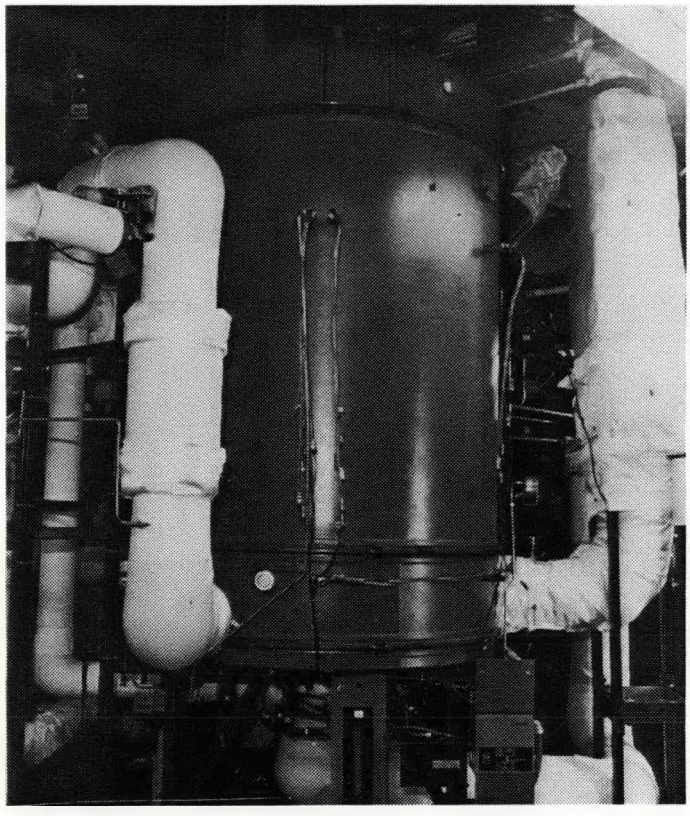

Figure 5.4–10. *Fuel Processor Photograph*

Fuel Processor Testing

Prior to actual operation of the fuel processor, the catalytic beds in the Low Temperature Assembly (LTA) were preheated to the required operating temperatures. The heatup rate was slower than expected; the predicted heatup rate was 14-hours compared to an actual of 24-hours. The slower rate was attributed to higher-than-expected internal thermal resistances. Even though the slower heatup did not impact actual fuel processor start or operation, heater setpoints were readjusted to decrease heatup time on subsequent starts.

The fuel processing system was operated for over 350-hours with 45 thermal cycles above 1000°F. As shown in Table 5.4–1, operating conditions were generally as expected based on previous reformer testing in Subtask 5.3 and analytical predictions. Two significant exceptions were noted:

1. Reformer fuel conversion was 6 percent lower than expected at the same efficiency.
2. The reformer process pressure drop was 70 percent higher than expected.

Each of these exceptions are discussed in more detail in the following sections.

Table 5.4–1. Fuel Processor Operation at 200-kW

Item	Expected	Fuel Processor Test Data
Process Fuel Flow	84.2 pph	85.9 pph
Process Steam Flow	297 pph	335 pph
Burner H_2 Flow	7.2 pph	7.6 pph
Burner CH_4 Flow	6.9 pph	8.2 pph
Top Tube Ave. Temp.	1510°F	1522°F
Bottom Tube Ave. Temp.	762°F	749°F
Efficiency	86%	86%
Fuel Conversion	89%	83%
CO at HTS Exit	5.5 - 7.0%	6.4%
Reformer Process Pressure Drop	45 IWG	77 IWG
Process Exit Temp	817°F	810°F
Burner Exit Temp	821°F	812°F
CO at LTSC Exit	0.5%	0.5%

Reformer Fuel Conversion

The 6 percent loss in fuel conversion is equivalent to a 3 percent flow error and indicates a reduction in fuel conversion equivalent to the 3 percent performance loss. This discrepancy was attributed to flow measurement errors and leakage, since the process exit and burner exhaust temperatures remained virtually unchanged. Post-test calibration data indicated a 3 percent error in process fuel flow and a 5 percent error in H_2 burner flow. These errors accounted for a 2 percent performance loss. In addition, stains observed after the test adjacent to a damaged fuel line gasket suggest leakage of burner fuel.

Reformer Pressure Drop

Figure 5.4–11 provides the reformer process pressure drop history during its 1000-hours of operation. Two significant pressure changes occurred: when the high-temperature shift catalyst was added (predicted) and during the low temperature shift catalyst activation procedure and burner light off trials (not predicted). This differential pressure increase occurred as almost a step change. Although it did not present a performance or operational problem, it was determined that an investigation into the cause should be undertaken.

The reformer catalyst investigation confirmed the catalyst had "slumped" below the top tube thermocouple location. Removal and examination of the catalyst followed. The catalyst was sieved and whole pellet distribution along the reform tube was determined. Figure 5.4–12 shows the distribution of broken pellets along the length of the reform tube. Figure 5.4–13 also shows that the crush strength of catalyst samples from the bed compare favorably with as-received catalyst. Comparison of reformer heat-up rates and operating parameters during the light off trials and during the low-temperature shift catalyst activation indicated that the outside reformer tube could be heating at a significantly faster rate than the regenerator tube. This would cause thermal differential growth of the annulus, allow the catalyst to shift and subsequently crush when thermal equilibrium is established. The review centered on differences from earlier testing, thermal predictions using an IFC computer model, and structural predictions based on the real and computer-generated data as shown in Figure 5.4–14. The thermal model and the structural analysis predict the highest stress occurs where the most severe crushing occurred (at the 50" location), but does not predict crushing at that location or at the base of the reform tube. Instrumentation was added to the regenerator tube to measure the magnitude of the thermal differential during future verification testing.

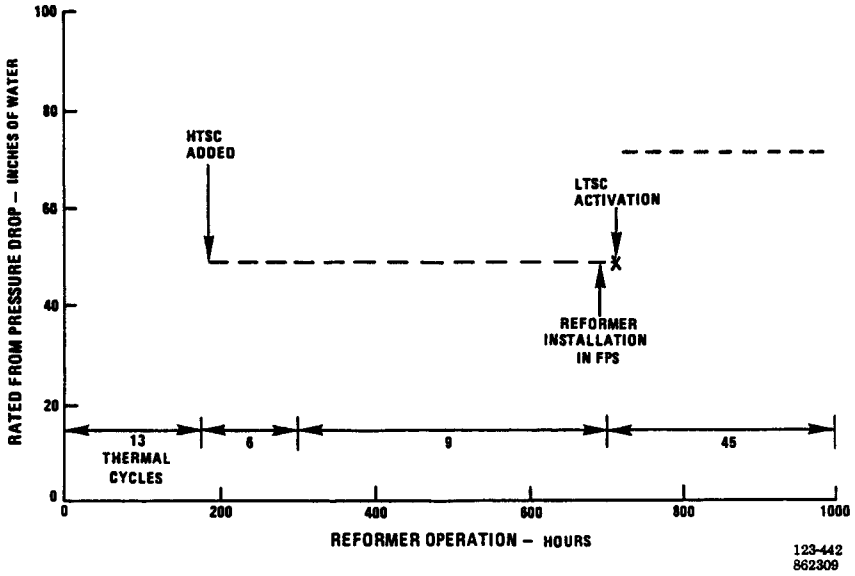

Figure 5.4–11. *Reformer Pressure Drop History*

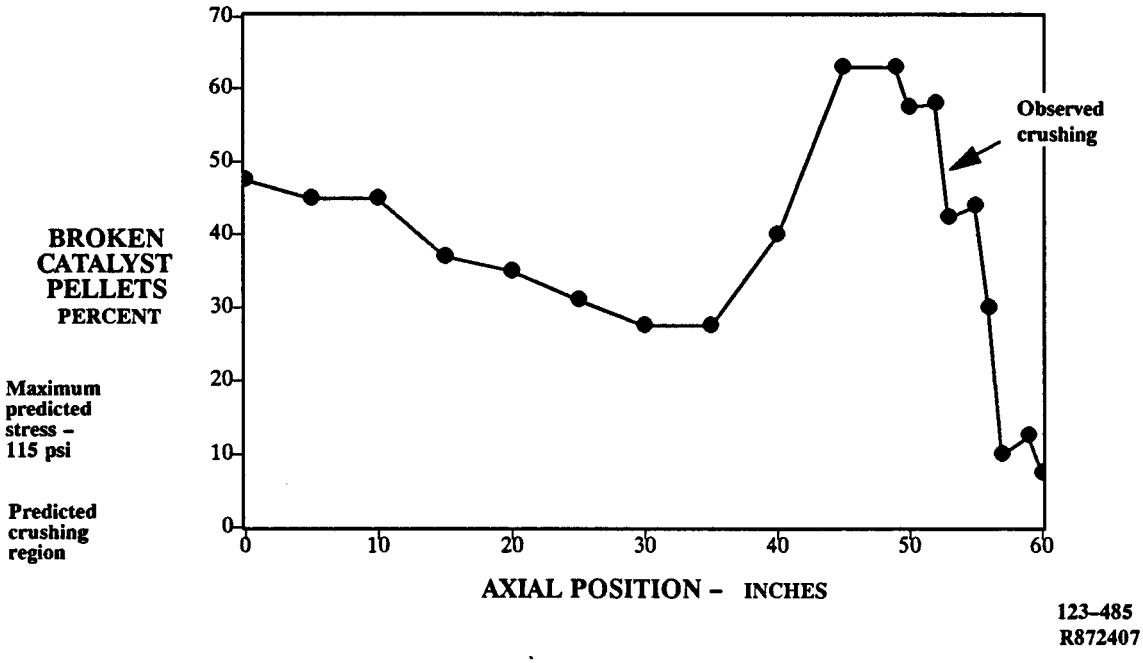

Figure 5.4–12. *Reformer Catalyst Condition Over Tube Length*

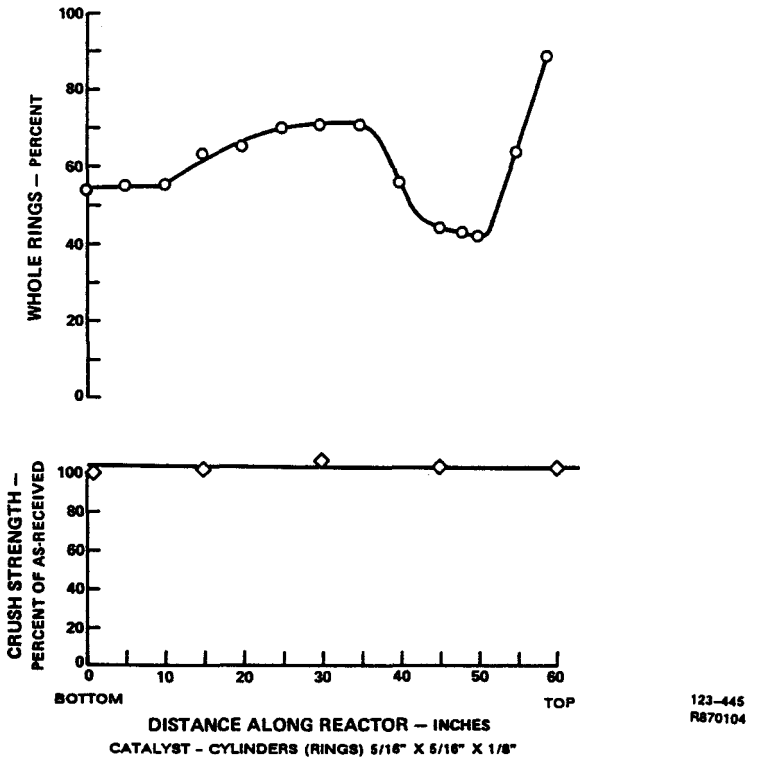

Figure 5.4–13. *Reformer Catalyst Strength Over Tube Length*

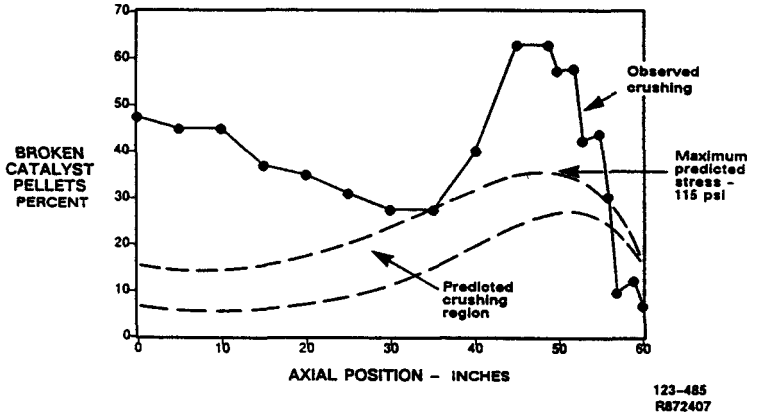

Figure 5.4–14. *Comparison of Observed and Predicted Catalyst Crushing*

During the examination of the reform catalyst, the high-temperature shift (HTS) catalyst was removed from the reformer regenerator tubes to evaluate its physical characteristics. Volume of the catalyst had been reduced by about 35 percent. Most of the catalyst shrinkage was in the upper 20 percent of the bed where temperatures were expected to cause some shrinkage. The HTS catalyst was also replaced due to uncertainties in tube-to-tube flow distribution associated with refilling with the "old" catalyst.

VTA Installation and Checkout

After completing the catalyst inspections described in the previous section, catalyst was removed from all six (6) reformer tubes and replaced with fresh reform and HTS catalyst. Cold nitrogen flow checks were conducted on the individual reformer tubes to ensure proper flow distribution. The differential pressures were acceptable and uniform tube to tube. Flow distribution was +3 percent to –4 percent from the median (Figure 5.4–15). The catalyst bed heights and weights were within 2 percent.

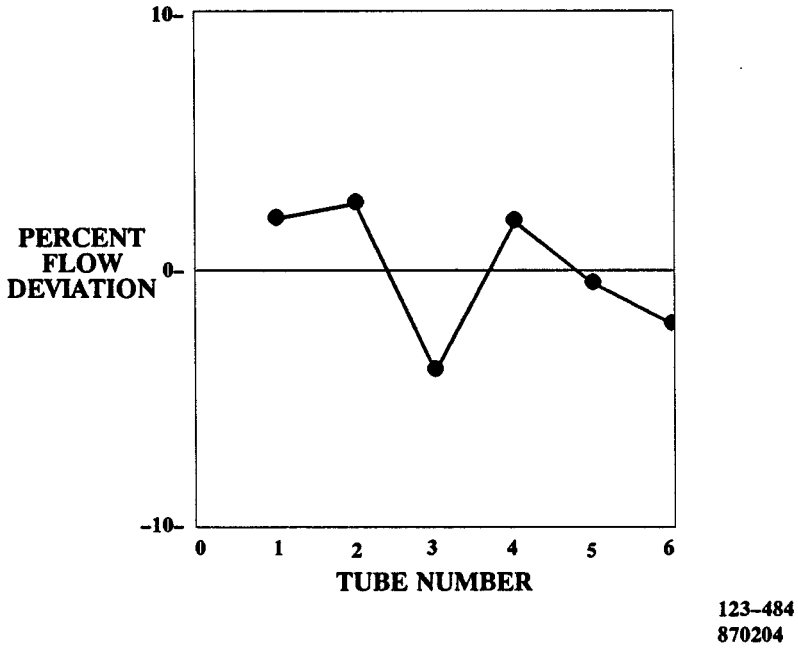

Figure 5.4–15. *Nitrogen Flow Distribution*

The interior of the reformer was examined and the insulation, tubes, and all internals appeared unchanged from earlier testing except for a small iron oxide stain on the burner splash shield. This has been attributed to rust carry-over from carbon steel piping recently installed in the test stand.

The reformer was reassembled and, along with the rest of the fuel processor, moved to the Verification Test Article (VTA) test stand for final checkout. The process fuel water and

steam lines were pressure checked. Additional Fuel Processing System (FPS) testing in the VTA test stand resumed after installation of a new integrated heat exchanger. The objective of the test was to check out the FPS with the Water Treatment System (WTS) prior to installation of the cell stack. This testing established operational start-up sequences and procedures for open loop stack "break-in" in the VTA. The FPS/WTS microprocessor controllers were interconnected, and testing was conducted through all operational states including shutdowns. The burner used natural gas throughout the test rather than a simulated stack anode exhaust gases. Process fuel was controlled by manually setting the desired flow. Operating flow parameters were evaluated up to 35 percent of the rated power point.

The checkout involved the confirmation of all components, sensors, actuators, meters, and indicators that had been verified in earlier FPS testing. Additional instrumentation, components, and concerns identified prior to testing were also included, evaluated and/or addressed. The major items included improvements in the microprocessor control of the cathode air valve; confirmation of the recalibrated reformer inlet process fuel and anode fuel flow meters; and establishment of a reduced thermal stress heatup rate for the reformer.

The addition of the internal thermocouples to tube No. 3, prior to this test, provided thermal differential measurements between the reformer tube wall and the regenerator tube wall. These measurements were used to confirm the predicted high-temperature shift catalyst bed temperatures and to check temperature differences during various heat-up, operational, and cool down modes. The temperatures at both the top and the bottom of the tube for two heat-ups are shown in Figure 5.4–16 and 5.4–17. The reduced heat-up rate shown in Figure 5.4–17 was accomplished by reducing burner flows by 33 percent for the initial 45 minutes and then completing the heat-up at the baseline conditions. The reduced heat-up rate was used during initial VTA testing to minimize thermal stress.

This concluded all preliminary testing of the FPS. All subsequent FPS evaluations are reported under Subtask 7.2 Verification Testing.

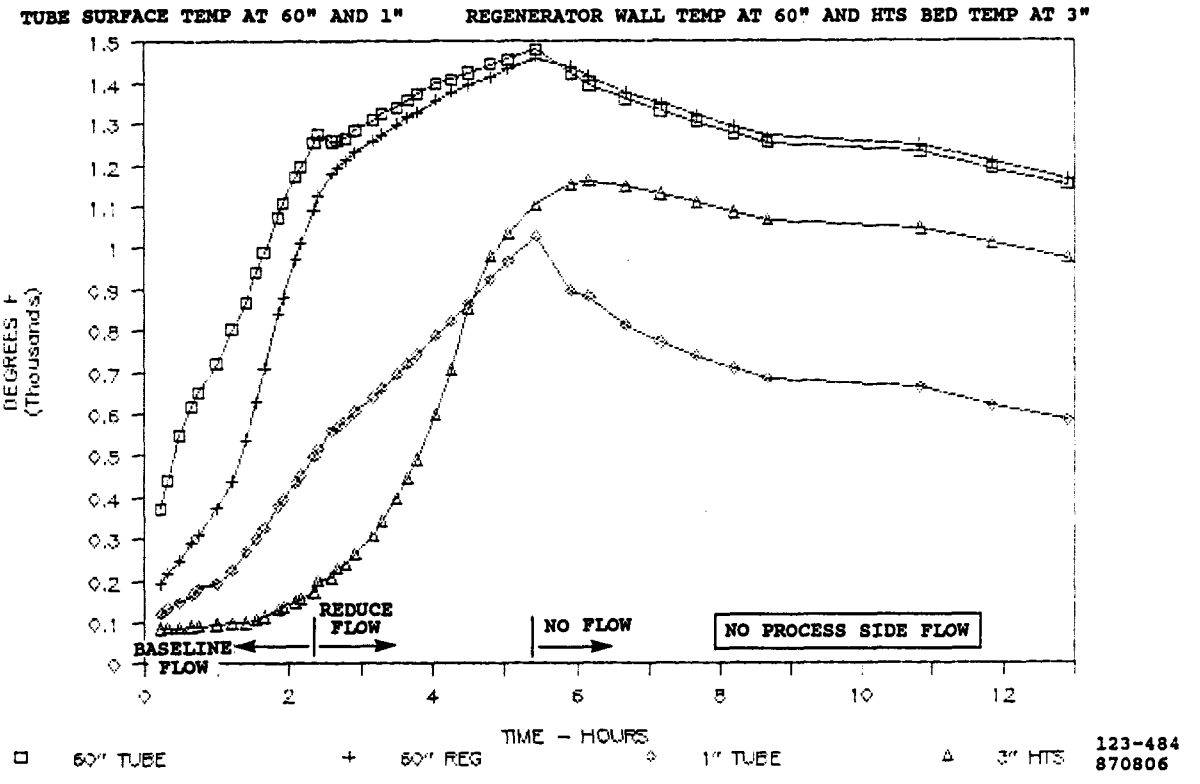

Figure 5.4–16. *Reformer Heatup With Baseline Burner Flows*

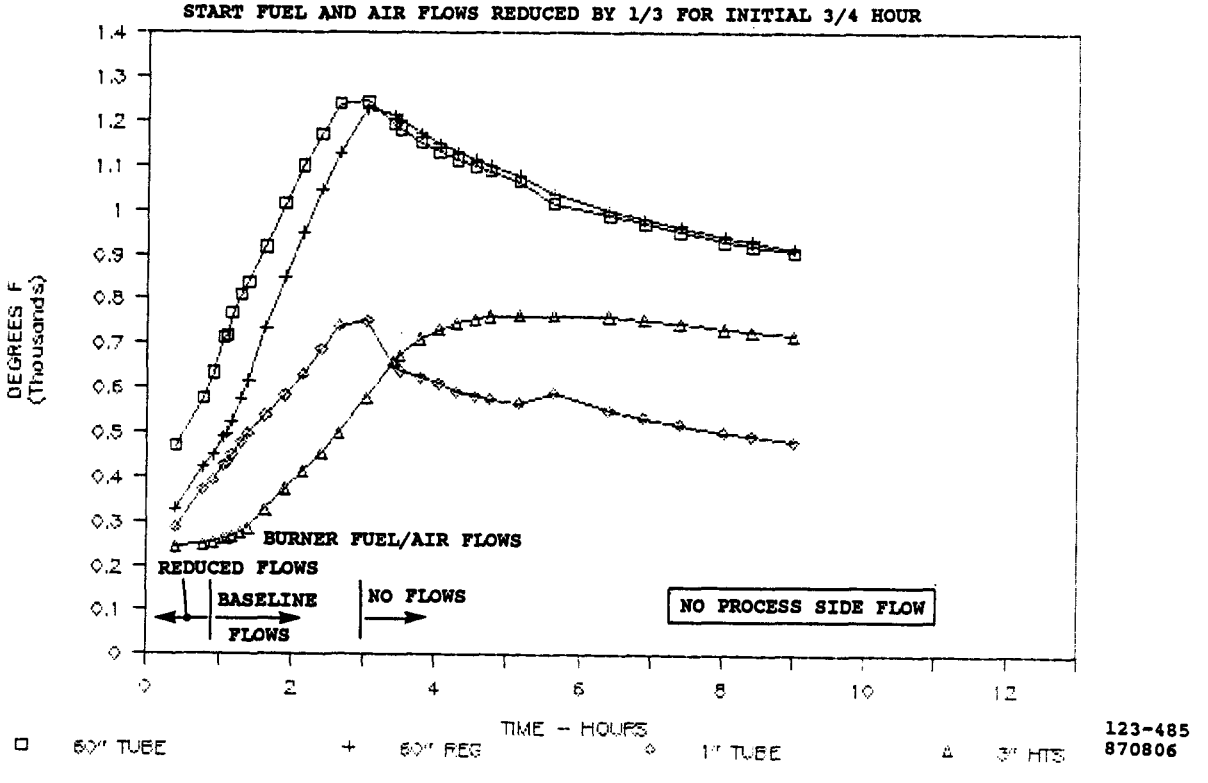

Figure 5.4–17. *Reformer Heatup With Reduced Burner Flows*

TASK 6 - ASSESS PREPROTOTYPE AND VERIFICATION TEST RESULTS

OBJECTIVE

The objective of this task was to review operating experience of early 40-kW power plants. The results of this review were assessed to determine whether additional technology development activities or changes in emphasis are required to overcome these power plant reliability deficiencies in future power plants.

SUMMARY

The shutdown experience of six early 40-kW power plants was reviewed. Each unscheduled shutdown was examined to determine the cause of the failure and then classify the failure. In addition to pointing out design and procedure changes for the 40-kW Power Plant Field Test Program, several development activities in this program were redirected to develop an improved basis for the design of future on-site power plants.

DISCUSSION

The shutdown experiences of the verification power plant, three DOE/NASA preprototype field test power plants, and three private preprototype field test power plants were analyzed to provide additional reliability information for use in the prototype technology design and development program.

These early power plants were operated as field development units to identify improvements to: power plant components, manuals, and training, which would result in improved operating experience for the power plants in the 47 unit field test program. Deliveries under this program began in the Fall of 1983. The 47 Power Plant Program was sponsored by GRI and DOE and managed by NASA under Contract No. DEN3-255.

Power plant shutdowns were reviewed to determine if they were scheduled or unscheduled. Unscheduled shutdowns were defined as power plant failures and were reviewed further to define primary cause. Failures were then classified into the following categories:

Non-Relevant Failure - Failures arising from circumstances not normally found in the intended application.

Relevant Failures - Failures caused by circumstances or conditions relevant to power plant technology and development.

Process Failure - A failure attributed to a power plant function performed unsatisfactorily by one or more components.

Inadequate Component Failure - A failure caused by a component that satisfies specified design requirements but predictably limits power plant operation.

Component Failure – A failure caused by a component that meets specified design requirements. Failures of this type are often referred to as random failures.

Non-relevant failures, which represented only about 2 percent of the shutdowns reviewed, were excluded from further consideration.

Table 6–1 shows the percent of relevant power plant failures by cause. All process failures were associated with water system issues. Corrosion products deposited in flow restrictions which control coolant distribution in the cell stack resulted in one of the largest changes in this and complementary programs. In the GRI Technology Development Program, alternative designs for the flow restrictions, alternative water loop configurations, materials, and approaches were evaluated in subscale rigs, and the mechanisms of corrosion product deposition were also evaluated. Results of these activities were used to modify cooling systems used in 40-kW power plants and subscale and full-scale rigs in this program (see Tasks 2 and 7). In addition, an alternative cooler configuration, the serpentine cooler, was developed to eliminate flow restrictions and, therefore, improve tolerance to corrosion product deposition.

The issue of inadequate components were also addressed in this program and the complimentary GRI program. Guidelines for avoiding logic control problems were established. In addition, control concepts were developed to reduce the number of parts by using more highly integrated control logic elements, modifying control strategies, and changing the method of control valve actuation. Pump and heat exchanger alternatives which increase design margin and, therefore, reliability were also identified. Results of many of these activities were demonstrated in the Verification Test Article (VTA) in Subtask 7.2.

Table 6–1. Percent Failures by Cause

	Percent of all Failures
Component Failures	7
Inadequate Components	78
Process Failures	7
Human Errors	8
All Causes	100%

TASK 7 VERIFICATION TESTING

Subtask 7.1 – Define and Fabricate Test Article

OBJECTIVE

The objective of this task was to define an approach to verify critical aspects of the power plant and fabricate a full-size Verification Test Article (VTA) for testing in Subtask 7.2.

SUMMARY

The Verification Test Article (VTA) was defined to include the following major system elements:

1. Full-height stack
2. Fuel processing System (FPS)
3. Water Treatment System (WTS)
4. Thermal Management System (TMS)

The full-height stack was fabricated in Subtask 2.4. The FPS was fabricated and checked out in Subtask 5.4. The WTS and TMS were fabricated in a complementary GRI program. Activities in this task included integration of the various system elements into the VTA, definition and assembly of facility support equipment, and preparation of a test plan.

The VTA was designed to deliver up to 220–kWdc of power. Industrial microprocessor – based controllers were set up for semi–automatic operation allowing evaluation of control approaches and algorithms which will be required in future fully–automatic power plants.

ACCOMPLISHMENTS/CONCLUSIONS

By April of 1987, all equipment was operational, and the VTA was ready for initial testing. The VTA was tested as part of Subtask 7.2.

DISCUSSION

The Verification Test Article (VTA) was defined to allow evaluation of key aspects of the process systems in 200–kW fuel cell power plants. (The inverter, the device which converts the dc power to utility grade AC power was developed separately in Subtask 3.0 and complementary GRI programs and not included in the VTA). The process schematic for the VTA is shown in Figure 7.1–1. All equipment required to convert pipeline natural gas to hydrogen, supply process air to the system, recover and treat water, and reject waste heat from the system is included. Heat rejection was simplified by connecting the VTA glycol water loop to the IFC facility heat rejection, but instrumentation was added to confirm performance of heat exchangers and measure heat which would be available for cogeneration.

As shown in the floor plan, Figure 7.1-2, the VTA was arranged as a "bread board" and not packaged as a commercial power plant prototype. Aisle ways and spaces between major subsystems were incorporated to allow easy access for assembly, maintenance, and testing. Facility services and equipment (rather than equipment appropriate for power plant use) were selected for some non-critical power plant functions to reduce program cost. Photographs of the completed subsystems, microprocessor - based controllers, and the test stand are shown in Figures 7.1-3 through 7.1-6. Results of Fuel Processing System and Water Treatment/ Thermal Management System checkouts (before operation of the VTA) are discussed in Sections 5.4 and 7.2, respectively. Section 7.2 also discusses verification testing of the VTA.

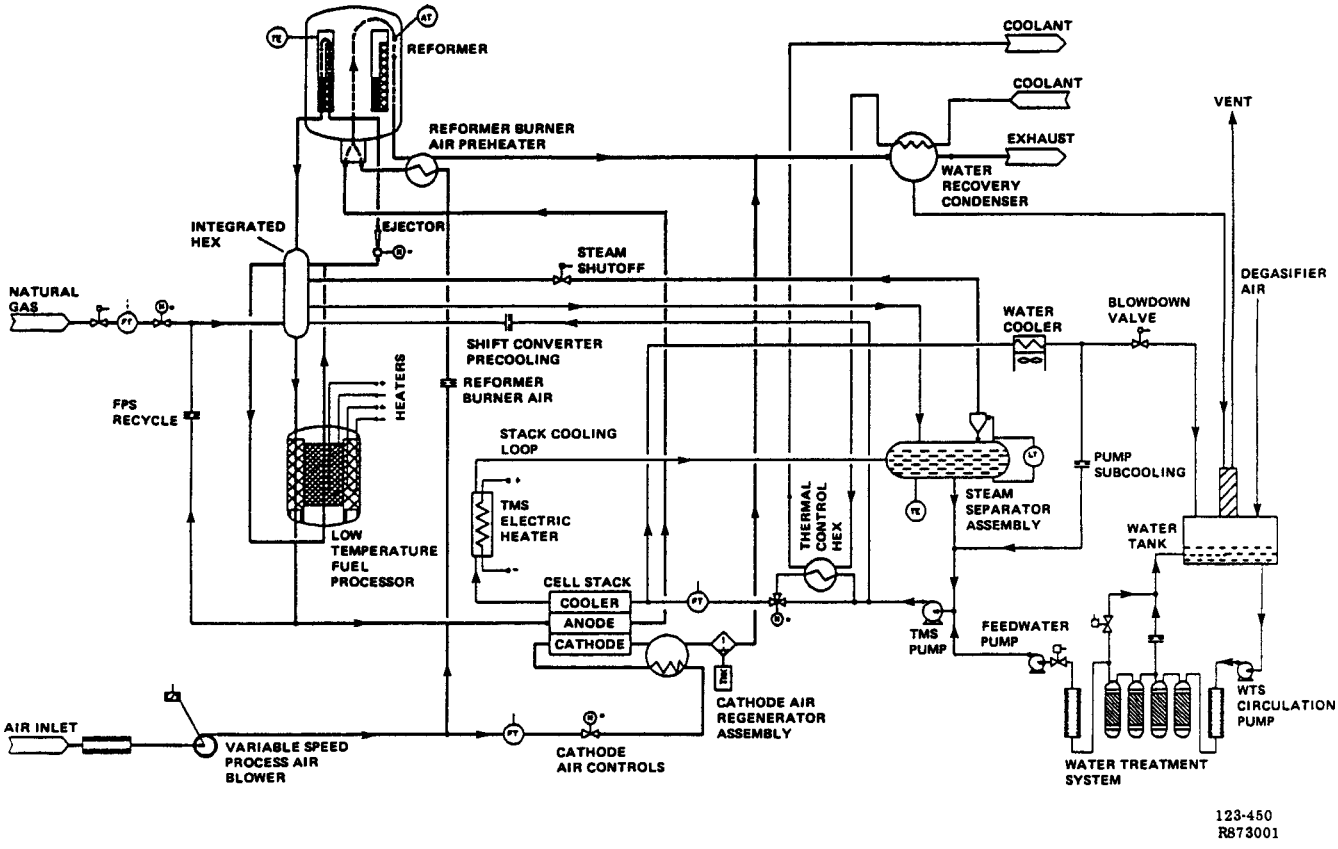

Figure 7.1-1. *Process Schematic*

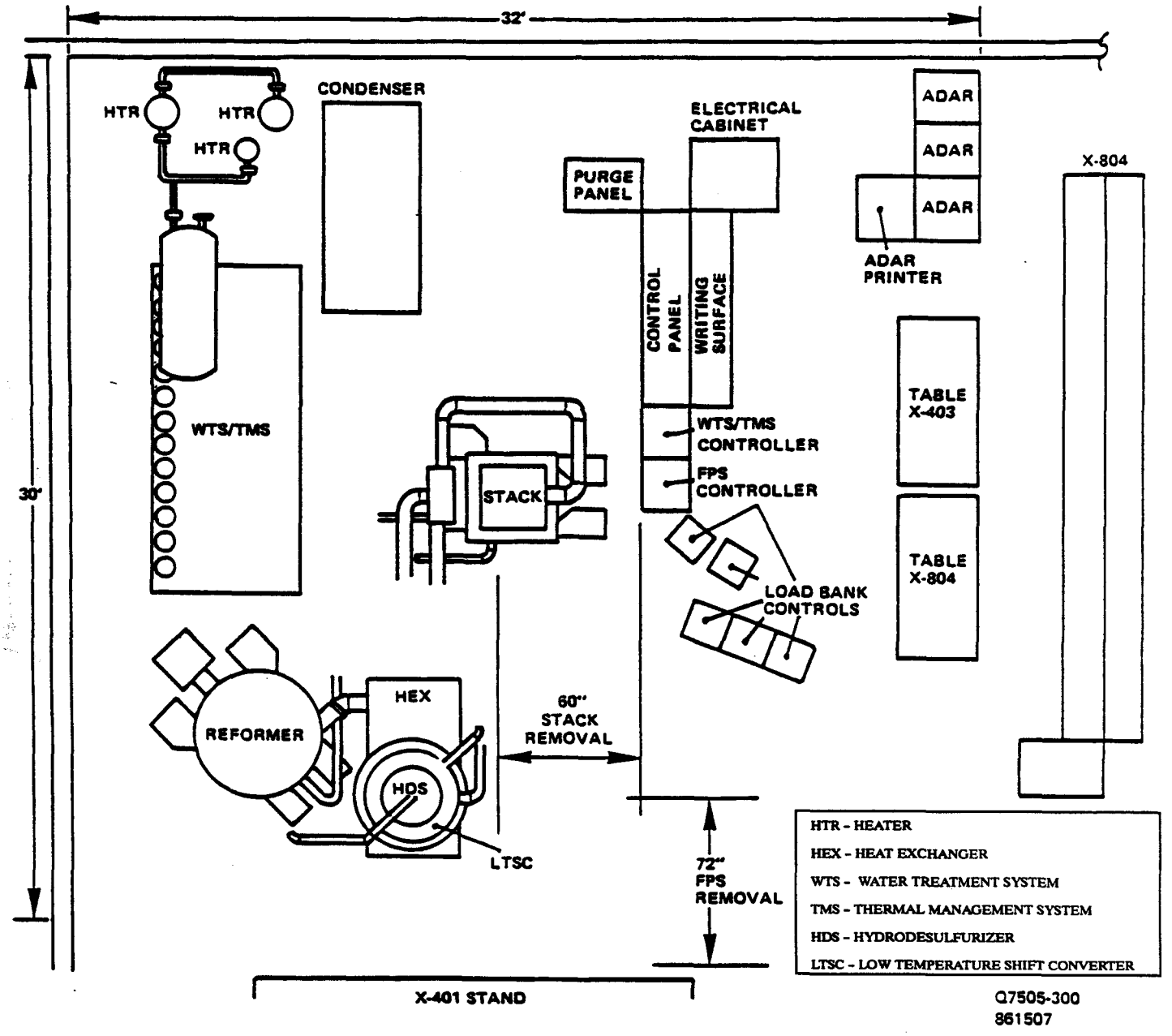

Figure 7.1–2. *VTA/Facility Floor Plan*

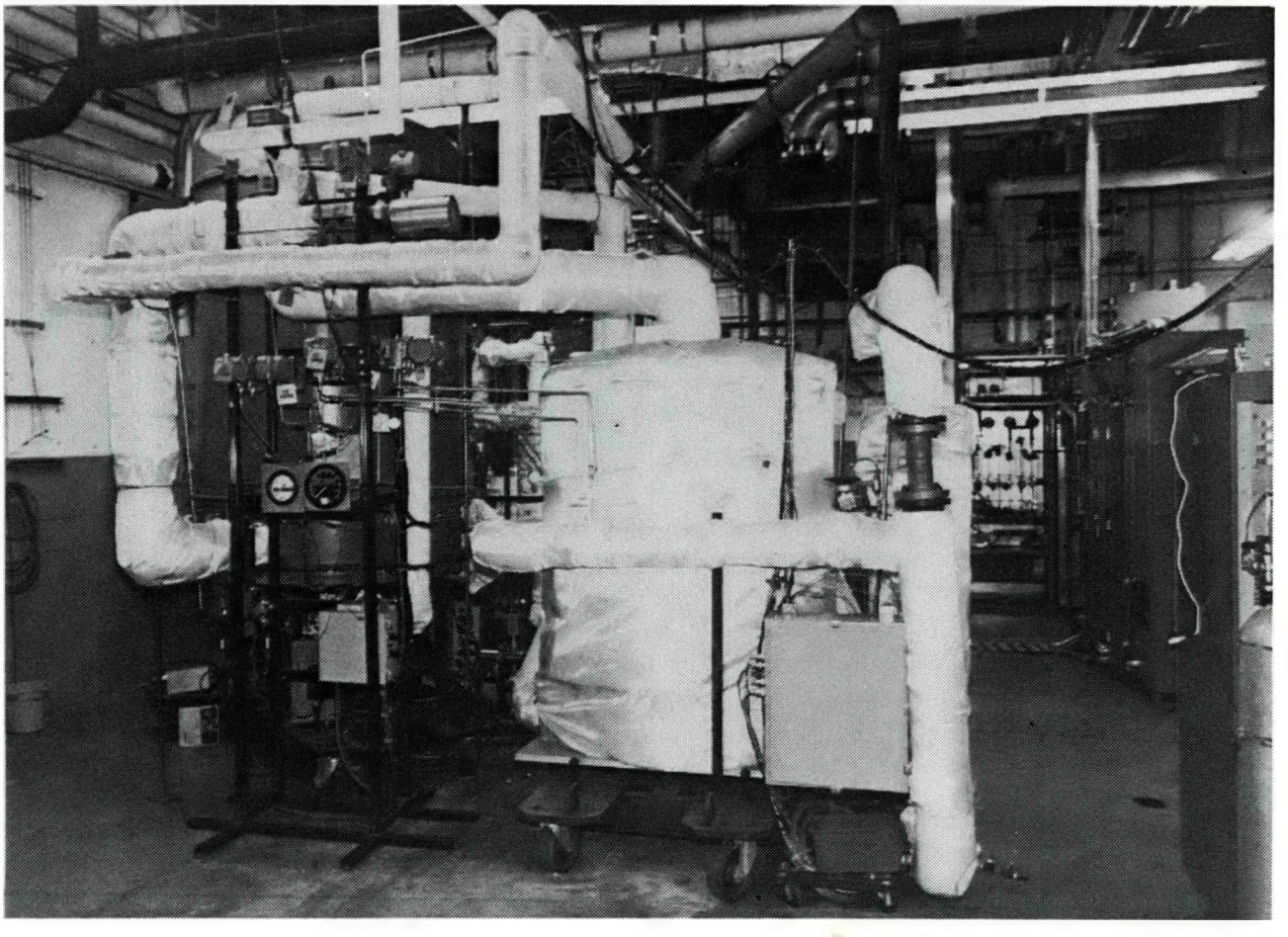

(WCN-14307-1)

Figure 7.1-3. *VTA Fuel Processing System*

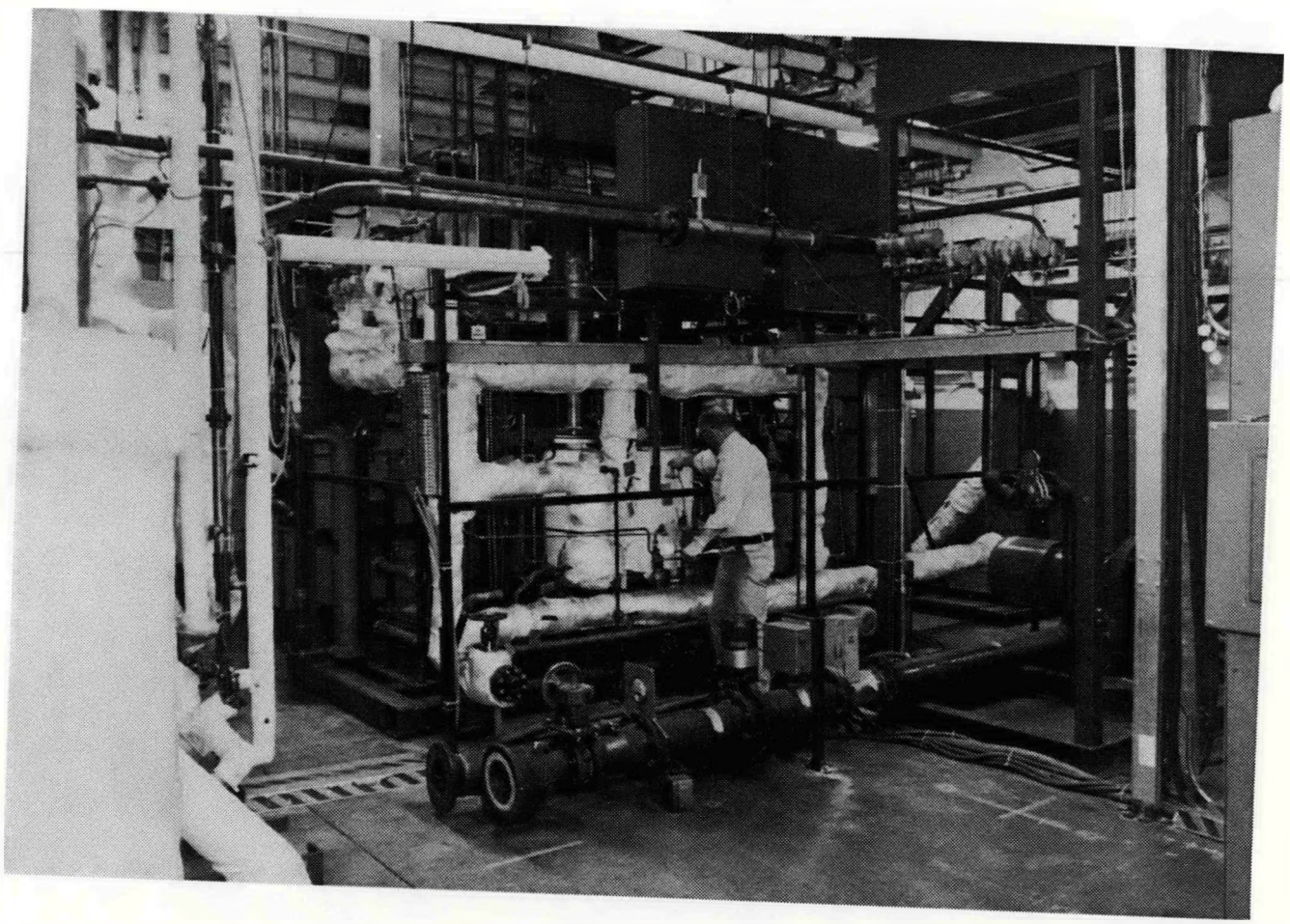

(WCN-14307-7)

Figure 7.1-4. *VTA Water Treatment System*

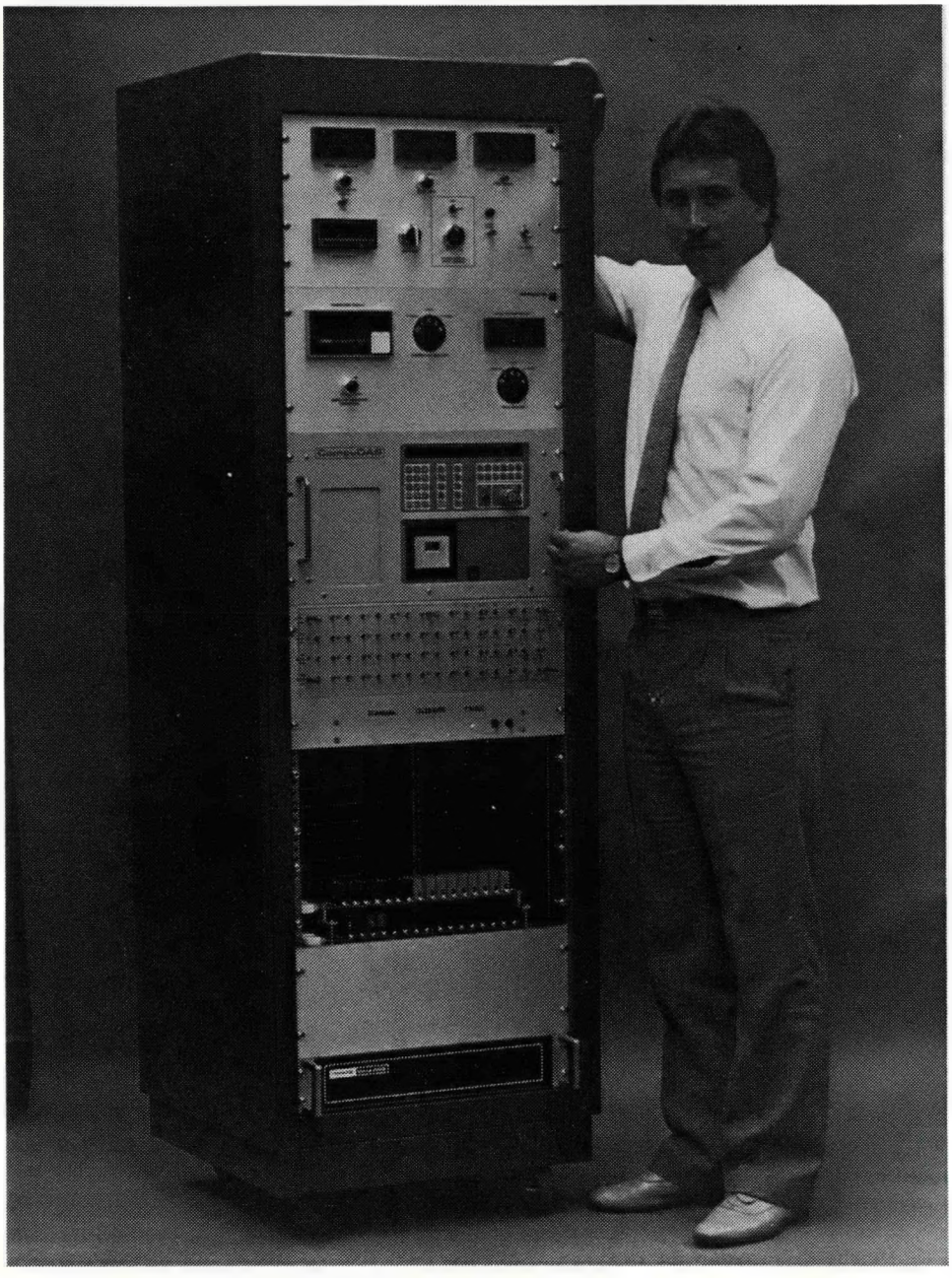

(WCN-13718)

Figure 7.1-5. *Fuel Processor Controller*

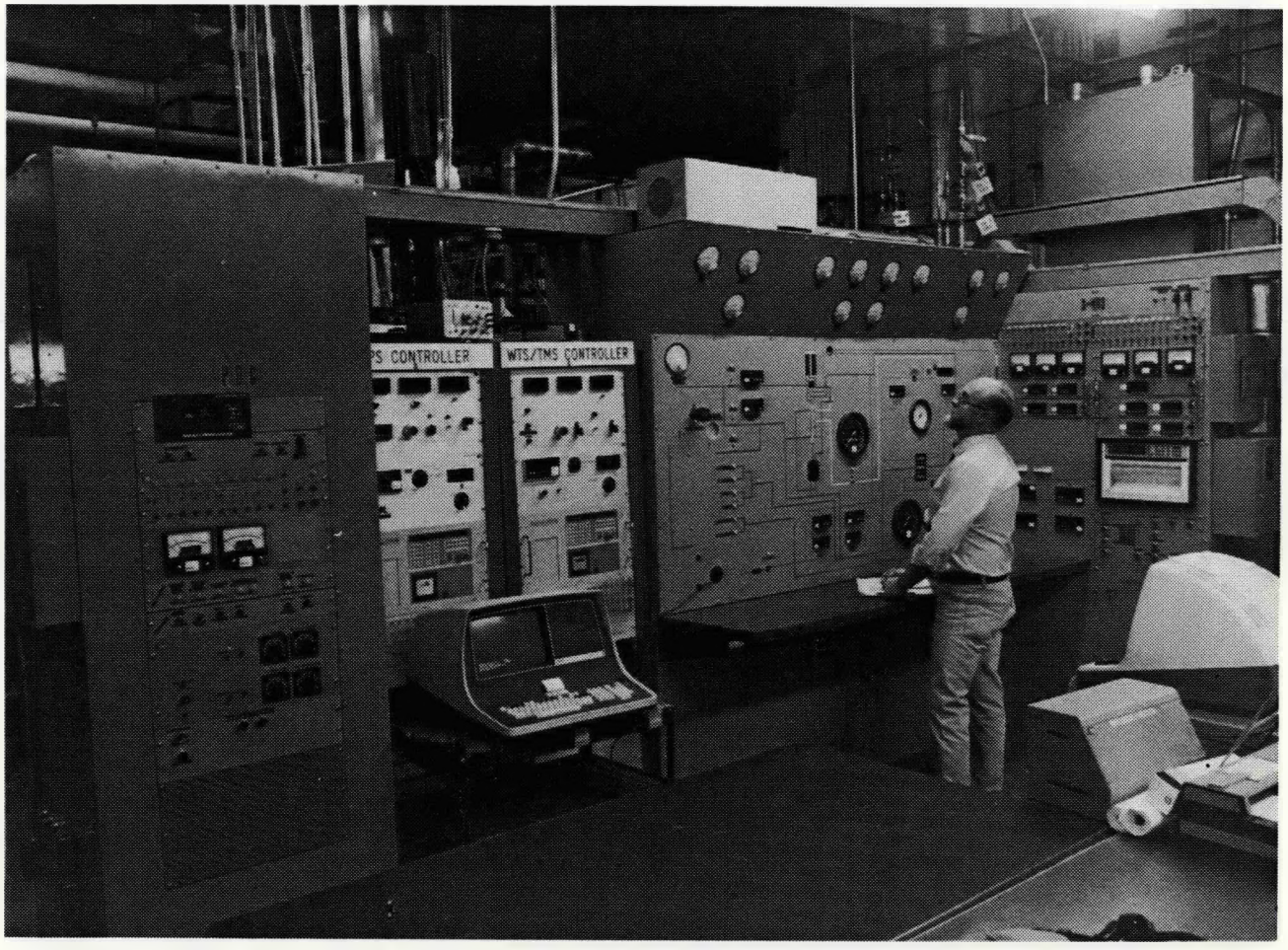

(WCN-14307-11)

Figure 7.1-6. *VTA Control Panel*

Subtask 7.2 - Verification Test

OBJECTIVE

The objective of this task was to verify the integrated operation of the full-scale Verification Test Article (VTA) fabricated in Subtask 7.1 and to provide a test bed for advanced component evaluation. The VTA consists of a full-height cell stack, water treatment and thermal management systems, a fuel processor, and controls.

SUMMARY

Early activities in this task were focused on subscale and full-scale verification of water treatment and cooling system improvements. Over 2100-hours of development testing without flow restriction preceded VTA testing and confirmed feedwater and cooling water improvements planned for the VTA.

On April 23, 1987, the VTA was successfully started in the open-loop configuration. The open-loop configuration was selected to facilitate cell stack "break-in." After completing cell stack "break-in," the VTA was reconfigured into the normal (closed-loop) power plant configuration and restarted.

Initial operation of the VTA confirmed operation over the full power range (up to 210 kWDC) with the performance of the cell stack exceeding the program goal of E + 20 mV. The reformer and water treatment systems performed satisfactorily.

Continued operation of the VTA afforded the opportunity to correct component deficiencies which were recognized during initial testing. The start burner for the reformer was modified to prevent flame-outs during fuel-steam transitions, a new type of coolant pump was installed to improve durability, water treatment changes were implemented to simplify the system and reduce cost without sacrificing water quality, a new steam ejector was installed to improve durability and transient response, a preoxidizer was added to allow operation with peak shave gas, and a new type of anode filter material was evaluated.

After nearly 2700 hours of operation, substack No. 13 in the full-height stack lost performance during an up-transient, and the VTA was shutdown. The stack was removed from the VTA for inspection after a brief diagnostic run. Operating times of the VTA during the twenty-seven (27) runs with the cell stack are listed in Table 7.2-1.

Table 7.2-1. VTA Cell Stack Operating Times

Open-Loop Load Time	182 Hrs
Closed-Loop Load Time	2491 Hrs
Total Load Time	2673 Hrs

The full-scale fuel processor and water treatment system were operated an additional 7 (seven) times for about 250 hours after removal of the stack. The extended testing afforded the opportunity to verify simplifications to the preoxidizer, improvements to steam ejector sealing and actuation, and evaluation of alternative feedwater injection points to improve thermal stability of the cooling water loop.

At the conclusion of the VTA test program the cell stack was properly conditioned for tear-down and analysis and removed from the VTA rig. At that point it was transferred to the DOE Advanced Water-Cooled Phosphoric Acid Fuel Cell Development Contract (DE-AC21-88MC24221).

ACCOMPLISHMENTS/CONCLUSIONS

In general, the Verification Test Article (VTA) demonstrated advances in system, major component, and ancillary component technologies which overcome deficiencies identified in the 40-kW field test, reduce cost, and improve reliability. Specific accomplishments are listed below:

1. Ability of all major components and controls to accommodate system operating requirements associated with startup, power generation, and shutdown to either a "hot hold" or cold condition. Startups were typically completed in less than 4-1/2 hours from a cold condition in the cell stack and reformer and were consistently below the 5-hour goal; restarts from "hot hold" were performed in as little as 30 minutes.

2. Stable system operation over full power range up to the rated power of 210 kWDC. Nearly two-thirds of the VTA operating time was accumulated at 180 kW (300 ASF) or above.

3. Cell stack performance which exceeded the program goal of E + 20 mV. As shown in Figure 7.2-1, this performance is significantly above the stack performance demonstrated in 40-kW on-site power plants.

4. Successful operation of a new water treatment system which significantly improved water quality (over previous 40-kW on-site power plant field experience) with no signs of cooling water flow restriction. See Figures 7.2-2 and -3. Continued operation provided the opportunity to verify simplifications such as reduction in the number of resin beds, elimination of filters, and removal of the air regenerator (acid condenser) assembly from the system.

5. Emission characteristics better than program goals even though goals were established to be at least an order of magnitude below existing federal and state standards. See Figure 7.2-4.

6. Successful operation on peak shave gas mixtures containing propane and air by adding a preoxidizer to eliminate oxygen. Further testing identified a simplified preoxidizer configuration which could reduce catalyst volume by up to 85% when compared to the original unit.

7. Full power transient capability within 15-seconds was demonstrated. Analytical projections indicate that transient response requirements for both grid-connect and grid-independent power plants can be met with identified improvements to the steam ejector and oil control.

8. A new steam ejector with improved sealing to prevent leakage without binding and faster response actuator to increase transient capability.

9. Full water recovery at rated power with conditions simulating operation on a 95°F day.

10. Successful development and verification of feedwater and cooling water pumps for on-site power plant service.

11. System simplifications such as eliminating the centrifugal steam separator, downsizing the steam drum, and integrating a new anode filter material into existing fuel processor vessels.

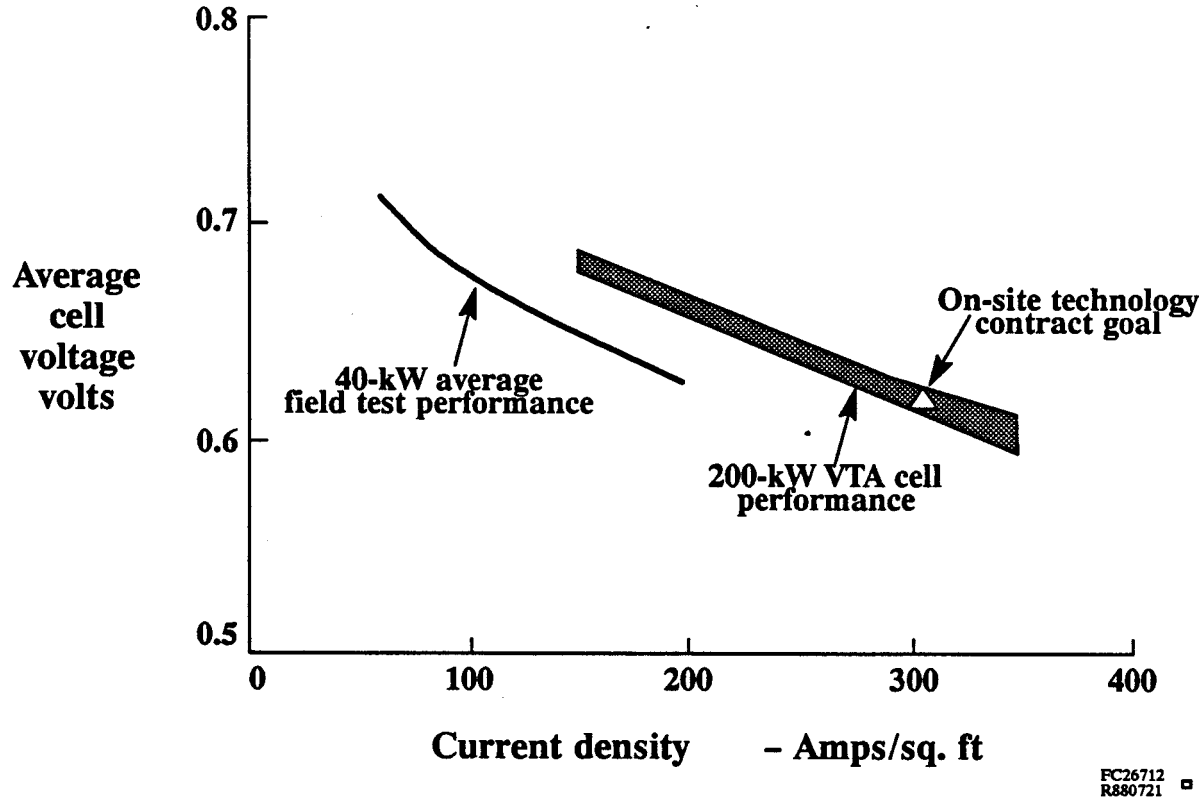

Figure 7.2–1. *On–Site Cell Stack Performance Comparison*

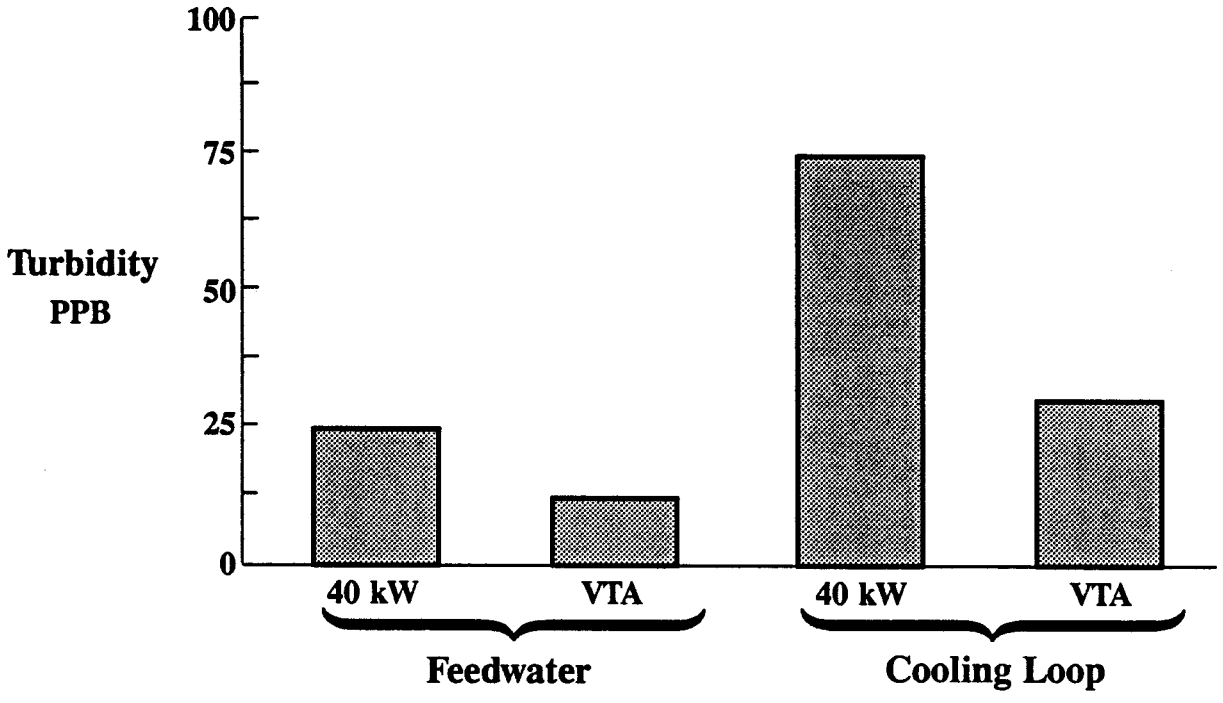

Figure 7.2–2. *Water Quality Comparison*

VTA COOLING WATER EQUIVALENT ORIFICE DIAMETER

295 - 305 ASF

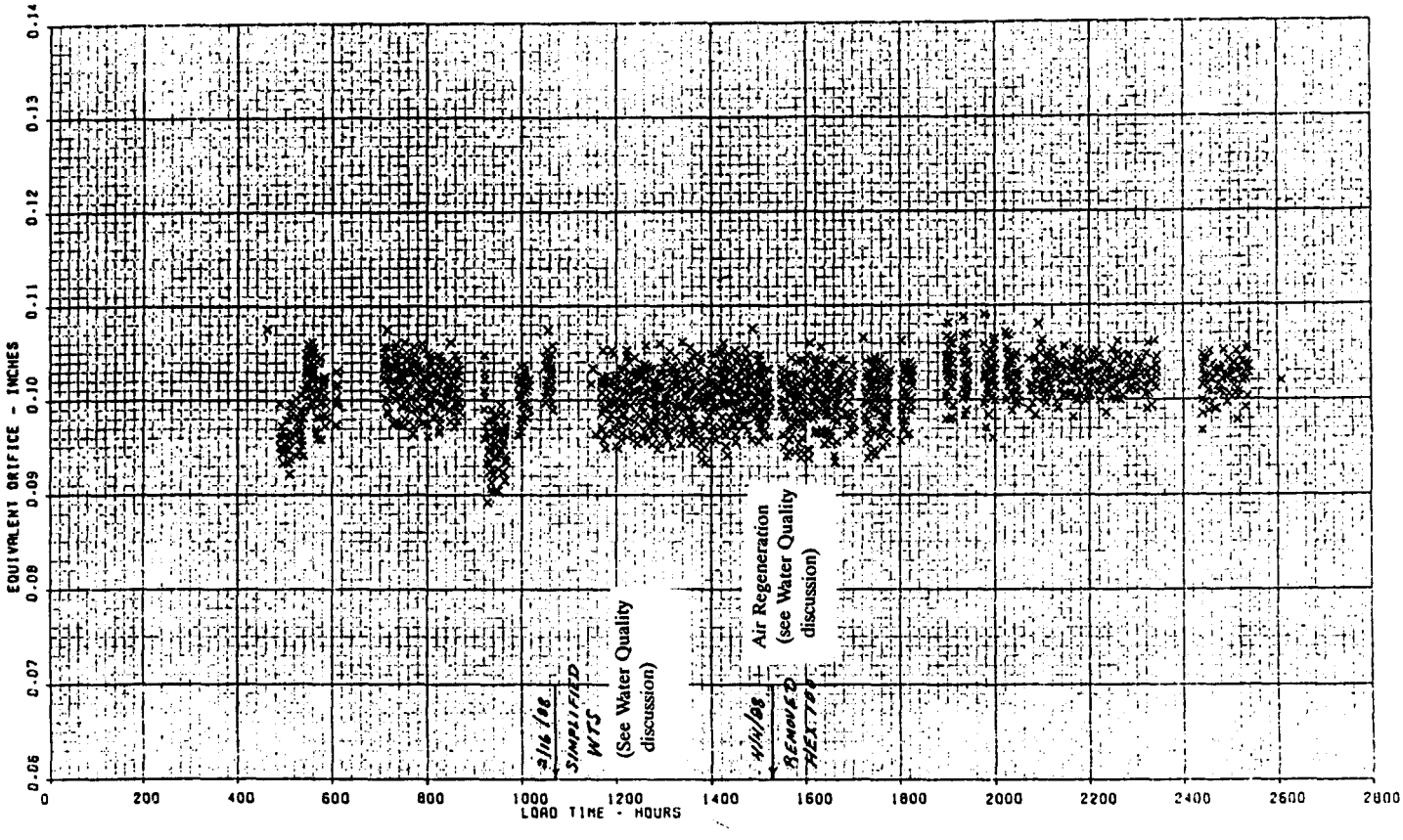

Figure 7.2-3. *VTA Flow Resistance History*

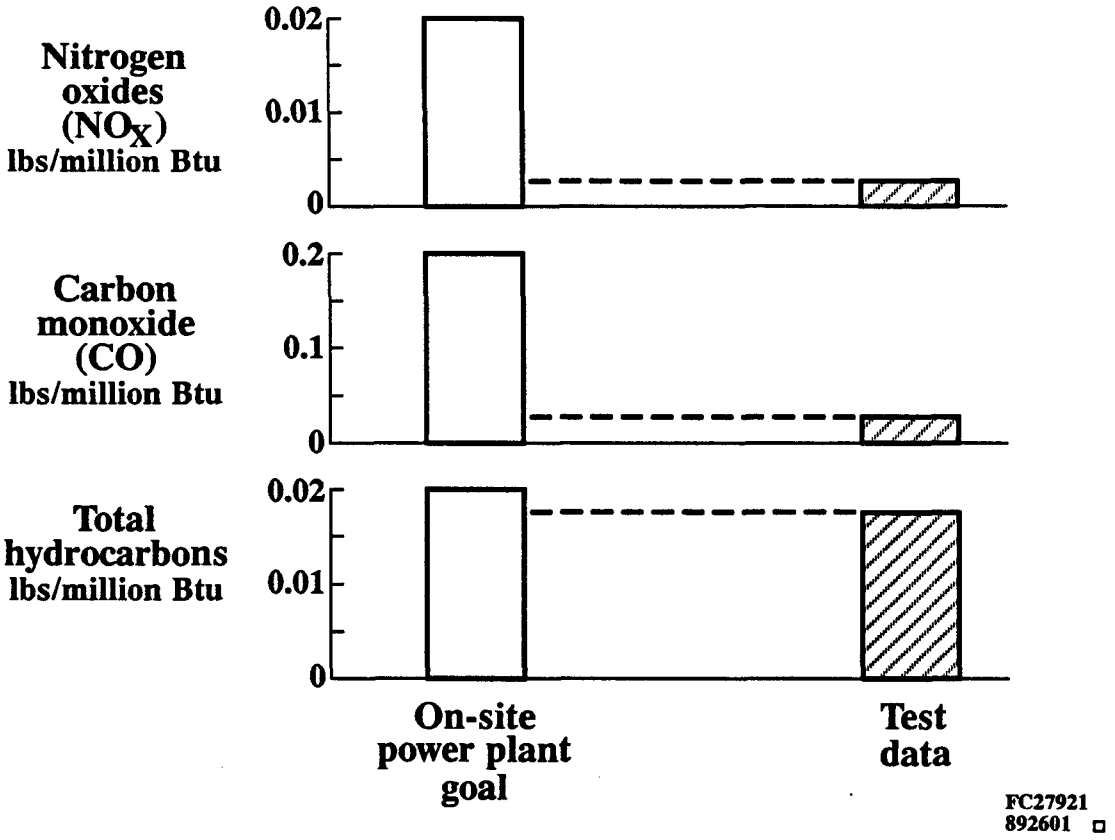

Figure 7.2–4. *Verification Test Emissions*

DISCUSSION

The thirty-three (33) runs of the Verification Test Article (VTA) afforded the opportunity to investigate many modes of power plant operation. The first sections discuss various subjects investigated during the 2900 hours of operation and results of these activities. The final section (VTA Test Activities) provides an operating history of the VTA including brief description of each run.

Cell Performance

The initial full–height cell stack performance was generally good. Figures 7.2–5 and 7.2–6 show that average cell performance is 15 to 25 mV above E–line, and that the performance goal of E + 20 was met above 120 ASF. During Run 8, at approximately 500–hours of load time, a stack performance calibration was conducted over the full power range up to 365 ASF current density. As shown in Figures 7.2–7 and 7.2–8 cell performance was slightly better than short stack No. 3 and about 30–mV above E–line between 200 and 365 ASF.

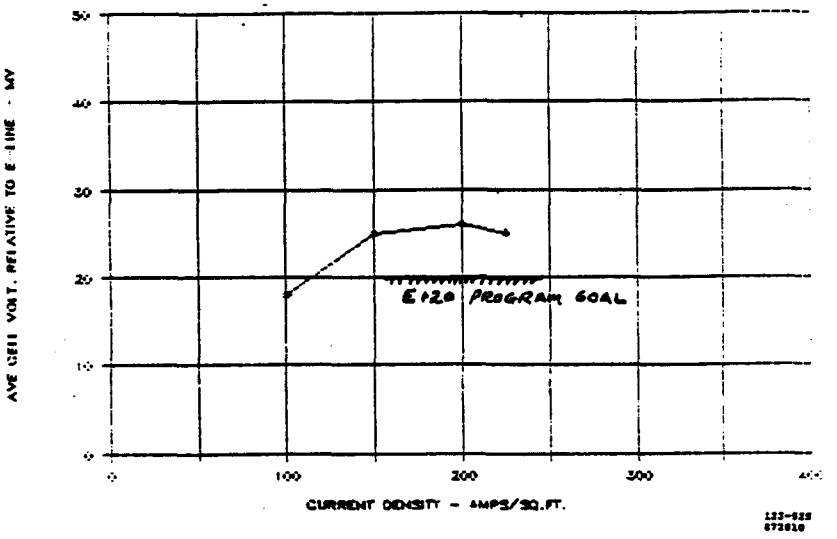

Figure 7.2–5. *Initial Cell Performance Calibration*

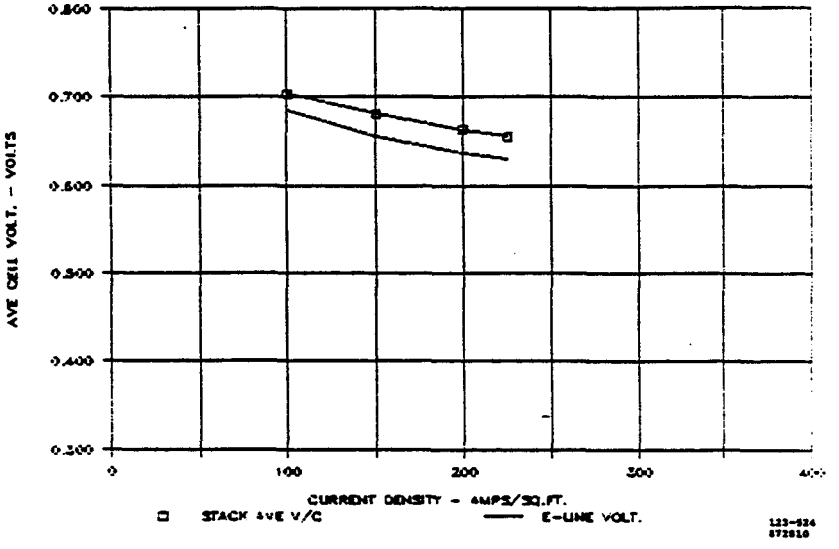

Figure 7.2–6. *Initial Performance Calibration Comparison*

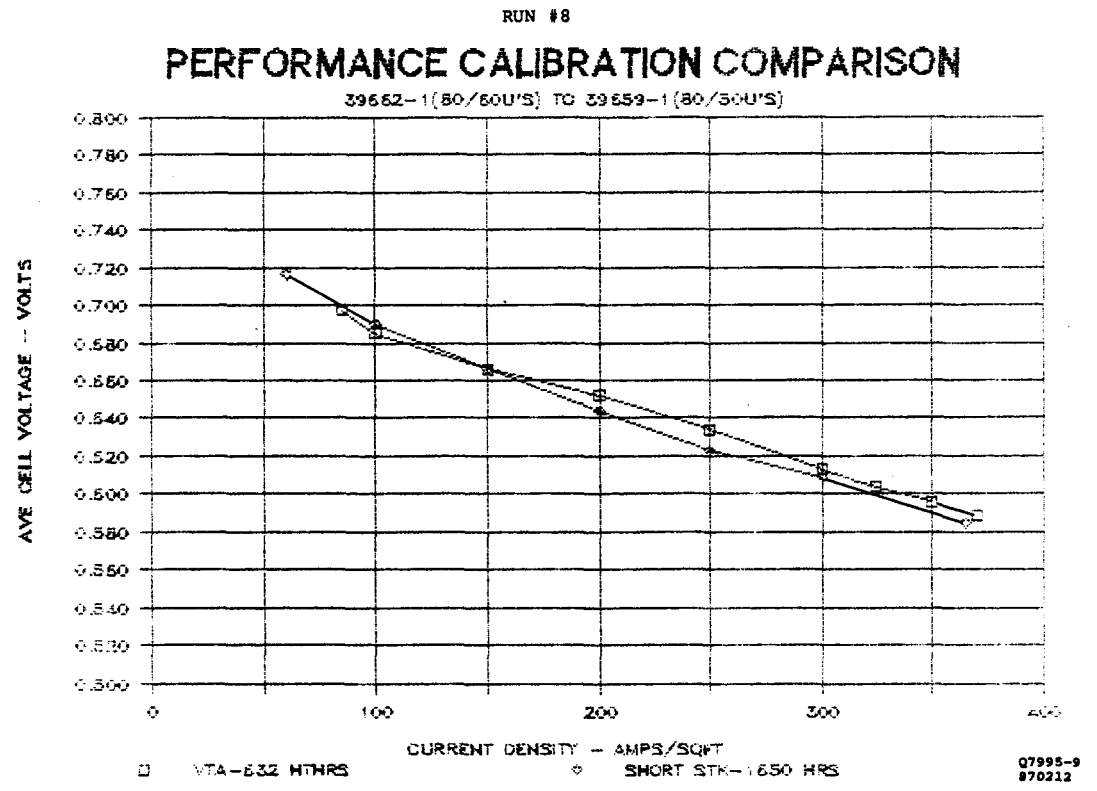

Figure 7.2–7. *500–Hr. Stack Performance Comparison*

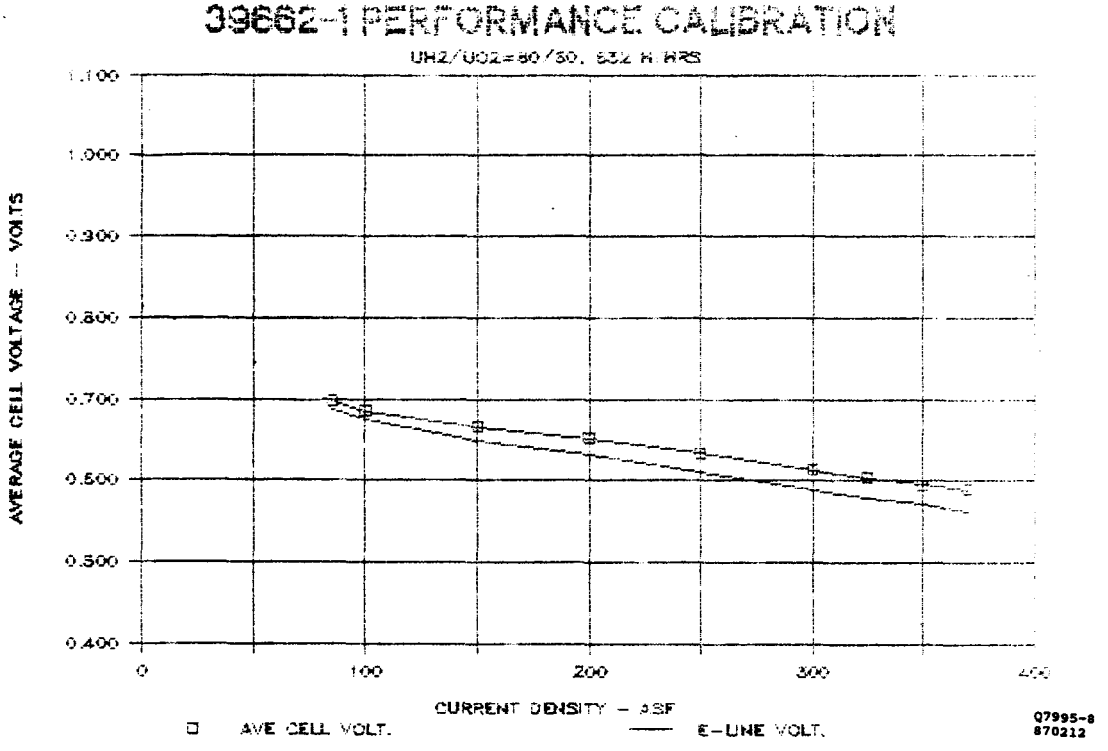

Figure 7.2–8. *500–Hr. Stack Performance Calibration*

The stack performance at 300 ASF through nearly 2700-hours of load time is shown in Figure 7.2-9. The performance was stable during periods of extended operation (without shut-downs) at or below 300 ASF. Runs 15 and 26 are examples of runs over 450-hours without significant decay. Figure 7.2-10 shows the stability of stack performance at various current densities during Run No. 26.

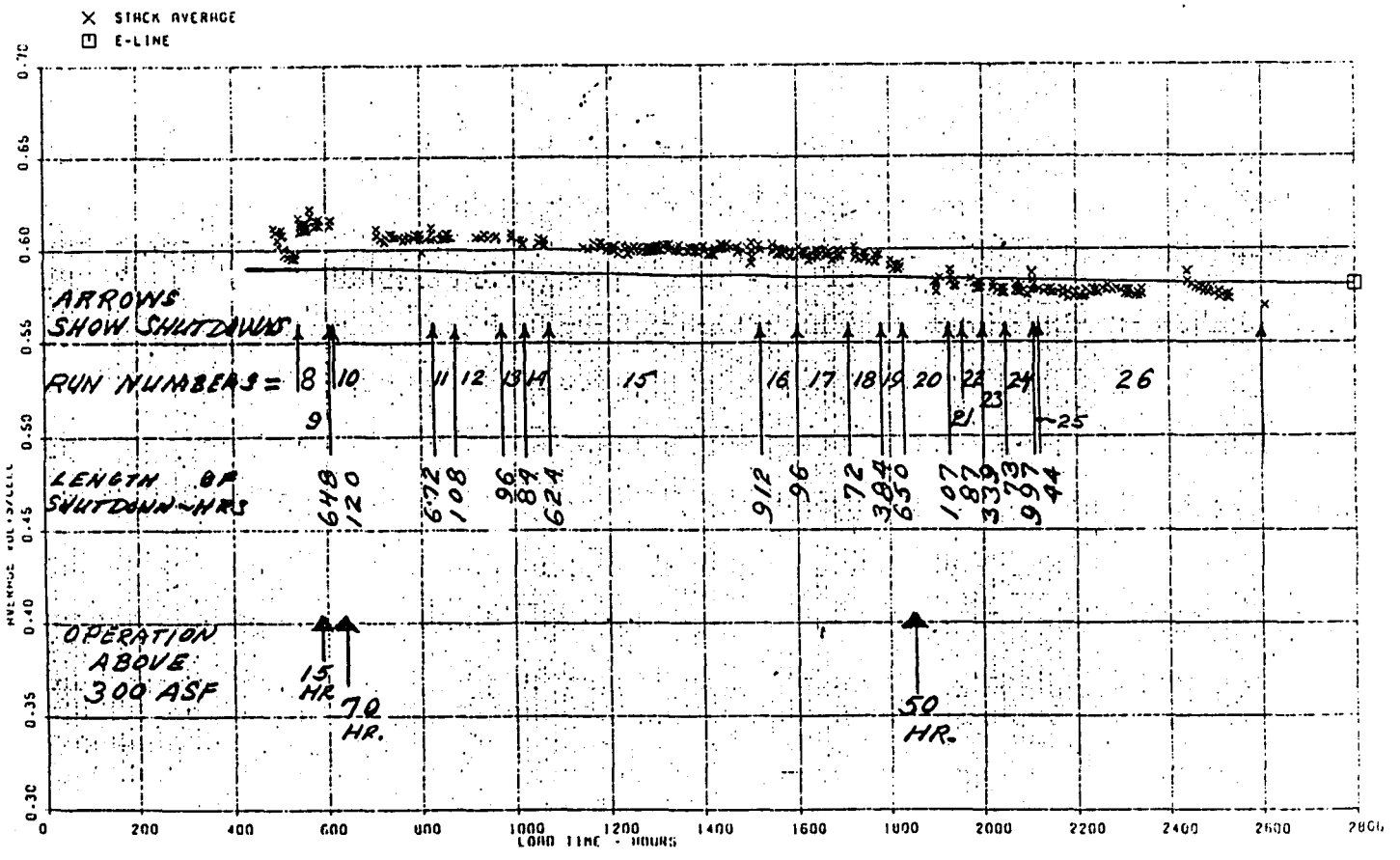

Figure 7.2-9. *VTA Stack Performance History at 300 ASF*

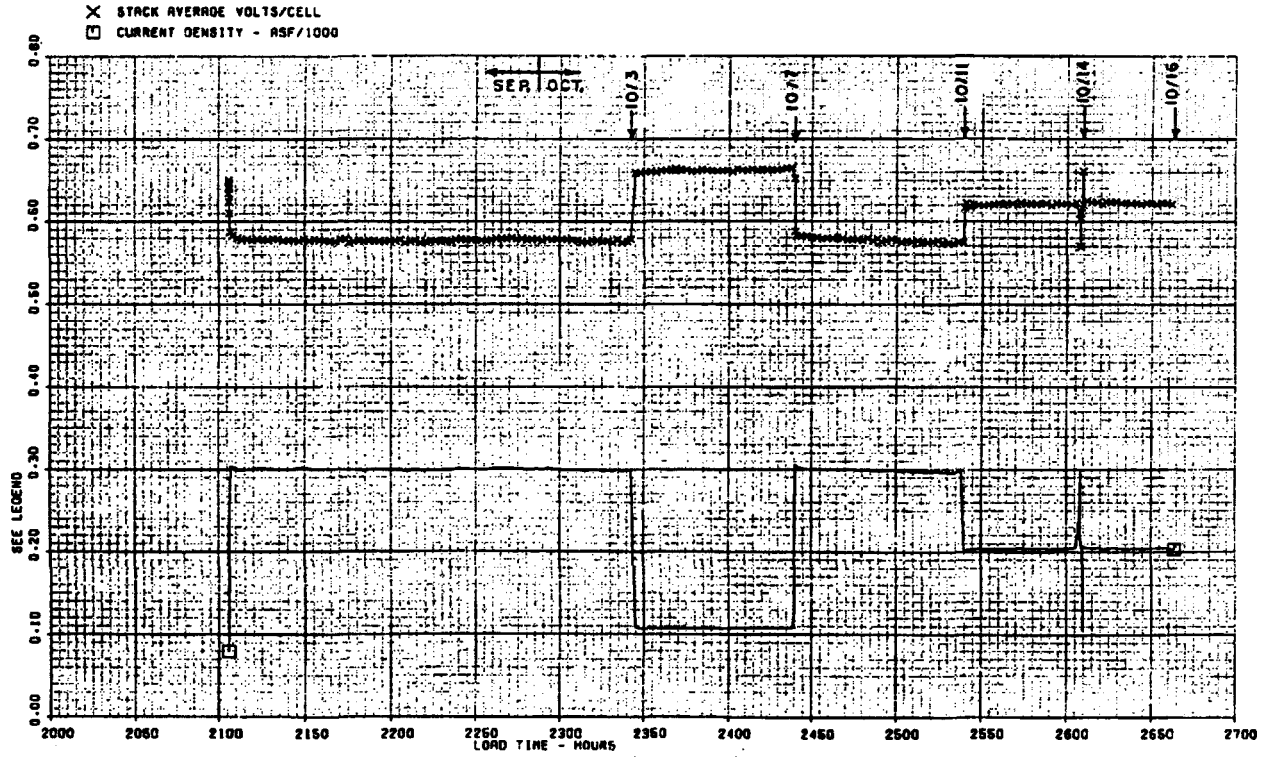

123-630
882911 ●

Figure 7.2–10. *VTA Stack Performance During Run 26*

The loss of performance evident in Figure 7.2–9 is primarily associated with startup and shutdown cycles. While the 36 startup/shutdown cycles experienced on the VTA is associated with the test program and is not typical of the number expected in production power plants, efforts were made to minimize these losses by modifying the passivation purges during start/stops and limiting the time at open circuit. Unfortunately, there was inadequate time to evaluate these improvements.

Figure 7.2–11 shows a comparison of substack No. 13 performance to average cell performance during operation on Run 26. The drop–off in substack No. 13 performance during the transient from 200 to 300 ASF can be clearly seen. A review of data during and following the up–transient indicates that one or two cells in the bottom of the substack are involved. It was decided to perform standard cell stack diagnostics. The hydrogen gain test (Figure 7.2–12) clearly showed an anode problem in Substack No. 13 and the cell stack was removed from the VTA for teardown inspection under a complementary technology program.

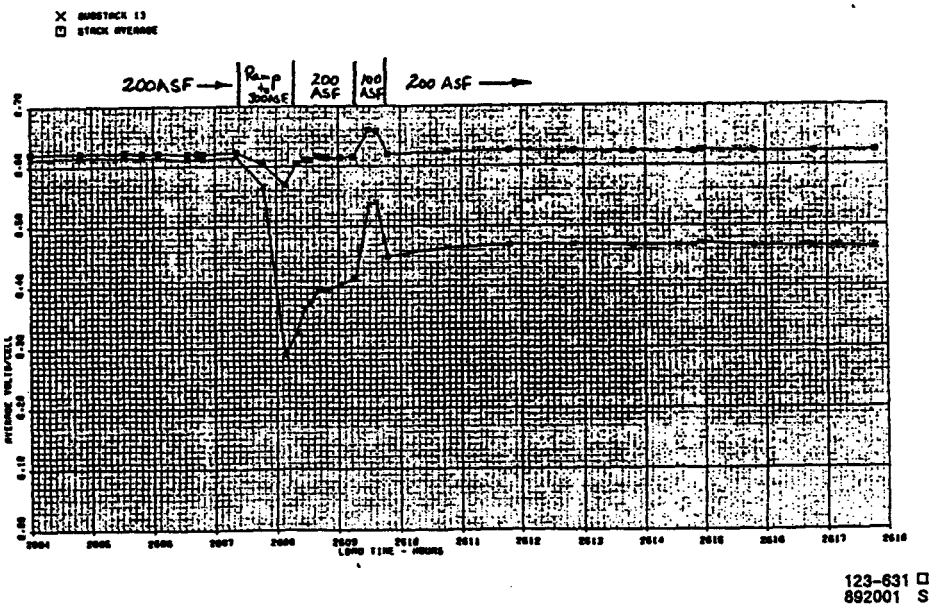

Figure 7.2-11. *VTA Substack 13 Performance on 10/14/88*

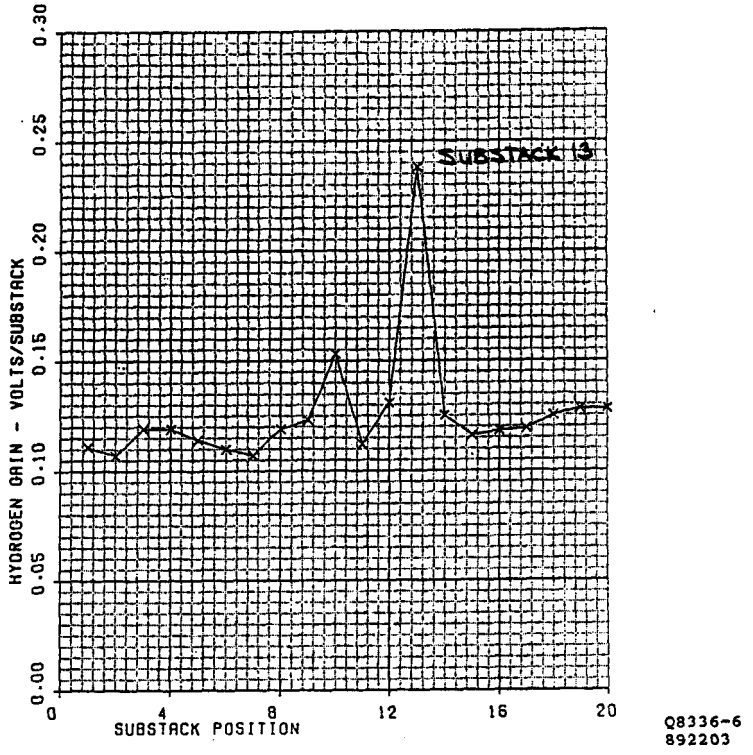

Figure 7.2-12. *Hydrogen Gain at 100 ASF*

A few other performance anomalies were noted during the nearly 2700-hours of operation and special diagnostic tests which were conducted prior to removal of the stack from the VTA. The following items were noted and will be investigated during the stack teardown inspection in a complementary program:

1. Two substacks (numbers 12 and 29) were unusually low in performance. As shown in Figure 7.2-13, the performance discrepancy between these two substacks and the remainder of the substacks increased when current density was raised from 100 to 225 ASF.

   Because of this discrepancy, the VTA was reconfigured in the open loop mode to allow a pure hydrogen supply to the cell stack for diagnostic purposes. Two diagnostic runs (Runs 6A and 6B) were conducted. The hydrogen/air performance of the cell stack was evaluated up to 325 ASF. The H_2 gains were normal, but the O_2 gain test shown in Figure 7.2-14 clearly indicated that substacks 12 and 29 were sensitive to air flow and probably had a cathode problem. Under these conditions, the substacks could be operated stably over the full power range, and immediate cell stack repair was not required. Figure 7.2-15 shows the two substacks did operate stably for the remainder of testing.

2. As shown in Figure 7.2-16, two substacks (numbers 28 and 35) were more sensitive to reactant cross-pressure than other substacks during open-circuit diagnostic tests indicating higher reactant leakage in these substacks.

3. Substacks in the top-half of the cell stack were unusually sensitive to hydrogen flow during open-circuit diagnostic tests. See Figure 7.2-17.

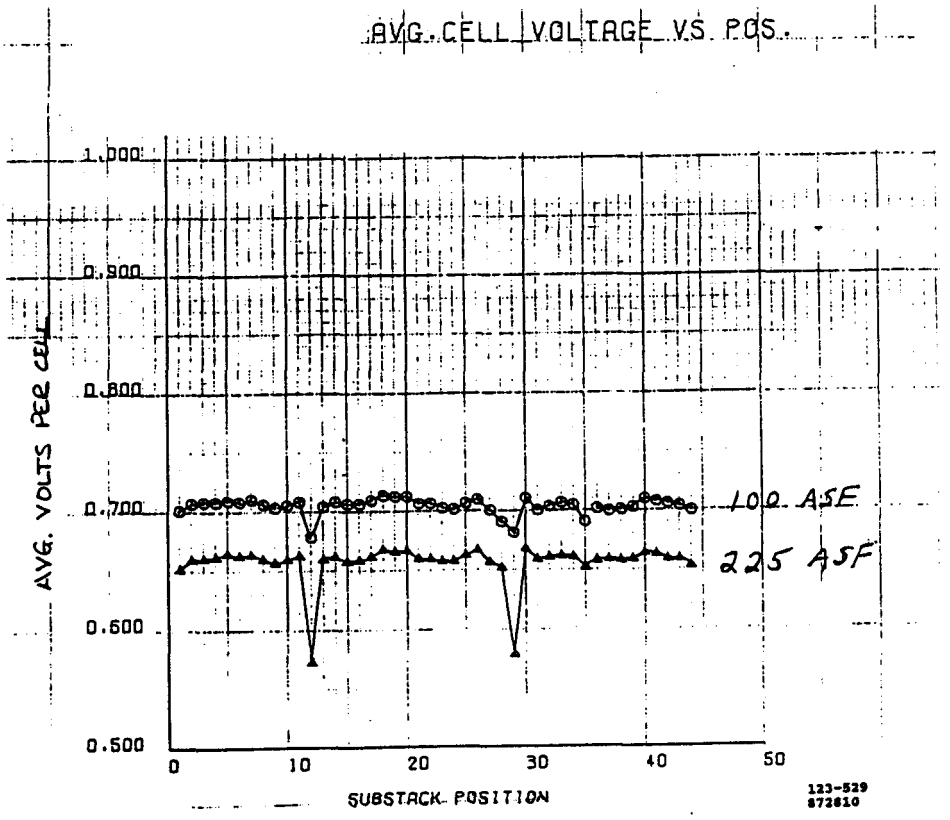

Figure 7.2–13. *Average Cell Voltage Versus Position*

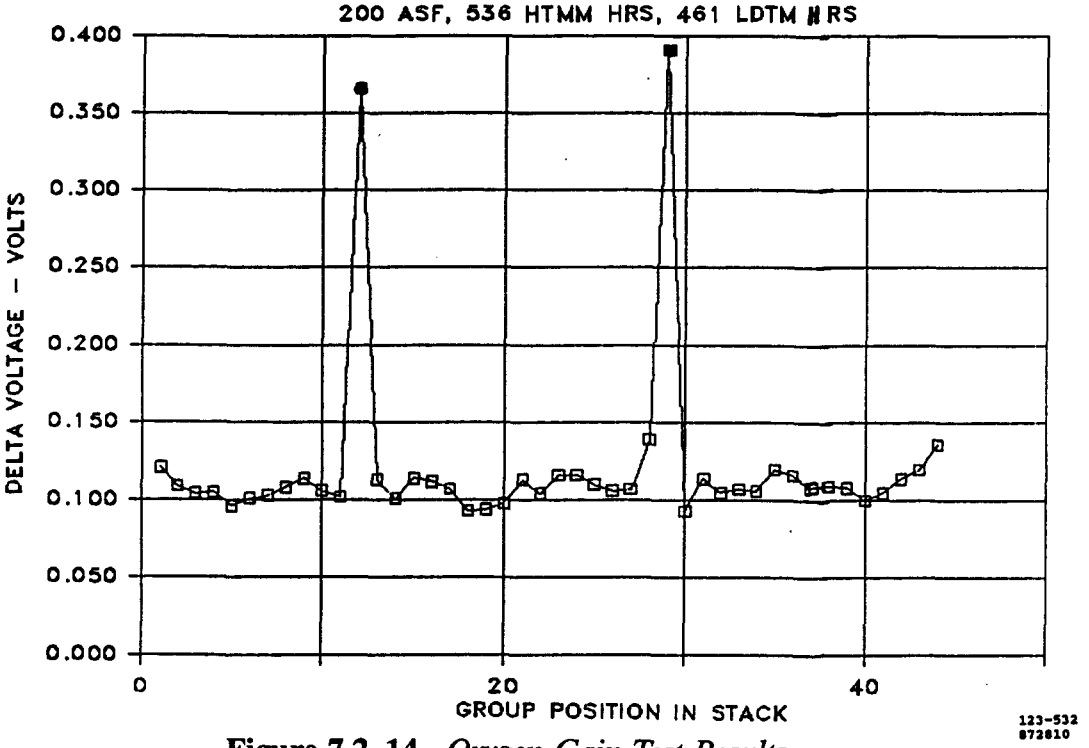

Figure 7.2–14. *Oxygen Gain Test Results*

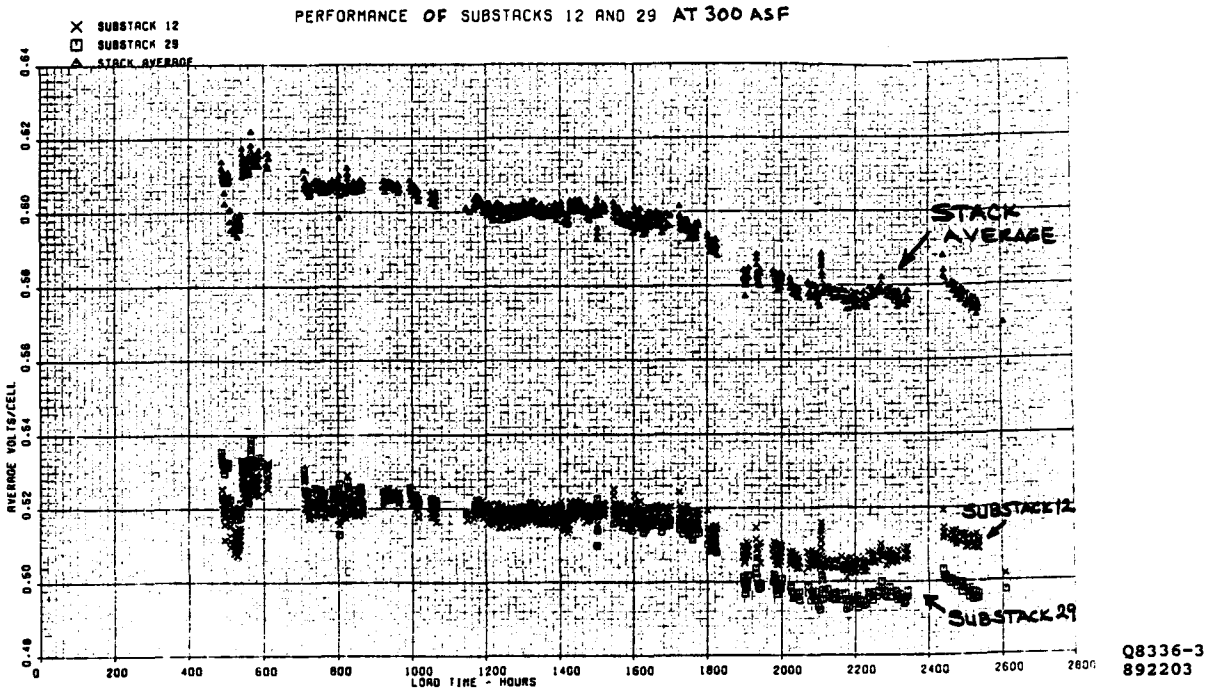

Figure 7.2–15. *Performance History of Substacks 12 and 29*

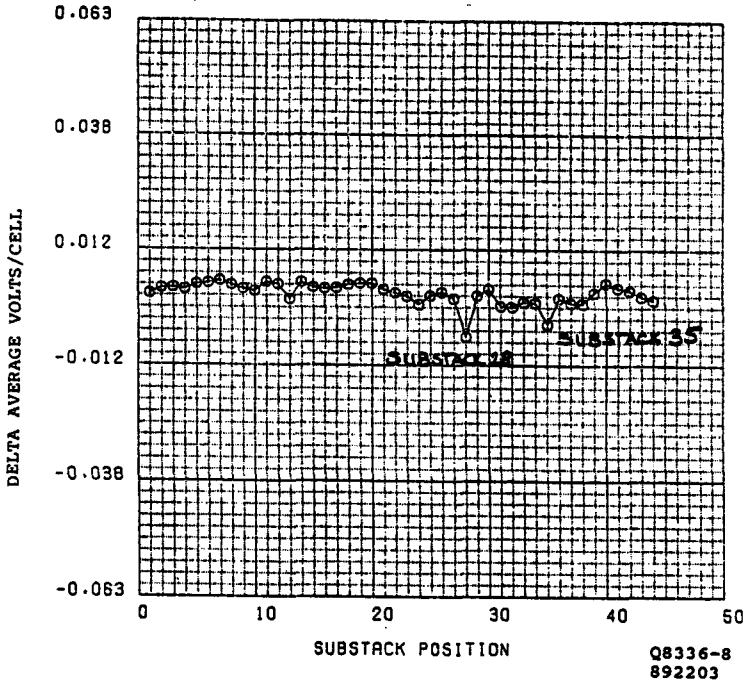

Figure 7.2–16. *Effect of Reactant Cross–pressure at Open–Circuit*

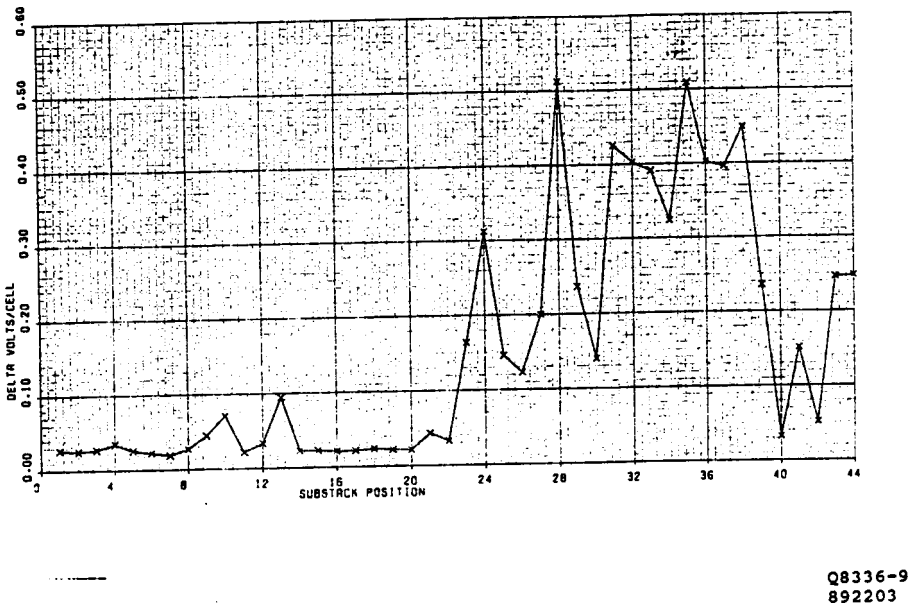

Figure 7.2–17. *Effect of Hydrogen Flow on Open–Circuit*

Water Quality

A significant effort in this program was directed toward eliminating the cooler deposition problem experienced in the 40–kW power plant field test program. Cell stack coolers in 40–kW power plants typically required chemical cleaning every 2000–hours. As discussed in Subtask 2.3, the coolers were redesigned to be more tolerant to buildup of impurities in the water. The thrust of this task was to improve the water chemistry and, thereby prevent deposition.

Water chemistry goals for the new water treatment system were empirically established based on data from a hydrogen–fueled 40–kW power plant. This power plant operated for over 7700–hours without requiring cleaning of the coolant system. This successful operation without deposition is credited in-part to the cleanliness of the feedwater.

A subscale test rig incorporating features of the new water treatment approaches was built and tested with a 32–cell short stack. A test section of three flow control orifices of the early 40–kW design (.055 inch diameter) was included to provide a very early indication of corrosion product disposition. The test rig operated for 2163 hours with excellent results. The feedwater quality was markedly better than typical 40–kW power plants and similar to the hydrogen–fueled unit. No evidence of corrosion product deposition was observed in the control orifice test section as determined by flow and pressure differential measurements and post test inspection of the coolant manifolds and ports after the test.

The next step was to scale-up for the full-size Water Treatment System (WTS) used in the VTA. A process schematic of the original WTS used in the VTA is shown in Figure 7.2-18. Initial results from the VTA were very encouraging; water cleanliness of the original full-scale WTS were similar to the subscale test rig. The only change made to the WTS during initial testing was to add a "splash pan" to the water tank (after Run 8) and, therefore, increase the marginally-acceptable oxygen level throughout the system.

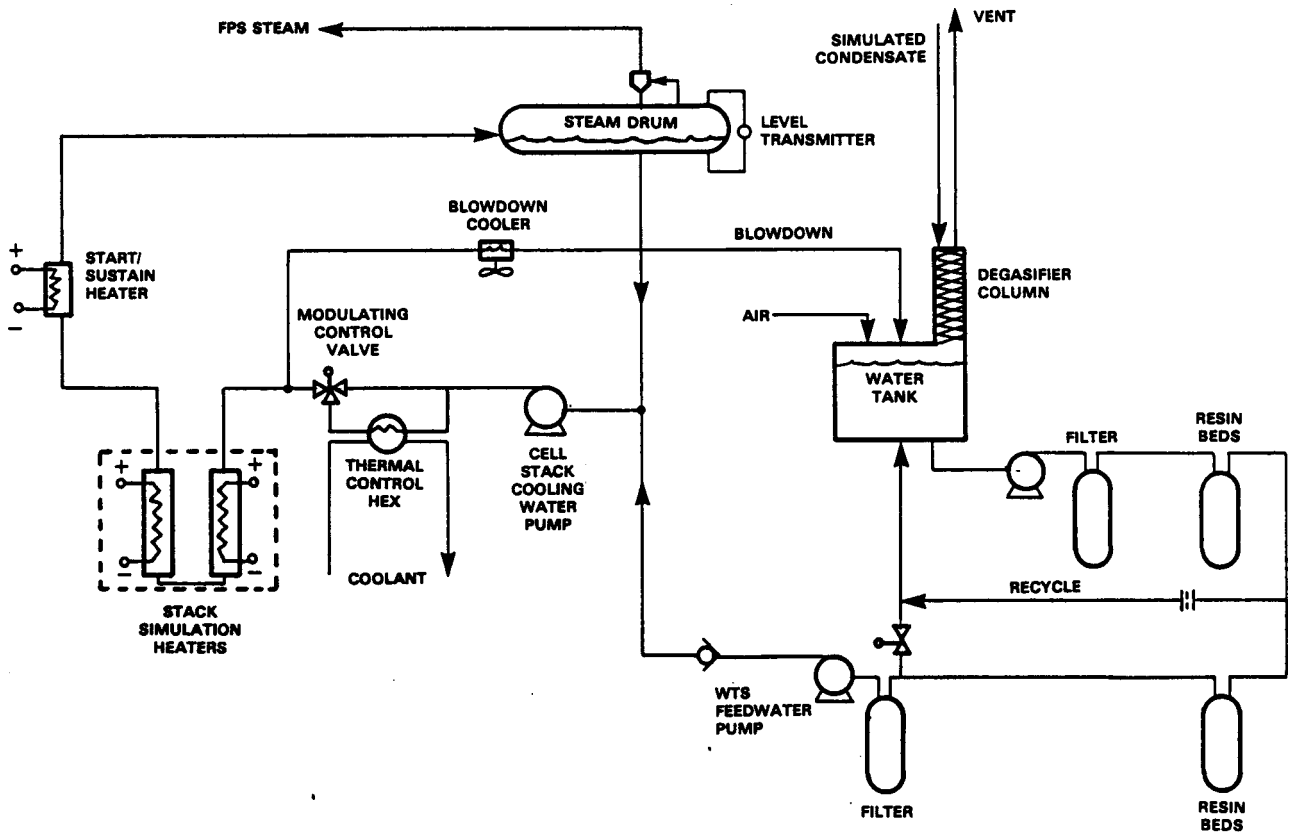

Figure 7.2-18. *Water Treatment and TMS Subsystems*

After about 1100-hours of operation without difficulty (before Run 15), the Water Treatment System was modified to simplify the system. The new configuration consisted of two bottles of mixed resin and a charcoal bed. This represents a reduction from 7 WTS bottles to 3. After Run 15, the system was further simplified by removing the air regenerator (acid condenser) from the VTA. As shown in Tables 7.2-2 and 7.2-3, the performance of the new simplified WTS is comparable to previous successful systems.

Based on results at the end of VTA testing, the 2-mixed beds in the simplified WTS are effective for about 1000 load hours; and 4 beds will be required to increase the service interval to 2000-hours. More importantly, however, there were no indications of cooler deposition problems.

Table 7.2–2. Feedwater Water Analysis Data

		Standard 40 kW	Hydrogen Fuel 40-kW	Subscale VTA	VTA Testing Original WTS	VTA Testing Simplified WTS
Conductivity, μ MHO		0.285	0.2	0.11	0.28–0.3	0.2
PPM Alkalinity		0.29	BDL	BDL	1.025–1.1	-
pH		7.96	-	6.97	6.3–6.5	6.0–6.5
PPB Fe		51	< 40	< 10	25	< 5
PPB Cu		28	< 30	< 10	< 10	< 5
Anions - PPB	SO_4	295	< 30	< 40	< 50	< 10
	CL	76	< 10	< 10	< 50	< 40
	F	153	< 10	< 10	< 50	-
	PO_4	148	< 40	< 50	BDL	< 40
	NO_3	88	< 30	< 40	BDL	< 10
	NO_2	55	< 10	< 10	BDL	-
PPM Total SiO_2		-	-	< 1	-	-
PPM Reactive SiO_2		-	-	< 1	-	-
Organics - PPM C.O.D.		-	-	8.8	-	-
- PPM T.O.C.		-	-	< 0.5	-	-
Dissolved O_2, PPM		-	-	4–5	3–6	3–6

Notes:
BDL - Below Detection Limit

Table 7.2-3. Cooling Water Analysis Data

	Standard 40 kW	Hydrogen Fuel 40-kW	Subscale VTA	VTA Testing Original WTS	VTA Testing Simplified WTS
Conductivity, μ MHO	0.653	0.80	0.33	0.36	0.4
PPM Alkalinity	1.5	BDL	BDL	0.5	-
pH	7.88	-	7.14	6.5	6.3
Turbidity, PPB	50-75	BDL	BDL	10	10
PPB Fe	(70)	< 40	< 10	65	6
PPB Cu	21	< 30	< 10	< 10	< 5
Anions - PPB SO_4	353	< 30	< 40	< 50	< 10
CL	90	< 10	< 10	< 50	< 10
F	188	< 10	< 10	< 50	-
PO_4	84	< 40	< 50	BDL	< 40
NO_3	124	< 30	< 40	BDL	< 10
NO_2	78	< 10	< 10	BDL	-
PPM Total SiO_2	-	-	< 1	-	-
PPM Reactive SiO_2	-	-	< 1	-	-
Organics - PPM C.O.D.	-	-	7.0	-	-
- PPM T.O.C.	-	-	0.4	-	-
Dissolved O_2, PPB	20-40	-	30-100	30-80	30-60

BDL - Below Detection Limit

Emission Characteristics

The VTA emission goals were established to meet world-wide emission requirements and be below present Federal (EPA) and state standards by nearly an order-of-magnitude. For example, the South Coast Air Quality District (SCAQD) has the most stringent standards in the United States for NOx and CO emissions from reciprocating engine generators. The SCAQD standard for NOx is 90 ppm, the VTA goal is 9.5 ppm. Similarly, the SCAQD standard for CO is 1500 ppm, the VTA goal is 150 ppm.

Emissions testing was performed at power levels ranging from full power to minimum power during Run 10. Burner air flows were initially adjusted to the normal equivalency ratio (E.R.)

of 1.2. E.R. values of 1.05 to 1.4 were also evaluated. Emissions recorded during these tests are shown in Figure 7.2–19. The measured VTA emissions were better than expected levels.

- NOx emissions were less than 1 ppm compared to the goal of 9.5 ppm.
- CO emissions (at the normal E.R. of 1.2) were 20 ppm compared to the goal of 155 ppm.
- Total hydrocarbons (THC) were 25 ppm compared to the goal of 28 ppm.

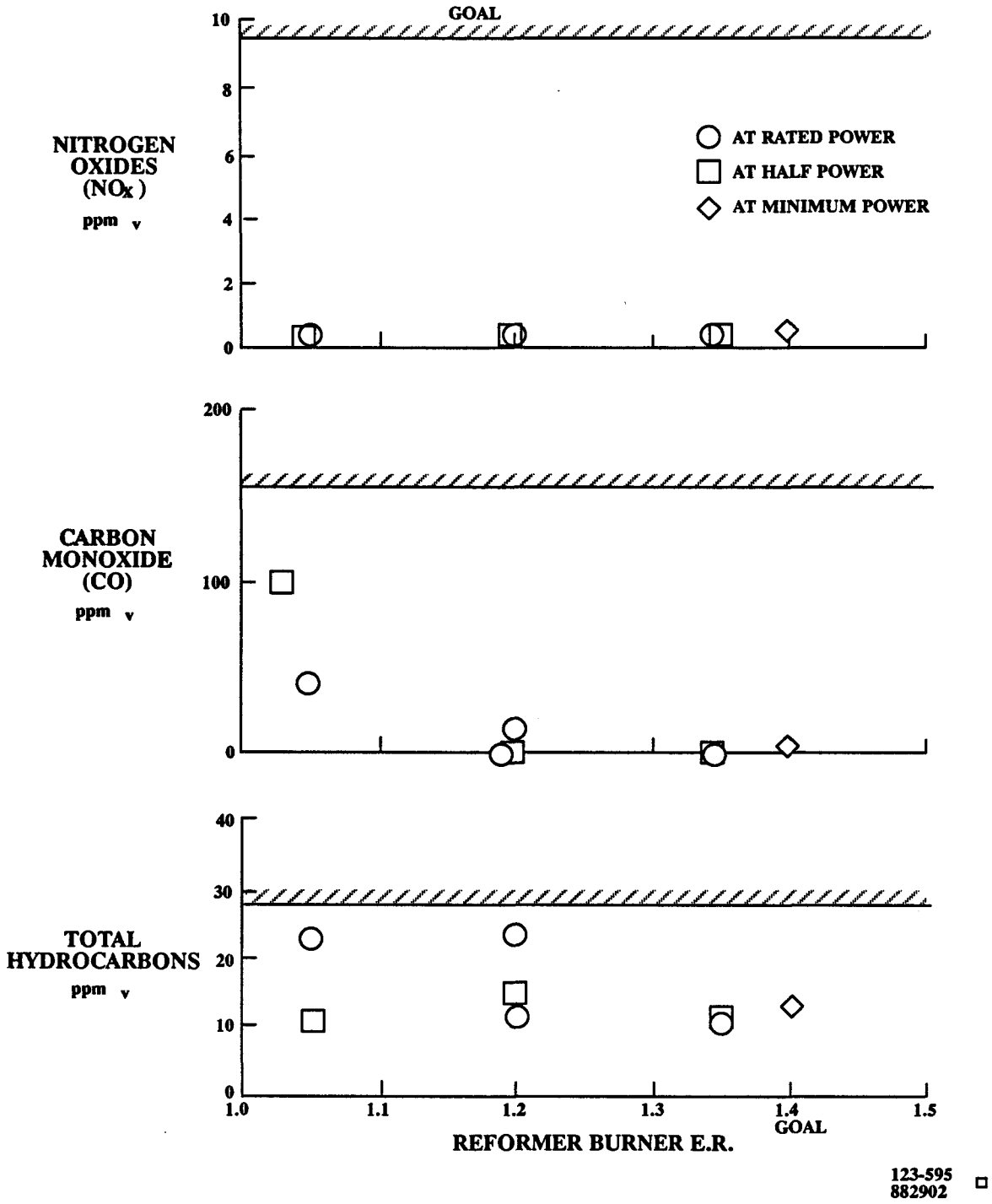

Figure 7.2–19. *VTA Power Plant Emissions*

Preoxidizer Testing

Peak shave gas typically contains a mixture of propane and air to replace a portion of the pipeline natural gas during fuel shortages. While many gas distribution systems do not utilize propane/air peak shaving, some U.S. companies (including the one servicing by IFC) do utilize propane/air peak shaving. Oxygen in the air of the peak shaved gas is detrimental to the reforming catalyst and must be removed from the fuel stream prior to it getting to the reformer. Several runs of the VTA were shortened by the introduction of peak shave gas by the local utility since the VTA was not designed to handle the oxygen in peak shave fuel mixtures. Prior to Run 15 of the VTA, a preoxidizer was added to eliminate the oxygen in peak shave fuel mixtures and allow continued operation. This change is beneficial in preventing shutdowns of the VTA and establishes a basis for future power plant designs.

The preoxidizer system which was added consisted of a preoxidizer containing noble metal catalyst, a 3–way valve, a simple electronic controller, and a recycle bypass valve. After several successful tests with air added to normal facility gas, the preoxidizer was successfully operated for about 20 continuous hours on actual peak shave fuel from the local utility. Figure 7.2–20 shows the response of the preoxidizer controls to the introduction of peak shave gas and elimination of the peak shave mixture. At all times, the preoxidizer exit temperature was held near its 600°F setpoint. Figures 7.2–21 shows that cell stack performance was not effected by operation with peak shave gas.

Prior to Run 25A, a new preoxidizer configuration which was simplified and smaller than the original preoxidizer was installed in the VTA for evaluation. Initial tests with air added to normal utility gas did not produce the desired reaction, but successful ignitions were achieved after adjusting valve settings to improve the mixing of the natural gas with fuel processor recycle streams. Judging from temperature rise in the bed, most of the reaction was occurring in the first third of the bed, and no oxygen slip was measured at the preoxidizer exit.

The testing described above was performed with fresh catalyst. Since the reaction characteristics of the catalyst can be influenced by sulfur odorants in the natural gas, it was decided to flow natural gas (with 2 ppm sulfur) through the preoxidizer for a period of time and then re-evaluate the ignition characteristics. Natural gas was allowed to flow through the bed for about 12-hours, to establish a sulfur coating on the catalyst surface, and then the rated power air injection test (which was previously successful) was repeated. As illustrated in Figure 7.2-22, a shift in the reaction from the inlet to the exit of the preoxidizer and oxygen slip were noted. Apparently, sulfiding of the catalyst had caused a loss in activity. At this point, tests were run to establish new thermal requirements for sulfided catalyst. After establishing these limits, all ignitions were successful with ignitions occurring at the inlet of the bed.

Testing of the simplified configuration was beneficial in showing that the volume of preoxidizer catalyst could be substantially reduced by using alternative catalysts which are industrially available. The volume of the simplified bed was about 30% of the original configuration tested in the VTA, and testing of the simplified configuration showed that it was still about 3 times larger than necessary. The net result is a potential 85% reduction in catalyst from that used in the VTA.

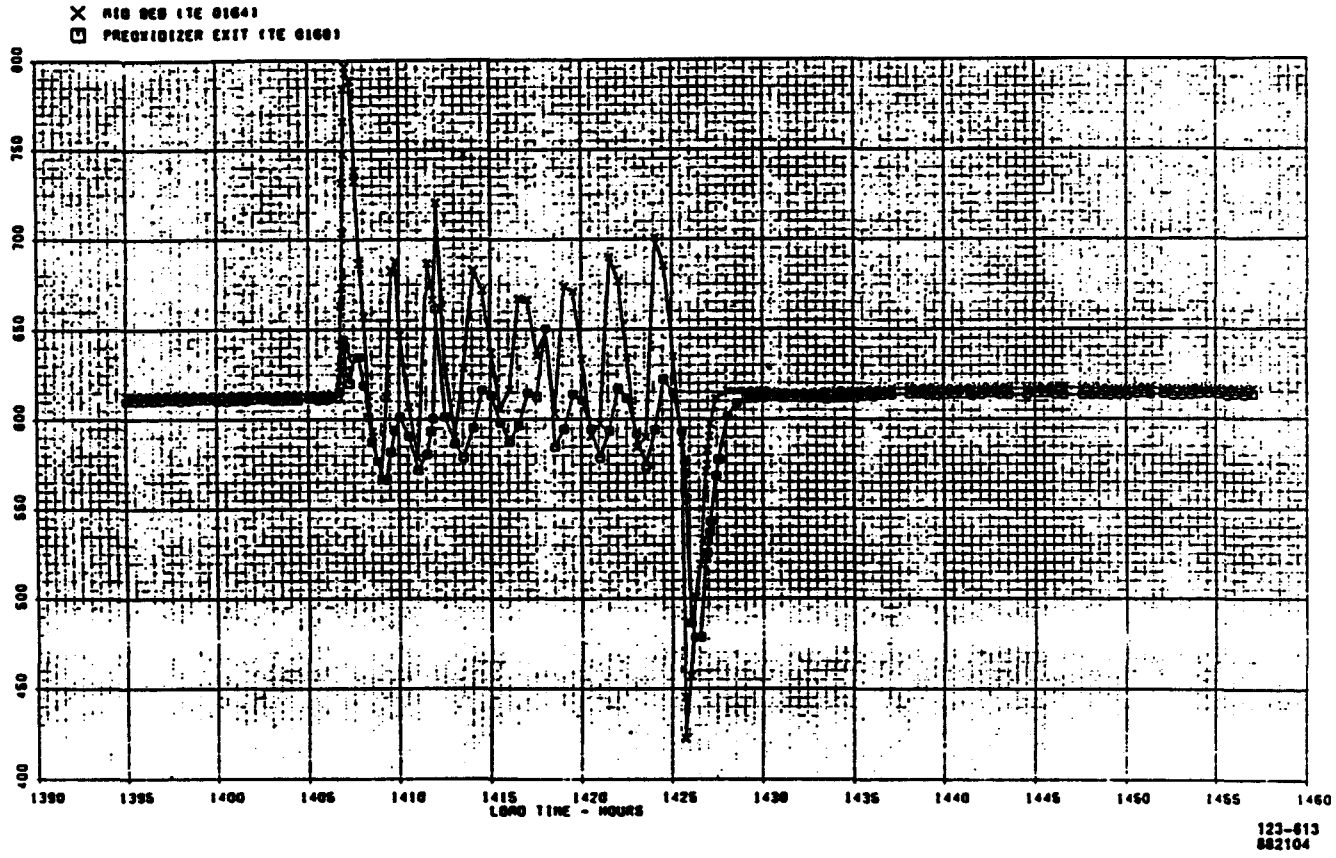

Figure 7.2–20. *VTA Pre–oxidizer Temperatures During CL&P Peak Shaving*

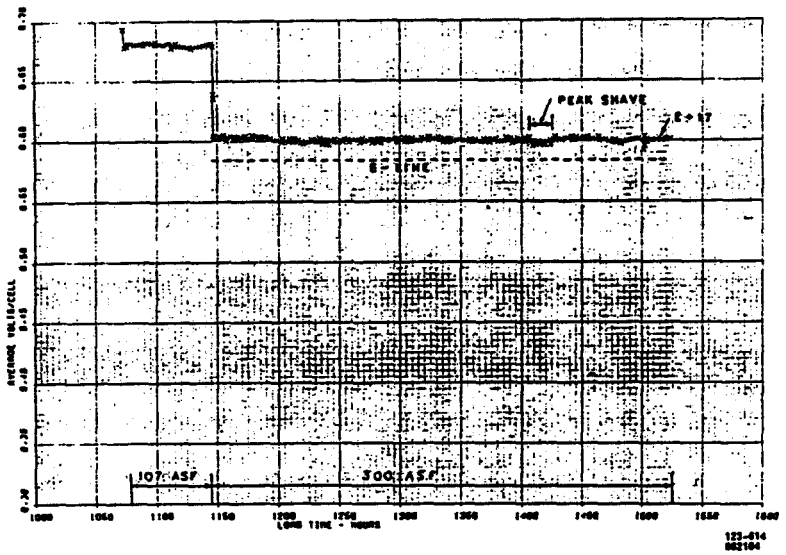

Figure 7.2–21. *VTA Stack Performance During Peak Shaving*

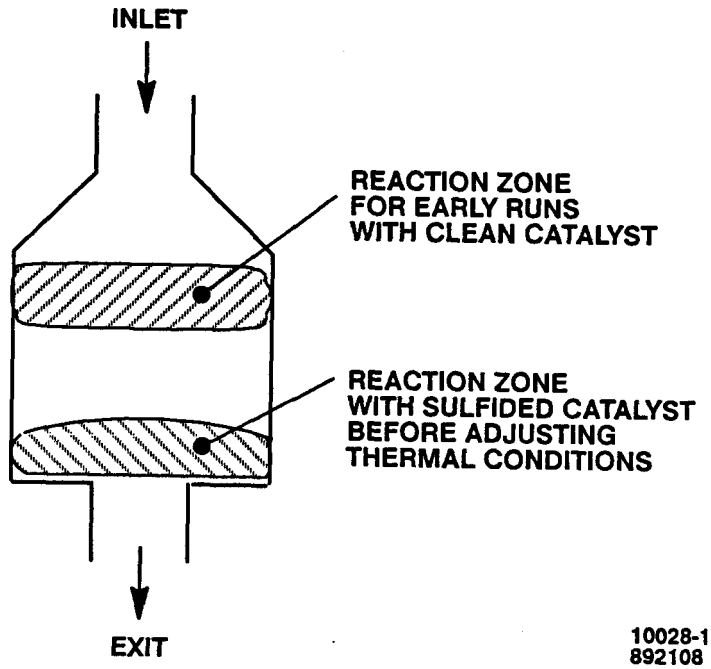

Figure 7.2–22. *Ignition Zones in Simplified Preoxidizer*

Transient Capability

The ability to perform power transients is important to both future grid-connect and grid-independent fuel cell power plants. A series of load transients were performed on the VTA to establish the capability of the VTA with "as is" controls. The transients performed during Runs 12, 13, and 14 are listed in Tables 7.2-4, 7.2-5, and 7.2-6, respectively. These transients established the following capabilities:

1. The VTA performed full power transients in 15-seconds. See Figure 7.2-23.

2. The VTA performed 80 ASF (about 30-kW) instantaneous (step) transients. See Figure 7.2-24 through 7.2-26.

TABLE 7.2-4. RUN 12 TRANSIENT TESTS

Test Number	Current Density Initial	Current Density Final	Type of Load Change
1.	80 ASF	100 ASF	20 ASF Step Up
2.	100 ASF	140 ASF	40 ASF Step Up
3.	140 ASF	200 ASF	60 ASF Step Up
4.	200 ASF	240 ASF	40 ASF Step Up
5.	240 ASF	300 ASF	60 ASF Step Up
6.	300 ASF	360 ASF	60 ASF Step Up
7.	360 ASF	340 ASF	20 ASF Step Down

TABLE 7.2-5. RUN 13 TRANSIENT TESTS

Test Number	Current Density Initial	Current Density Final	Type of Load Change
8.	80 ASF	190 ASF	6-second ramp
9.	190 ASF	300 ASF	6-second ramp
10.	300 ASF	80 ASF	11-second ramp

TABLE 7.2-6. RUN 14 TRANSIENT TESTS

Test Number	Current Density Initial	Final	Type of Load Change
11.	300 ASF	80 ASF	Step
12.	56 ASF	118 ASF	Step
13.	118 ASF	162 ASF	Step
14.	162 ASF	202 ASF	Step
15.	87 ASF	178 ASF	Step
16.	178 ASF	255 ASF	Step
17.	255 ASF	325 ASF	Step
18.	80 ASF	325 ASF	15-Second Ramp

Comparisons of the results of step transients to predictions of transient capability showed that 80 ASF step transients from 61-kW, 118-kW, and 162 kWdc were very similar to predictions. Figures 7.2-27, 7.2-28, 7.2-29 compare typical results to predictions. As shown in Figure 7.2-30, the predicted power step capability closely matches VTA data over the full power range.

Further analyses were performed to understand changes needed to meet future power plant transients requirements. These studies indicated the need for improved response of the steam ejector and cathode air controls. A new ejector with high-speed actuator was installed in the VTA. See Steam Ejector for details. Unfortunately, there was inadequate time for transient testing before operation with the cell stack was terminated, but observations of ejector operational speed indicate response will be adequate for both grid-connect and grid-independent operation.

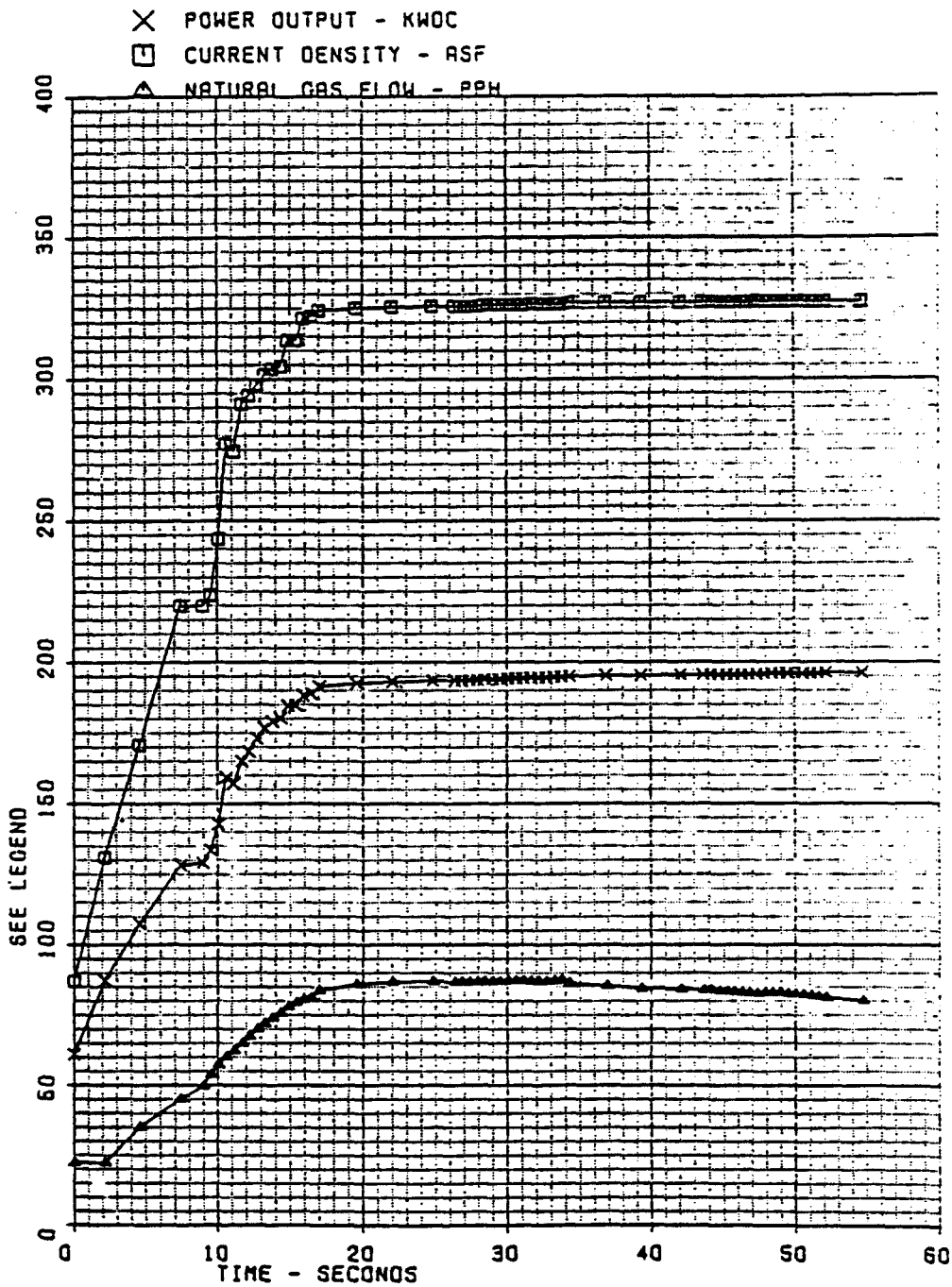

Figure 7.2–23. *15 Second Full Power Ramp (2/10/88)*

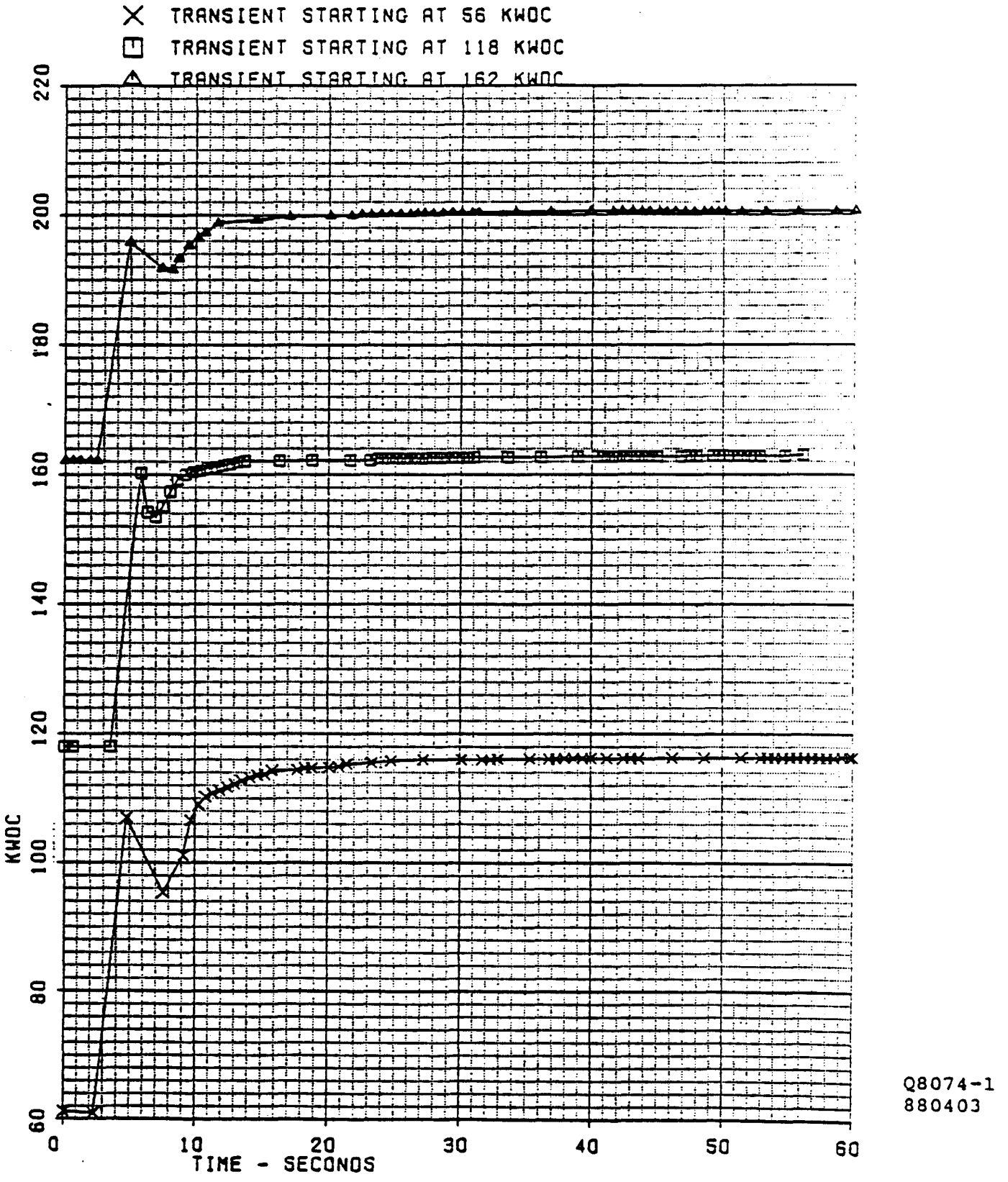

Figure 7.2–24. Power Output During 80 ASF Step Transients (2/9/88)

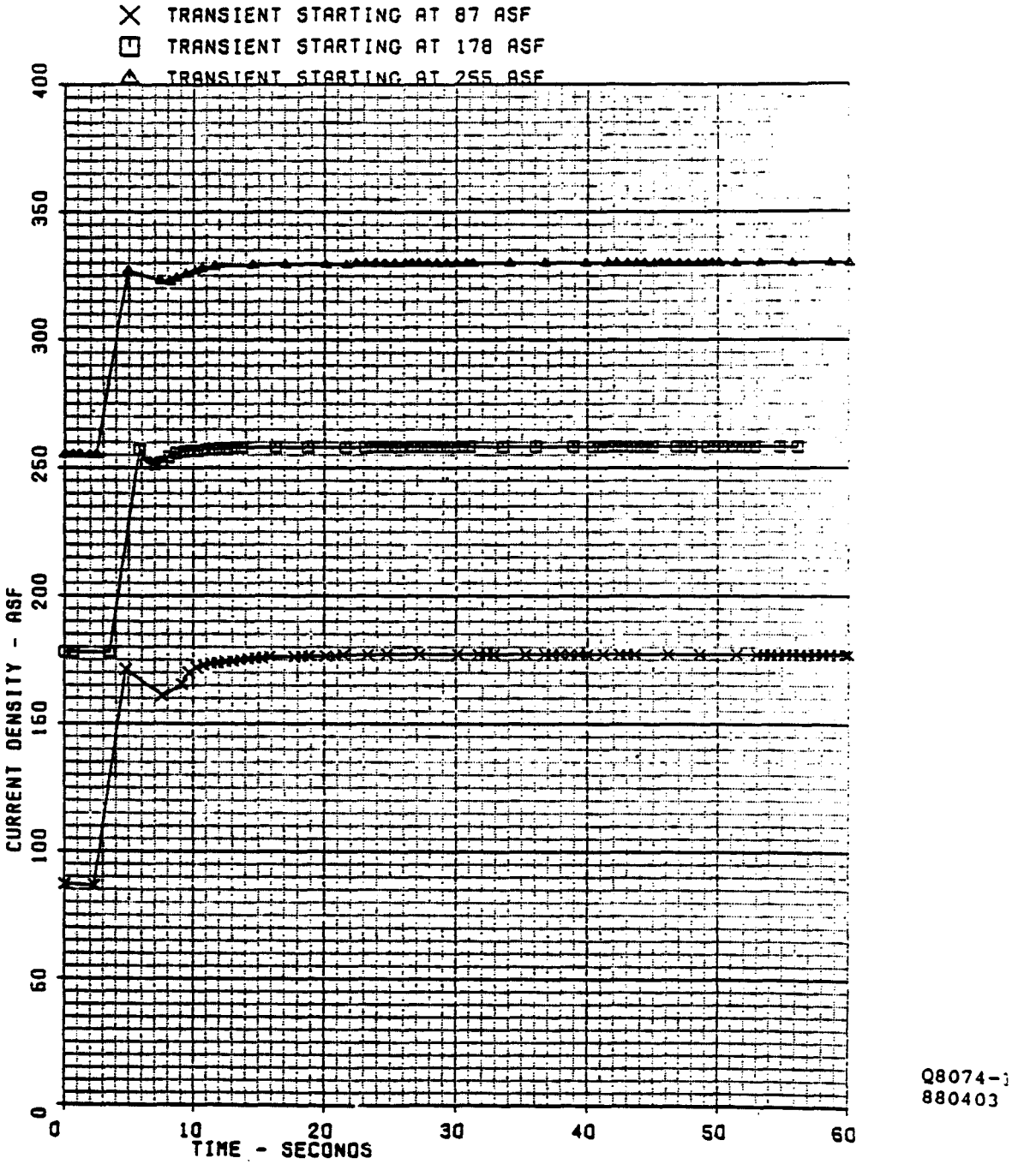

Figure 7.2-25. *Current Density During 80 ASF Step Transients (2/9/88)*

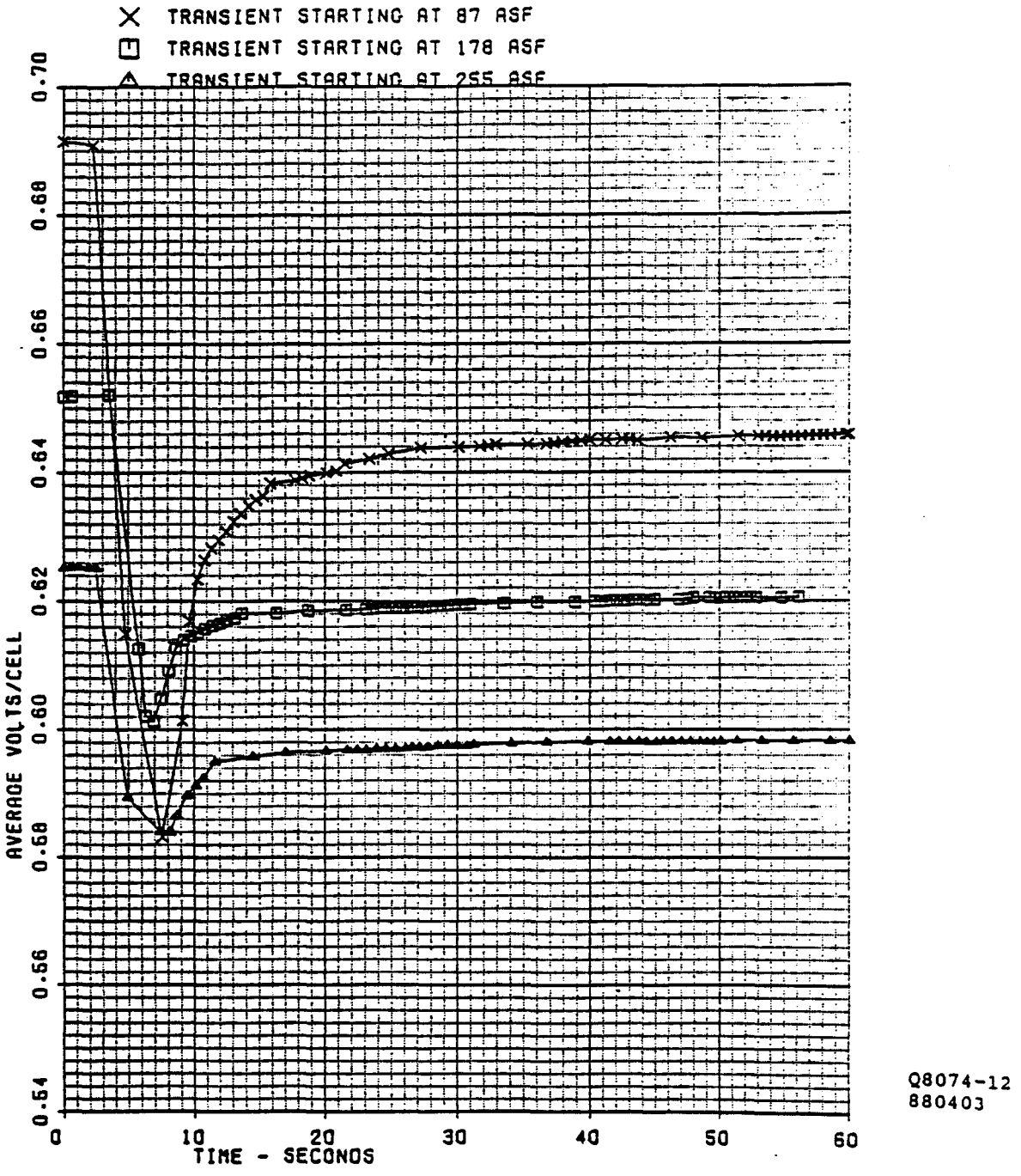

Figure 7.2–26. *Cell Voltage During 80 ASF Step Transients (2/9/88)*

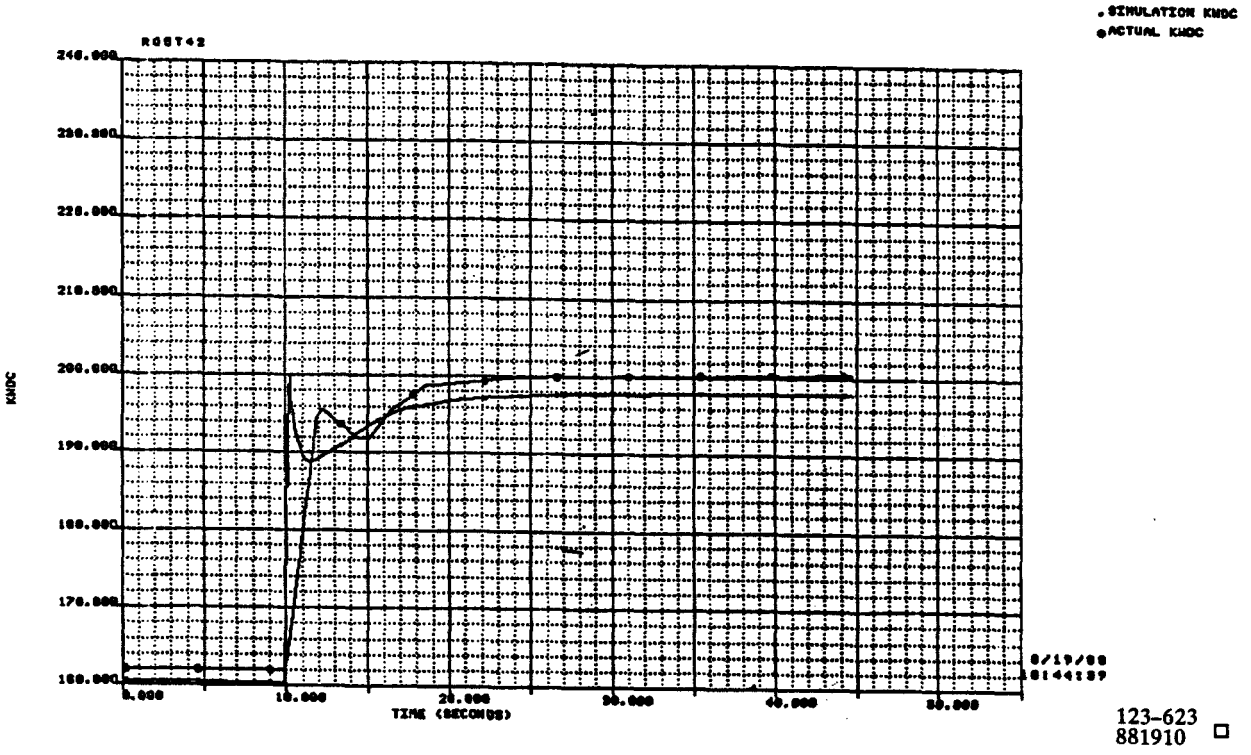

Figure 7.2–27. *Comparison of Power Change During VTA Transient to Prediction*

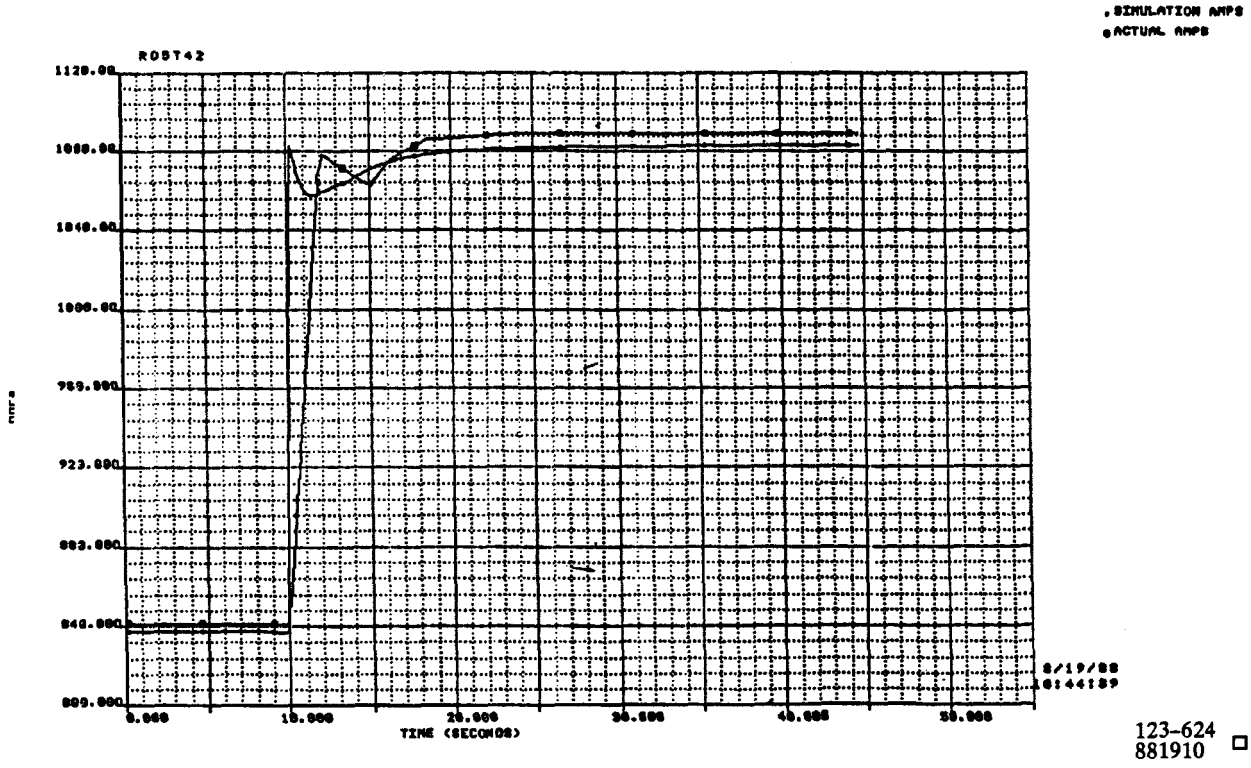

123-624
881910 □

Figure 7.2-28. *Comparison of Current Change During VTA Transient to Prediction*

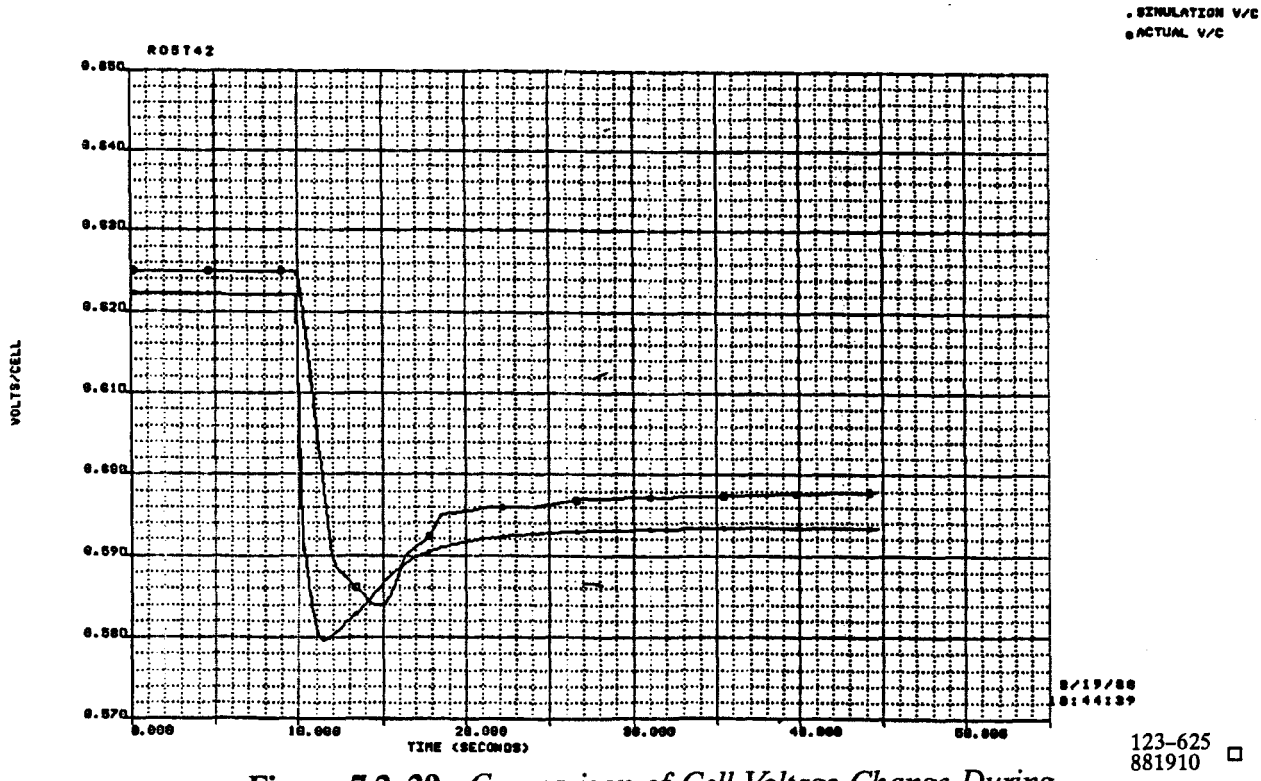

123-625
881910 □

Figure 7.2-29. *Comparison of Cell Voltage Change During VTA Transient to Prediction*

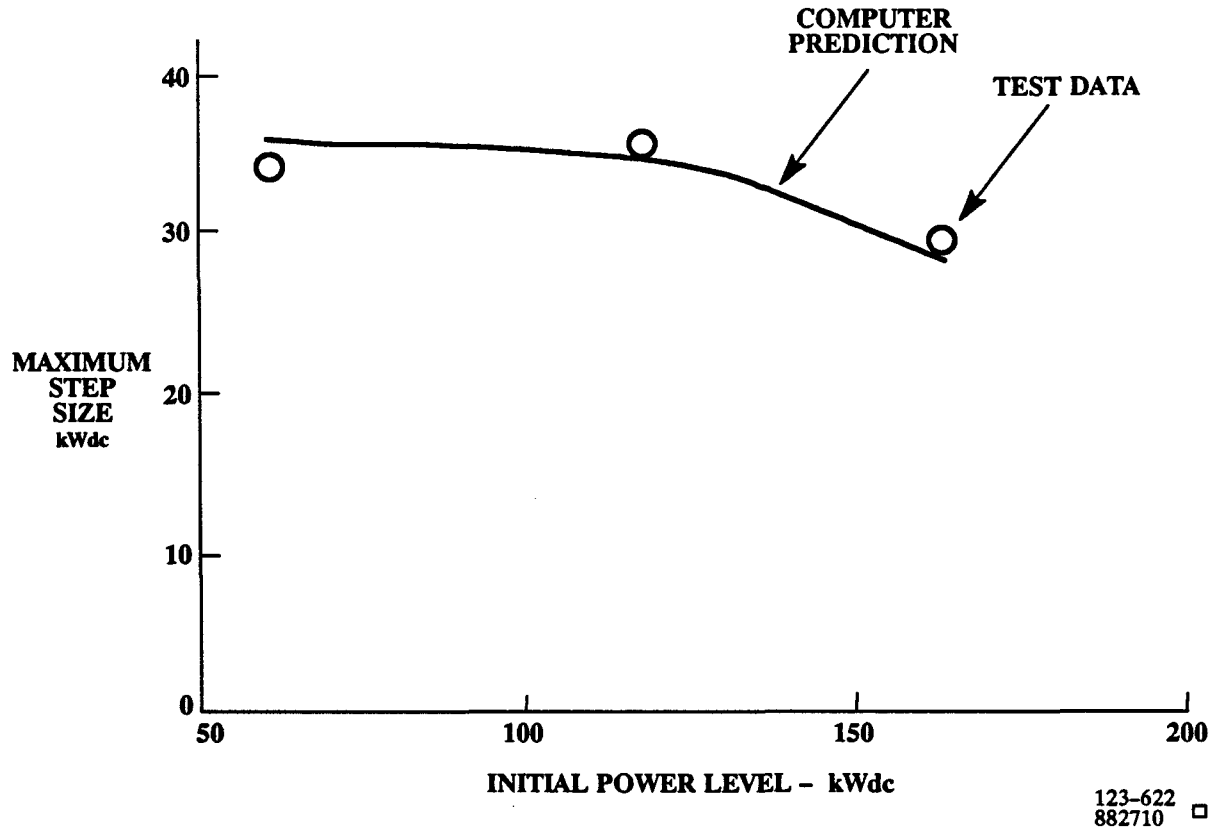

Figure 7.2–30. *Comparison of Predicted Maximum Power Step Size to VTA Data*

Water Recovery Condenser

The fuel processors in on–site fuel power plants require steam to convert the natural gas to usable hydrogen fuel. In order to meet this steam flow requirement without water addition by the customer, water is condensed from the power plant exhaust. The 40-kW power plants were capable of condensing adequate water to meet rated power demands on ambient temperature days up to about 70°F. Since it is desirable to increase the operating range of future on–site power plants, the condenser in the VTA was designed for water recovery at rated power on a 95°F day.

In July of 1988, the glycol/water temperature at the inlet of the water recovery condenser was increased to simulate operation on a 95°F day. Figure 7.2–31 shows the results of condenser testing. The condenser performed "as expected" recovering 56 pph more water than was required by the process. Fifty–six (56) pph of extra water corresponds to a 20 percent excess. In theory, the excess can be reduced to zero and still retain full water recovery. Figure 7.2–32 shows that the condenser volume could be reduced by more than 50 percent at zero excess.

Iron corrosion products were found in the water tank during Runs 11, 12, and 22. The rust was traced to the condenser so inspection ports were added to the condenser, and the condenser

was inspected. The first stainless steel core section (hot side inlet) of the condenser was found to be in excellent condition, and the next carbon steel section showed only minor corrosion on the fins. The remainder of the cores were in excellent condition. The largest amount of corrosion was noted on the shell, and a material upgrade may be required in future designs.

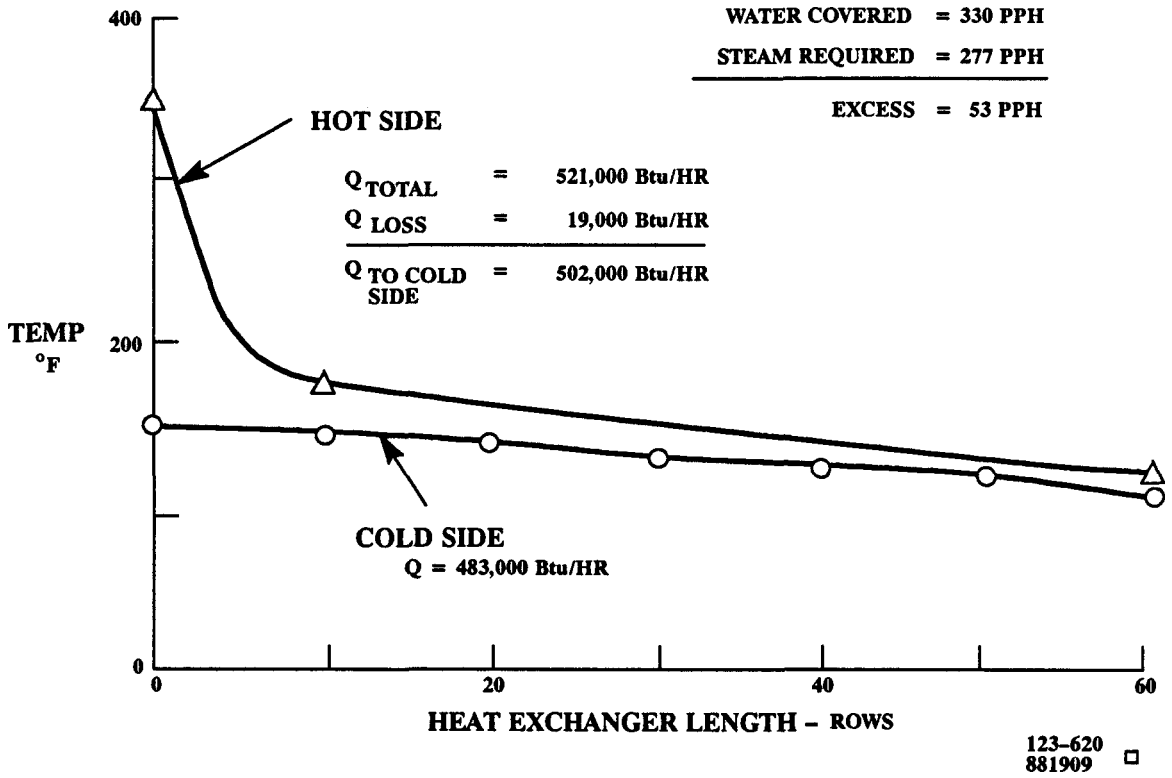

Figure 7.2-31. *VTA Water Recovery Condenser Test Results*

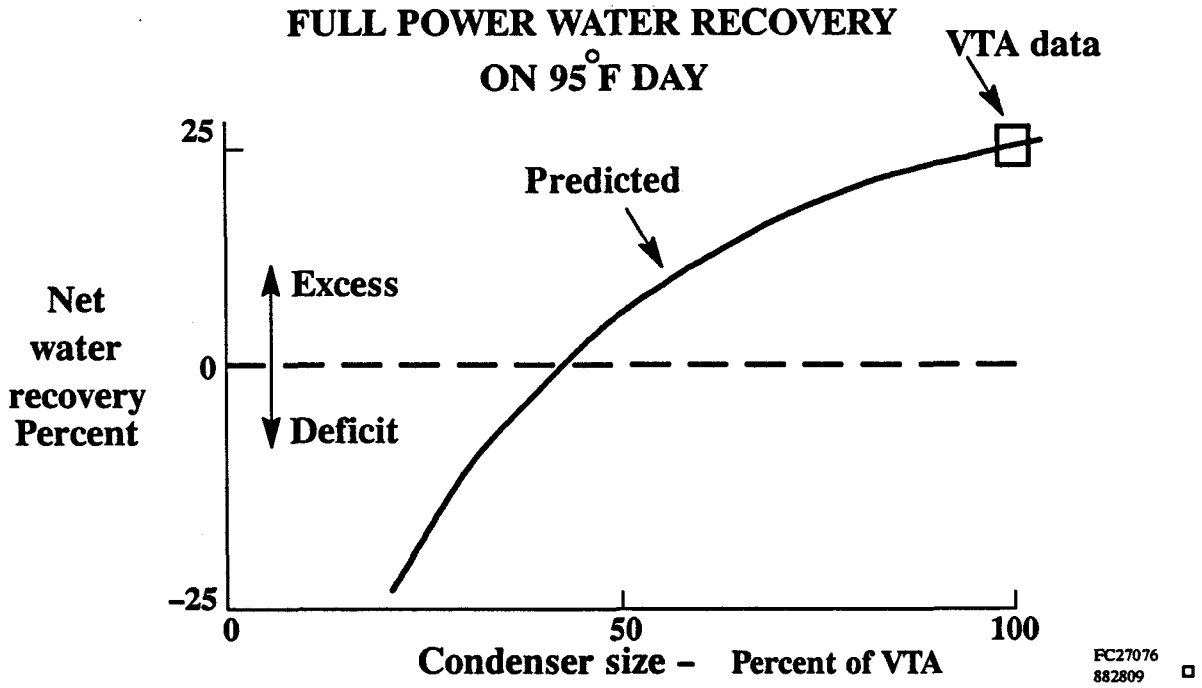

Figure 7.2–32. *Condenser Size Versus Water Recovery*

Cooling Water Pumps

One objective prior to actual operation of the VTA was to identify and evaluate reliable, low–cost coolant pumps for circulating the cooling water through the cell stack coolers. Three design alternatives were selected for bench testing. Candidate A represents magnetically coupled unit, B is the ANSI double–seal, and C is the canned–motor version. FIgure 7.2–33 shows the three pump candidates installed in a test rig.

Candidate A successfully completed 27,050 hours without experiencing excessive bearing wear or oxide buildup. Candidate B was plagued with oil seal leakage and was removed from testing. Candidate C initially experienced rapid bearing wear but successfully completed 22,670 hours of testing after the factory rebuilt the pump and recommended a change in the startup procedure to prevent air entrapment.

Based on the above bench test experience, a pump similar to Candidate A was selected for the VTA. Unfortunately, the pump experienced several bearing failures and was replaced after about 500–load hours. Data from a complementary GRI program indicated that the failures were associated with start/stop cycles of the VTA and that a canned–motor pump similar to candidate C may be more acceptable. The canned–motor pump was installed in the VTA and operated flawlessly for an additional 1200–hours and 11 thermal cycles. At that point, a newer model from the same vendor was installed and operated flawlessly for the remainder of verification testing.

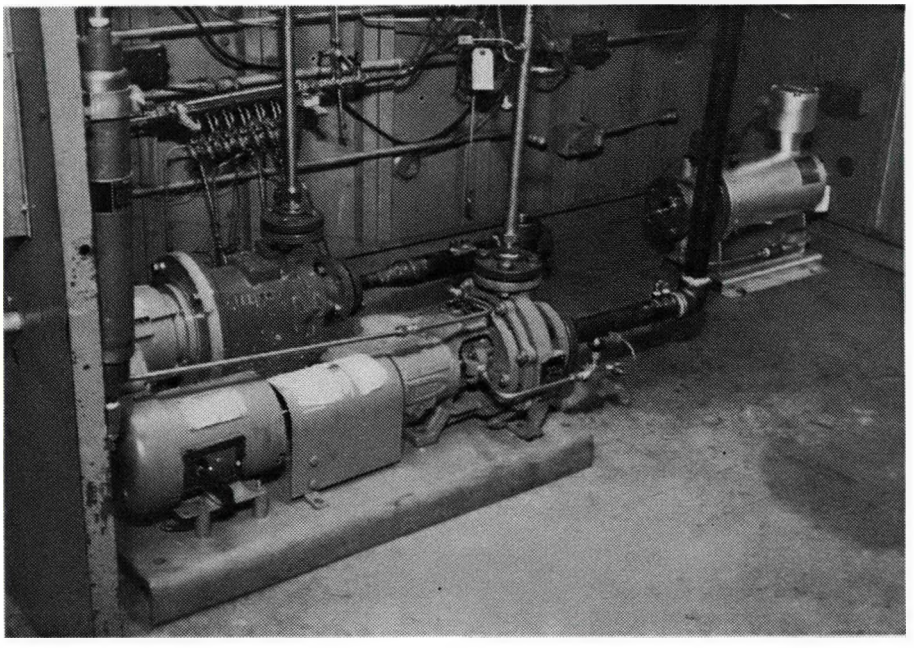

(WCN-13263)

Figure 7.2–33. *200–kW Circulation Pump Candidates*

Feedwater Pumps

The water treatment system feedwater pump requirement was met with multi–stage centrifugal pumps. Three candidates, shown in Figures 7.2–34, 7.2–35, and 7.2–36 were selected for operational experience testing. The endurance test for this set of pumps is one with a 50 percent duty cycle with the pumps on for 5 minutes and off for an identical time span. Between 13,100 and 19,800–hours were accumulated on each of the candidates. The only failure experienced in this testing has been with Candidate A, apparently overheating, damaging the plastic impeller and diffuser assembly. This pump was rebuilt utilizing improved plastic internals having a higher temperature rating.

Two pumps similar to candidate A were selected for evaluation on the VTA. Other than problems associated with rust occasionally restricting the feed lines and stages, no problems were encountered during full–scale VTA testing.

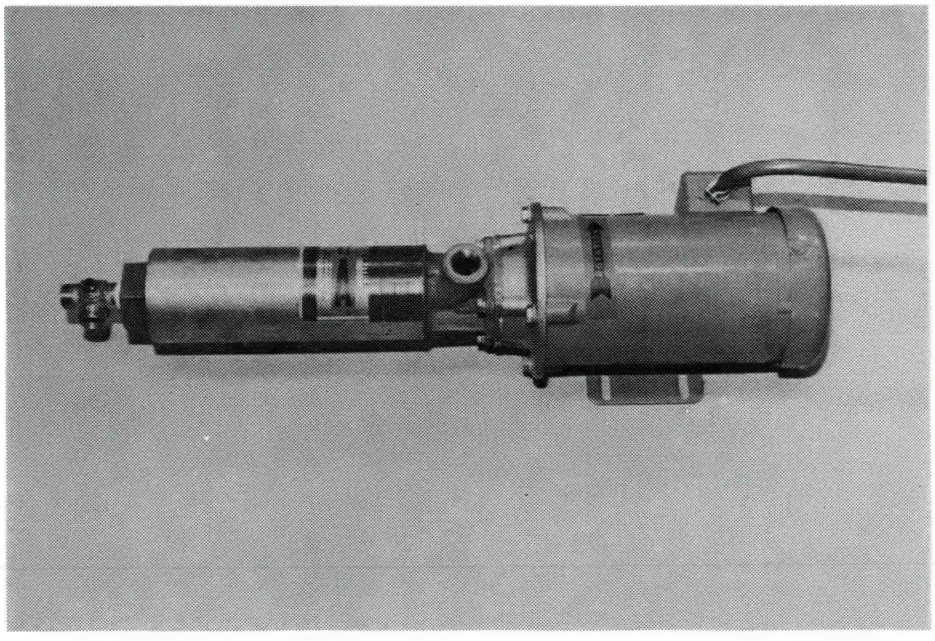

(WCN-13439)

Figure 7.2–34. *Candidate "A" Feedwater Pump*

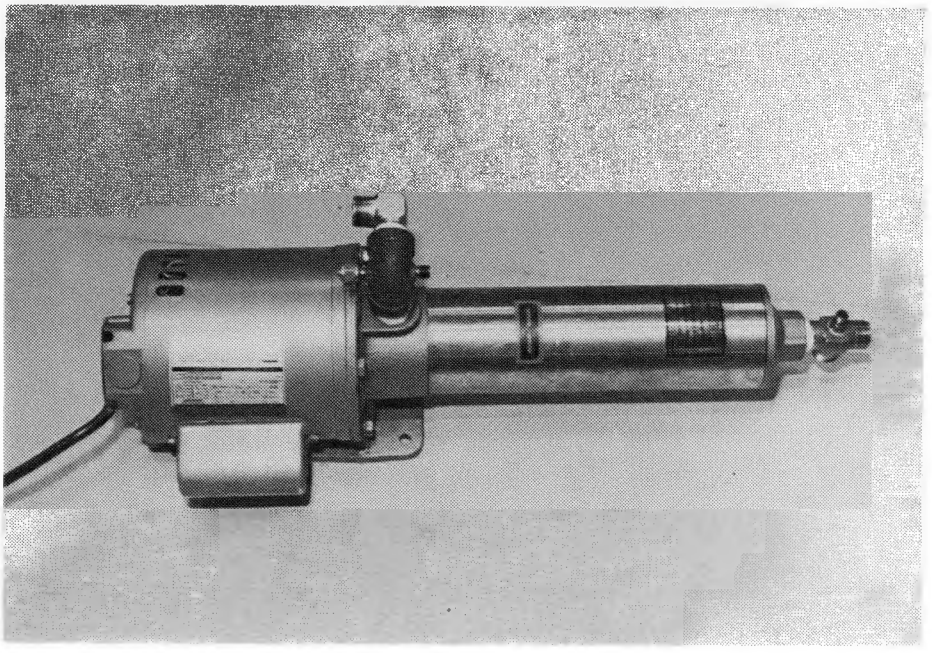

(WCN-13440)

Figure 7.2–35. *Candidate "B" Feedwater Pump*

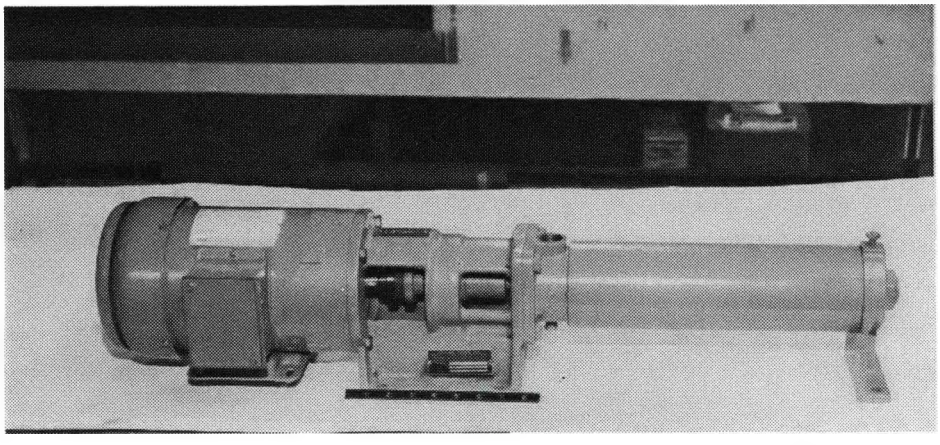

(WCN-13114)

Figure 7.2–36. *Candidate "C" Feedwater Pump*

Steam Ejector

The steam ejector uses the energy in high pressure steam to drive the fuel through the fuel processor and cell stack. While the original development steam ejector in the VTA was usable, testing did point several deficiencies:

1. The pintle (valve stem) occasionally stuck. Two incidences of sticking were noted during VTA testing. Typically, re-alignment, lubrication, and readjustment restored normal operation.

2. The actuator was acceptable for grid-connect transient duty with 15-second ramps but not acceptable for large grid-independent step transients.

3. The ejector (as tested in Subtask 5.4) was not capable of fuel flows above 110 percent of rated.

An alternative steam ejector developed on a complementary on-site program to address deficiencies noted with the original VTA ejector was purchased. The unit has the following features:

1. A new seal and guide configuration which minimizes chance of binding.

2. An actuator capable of stroking the pintle in 1/2 the time of the original unit.

3. An improved internal flow configuration which allows 125 percent of rated flow to be pumped through the system.

The new steam ejector was installed on the VTA after Run 24. Operation of the new unit has been flawless.

Reformer Performance

Reformer efficiency reflects the energy expended by a fuel cell power plant to convert natural gas feed into hydrogen consumed by the fuel stack in producing electric current. Reformer efficiency is defined as follows:

$$\eta_{reformer}\ (\%) = 100 \times \frac{\text{Hydrogen consumed (pph)} \times \text{LHV}_{H_2}\ \text{(BTU/lb)}}{\text{Natural gas feed (pph)} \times \text{LHV}_{NG}\ \text{(BTU/lb)}}$$

As discussed in Subtask 5.3, the expected reformer efficiency in the VTA was about 86 percent at rated power.

Originally, discrepancies between natural gas flow measurements by two mass meters (FT012 and FT012A) prevented accurate determination of reformer efficiency. A third flow meter, a

positive displacement meter (FT012B), was added. As shown in Figure 7.2–37, reformer efficiency based on the positive displacement meter was 3 percent – 6 percent below predictions and generally between mass meter readings.

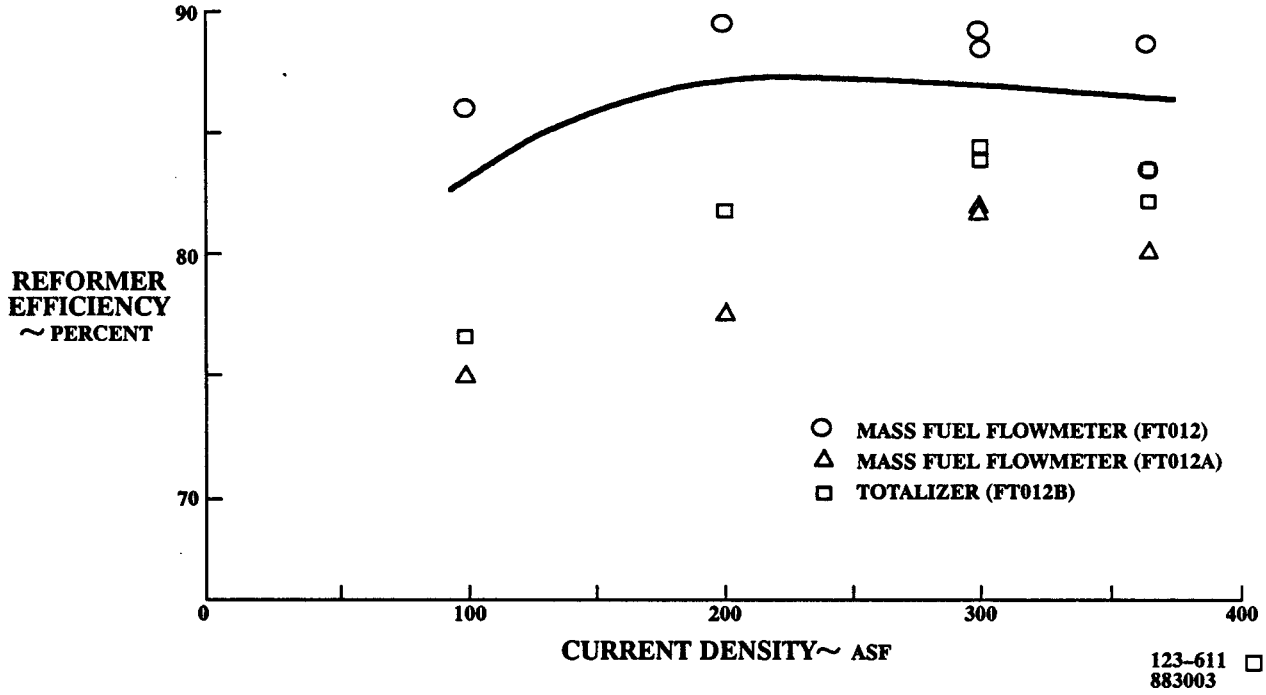

Figure 7.2–37. *VTA Reformer Efficiency*

Efforts to resolve flow measurement differences and understand the apparent reformer efficiency discrepancy continued throughout VTA testing. Reasonable agreement between the mass meter and the positive displacement meter was achieved by in-place calibrations of the meters. Apparently, the mass meters are very configuration sensitive. As shown in Figure 7.2-38, the measured reformer efficiency at rated power by both the mass meter (FT012) and the gas totalizer was about 82% for the last 600-hours of closed-loop testing. This represents a discrepancy of 4% between the predicted and the measured efficiency.

The primary reason for the lower-than-expected efficiency was stack shorting. Shorting causes an unexpected (and normally unmeasured) increase in hydrogen consumption. Special diagnostics on the cell stack indicate that shorting caused about a 3% loss in reformer efficiency. The remaining 1% loss in reformer efficiency was caused by high heat loss and reactant gas leakage.

Figure 7.2-39 shows the pressure drop history of the reformer during VTA testing at 300 ASF. Most of the variations in pressure drop were caused by changes in operating conditions; however, a small (5-15%) increase in pressure drop was noted after normalizing data. Most of this increase appears to have occurred in the first 1500-hours of testing. The reformer start se-

quence was modified from the typical two-step heatup to a simpler single-step heatup for the last six startups of the VTA. No further increase in reformer pressure drop was noted. Table 7.2-7 compares the maximum measured temperature differential between the reformer and regenerator walls during two-step and simpler single-step heat-ups to values experienced during normal operation. Since the maximum temperature differential for the single step heatup is less than temperature differentials during normal operation neither catalyst damage or reformer pressure drop increase was expected.

Table 7.2-7. Maximum Temperature Differential between Reformer Tube Wall and Regenerator Wall

Reformer Heatup	
Two-step	294°F
Single-step	337°F
Normal Operation	
Steady-state	400°F
Transient	425°F

Figure 7.2-40 shows fuel conversion at 300 ASF as a function of operating time. A 7% reduction was noted during testing between 800-hours and 2500-hours. All of this reduction is explainable by changes in operating conditions, and no change in catalyst activity is apparent. The steam-to-carbon ratio of the reformer process feed was reduced from 3.35 to 2.95. This changed resulted in a 4% reduction in fuel conversion. Figure 7.2-41 shows the change in reformer top tube temperature during testing. The average top tube temperature dropped 35°F causing an additional 3% reduction in fuel conversion, bringing the total of the two operating condition changes to 7%.

Anode Filter

A new type of filter material was evaluated for removing copper fines from the processed fuel stream before the gas stream enters the anodes. The material is compatible with fuel processor operating conditions and, therefore, can be integrated in existing fuel processing vessels without a separate housing.

Table 7.2-8 lists results of the laboratory analysis of the new filter material after about 1100-hours of operation in the VTA. The analysis shows that most copper was collected on the top surface of the first layer. In addition, only background levels of copper were detected in downstream diagnostic filter.

Table 7.2-8. Anode Filter Analysis	
	Copper Level (mg/in3)
First Layer	
Top	1.3
Bottom	0.3
Second Layer	
Top	0.2
Bottom	0.2

Verification Test Activities

This section briefly describes test activities during each run of the Verification Test Article (VTA) in chronological order including results of post-test inspections and preparations for the next run. The run-by-run descriptions support the following conclusions:

1. Very few problems were experienced in starting the VTA, and those which were experienced were later corrected. Nearly 90 percent of all runs were successful in achieving "load".

2. About 36 percent of the shutdowns were caused by test facility problems or local utilities imposing conditions beyond design limits of the VTA. The VTA was not originally designed to handle peak shave fuel or to power itself during power interruptions. Most of these shutdowns could be avoided by power plants designed for peak shave fuel and capable of operating in the grid-independent mode (as at least a back-up to grid-connect operation when power fails).

3. Less than 30 percent of the shutdowns were caused by component failures. With the exception of the cell stack problem, problems encountered during operation were addressed, and solutions were demonstrated during subsequent testing.

4. The automatic control system functioned properly to maintain safe conditions in response to all facility and VTA malfunctions.

5. A number of improvements to the original VTA equipment were introduced to extend the VTA operating capability and improve reliability. The addition of a preoxidizer and replacement of the cooling water pump and ejector with improved units, and water treatment simplification are examples of this activity.

6. The logistics of procuring, installing, and maintaining experimental test equipment with minimal spare parts combined with program interruptions to significantly extend the calendar time required to achieve the nearly 3000-hours of VTA operation.

Run 1 (April 22 – 24, 1987)

The VTA was successfully started and operated on–load for 19–hours. It was operated in the open–loop configuration to facilitate cell "break–in." A voltage spike from the utility line caused the process air blower speed control to trip and shut down the power plant before "break–in" was completed.

After the run, the process air blower speed control was temporarily connected to an in–house motor generator to prevent reoccurrence of the problem described above. A long–term solution was eventually defined with assistance of the vendor and implemented. Further problems of this type were not experienced.

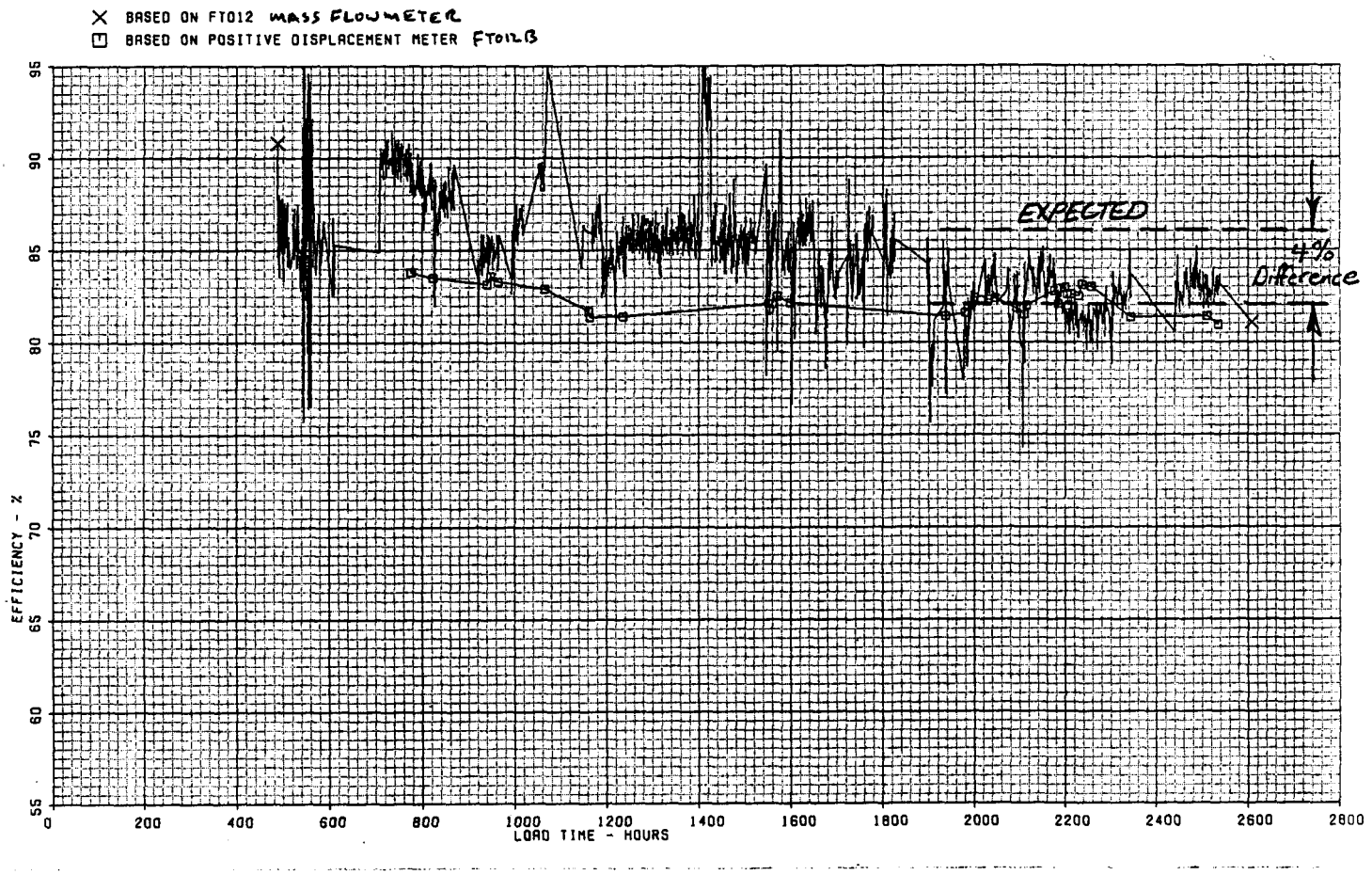

Figure 7.2-38. *VTA Reformer Efficiency History*

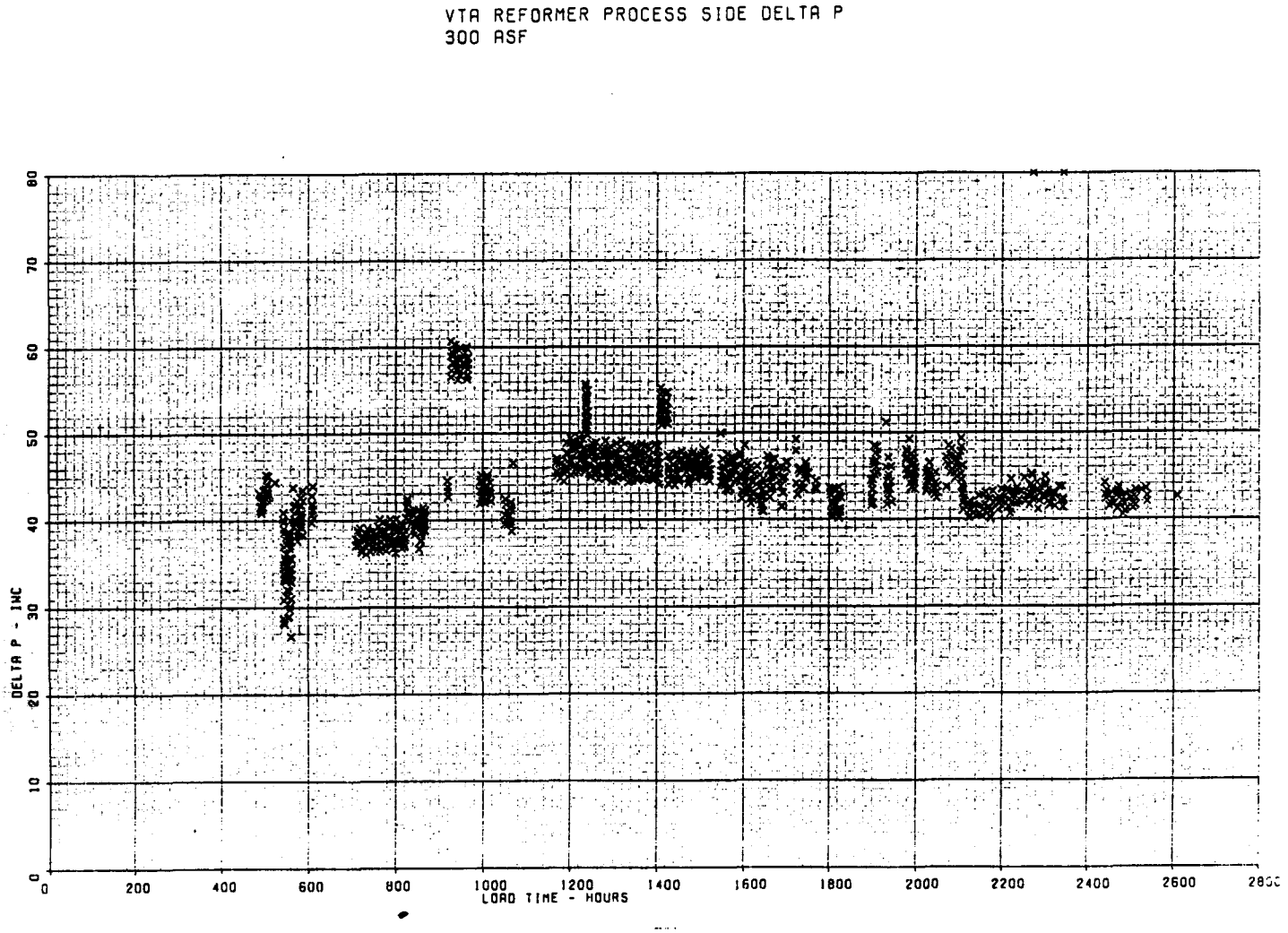

Figure 7.2–39. *VTA Reformer Pressure Drop History*

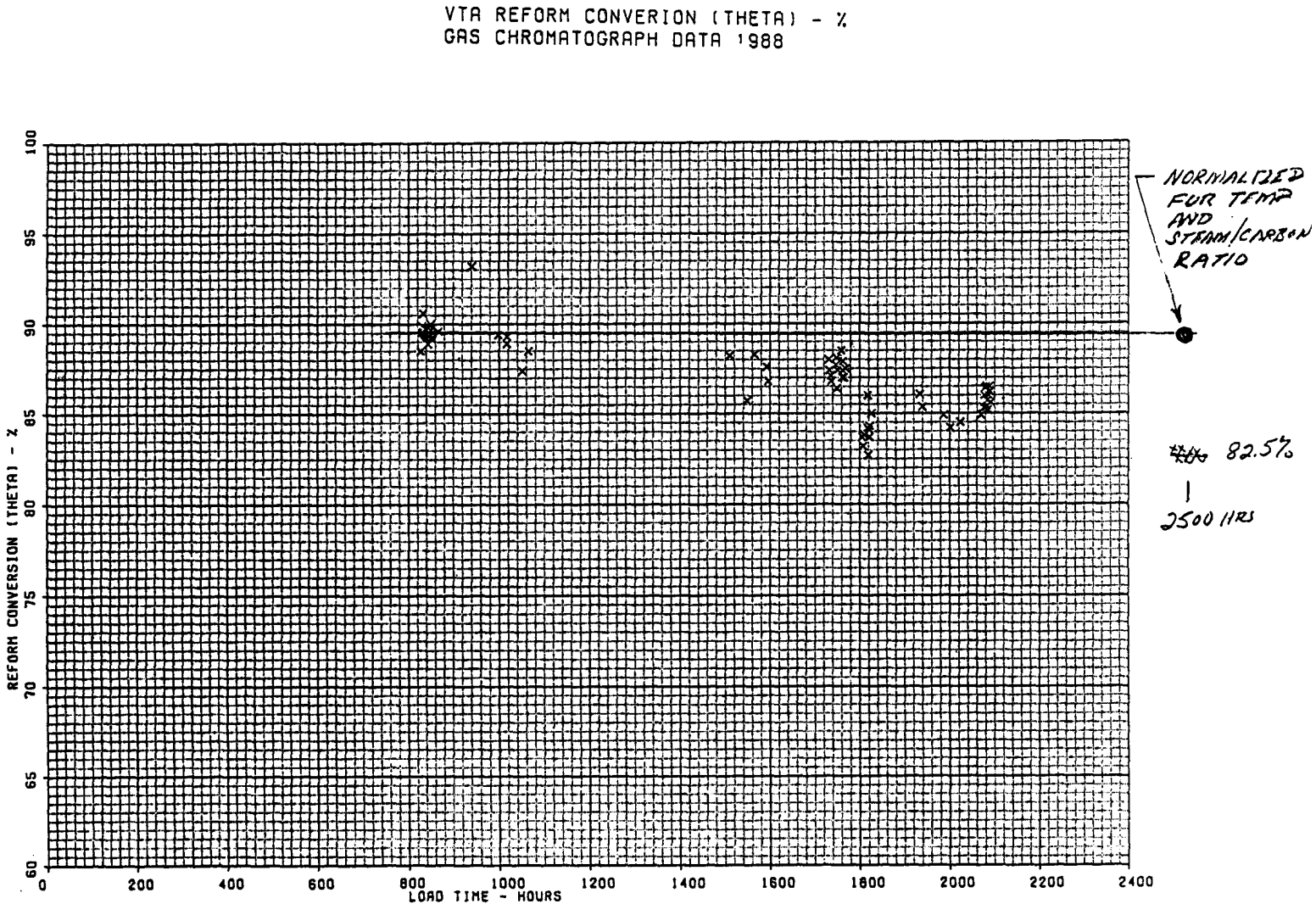

Figure 7.2–40. *VTA Reformer Fuel Conversion History*

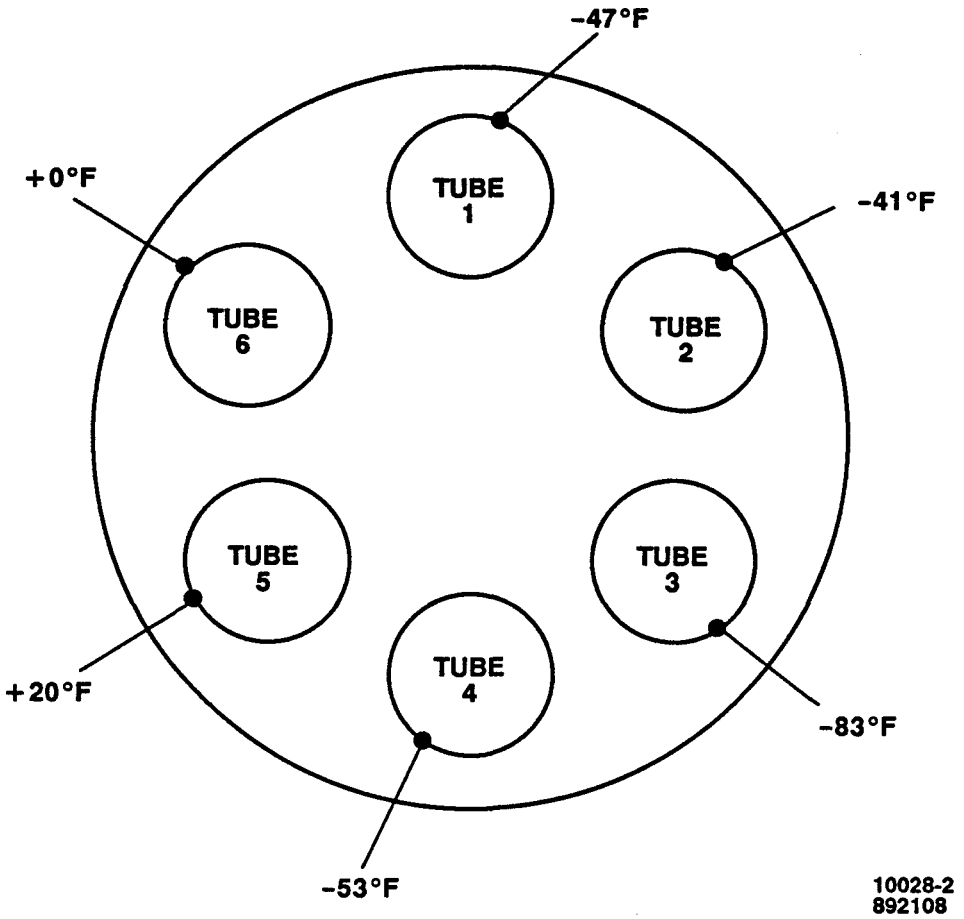

Figure 7.2–41. *VTA Reformer Top Tube Temperature Change Between 800 Hours and 2500 Hours*

Run 2 (April 30 – May 7, 1987)

The VTA was restarted to complete the cell "break–in" begun in Run 1. As shown in Figure 7.2–42, the cell stack operated for 165–hours of load time during Runs 1 and 2 at up to 175 ASF. The VTA was voluntarily shut down after completing cell "break–in", and it was then prepared for closed–loop operation as follows:

- The anode exhaust plumbing was modified to operate the reformer burner would operate on anode exhaust.. Burner light trials were conducted to establish the operating envelope.
- The cathode and burner exhaust plumbing was modified to include the condenser.

Other maintenance activities performed during the period are listed below:

- Water Treatment System (WTS) resin beds were cleaned and re–filled to provide a proper basis for evaluating time-between-maintenance requirements. A charcoal bed was relocated, and two organic resin beds were deleted.
- The stack cooling water pump was rebuilt with a new case provided by the vendor. Increased output and improved stability were noted.

Run 3 (June 10, 1987)

Repeated reformer burner flame–outs occurred during heat–up. The VTA was manually shut down to perform burner stability mapping. As shown in Figure 7.2–43, burner stability is influenced by nitrogen purge flow entering the burner through the anode exhaust port. This data was used to define new flow settings for stable operation.

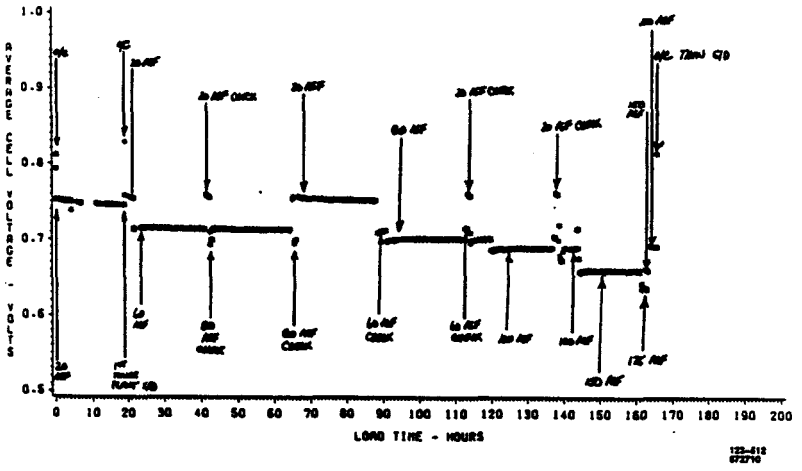

Figure 7.2–42. *VTA Open–Loop Performance History for Runs 1 and 2*

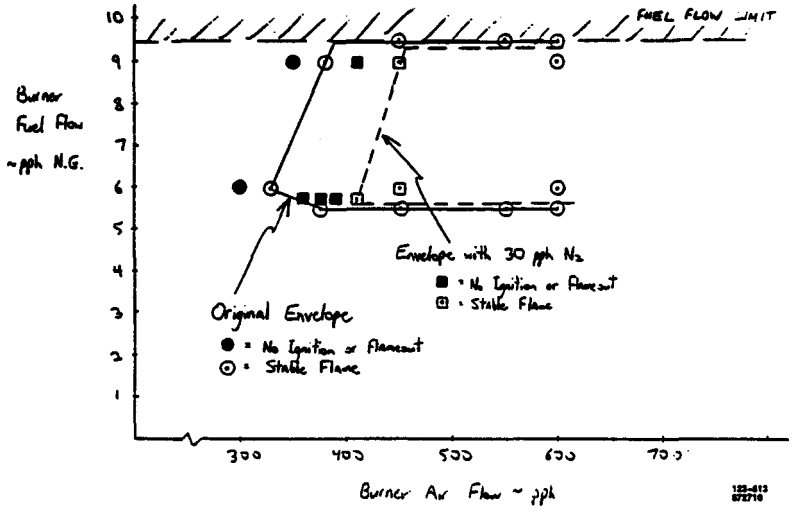

Figure 7.2–43. *Reformer Burner Ignition and Stability Envelopes*

Run 4 (June 11, 1987)

Burner air flows were adjusted to allow stable burner operation, and the VTA was successfully started in the closed–loop mode. After going on–load, cell performance was unusually sensitive to air flow in three substacks (see Figure 7.2–44), and the VTA was manually shut down for diagnostics. Leakage was found in the air regenerator, and the unit was resealed.

Run 5 (July 7, 1987)

This run was terminated because of a problem with the facility cooling system.

Run 6 (July 8 – July 20, 1987)

The VTA was successfully operated for 286 hours with the power profile shown in Figure 7.2–45.

During Run 6, subsystem evaluations were performed. Figure 7.2–46 shows that the controllability of the cell stack temperature control was within $\pm$ 2°F. Water quality generally agreed with subscale testing and was better than 40–kW experience, except the dissolved O_2 level in cell stack water was at the low limit of 40 ppm. Minor changes were defined to increase the O_2 level on later runs. See the discussion of Water Quality for more details.

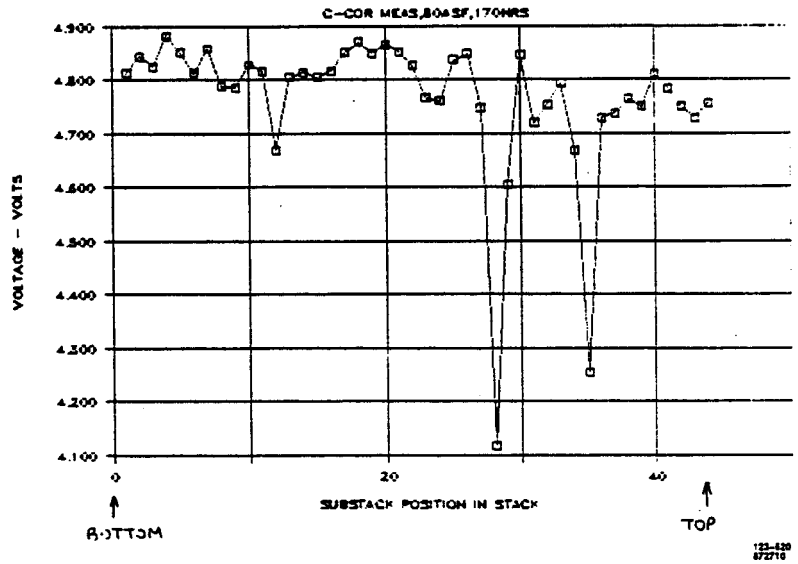

Figure 7.2–44. *Substack Voltages versus Position*

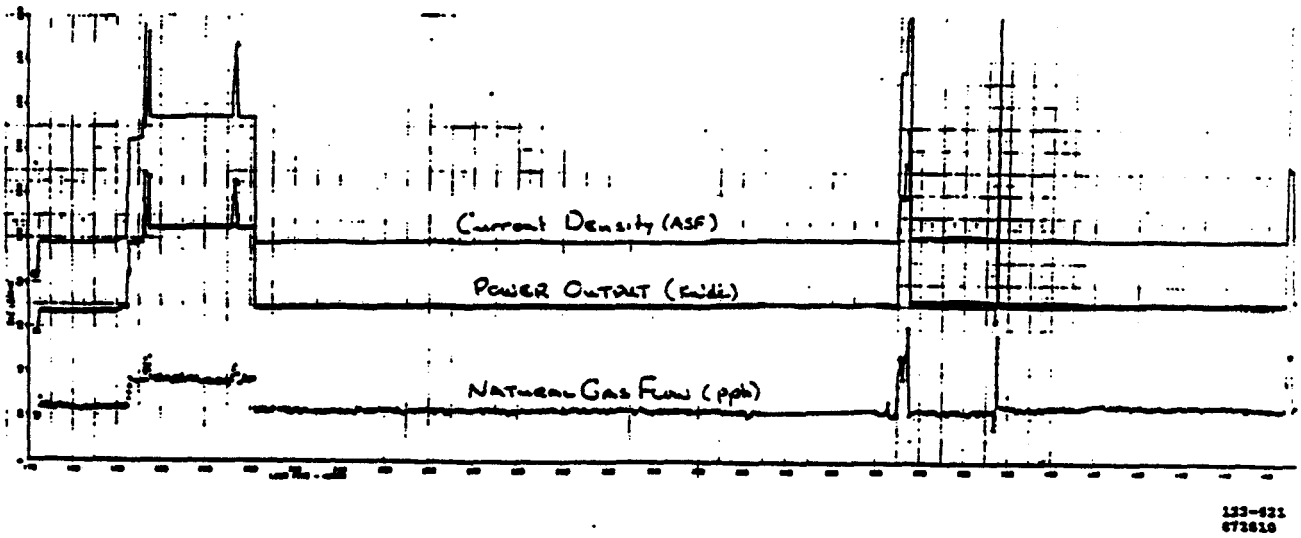

Figure 7.2–45. *VTA Operating Profile for Run 6*

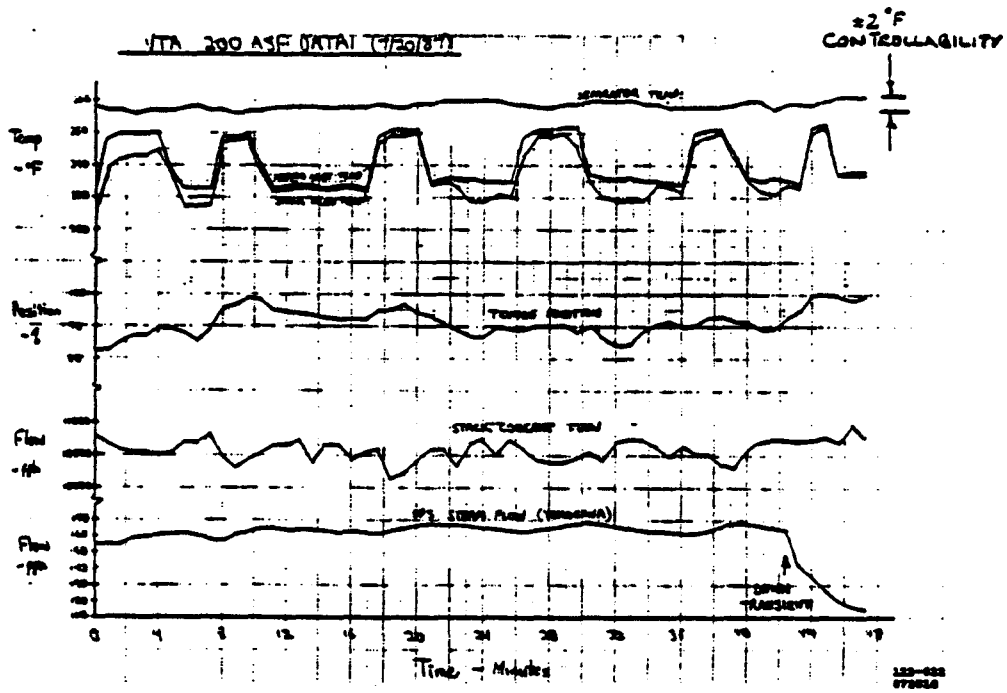

Figure 7.2–46. *VTA 200 ASF Data*

Also, during Run 6, a possible problem with two substacks (numbers 12 and 29) was identified, and the VTA was shutdown and reconfigured for open–loop diagnostics. Two runs (Runs 6A and 6B) were conducted for a total of 7–hours of load time. As discussed in the Cell Performance section, it was determined that the substacks were stable, and the VTA was returned to the normal (closed–loop) configuration to continue testing.

Run 7 (October 5 – 8, 1987)

The VTA was successfully started in the normal (closed–loop) configuration on 10-5-87. A power level of 210 kW was achieved the following day. After a few hours of operation at high power, it was discovered that the steam ejector pintle was stuck. The VTA ran at a constant output of 180 kW until voluntary shutdown. Figure 7.2–47 shows the operating power profile for the run. Other observations during the run were a lower than expected stack temperature at the 180 kW level, some instability in the fuel control operation and higher–than–expected shift converter exit temperature.

During cooldown of the VTA, the coolant pump bearings showed evidence of high wear rate by virtue of high noise level and TMS loop contamination. The pump was rebuilt and re–installed prior to Run 8. (This pump was eventually replaced with an alternative design which proved to be far superior. See Coolant Pumps discussion.)

The stuck steam ejector pintle encountered was the result of a "dry" pintle stem packing and an over–torqued packing gland nut. The packing was lubricated and the nut set to a lower torque value and proper operation was achieved. (This ejector was later replaced with an alternative design. See Steam Ejector.)

In response to problems noted on Run No. 7, several changes were made to the VTA prior to the start of Run No. 8. Piping to the shift converter precooler was enlarged and relocated to provide more flow and cooler fluid to the precooler, and an offset adjustment was made to the separator temperature control software to provide more accurate stack temperature control. In addition, the coarse WTS filter was bypassed to provide data which could result in its permanent removal from the system.

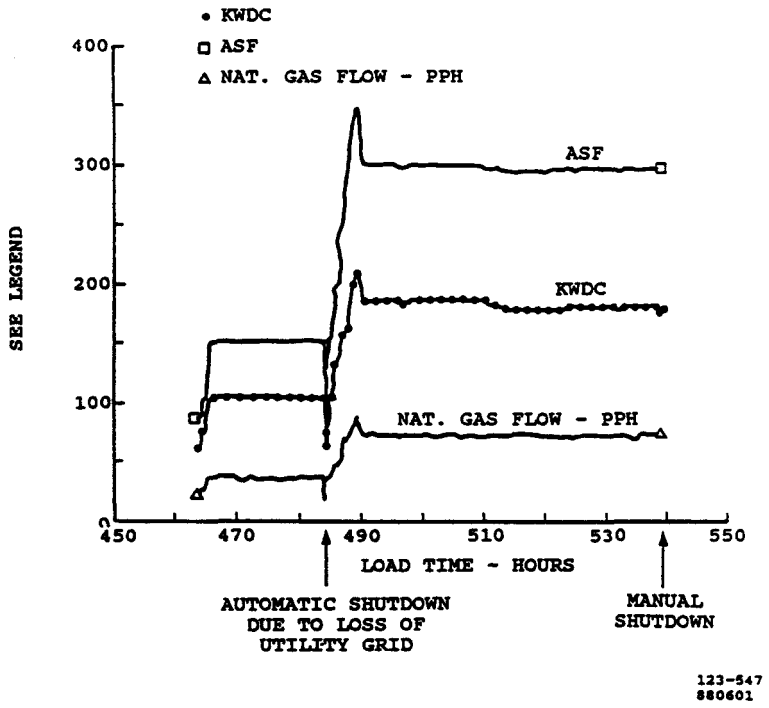

Figure 7.2–47. *VTA Operating Profile for Run 7*

Run 8 (November 9 – 12, 1987)

Startup of the VTA was achieved and cell stack load set at 300 ASF. The instability noted in Run No. 7 of the fuel control was again noted, and a short shutdown was initiated to adjust the gain of the fuel control. Restart confirmed stable operation of the fuel control. Figure 7.2–48 compares operation of the fuel control before and after the gain adjustment as reflected by fuel flow and reformer operating temperature. Operation of the VTA throughout the remainder of the run was stable over the operating range shown in Figure 7.2–49.

The offset to the separator control resulted in excellent stack operating temperature control as shown in Figure 7.2–50.

The VTA was shutdown manually after the local utility began using peak shaved gas.

Prior to the shutdown, an increase in water turbidity was noted due to failing coolant pump bearings. While shutdown the coolant pump was replaced with an alternative design (see Cooling Water discussion). Other changes included addition of gas totalizer on the natural gas supply to resolve flow measurement inconsistencies and a splash pan to the blowdown entrance into the water tank for purposes of increasing oxygen level in the entire WTS/TMS system.

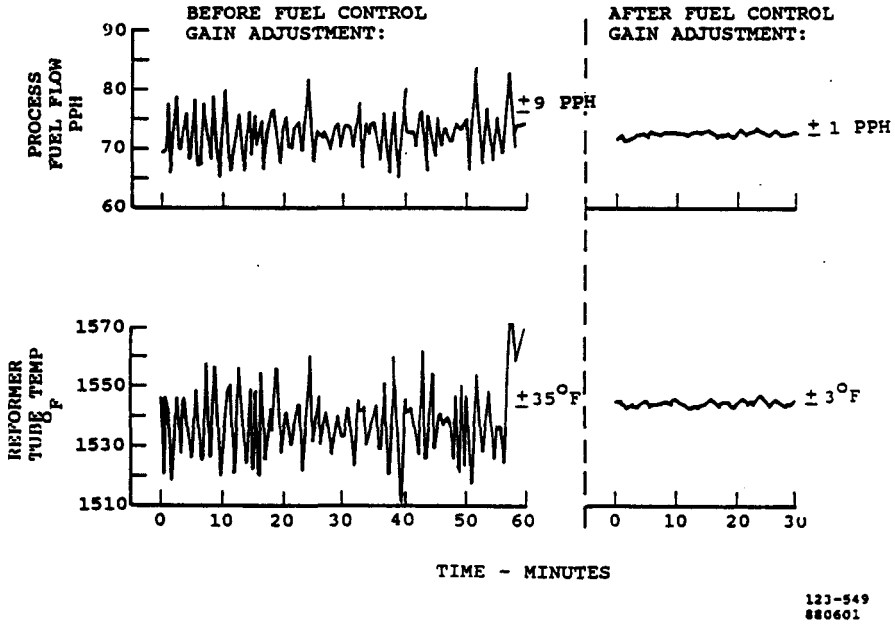

Figure 7.2–48. *Fuel Control Operation (at 300 ASF) During Run 8*

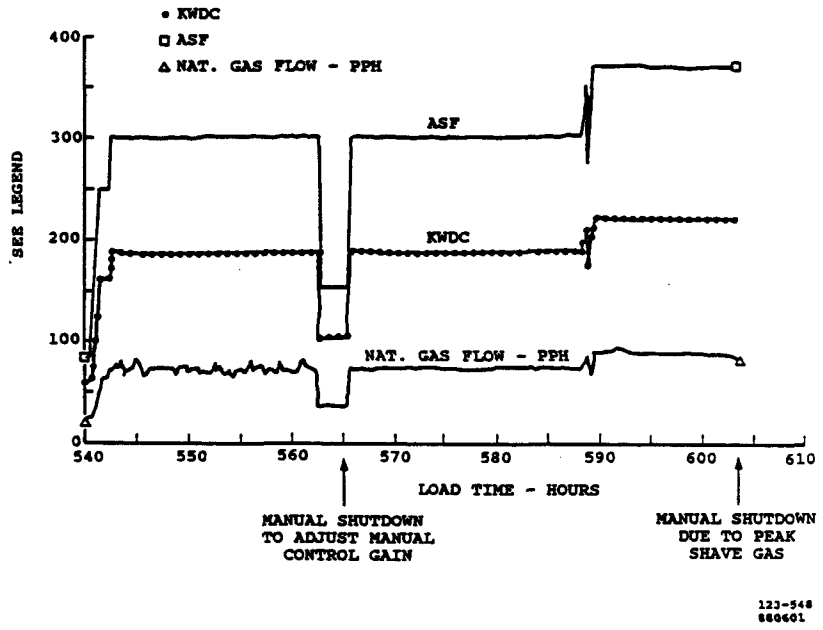

Figure 7.2–49. *VTA Operating Profile for Run 8*

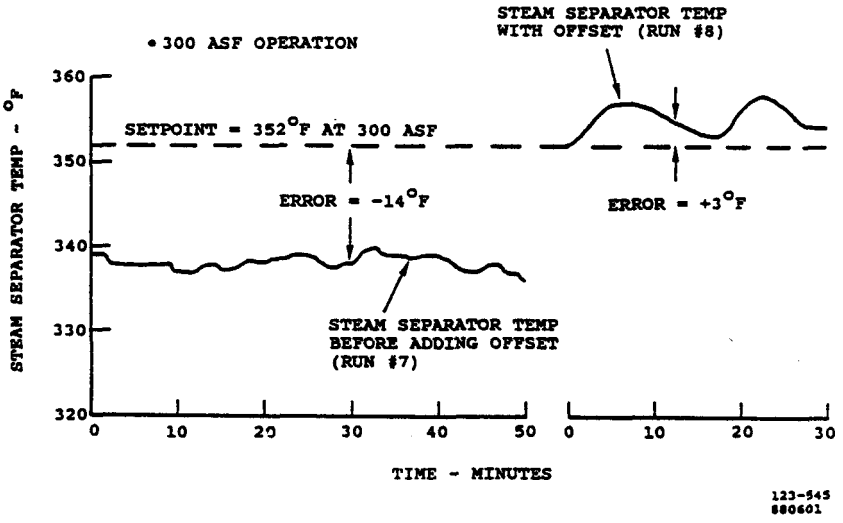

Figure 7.2–50. *Stack Cooling Water Loop Temperature Control*

Run 9 (December 9, 1987)

The VTA was started successfully after installation of the new coolant pump. An automatic shutdown occurred after six hours of operation due to an electrical breaker trip in the new coolant pump circuit. After installing a higher rated thermal breakers in the coolant pump circuit, no further pump problems were experienced.

Run 10 (December 14 through December 23, 1987)

The VTA was started and voluntarily shut down 9 days later in preparation for a holiday. The power profile for this run is shown in Figure 7.2–51. The coolant pump performed well throughout the run (and subsequent runs), and water quality remained acceptable.

During this run, emission testing was performed at various power levels and flow conditions and found to meet program goals. See Emissions Characteristics for more details.

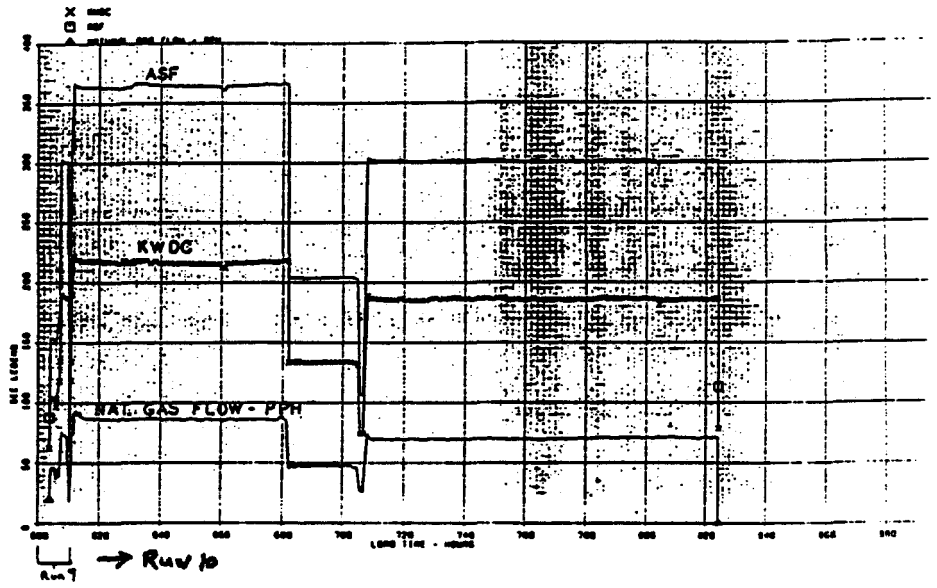

Figure 7.2–51. *VTA Operating Profile for December, 1987 (Runs 9 and 10)*

Run 11 (January 18 – 20, 1988)

During system checkout prior to starting Run No. 11, it was determined that the process air blower speed control was not providing proper control. A vendor service representative replaced the main microprocessor chip in the speed control and proper operation was achieved.

Startup was successfully achieved, and the power level was set at 300 ASF to confirm previous reformer efficiency measurements. Data was found to duplicate previous results.

During the third day of operation, the automatic data recording system showed a rapidly dropping Water Treatment System (WTS) flow rate. The feedwater pump continued to pump water into the Thermal Management System (TMS) loop, but the conductivity of the WTS water started to increase because of the low flow in the WTS. The VTA was shutdown to investigate the problem. Disassembly of the boost pump showed slight evidence of damage to the interstage impeller seals, and the pump was rebuilt. The pump vendor suggested that this type of damage sometime results from a restriction at the pump inlet. Piping upstream of the pump was checked, but no evidence of restriction was found. The pump was put back into service. See Run 12 for further observations. Load time on Run 11 was 49 hours.

Run 12 (January 25 – 29, 1988)

The VTA was restarted, and a series of transient tests were conducted to determine the response characteristics of the VTA. No difficulties were encountered as a result of these transients. The operating profile is shown in Figure 7.2–52 for Runs 11 and 12. Run No. 12 was terminated after 98 hours of operation due to the introduction of peak shave gas in the pipeline.

During this shutdown, a loss of WTS boost pump discharge pressure was observed. Sediment was found in the WTS water tank and in the boost pump strainer. The sediment was sent to the laboratory for analysis. Laboratory results identified sediment as iron corrosion products which were then traced to the condenser. See Water Recovery Condenser for more details.

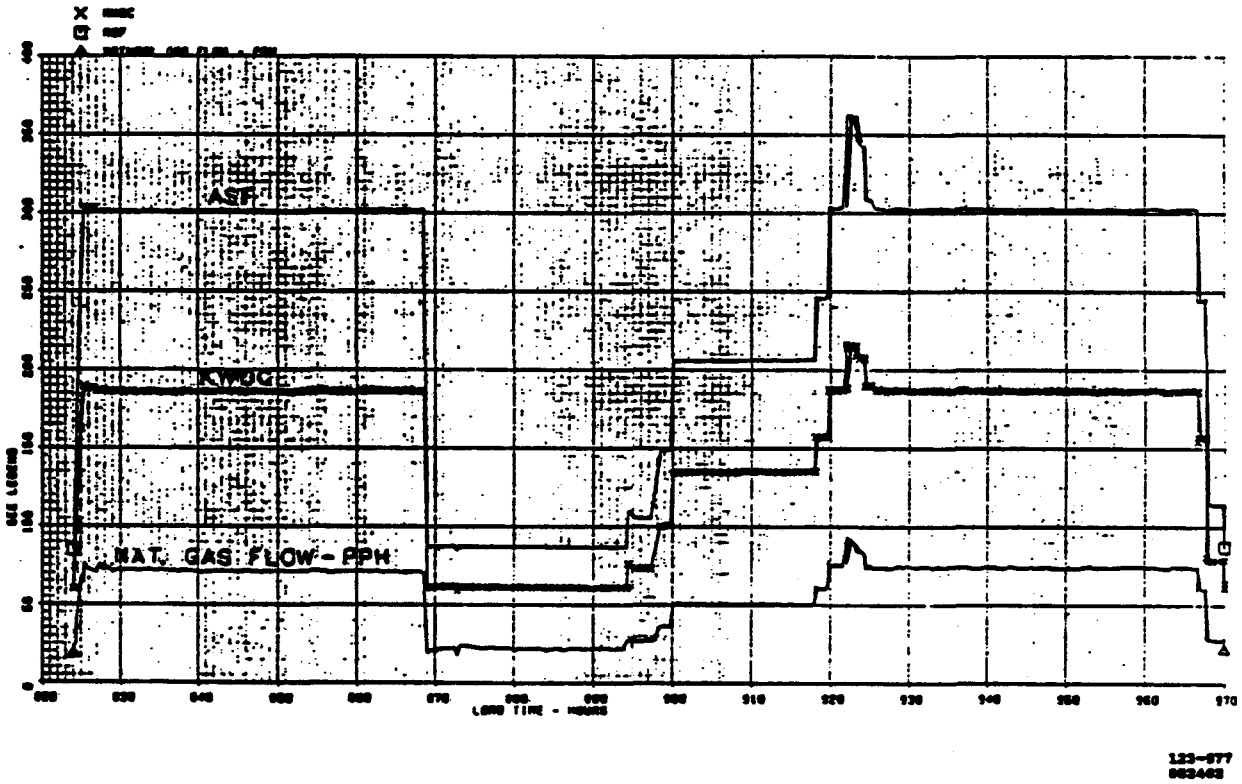

Figure 7.2–52. *VTA Operating Profile for January 1988 (Runs 11 and 12)*

Run 13 (February 2 – 4, 1988)

Startup was accomplished with no anomalies, and power transient testing continued per the planned program. There were no problems encountered with any of the transients. Testing was interrupted when utility peak shave gas forced a manual shutdown.

Run 14 (February 8 – 10, 1988)

Startup was accomplished and transient testing resumed. A manual shutdown was again initiated due to utility peak shave gas. The operating profile is shown in 7.2–53 for Runs 13 and 14.

The VTA was capable of 30 – 35 kWdc power steps and full power up–transients within 15 seconds. See Transient Capability for discussion.

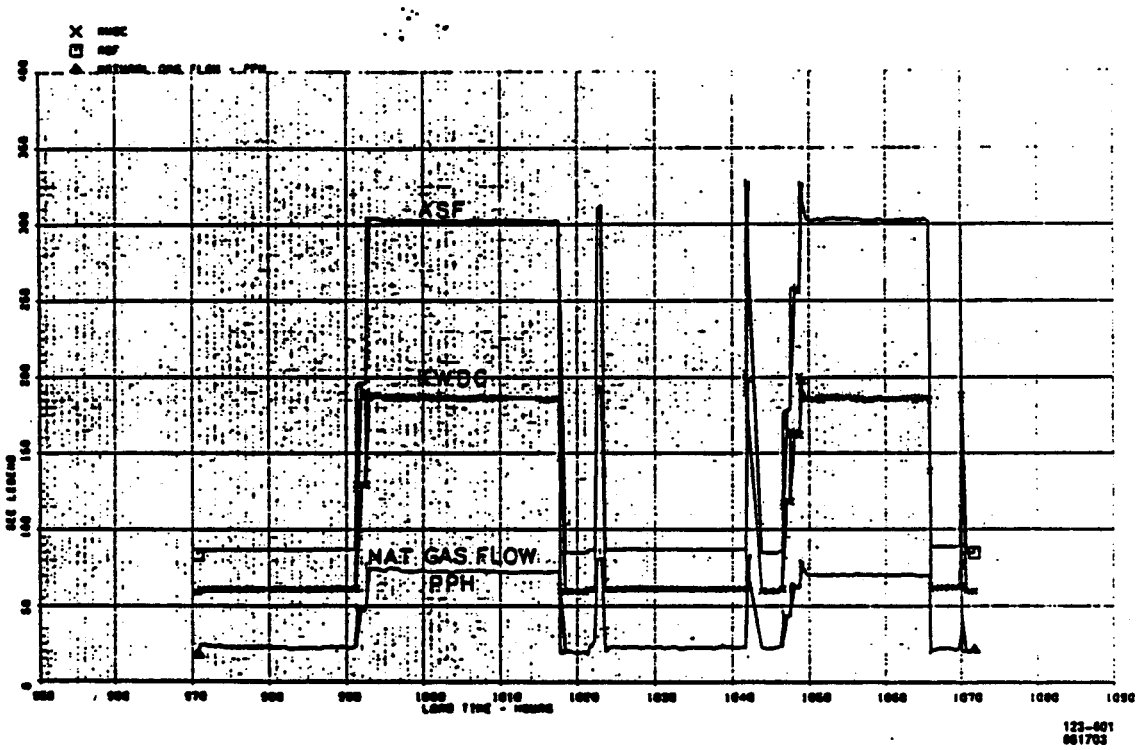

Figure 7.2–53. *VTA Operating Profile for February 1988 (Runs 13 and 14)*

Run 15 (March 8 – 26, 1988)

Prior to startup a preoxidizer was installed in the fuel system in order to give the VTA peak shave gas capability. See Preoxidizer Testing for discussion of configuration and test results.

Water conditioning with the new WTS started on March 3, 1988 and starting of the VTA was accomplished on March 7, 1988 without problems.

As peak shave gas was not available, the first trials of the new preoxidizer were run from March 8, 1988 until March 11, 1988 using air injection into natural gas to simulate peak shave gas at levels up to 18 percent. This first testing was conducted at approximately 100 ASF power level. Several changes in control setpoint and control concepts were tried. The best performance resulted in paralleling the inlet and exit preoxidizer bed thermocouple readings and setting 625°F.

On March 10, 1988, the load was increased to 300 ASF and a simulated peak shave gas was run again with good results.

On March 21, 1988, the local utility started peak shaving for about 18 hours. Control of the preoxidizer was excellent with no HDS overtemperature.

Until utility power loss caused a facility-induced shutdown, the remainder of this run was spent documenting stack performance, evaluating reformer efficiency, and lowering the steam drum water level to determine if a smaller drum might be used in future units. The results of the lower water level testing were not conclusive, but a reduction from 11.25" to 8.25" in level was possible at steady state 300 ASF. The operating profile for this run is shown in Figure 7.2–54.

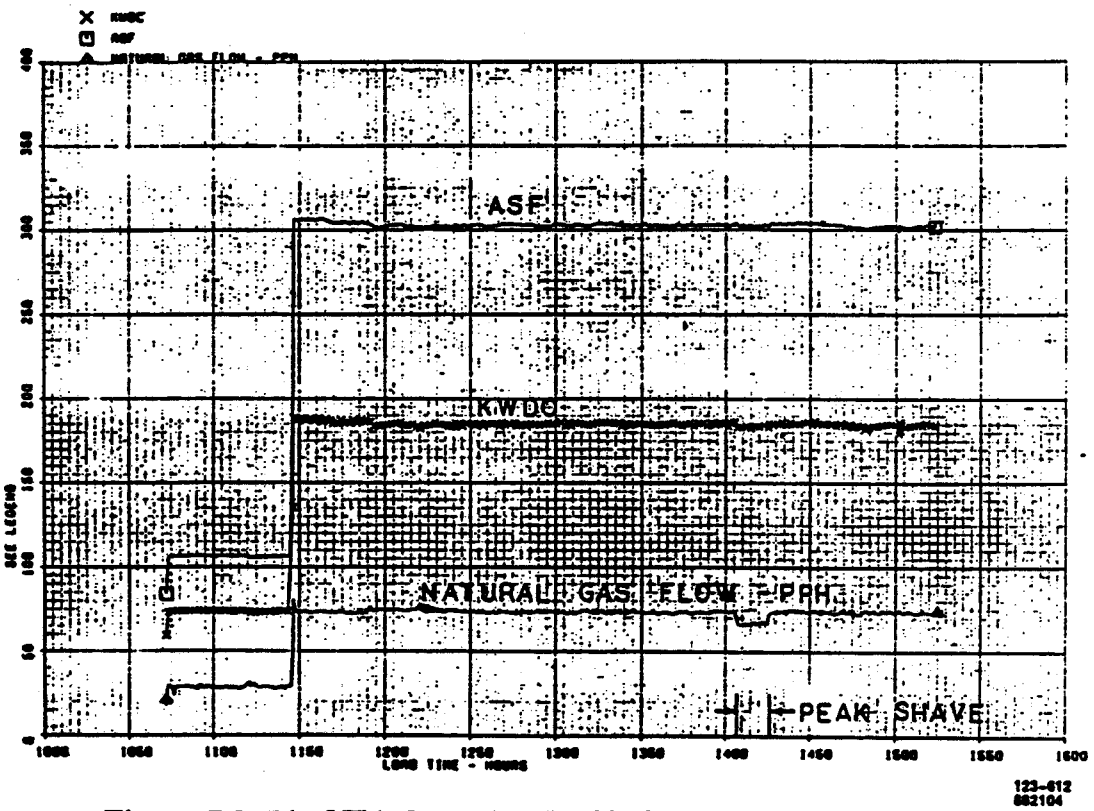

Figure 7.2–54. *VTA Operating Profile for March 1988 (Run 15)*

Run 16 (May 3 – 6, 1988)

Prior to Run 16, the steam separator and stack air regenerator were removed, and new filter material was added to the copper fines filter assembly. In addition, several leaks in the burner air and exhaust system and the fuel system were found and repaired. A separate leak check of the cell stack showed no change from previous checks.

Burner air and exhaust leakage was found at two (2) locations on the VTA: the Burner Air Preheater (Hex 910) and the penetrations of the fuel inlet and exit piping through the re-

former shell burner cavity. Total leakage before repair was 220 pph N_2 at 5 IWC. After welding HEX 910 joints and installing packed sleeves around fuel inlet and exit penetrations, total leakage was reduced to 60 pph N_2 at 5 IWC.

Initial fuel system leakage was greater than 2 pph N_2 at 8 IWC. Leaks were discovered at seven (7) fuel piping connections where the clamping devices had lost all or most compression on the joints. In all cases, repair was made by re-torquing these clamps. Final fuel system leakage excluding the cell stack was at 0.2 pph at 8 IWC.

Also, as part of an effort to improve fuel measurement accuracy, a new fuel flowmeter (at the natural gas supply) was received, calibrated and installed in place of the present FTO12A.

Startup and on-load operation up to 300 ASF was without incident, and a slight improvement in VTA operating efficiency was noted. During this run, the new integrated filter material ran at predicted pressure drop levels, and there was no evidence of water carry over from the steam drum without a separator. No problems were evident as a result of stack air preheater removal. This run was manually terminated on May 6th because of a stuck steam ejector pintle which limited further testing. The ejector sticking problem was traced to misalignment between the actuator motor mounting flanges and the pintle assembly. Shims were added to the assembly, and satisfactory cold operation was achieved after repair. (As described in the Steam Ejector section, the original ejector was eventually replaced with an improved design.)

Run 17 (May 10 - 14, 1988)

Startup and transition to load was successfully completed on May 10th. VTA efficiency was evaluated up to 300 ASF with slight improvement from Run 16. Several times during this run, unexpected changes in process air blower speed were noted at constant load. On May 14th, the VTA shutdown because of an indicated utility power loss. As there was no other evidence in the facility of a power loss, the problem was most likely caused by the UPS which is installed in the test stand to maintain power to the VTA controllers in the event of a momentary building power glitch. The UPS was bypassed for the next run(s) and monitoring equipment was added to the UPS to detect malfunctions.

Run 18 (May 17 - 26, 1988)

On May 17th the VTA was started again with no problems, and the load increased to 300 ASF. The operating profile for Runs 16, 17, and 18 are shown in Figure 7.2-55. Powerplant operation was normal until process air blower speed started to drop suddenly on May 20th.

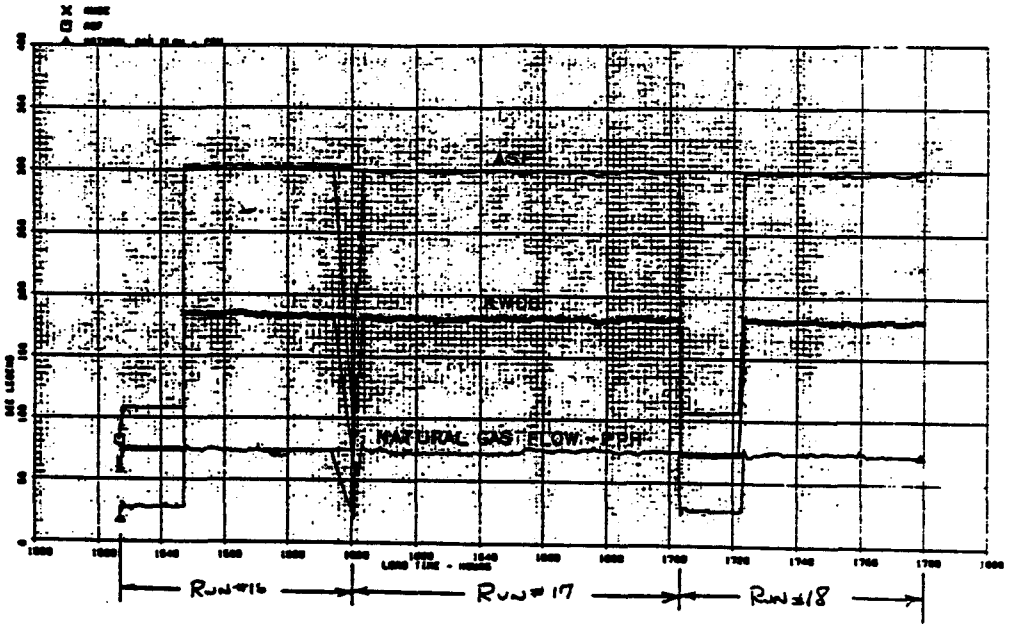

Figure 7.2–55. *VTA Operating Profile for May 1988 (Runs 16, 17, and 18)*

The VTA was shutdown to troubleshoot. Special monitoring equipment was setup and the blower was operated continuously. On May 26th, the blower speed started to drop and monitoring equipment showed that the FPS controller signal to the speed control had become erratic. Further troubleshooting indicated a bad power supply card in the FPS controller. In addition, the UPS malfunctioned during this period, thus confirming the reason for the Run 17 shutdown.

Because of the continuing discrepancies in measuring fuel flow, all three fuel flow meters were removed and calibrated simultaneously.

Run 19 (June 6 – 8, 1988)

Prior to Run 19, the coolant pump (PMP 400) which has performed flawlessly for almost 1200–hours was removed for vendor evaluation and replaced with a new unit from the same vendor. (The original pump was on loan to IFC from the vendor; the new pump was purchased for this contract. See the discussion of coolant pumps for more details.)

Startup and on load operation was achieved on June 6 without incident. VTA performance was checked up to 300 ASF through the following day, but on June 8 a gas leakage was discovered emanating from under insulation on the reformer burner external housing. The VTA was shut down to investigate. The operating profile for the run is shown in Figure 7.2–56.

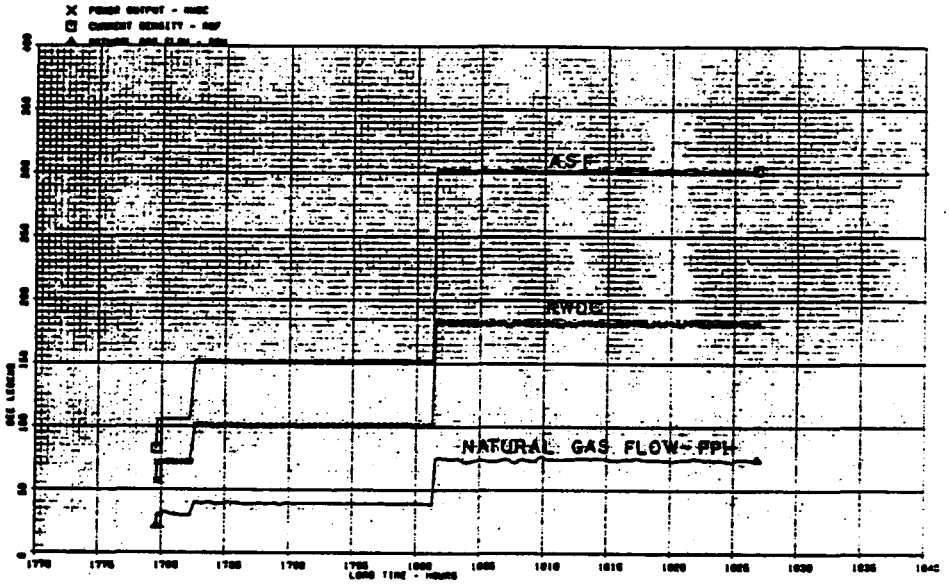

Figure 7.2–56. *VTA Operating Profile for June 1988 (Run 19)*

Pressure check and subsequent visual examination of the burner assembly showed that a gasket had burned away from a flange joint connection at the main burner body. The most probable cause for this failure was a result of subjecting this gasketed joint to hot burner flame very early in the VTA test program during burner development. Further temperature and pressure cycles resulted in failure of the joint. A decision was made to replace the entire burner assembly. Disassembly of the burner was made difficult by apparent thermal growth expansion and distortion of the burner in the reformer housing. As part of the new burner installation the gasket material was upgraded, and flat washers were added to establish proper bolt torque.

Run 20 (July 5 – 9, 1988)

Startup and on–load operation was achieved on July 5, 1988 with no problems. This was the first start for the new reformer burner (which was inserted after a seal failure in the old unit); burner operation was excellent.

While data was being gathered to evaluate stack performance, a test was run to determine effectiveness of the condenser (HEX 981) at design conditions. The water/glycol coolant temperature at the inlet to the condenser was increased to simulate power plant operation on a 95°F day, and water recovery was measured as described in the discussion of Water Recovery, the condenser performed "as expected", exceeding full water recovery at rated power on a 95°F day.

This run continued until July 9, 1988 when a loss of utility power forced a shutdown.

Run 21 (July 13 – 14, 1988)

Startup and on load operation was achieved with only a minor problem with a malfunctioning burner start fuel solenoid. The valve was rebuilt and then functioned properly. A lightning strike on local utility lines resulted in loss of building power, and the VTA shut down.

Run 22 (July 18 – 20, 1988)

Startup and on load operation was achieved on with no problems. Two days later, another local utility power interruption caused a shut down. The operating profile for the Runs 20, 21, and 22 is shown in Figure 7.2–57.

An attempt to restart on July 21, 1988 was terminated when it was discovered the Thermal Control Valve (TCV 400) had significant water leakage at one of the main assembly body gaskets and the valve stem packing. Total hot time on this valve including rig testing before VTA operation is about 5000 hours. After repair of the valve, problems were encountered in establishing the proper WTS loop flows. Rust from the water tank was found in the external filter, and the WTS circulation pump flow was almost zero. The rest of July was spent rebuilding the pump, installing a sparger–type filter in the water tank, and cleaning up the water.

Run 23 (August 3 – 5, 1988)

Startup and load operation was achieved without problems. The load was set at 150 ASF and then increased to 300 ASF the following day. On August 5, 1988 the VTA shut down when a facilities work crew working on building modifications inadvertently shut off the natural gas supply. This resulted in a burner flame out and shutdown.

Run 24 (August 8 – 10, 1988)

Startup and transition to load was accomplished without problems. On the following day, the load was increased to 300 ASF. During that day, two malfunctions in steam drum water level control were noted whereby the water level signal suddenly indicated a drop to zero output. A separate level indicator, a lower cost unit installed to evaluate product improvements, showed that the drop was not real. Operation returned to normal after a few minutes and remained normal for the rest of the run.

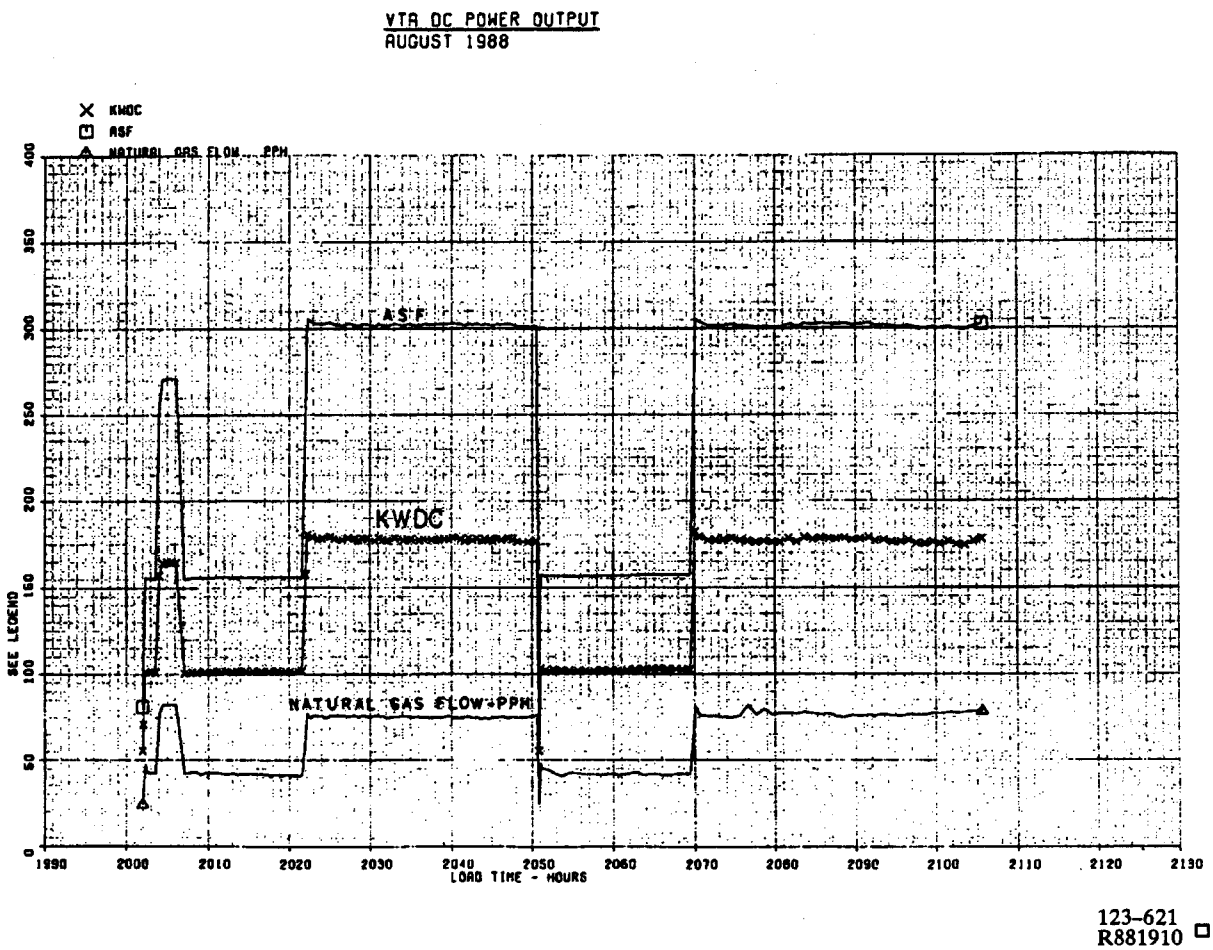

Figure 7.2–57. *VTA Operating Profile for July 1988 (Runs 20, 21, and 22)*

On August 10, 1988 the test operator manually shutdown the VTA when he observed water flowing from the top of the degasifier. The overflow of water was due to test conditions where a large excess of water was being condensed (humid day, low condensing temperature) and all water entering the water tank could not be dumped overboard. The overboard vent line was increased in size to 3/4 inch to prevent a reoccurrence.

Subsequent investigation into the water level sensor problem showed the pressure transducer used to measure water level had a "dead" spot in its operating band. It was replaced when one chamber in the transducer was found plugged with rust. The rust had apparently drained from the bottom of the steam drum into the transducer. A sediment trap was also installed with the new transducer. The operating profiles for Runs 23 and 24 in August of 1988 are shown in Figure 7.2–58.

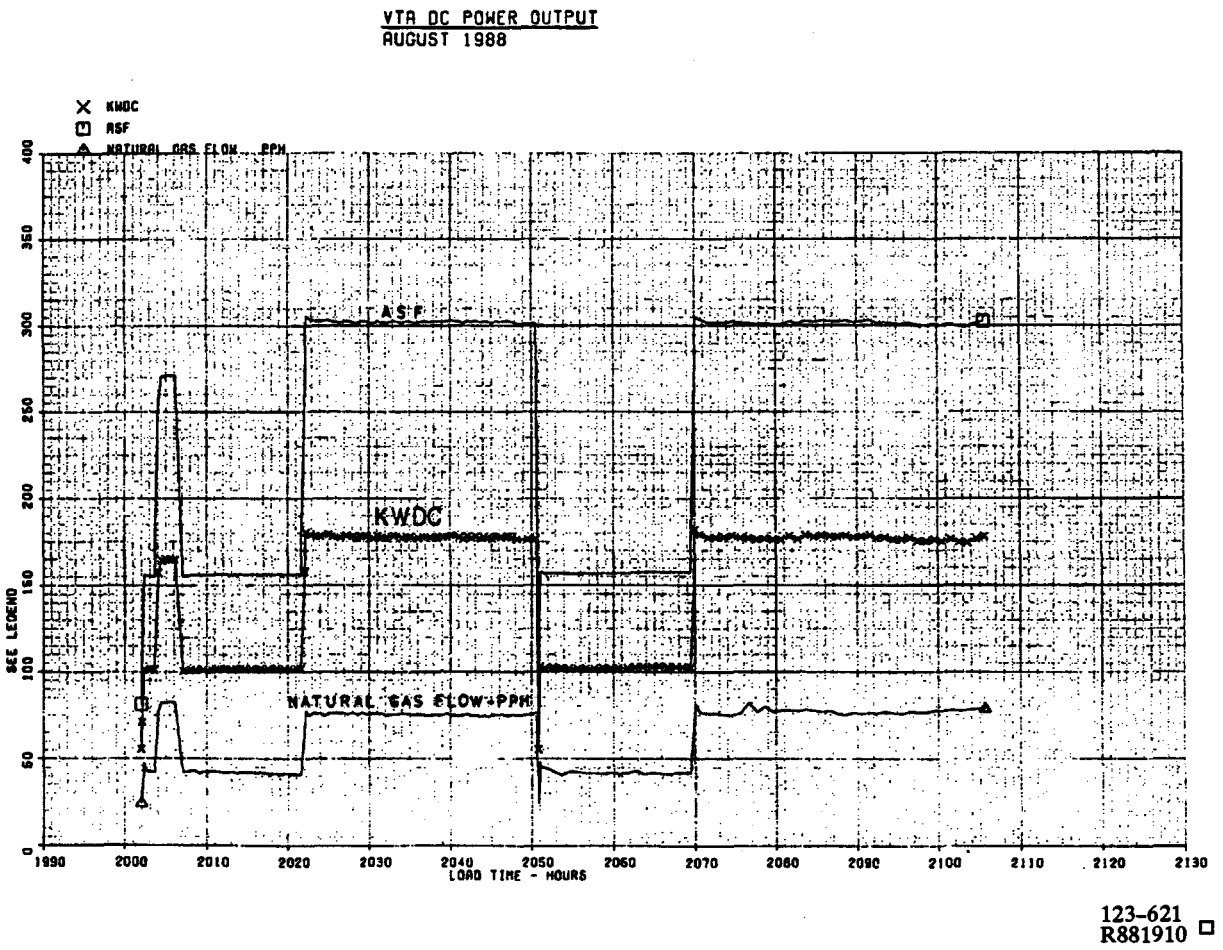

Figure 7.2–58. *VTA Operating Profile for August 1988 (Runs 23 and 24)*

Run 25A (September 20, 1988)

Prior to Run 25A, a decision was made to modify the system to improve operating characteristics and inspect the condenser. The following system modifications were made:

- Installation of high–speed ejector with improved seals
- Installation of smaller and simpler preoxidizer with simpler control
- Installation of a new purge system to control stack voltage
- Addition of inspection ports in condenser for viewing the core

The condenser was examined after adding view ports to the condenser. The first stainless steel core section (hot side inlet) of the condenser was found to be in excellent shape, but the next carbon steel section showed some minor fin corrosion. The remainder of the cores were in excellent condition. At this time inspection was completed and view ports were closed.

After completing modifications, a start was attempted on September 20, 1988. The run was terminated when all FPS controller outputs went to "zero", and an automatic shutdown took place. A loose wire was found on the "watch dog timer" circuit (this circuit monitors controller operation and shuts down the VTA if a controller failure is detected). This wire and several other terminals were checked and tightened.

Run 25 (September 21, 1988)

The VTA was restarted after correcting a controller software error. After about 20 minutes on load, the VTA automatically shutdown when all outputs lost power. Although the exact cause of the problem was not found, the "watch dog timer" contacts were again cleaned, and the problem did not reoccur on subsequent runs.

Run 26 (September 1 – October 16, 1988)

Startup of the VTA for this run was accomplished without incident, and the load set at 300 ASF. All VTA operating parameters were as expected. By October 3, the stack had operated continuously at 300 ASF for 237 hours. After the initial settling of stack performance after restart, there was no measurable decay for the last 175 hours of this 300 ASF operation.

At the point, the power level was reduced to 100 ASF in preparation for peak shave gas testing. In this particular testing, air was injected into the natural gas supplied to the VTA to simulate peak shave gas mixtures. In the first test, no reaction took place in the preoxidizer. The lack of a reaction in the preoxidizer was assumed due to inadequate thermal conditions in the preoxidizer. Control valving was adjusted to redirect the incoming fuel and recycle flows to the preoxidizer and, therefore, improve the thermal conditions within the preoxidizer catalyst bed. After several attempts, a short duration injection of air into the natural gas achieved a reaction in the preoxidizer. Although a reaction was achieved, a rise in HDS temperature showed that the reaction was not complete. Another trial produced similar results. Further testing was postponed to later runs where proper thermal conditions were established.

During the 98–hour period at 100 ASF, cell performance improved slightly. On October 7, the power level was increased to 300 ASF. Initial cell performance was higher than previous 300 ASF operation, but stack performance decreased to the previous level over the next 100–hours. On October 11, the power level was reduced to 200 ASF and maintained at this level for the next 3 days. No change in stack performance occurred during this period.

On October 14, the power level was again increased to 300 ASF. Shortly thereafter, a data monitoring alarm sounded indicating an out of limits condition in substack No. 13 voltage. At 100 ASF, the substack No. 13 performance improved to a point where the load could be increased to 200 ASF. Unfortunately, the VTA was shutdown two days later because substack No. 13 voltage was again dropping. Figure 7.2–59 shows the complete operating profile for Run 26.

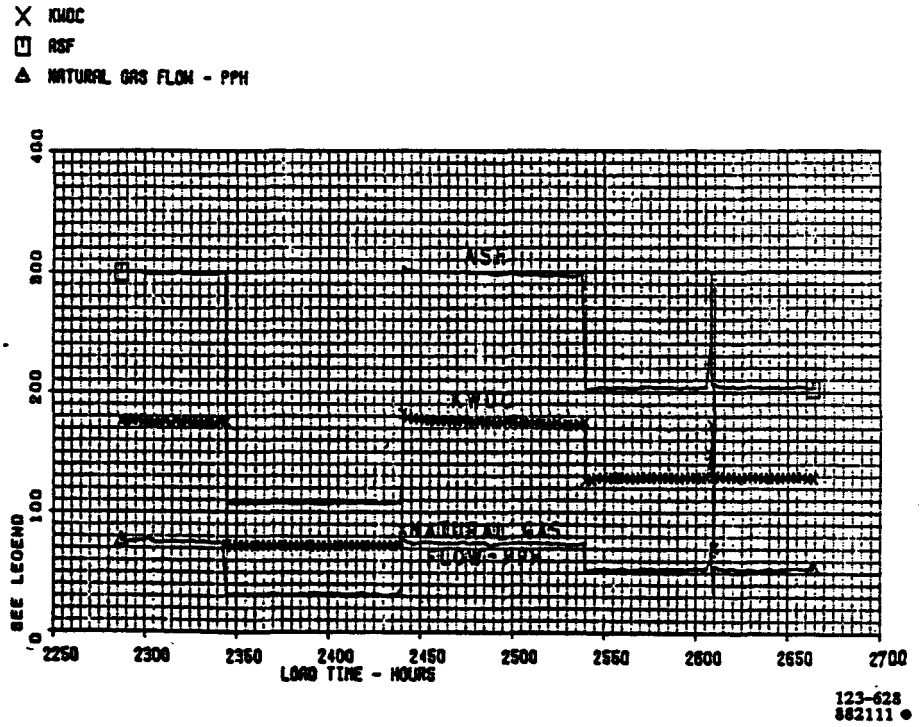

Figure 7.2–59. *VTA DC Power Output for Run 26*

A decision was made to inspect the cell stack. Fuel and air leakage tests and stack compressive load tests were conducted and all were within expected limits. Prior to the next run, the VTA was reconfigured for open–loop operation where the cell stack could be operated with a mixture of hydrogen and nitrogen flowing to the anodes for diagnostic purposes.

Run 27 (January 23, 1989)

Cell stack diagnostic tests were performed after reconfiguring the VTA for open-loop operation. A hydrogen/nitrogen gas mixtures was delivered to the anode to simulate the reforming mixture normally supplied by the fuel processing system of the verification test article, and the anode exhaust was vented overboard.

As discussed in the Cell Performance section, diagnostic tests confirmed an anode problem in Substack 13. After completing diagnostic tests, the cell stack was shutdown, and the electrolyte was conditioned. Post-test electrical and pressure tests were then performed before the cell stack assembly was removed on February 10, 1989.

Run 28

After removal of the cell stack, the VTA was reconfigured to operate the Fuel Processing, Thermal Management, and Water Treatment Systems without the cell stack. Fuel normally flowing to the cell stack was vented overboard, and the reformer burner was fueled by natural gas.

An attempt to start on February 22, 1989 was terminated when a steam leak developed in the superheater steam inlet to the steam/fuel ejector connection flange. A failed gasket was replaced, and other flange connections were checked and re-torqued.

The VTA was successfully restarted in early March. Equipment and procedures required to evaluate the preoxidizer were checked and verified. The rig was then shutdown to replace preoxidizer catalyst.

Run 29 (March 27, 1989)

This run was started and terminated on the day when an air leak in a test gage caused the preoxidizer to ignite immediately on introduction of natural gas. The leak was repaired, and VTA was prepared for restart.

Run 30 (March 29 – 31, 1989)

The VTA was successfully restarted and (5) five preoxidizer trials were run using simulated peak shave gas.

The first three trials were only partially successful. There was immediate ignition, but it occurred only on the outer edges of the bed, allowing some oxygen slip. System valving was then adjusted to improve mixing of the fuel and recycle gas streams. As illustrated in Figure 7.2–60, subsequent trials were completely successful with immediate ignition at the front of the bed and no oxygen slip.

The VTA was voluntarily shutdown for the weekend.

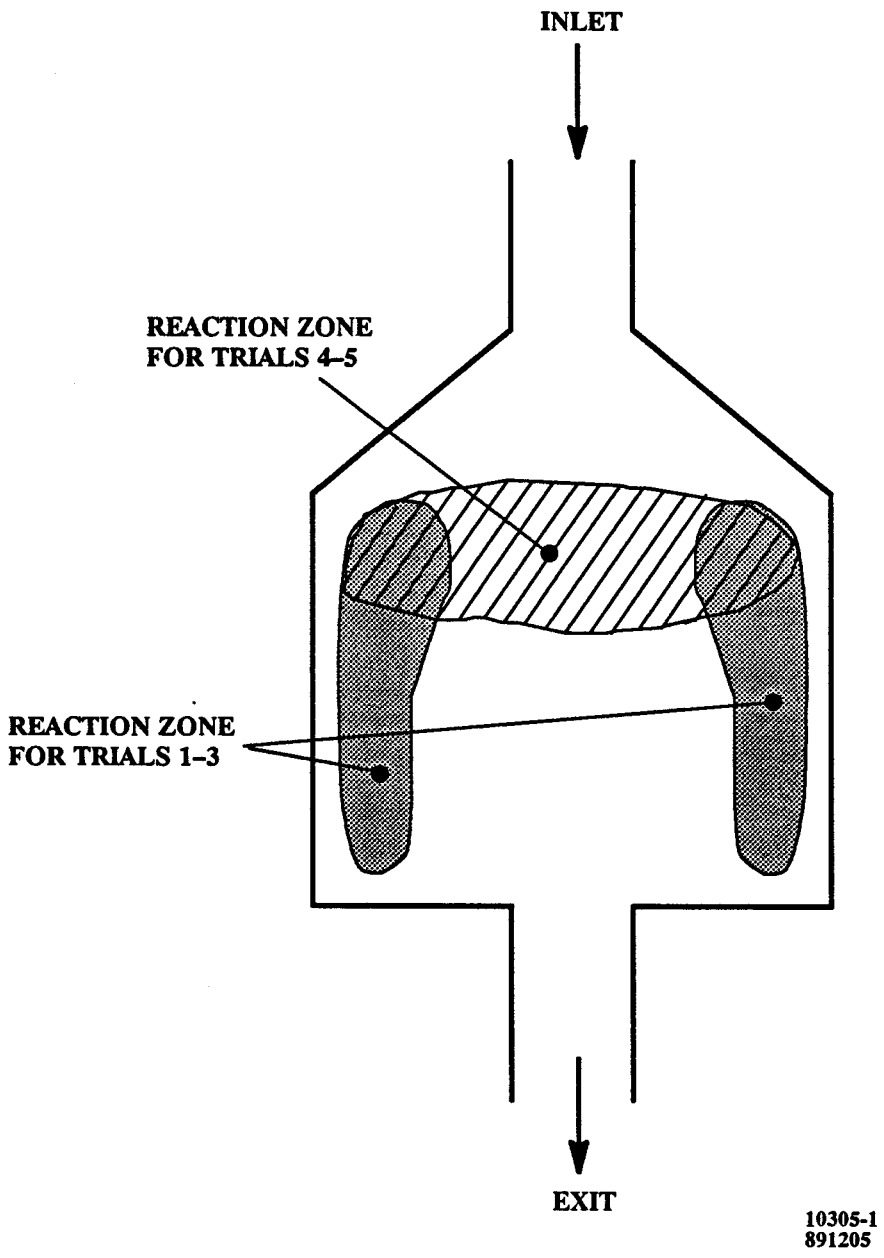

Figure 7.2–60. Preoxidizer Ignition Zones

Run 31 (April 4 – 5, 1989)

Startup of the VTA in the open-loop configuration (without the cell stack) was completed on April 4, 1989.

Simulated full power conditions were then set and peak shaving up to 22% air was simulated. All ignitions of the preoxidizer were successful.

The VTA was shut down by the operator when a low water level alarm in the water tank sounded. Subsequent investigation found nothing wrong with VTA, and a facility water supply interruption was suspected.

Run 32 (April 6 – 7, 1989)

The VTA was started, and minimum power conditions were set. A short preoxidizer test was successfully conducted with 22% air.

Since all runs up to this point had been conducted on fresh catalyst, it was decided to investigate the preoxidizer performance after sulfiding the catalyst. Sulfiding was accomplished by running natural gas (with about 2 ppm sulfur odorant) through the bed for about 12 hours. Testing on the following day with sulfided catalyst showed a deterioration in ignition characteristics. Ignition occurred initially at only the exit of the bed (see Figure 1), and some oxygen slip was noted for a short time. It was apparent from this data that sulfiding had caused some loss in catalyst activity, and that operating conditions would have to be modified to provide consistent ignitions.

The VTA was shutdown on April 7, 1989 for the weekend.

Run 33 (April 11 – 14, 1989)

Startup of the VTA was accomplished, and minimum power conditions were set overnight.

Thermal conditions within the preoxidizer were adjusted to determine minimum requirements for successful ignitions. Subsequent trials were successful and ignitions occurred at the inlet of the bed with no oxygen slip.

The VTA was shutdown due to local utility power outage.

Run 34 (April 24 – 28, 1989)

VTA startup was accomplished, and maximum power conditions were set.

Since previous VTA data showed a correlation between feedwater fill cycles and cell stack cooling water loop thermal stability, an alternate feedwater inlet location was evaluated.

Figure 7.2–61 shows typical cycling of separator temperature, stack inlet temperature, and thermal control valve position over a 30 minute period. About a 29°F range in stack inlet

temperature was experienced. Figure 7.2–62, is a plot of the same parameters with the alternate feedwater inlet location. Stack inlet temperature cycling was reduced by about 50% to 14°F. Further improvement might be possible by tuning the temperature control gains.

Three preoxidizer trials were also conducted during the week of testing. Ignitions were successful with simulated peak shave gas, the data indicated that the required preoxidizer bed size could be 50% smaller than the present size and 85% smaller than the original configuration.

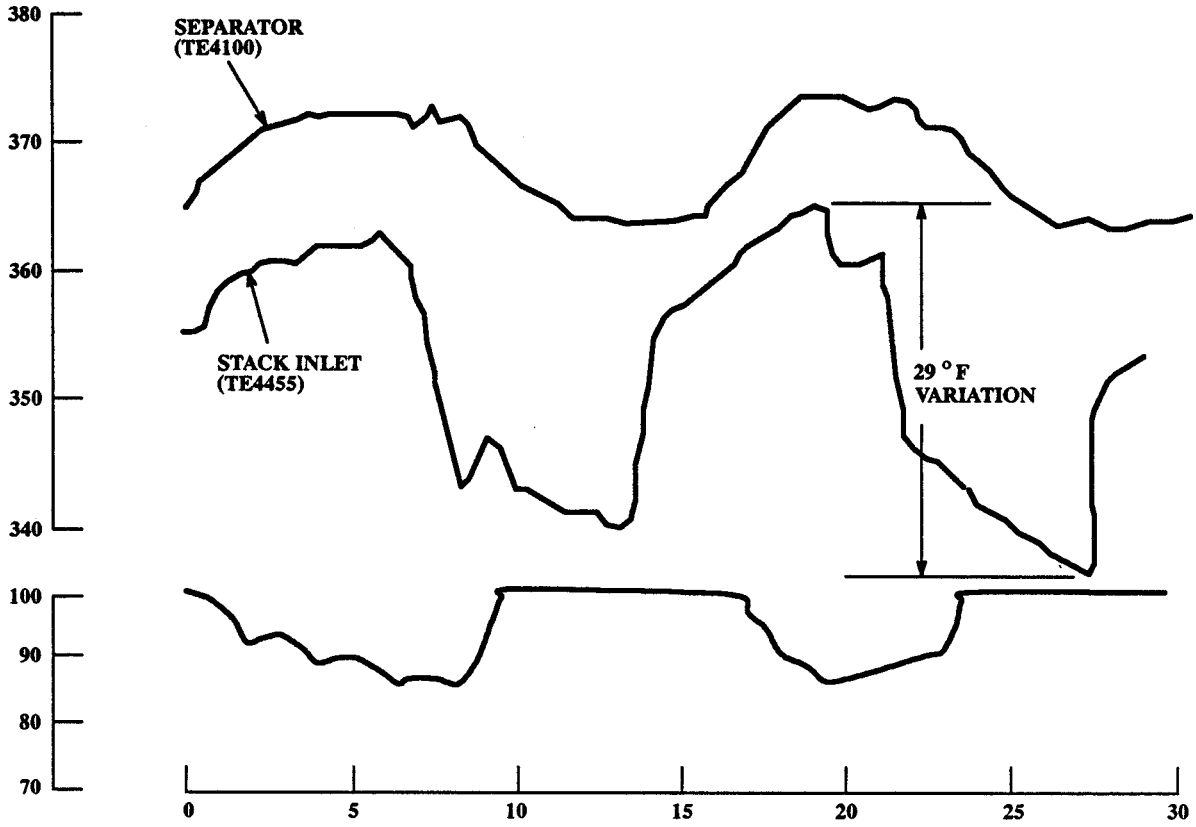

Figure 7.2–61. Transient Characteristic With Normal Feedwater Location

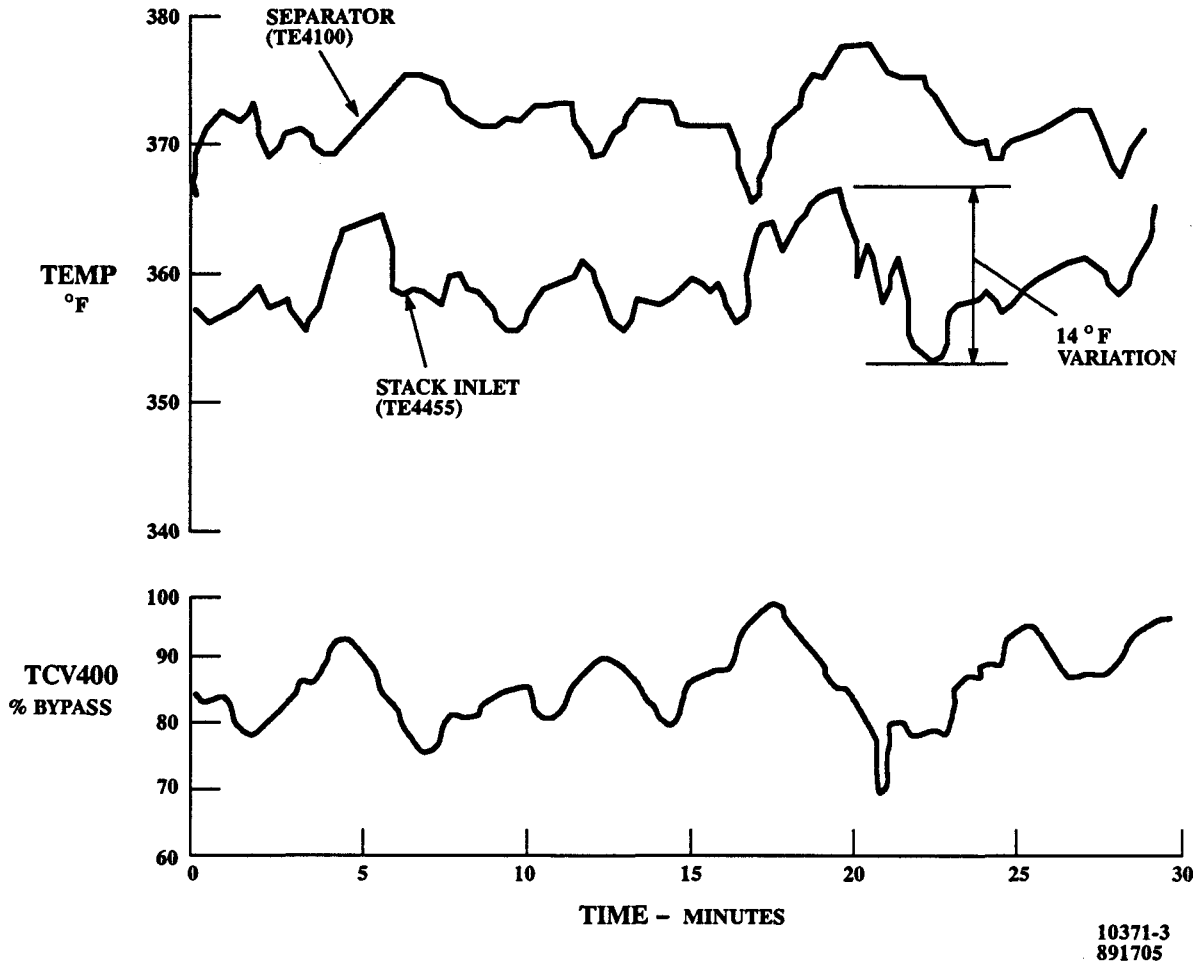

Figure 7.2–62. Transient Characteristic With Alternate Feedwater Location

VTA Storage

After conducting VTA test activities in this program, the VTA was stored for future use by complementary programs. Storage activities included the following:

1. Cell stack cooling water system heated to 250°F and then drained and purged.
2. Water tank drained and disinfected.
3. WTS instrument lines drained, but water left in resin beds.
4. Controllers cleaned and covered.
5. Air blower inlet cleaned and sealed.
6. FPS purged and sealed.